Microbiological approaches for the improvement of industrial biogas production

Submitted by Barbara Mary Shannon to the University of Exeter as a thesis for the degree of Doctor of Philosophy in Biological Sciences in October 2017.

This thesis is available for Library use on the understanding that it is copyright material and that no quotation from the thesis may be published without proper acknowledgement.

I certify that all material in this thesis which is not my own work has been identified and that no material has previously been submitted and approved for the award of a degree by this or any other University.

Signature: ……..

Abstract

Biogas is an alternative fuel source, composed of methane and carbon dioxide, formed during the microbial process of anaerobic digestion (AD). Biogas production has the potential to be used as a substitute for natural gas and ease problems associated with global warming, energy security and waste management. However, AD can often be unreliable due to the instabilities that can arise during the process. The work described in this thesis, focuses on the discovery and development of micro-organisms for use in synthetic bio-methane producing microbial communities. Two main sources of instability within AD were focused on: oxygen-sensitivity of methane-producing microbes (methanogens) and volatile fatty acid (VFA) accumulation.

The estuarine tidal mudflats of the River Exe Estuary, Exmouth, Devon, UK, were chosen for the search of potentially oxygen-tolerant methanogens, due to its intermittent oxygen exposure. Initially, 16S rRNA screening indicated the presence of methanogens in the very surface layer of the sediment, which was later confirmed by enrichment experiments. Whole genome shot-gun sequencing suggested *Methanosarcina mazei*, a methanogen known to have oxygen-tolerant capabilities, or a closely related organism, had been successfully enriched.

The second part of this investigation focused on the use of *E. coli* as a model organism, for the engineering of a negative feedback loop against acetate production, a common VFA. The glutamine synthetase promoter, found to be sensitive to external pH and acetate concentration, was used to control the production of antisense RNA targeting the *pta* gene, involved in acetate production. Results indicated that expression of *pta* was successfully reduced, however overall acetate production was not found to decrease.

Acknowledgements

Firstly, I would like to thank both my supervisors, Rick Titball and David Studholme, for their support and guidance throughout my PhD. Your supervision has been indispensable to my growth as a scientist.

Thank you to Orkun Soyer and members of the wider sLola research group. Our meetings, conferences and collaborations have taught me so many new skills.

Thank you to the Exeter Sequencing Service for providing me with excellent service and support during my sequencing projects, especially Karen Moore.

Thank you to Anke Lange, who taught me everything I know about qPCR and met with me on several occasions to help guide me through my data analysis.

To every single member of the 4th floor lab, both past and present, thank you for making this period so enjoyable. I will miss you all. Thank you to Andrea Gori for insisting on coffee breaks. Thank you to Vanessa Francis, Monika Bokori-Brown, and Harriet Bare, for providing me with support at times when I have struggled, and allowing me to be an honorary ‘Squibbit’.

Thank you to my family and friends for listening to me ramble on about science, even though you had no idea what I was talking about.

Finally, my biggest thanks of all, must go to my lovely boyfriend Sam. Thank you for always believing in me and keeping me motivated. Thank you for providing me with food and shelter when I ran out of money. Thank you for supporting me in everything I do. I am forever indebted to you.

Table of Contents

List of Figures

List of Tables

Abbreviations

AMP	Adenosine monophosphate
ANOVA	Analysis of variance
ATP	Adenosine triphosphate
BLAST	Basic local alignment search tool
BMCs	Biomethane producing microbial communities
Bp	Base pairs
Bps	Base pairs
cDNA	Complementary DNA
CoA	Coenzyme A
COD	Chemical oxygen demand
CoM	Coenzyme M
Ct	Cycle threshold
DNA	Deoxyribonucleic acid
dNTPs	Deoxynucleotides
ds	Double stranded
DTT	Dithiothreitol
FLP	Flippase
FRT	Flippase recognition target
g	Gram
gDNA	Genomic DNA
GFP	Green fluorescence protein
H_4MPT	Tetrahydromethanopterin
hr/hrs	Hour/hours
HRT	Hydraulic retention time
IPTG	Isopropyl ß-D-1 thiogalactopyranoside
kDa	Kilodaltons
kV	Kilovaults
L	Litres

LB	Luria-Bertani
m	Milli or metres
M	Molar
MB	Mega base
MCR	Methyl-coenzyme M reductase
MFR	Methanofuran
mg	Milligram
min(s)	Minute(s)
mL	Millilitre
mm	Millimetres
mM	Millimolar
mRNA	Messenger RNA
MW	Molecular weight
n	Nano
NCBI	National Centre for Biotechnology Information
ng	Nanogram
NGS	Next generation sequencing
nm	Nanometre
NMR	Nuclear magnetic resonance
OD	Optical density
OD_{600nm}	Optical density (measured at 600nm)
OLR	organic loading rate
PCR	Polymerase chain reaction
pH	Potential of hydrogen-measure of hydrogen ions associated with acidity
qPCR	Qualitative real-time polymerase chain reaction
QS	Quorum sensing
RNA	Ribonucleic acid
ROS	Reactive oxygen species
Rpm	Revolutions per minute

rRNA	Ribosomal ribonucleic acid
RT-PCR	Reverse transcription-polymerase chain reaction
S	Subunit
SDS	Sodium dodecyl sulphate
Secs	Seconds
SEMs	Synthetically engineered microbes
SMCs	Synthetic microbial communities
SRT	Solid retention time
SS	Single substrate
TOC	Total organic carbon
UK	United Kingdom
USA	United States of America
UV	Ultraviolet
V	Volts
v	Volume
v/v	Volume per volume
w/v	Weight per volume
WGS	Whole genome sequencing
WT	Wildtype
x g	Centrifugal force
α	Alpha
∆	Delta
λ	Lambda
µ	Micro
µg	Microgram
µl	Microliter
µM	Micromolar
s	Sigma

1. Chapter one: Introduction

1.1. Introduction to anaerobic digestion technology

1.1.1. Energy crisis/global warming

Since the early industrial revolution, the utilisation of coal, oil and natural gas has shaped the world we live in. These fossil fuels have provided us with the energy to revolutionise our industries, power our electrical devices, run our vehicles and heat our homes. However, over recent years, concerns have developed over both future fuel security and global warming [1, 2]. Global carbon emissions from fossil fuels have significantly increased. Since 1970, carbon dioxide emissions have increased by approximately 90%, with emissions from fossil fuel combustion and industrial processes contributing about 78% of the total greenhouse gas emissions. Agriculture, deforestation, and other land-use changes have been the second-largest contributors [3]. This coupled with further growth of the global population, which is set to rise to 9.7 billion by the year 2050, has resulted in the demand for cleaner, renewable energy sources to be higher than ever [4].

In recent years biofuels have become a popular choice as an alternative to fossil fuels. Biofuels contain recently fixed carbon and are renewable. One group of biofuels are alcohols, such as bioethanol, which are formed from the fermentation of plant material, and are widely used in industry [5]. Despite being a popular alternative to fossil fuels, this form of fuel does carry controversy, as the space needed to grow the required amounts of plant material, reduces the land space available to grow crops for food, and there is concern that this could affect the food market [6].

1.1.2. Biogas as an alternative energy source

One promising example of a renewable and versatile energy source is biogas. Biogas is formed during the anaerobic breakdown of organic waste, through a process known as anaerobic digestion (AD), and is performed by a community of syntrophically related micro-organisms. Biogas is composed of approximately 60% methane and 40% carbon dioxide and can be used as an alternative to natural gas [7]. One of the first well-documented applications of anaerobic digestion technology was in 1859, when a digestion plant was created at a leper colony in Bombay, India [8]. However, it is also thought that biogas was used to heat thermal baths hundreds of years before this [9]. The technology continued to progress and in 1897, Exeter city's local government (Devon, UK) approved the use of methane gas generated from treatment of wastewater, to power the city's street lamps [10]. Anaerobic digestion technology is now applied on a variety of different scales, inside specially designed bioreactors, and can be used to breakdown many different forms of waste material. Some examples of different bioreactors and their applications are provided in Figure 1.1.

Despite its early discovery and development, historical interest in anaerobic digestion technology has varied. However, due to the growing energy and environmental concerns, recent years have witnessed a renewal in the interest in the technology, due to its ability to aid both the energy crisis as well as environmental issues [11]. A brief summary of the history of anaerobic digestion technology is provided in Figure 1.2 [12].

A)

B)

C)

D)

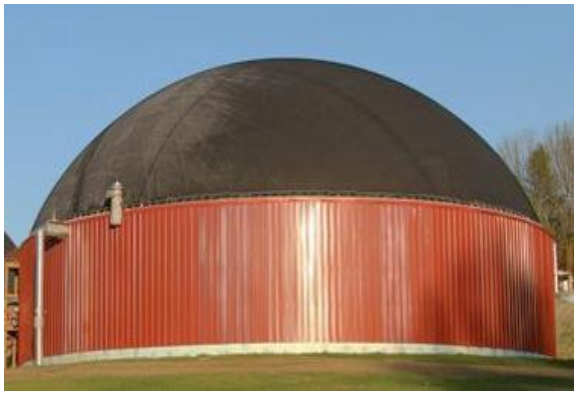

Figure 1.1: Examples of various types of anaerobic digester.

A) Homemade biogas reactor for food waste [13].

B) Sewage treatment works, Reading, UK [14].

C) Small-scale rural digester for agricultural waste [15].

D) Large-scale food waste digester [16].

Figure 1.2: History of anaerobic digestion technology.

Figure cited from the Anaerobic Digestion and Bioresources Association [12].

1.1.3. Uses and advantages of biogas

Biogas in its raw form can be burned and used for heating or to power electricity generators, or can be further purified (by removing non-combustible carbon dioxide) and fed into the gas distribution pipeline [17]. Unlike the burning of natural gas, which when burned, releases carbon fixed millions of years ago [18], the utilisation of biogas is considered a carbon-neutral process. This carbon-neutral status is achieved because the burning of biogas only releases carbon recently fixed from the atmosphere [19]. In addition to this, anaerobic digestion runs using waste material, such as manure, which is often left in the open environment to naturally decay. This waste can be a large source of methane on many agricultural sites, such as swine and dairy farms, which do not currently use anaerobic digestion technologies to handle their waste. Therefore, channelling organic wastes into anaerobic digestion achieves both the capture of methane and its utilisation as an energy source. This results in an overall reduction of methane emissions into the atmosphere. This process generates carbon dioxide and water only [20, 21]. As methane is a highly effective greenhouse gas, roughly 25 times more effective than carbon dioxide [22], any reduction in greenhouse emissions is a further advantage of this renewable fuel.

As well as generating biogas, anaerobic digestion is a very useful technology for the treatment of the organic waste itself. Anaerobic digestion can help with odour suppression, reduction in water content of waste sludge and pathogen removal [23] . The digestate produced from this process can also be a useful by-product, as the process mainly draws out carbon, hydrogen and oxygen from the feedstocks, leaving behind nitrogen, phosphorus and potassium. This nutrient-rich digestate is regularly used and sold as fertiliser. Figure 1.3

summarises the various cycles involved in the anaerobic digestion technology process, highlighting its renewability and multifaceted nature [24].

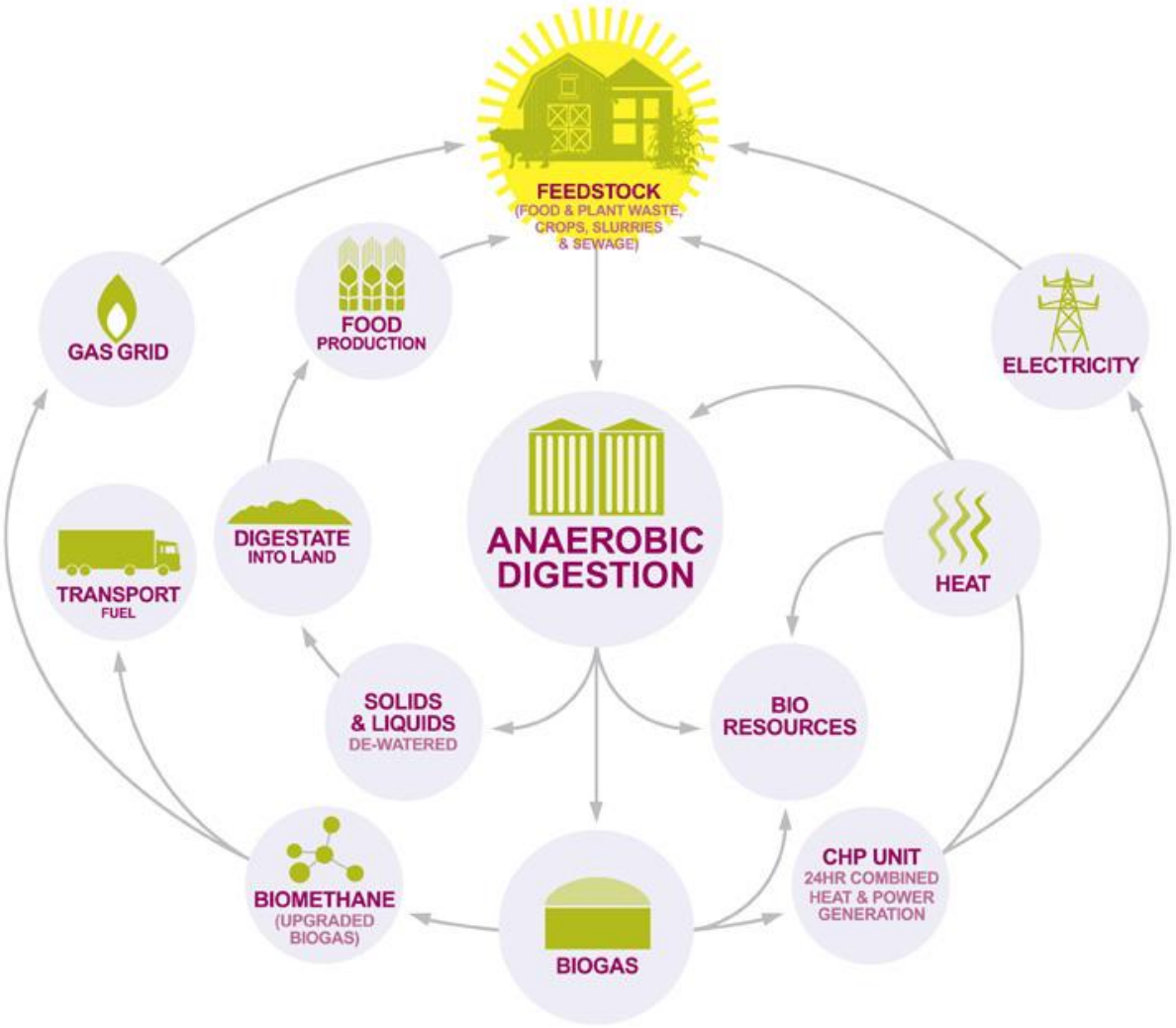

Figure 1.3: The anaerobic digestion cycle.

Figure cited from the Anaerobic Digestion and Bioresources Association [24].

1.1.4. Process of anaerobic digestion

Anaerobic digestion is a natural microbial process that takes place widely in the environment. Many different studies have identified methane-producing microbial communities inhabiting a diverse variety of both open and closed anaerobic habitats. Studies on open environments include peat bogs [25-29]; rice paddy soils [30-32], marine sediments [33-35], and freshwater sediments [36, 37]. The most common studies on closed anaerobic environments usually focus on the digestive tracts of mammals and insects [38-40]. The activity of anaerobic communities in the natural environment is a major source of global methane production and as a result, is a contributor to global warming [41] . The study of anaerobic microbial communities therefore has two very different strands, one that focuses on the contribution of these communities towards global warming, and one which focuses on their behaviour in anaerobic digesters for the improvement of biogas production.

A series of different biochemical steps are involved in anaerobic digestion. The first is a process known as hydrolysis. During hydrolysis, complex organic material containing carbohydrates, fats and proteins, is broken down into simpler units such as sugars, fatty acids and amino acids. This work is done by a group of bacteria that are able to produce the enzymes, such as cellulase, lipase and protease, required for the breakdown of the complex material [42]. This step can often be a slow, rate-limiting step, due to the complex nature of the organic material [43]. Hydrolysis is followed by acidogenesis, where simple monomers are fermented into an array of alcohols, carbonic acids and volatile fatty acids (VFAs). Following this step is acetogenesis, where previously formed compounds are converted into acetic acid. In addition to these products, hydrogen, carbon dioxide, ammonia, ammonium and hydrogen sulphide are also commonly

generated. Some of these products are also generated during the previous acidogenesis step [44]. These substrates feed the final step in the anaerobic digestion process, during which methane production occurs through a reaction known as methanogenesis. A schematic of the reactions involved in the anaerobic digestion process are detailed in Figure 1.4 [45].

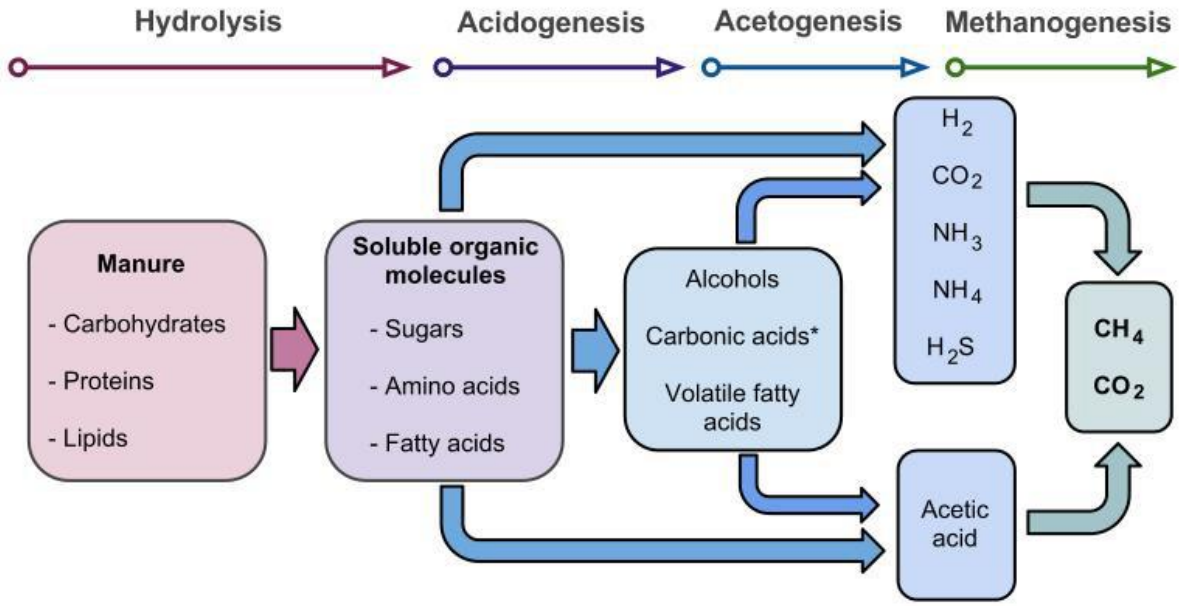

Figure 1.4: Biochemical reactions involved in anaerobic digestion.

Figure cited from Biodegradation in Animal Manure Management [45].

A variety of different microbes are involved in the different stages of anaerobic digestion and form a syntrophic microbial community. These microbial communities can vary greatly depending on reactor conditions and the type of waste being treated, and can have a significant impact of the performance of a digester, especially with regards to hydrolytic bacteria [46]. Microbes involved in the earlier stages of hydrolysis, acidogenesis and acetogenesis tend to be members of the Firmicutes phylum [47], with some bacteria able to perform

multiple steps in the process. Some examples of such bacteria include members of the *Clostridium, Acetivibrio, Selenomonas* and *Ruminococcus* species, and are often detected within the microbial communities of bioreactors [42, 48, 49]. The methane generated during methanogenesis, the final stage in anaerobic digestion, is produced by obligate anaerobic archaea known as methanogens. Due to their vital methane production, these microbes will be discussed in greater detail throughout the remainder of this chapter.

1.2. Methane generation

1.2.1. Discovery of methanogens

The foundation for the study of biologically produced methane was first laid by Alessandro Volta, an Italian physicist, who carried out experiments on combustible air collected from sediments and marshy landscapes [50]. He noted the gas formation in water-saturated decaying plant material. The years that followed witnessed adequate conformation by other researchers of Volta's findings, and almost a century later, sufficient evidence was obtained to confirm that methane production was a microbial process. By 1865, the term "methan" (methane) was proposed, and in 1892 an International Congress on Chemical Nomenclature confirmed this [51].

It was first thought that generated methane was produced from the bacteria that broke down cellulose, however this was proven incorrect, as fermenting cellulose cultures were found not to produce methane. This led to the idea that there were other associated organisms, existing as a microbial community, which used the products (hydrogen, acetate, carbon dioxide) created by the cellulose fermentation bacteria to produce methane. By 1940, a standard

aseptic technique had been developed for growing colonies of methanogens in the lab and different independent scientists continued to research methanogens [52].

1.2.2. Modern study of methanogens

Due to the limitations of traditional culturing techniques, methanogenic microbial communities have often been understudied, frequently because only a small fraction of microbes within a community can be successfully cultured and identified. These problems are intensified when dealing with fastidious anaerobes such as methanogens. Their low growth rate and obligate anaerobiosis has made them among some of the most difficult microorganisms to study by culture-based techniques [53].

Recent years have seen culturing problems overcome by the introduction of culture-free next generation sequencing techniques. The most common methods used for microbial identification are forms of comparative ribosomal RNA (rRNA) sequencing. Comparative rRNA sequencing works on the basis that rRNA molecules are extremely conserved in overall structure across all living organisms [54]. This conserved structure makes them an ideal target site for sequencing technologies. In particular the 16S rRNA sequence is generally used as a molecular marker, due to its ubiquitous nature and highly constrained sequence [55]. The sub-unit contains nine hypervariable regions (V1-V9) ranging from about 30-100 bases long [56]. The level of conservation can vary widely between hypervariable regions, with more conserved regions correlating to higher-level taxonomy and less conserved regions to lower levels, such as genus and species [57]. The use of 16S rRNA techniques allows for the identification or

at least phylogenetic assignment of the organism from which it originated, without the risk of bias, as no cultivation techniques are involved [58]. Oligonucleotide hybridisation probes and PCR primers can be designed to identify individual species or members of phylogenetically coherent groups with either variable or conserved tracts of the rRNA as hybridisation targets [53]. Many 16S rRNA PCR primers now exist for the characterisation of bacterial and archaeal species and claim to be universal. However, the specificity of these primers is disputed, due to the discovery of new taxa, which are not always complimentary to existing primers. Baker *et al* evaluated a series of 'universal' primer pairs and their recommendations are still widely used [59-62]. Despite the dispute, the use of 16S rRNA PCR primers and hydridisation probes is common practise when assessing the diversity of methanogenic microbial communities and all studies discussed in this chapter have used forms of 16S rRNA identification to aid their investigations.

Accompanying the use of 16S rRNA sequencing, are also methods of directly targeting methanogen DNA. These methods arose from the discovery of the methanogen-specific *mcrA* gene, which will be discussed in further detail below. Research has already identified the specificity of this gene to the methanogen, which has a highly conserved homologous nature amongst different strains of methanogen species [63]. The nature of this gene has made it a good target site for methanogen detection using specially designed PCR primers and DNA hybridisation probes. Knowledge of this gene also allows for the presence of methanogens to be detected in environmental samples without the need to recover methanogen isolates in culture [64].

Using modern molecular techniques in combination with culturing, methanogens have been isolated from many environments and characterised. These environmentally diverse organisms cover at least seven taxonomic orders: the Methanobacteriales, Methanococcales, Methanomicrobiales, Methanosarcinales, Methanopyrales, Methanocellales and Methanomassiliicoccales [65]. Basic information on each of these orders in supplied in Table 1.1.

Order	Families	Methane produced by:	Environment
Methanobacteriales	Methanobacteriaceae and Methanothermaceae	Reduction of CO_2 with H_2. Formate, CO, or secondary alcohols are used as alternative electron donors in some species.	*Methanobacteriaceae*: thermophilic or mesophilic *Methanothermaceae*: hyperthermophilic. [66]
Methanococcales	Methanocaldococcaceae and Methanococcaceae	Reduction of CO_2 with H_2. Many species can use formate as an alternative electron donor. Most species can grow autotrophically.	Methanocaldococcaceae: hyperthermophilic *Methanococcaceae*: thermophilic or mesophilic. [66]
Methanomicrobiales	Methanomicrobiaceae, Methanocorpusculaceae, and Methanospirillaceae	Reduction of CO_2 with H_2. Formate and secondary alcohols are used as alternative electron donors in many species.	Widespread [66]
Methanosarcinales	Methanosarcinaceae, Methanosaetaceae and Methermicoccaceae	Methanosarcinaceae : can produce methane from a methyl group and some can use acetate or H_2/CO_2. Methanosaetaceae: Can only split acetate. Methermicoccaceae: methanol and methylated aimines.	Widespread [66]
Methanopyrales	Methanopyraceae	Reduction of CO_2 with H_2.	Hyperthermophilic. [66]
Methanocellales	Methanocellaceae	H_2/CO_2 and formate.	Mesophilic. [67]
Methanomassiliicoccales	Methanomassiliicoccaceae	H_2-dependent methylotrophic methanogen.	Various environments. [68]

Table 1.1: Table to highlight some basic information on the seven orders of methanogens.

1.2.3. Biochemistry of the methanogens

1.2.3.1. Routes of methane production

Methanogens are only capable of producing methane from a limited number of simple substrates, mostly C1- and C2-compounds (e.g. carbon dioxide, carbon monoxide, methanol, methylamines, methyl sulfides, and acetate), which are converted to methane by the reduction of carbon [69]. Substrates are provided by syntrophically associated microorganisms that can break down complex substrates and take part in the earlier stages of anaerobic digestion (hydrolysis, acidogenesis and acetogenesis) [70, 71]. Methane generation occurs as a by-product of the methanogenesis pathway, which is the only metabolic pathway from which methanogens can generate energy for growth. The placement of methanogens within a microbial community is vital for them to obtain the sub-units to perform methanogenesis and generate energy [70]. There are three distinct metabolic pathways in which methanogens can generate methane. Some methanogens, can utilise all three pathways (such as members of the Methanosarcinales), whereas others can only use one distinct pathway and tend to have a more limited substrate range.

The first in the three distinct pathways, is the hydrogenotrophic methanogenesis pathway. Most methanogens can perform this pathway and are known as are hydrogenotrophic methanogens. This pathway involves the reduction of carbon dioxide to generate methane. The primary electron donor for this reduction is hydrogen. The reaction is detailed in equation 1.

Equation 1: $CO_2 + 4H_2 \rightarrow CH_4 + 2H_2O$

In addition to molecular hydrogen, many methanogens are also capable of using other substrates as the reducing agent. An example of this is the use of formate

[72]. During methane generation from this substrate, formate is first oxidised to generate carbon dioxide and hydrogen (equation 2A). Carbon dioxide is then reduced with hydrogen to form methane (equation 2B).

Equation 2A: $4HCOOH \rightarrow 4CO_2 + 4H_2$

Equation 2B: $4CO_2 + 4H_2 \rightarrow CH_4 + 3CO_2 + 2H_2O$

Other examples of substrates utilised for methane production by the hydrogenotrophic pathway are secondary alcohols, such as isopropanol (C_4H_8O) [73]. These secondary alcohols are first oxidised to a ketone, in this case acetone (C_3H_6O), detailed in equation 3A. The released hydrogen is used then used to reduce carbon dioxide into methane, equation 3B.

Equation 3A: $4C_3H_8O + CO_2 \rightarrow 4C_3H_6O + 4H_2 + CO_2$

Equation 3B: $4C_3H_6O + 4H_2 + CO_2 \rightarrow 4C_3H_6O + CH_4 + 2H_2O$

There are also species of methanogens that are capable of using carbon monoxide (CO) as a reductant of methanogenesis; however, this knowledge is limited to *Methanothermobacter thermautotrophicus* [74] and *Methanosarcina barkeri* [75] and is detailed in equation 4.

Equation 4: $4CO + 2H_2O \rightarrow CH_4 + 3CO_2$

The second type of methanogenesis pathway is the methylotrophic pathway. Methanogens that are capable of this pathway can utilise methyl-group

containing compounds such as methanol and methylated amines (monomethylamine, dimethylamine, trimethylamine). Equation 5A details the reactions involved in the utilisation of methanol. Some methanogens are also able to utilise methylated sulphides [76], such as dimethyl sulphide, detailed in equation 5B.

Equation 5A: $4CH_3OH \rightarrow 3CH_4 + CO_2 + 2H_2O$

Equation 5B: $2(CH_3)_2\text{-}S + 2H_2O \rightarrow 3CH_4 + CO_2 + 2H_2S$

Some methylotrophic methanogens are also obligate hydrogenotrophic methanogens. These methanogens are only capable of reduction of the methyl group if hydrogen is available, as detailed in equation 5C. The newly discovered *Methanomassiliicoccus luminyensis*, is an example of an obligate hydrogenotroph and methylotroph [77].

Equation 5C: $CH_3OH + H_2 \rightarrow CH_4 + H_2O$

During the utilisation of methylated compounds, the methyl-groups within the substrates are transferred by a methyltransferase protein. The methyl group is subsequently reduced to methane by the methanogenesis pathway. Due to the specific nature of the methyltransferases, only certain types of methanogens can utilise this pathway. To date, only members of the Methanosarcinales order and some members of the *Methanosphaera* genera, which belongs to the Methanobacteriales order, have been identified as methylotrophic [66].

The third type of methanogenesis pathway is the acetoclastic pathway. This pathway utilises acetate, which is a major intermediate in the anaerobic food chain. Up to two-thirds of biologically produced methane in the natural

environment is produced in this way [78]. Despite this perceived abundance, only two genera of methanogens, the *Methanosarcina* and the *Methanosaeta* are capable of this pathway. The pathway involves the physical splitting of acetate molecules. By doing this, the carboxyl group of acetate is oxidised, and the methyl group is reduced to methane, as detailed in equation 6.

Equation 6: $CH_3COOH \rightarrow CH_4 + CO_2$

1.2.3.2. Catalysis of methanogenesis

The equations detailed in the sections above are simplified versions of the actual reactions that take place during methanogenesis. For methane generation to occur, the nickel enzyme, methyl-coenzyme M reductase (MCR), is required, along with many cofactors.

The first stage of methane generation involves the attachment of a methyl group onto a coenzyme, named coenzyme M, to generate $\mathbf{CH_3}$-S-CH_2CH_2-SO_3^-, (methyl group highlighted in bold). This structure is often shortened to Me-S-CoM. The mechanism for attaching the methyl group onto coenzyme M depends on the substrate available and the mode of methanogenesis. The MCR enzyme catalyses the reaction between Me-S-CoM with another cofactor known as thiol coenzyme B, (CoB-SH). This reaction forms the heterodisulfide, CoB-S-S-CoM, detailed in equation 7. Methane gas is released as a by-product of this reaction. Methanogens then use CoB-S-S-CoM as part of their metabolism to generate energy, and is their only mechanism to do so [79].

Equation 7: $\mathbf{CH_3}$-S-CoM + CoB-S**H** → CoB-S-S-CoM + $\mathbf{CH_4}$

-components of methane are highlighted in bold.

1.2.3.3. Discovery of coenzyme M

In 1971, McBride and Wolfe reported that ‘a heat-stable, dialyzable cofactor of methyl transfer’ had been found in extracts of methanogens, whose addition was required for the formation of methane [80]. They named this cofactor coenzyme M (CoM). McBride and Wolfe continued to examine many methanogenic organisms and found CoM to be present in all of them. Detection studies were also carried out in non-methanogenic bacteria; however, these were unsuccessful. McBride and Wolfe indicated in their conclusions that the role of CoM was to ‘accept a methyl group and to donate it for methane biosynthesis’, indicating an explanation for the detection of CoM in only methanogenic organisms. Further work on CoM continued and in 1973, Taylor and Wolfe used data from infrared, proton NMR, ultraviolet spectroscopy, chemical tests and quantitative elemental analysis to reveal that the CoM was a 2,2’-dithiodiethanesulfonic acid [80, 81]. In 1979, Balch and Wolfe carried out further experimentation that confirmed CoM to be distinct to only methanogenic bacteria [63].

1.2.3.4. Assimilation of methyl group onto coenzyme M

Understanding the different modes of methanogenesis and the coenzymes involved provides insights into the different capabilities of various lineages of methanogens. It also aids our understanding of the sensitivities of methanogens, which will be discussed later.

During the hydrogenotrophic pathway, carbon dioxide is first transferred onto the coenzyme methanofuran (MFR). This reaction uses reduced ferredoxin as the direct electron donor which forms CHO-MFR. The formyl group is then

transferred to another coenzyme, tetrahydromethanopterin (H_4MPT) which forms CHO-H_4MPT and releases MFR in the process. The formyl group then undergoes a series of dehydration and reduction steps (using reduced coenzyme F_{420}, as the electron donor) to form methyl-H_4MPT. The methyl group is then finally transferred to CoM, with the release of H_4MPT. During growth on alcohols, specific coenzyme F_{420}-dependent secondary alcohol dehydrogenases are required for the oxidation of secondary alcohols to ketones before the released carbon dioxide can be fixed [82]. For carbon monoxide utilisation, carbon monoxide dehydrogenase ($CODH_2$) is required to first oxidise CO to CO_2, before the CO_2 is reduced to methane [74].

During the methylotrophic pathway, the methyltransferases required for the transfer of the methyl group onto CoM are substrate specific, which further restricts the substrate range of some methanogens [83]. As part of the methylotrophic pathway, the electrons required for the reduction of the further methyl groups to methane are obtained from the oxidation of additional methyl groups to CO_2 which proceeds step wise as the reverse of the hydrogenotrophic pathway [66].

During the acetoclastic pathway, acetate is first assimilated by coenzyme A (CoA) to produce acetyl-CoA, before being transferred to CoM by H_4MPT. Some methanogens use the low affinity acetate kinase-phosphate acetyl transferase (ACKA-PTA) pathway to assimilate acetate, while others use the high affinity adenosine monophosphate (AMP)-forming acetyl coenzyme A synthetase (AMP-ACS) pathway to assimilate acetate into the cell [84].

1.3. Sources of instability within anaerobic digestion technology

Despite the many advantages associated with generation of fuel via anaerobic digestion technology, the complex nature of the process makes it difficult to fully optimise. Many different approaches have been taken to improve the process; however, finding a universal solution to common anaerobic digestion problems is near impossible. One major contributor towards the difficulties optimising anaerobic digestion technology, is due to the complexity of the microbial communities involved. Each group of microbes involved in the process have their own physiological requirements. Certain conditions of a bioreactor can result in one group of microbes thriving whilst another group fails [85], and this can lead to overall failure of the process [86]. Many factors which can lead to process instability within anaerobic digesters are discussed below.

1.3.1. Operating temperature

Operating temperature of an anaerobic digester can have an important effect on the physicochemical properties of the digestion substrates formed. In addition, temperature can also heavily influence the growth and metabolism rates of the microorganisms within the community. These two effects can therefore can have an influence on the population dynamics. Depending on the type of waste being treated, anaerobic digesters are run either mesophilically (30°C – 40°C) or thermophilically (50°C – 60°C). Several studies stress the overall improved activity of certain wastes at thermophilic conditions. There is evidence to support that thermophilic reactors aid pathogen deactivation, increase the destruction rates of organic solids and produce higher biogas yields [87]. However other studies document that thermophilic reactors cannot sustain higher organic

loading rates (OLRs) compared with mesophilic reactors and have a higher rate of volatile fatty acid (VFA) manifestation due to the faster rate of the earlier acid-producing stages of anaerobic digestion [88, 89].

1.3.2. Operating pH

Operating pH can have important effects on the dynamics of the microbial communities present within an anaerobic digester. Different groups of microbes have different preferences in pH. For example, the bacteria involved in the hydrolysis and acidogenesis stages usually have an optimal pH of approximately 5.5-6.5 [90, 91]. In contrast, the optimal pH for the methanogenic archaea is approximately pH 7.0 [92]. Therefore, different operating pH levels favour different stages of anaerobic digestion. When conditions favour hydrolysis, intermediate substrates, especially volatile fatty acids (VFAs) tend to build-up and inhibit the methanogens, resulting in a lower methane output [93].

1.3.3. Organic loading rate

Organic loading rate (OLR) is the rate at which an anaerobic digester is loaded with organic material and is an important parameter of anaerobic digestion technology. Due to the day to day variability of many organic wastes, OLR can change significantly. For example, anaerobic digesters breaking down food wastes are subject to seasonal changes the foods being fed into the digester [94]. Large volumes of high strength organic material can create shock loads of organic material, resulting in an influx of intermediate substrates which can distort the anaerobic digestion process [95, 96].

1.3.4. Solid and hydraulic retention times.

The solid retention time (SRT) and the hydraulic retention time (HRT), refer to the average time that solids and liquids are held inside an anaerobic digester. The anaerobic digestion process can be directly affected by these two parameters. The length of the SRT can impact on the extent of the biological reactions able to take place. The length of the HRT can impact the density of the microbial population, as microbes are lost each time sludge is withdrawn. To avoid process failure, cell growth must be able to compensate for this removal [97].

1.3.5. Oxygenated feedstock

Due to the open nature of the environment in which digesters are operated, it is quite common for oxygen to unintentionally reach the inside of an anaerobic digester system. This oxygen is often introduced via dissolved oxygen within feedstocks or from of mixing of the digester [98-100]. Oxygenation can be a problem for the strict anaerobic archaea involved in anaerobic digestion, especially the methanogens, which have been widely documented in literature as strict anaerobic archaea, who have zero tolerance to oxygen [101, 102]. Exposure of methanogens to oxygen can result in their inhibition which causes an imbalance between the active microbes within the digester system.

1.4. Outcomes of instability

1.4.1. Build-up of volatile fatty acids

All factors mentioned above have been widely documented to have the potential to shift the metabolic patterns within anaerobic microbial communities, uncoupling volatile fatty acid (VFA) production and VFA consumption [103-105]. Instability can often lead to increased production of VFA from acidogenic and acetogenic bacteria, at a rate faster than methanogens can utilise them. This imbalance creates an overflow of VFAs within the digester system [106] and their accumulation results in the lowering of digester pH, which can inhibit the capabilities of the methanogens [107].

Many studies on both environmental communities and digester communities have noted a decrease in methanogen activity when pH decreases, and pH drops are often used as markers for digester failure [108, 109]. Research efforts have been made to discover the effects of pH on the activity of the methanogens. However, a decrease in external pH alone does not always directly correlate with a drop in methanogen activity. A study by Williams and Crawford, 1984 [110], found that when small amounts of acetic acid were added to certain peat bog samples, methanogenesis was strongly inhibited. However, when an inorganic acid, such as hydrochloric acid was added, the same effect was not observed. This result indicated that the presence of acetic acid was having other effects in addition to just decreasing pH. Many methanogens have been found to thrive in acidic environments, and it is now often accepted that a reduction in pH alone is not the only contributor towards methanogen inactivity [111, 112].

It is now widely acknowledged that it is the combination of both an accumulation of VFAs and a reduction in pH which causes the inhibition of

methanogens and many other microbes [113]. At low pH levels, VFAs exist in their protonated form. In this form they become highly lipophilic compounds, that can easily pass through cell membranes [114]. The greater the pH potential over the cellular membrane, the easier VFAs can cross. After crossing the cellular membrane, the alkaline pH of the internal environment causes the acid to dissociate. This dissociation results in a build-up of protons in the intercellular space, leading to an overall decrease in internal pH and acidification of the cytoplasm. This leads to toxic effects on the cell and metabolic disturbances by the anion, and can lead to a halt in cell growth and/or death.

The failure of the methanogens further exacerbates the problem of VFA accumulation. Inhibited acetoclastic methanogens become unable to convert generated acetic acid, one of the most abundant VFA in anaerobic environments, into methane. This additional accumulation often results in complete souring of the digester, causing toxicity and inhibition to other microbes within the community [115, 116].

1.4.2. Production of reactive oxygen species

Oxygen is a common stressor to anaerobes, particularly strict anaerobic methanogens, which are unable to form resting stages or spores [117]. It has been previously discussed how oxygen exposure to methanogens can result in severe inhibition or death. For example, *Methanococcus vannielii* and *Methanococcus voltae* have been found to lose their viability after a brief exposure to oxygen [101], and similar losses in viability have also been noted in other methanogens [102]. This loss of viability can cause substrate build-up

during anaerobic digestion and can cause major problems inside anaerobic digesters [99, 100].

The sensitivity of methanogens to oxygen is widely attributed to their evolution dating back to before oxygen was present in the Earth's atmosphere [118]. However, it has been unclear whether this sensitivity is due to the oxygen itself or an increase in redox potential [119]. Many studies now support that the presence of oxygen and not the reduction in redox potential cause damage to the methanogens. The process of methanogenesis requires many specific enzymes and coenzymes that usually contain metal cofactors [120], several of which were mentioned in section 1.2.3.4. The exposure of methanogens to oxygen can result in autoxidation of these flavoenzymes and metalloenzymes and produce reactive oxygen species (ROS). Generally, when anaerobic microorganisms meet oxygen, hydrogen peroxide (H_2O_2), superoxide radicals ($O_2^{\bullet -}$) and hydroxyl radicals (•OH) are formed [121, 122]. The production of reactive oxygen species is more prevalent in methanogens, due to the high number of cofactors that readily react with oxygen [123]. This reactivity causes oxidative damage to enzymes, coenzymes, cofactors and other macromolecules, potentially leading to cell death [124].

The presence of oxygen has been shown to lead to the rapid degradation of methyl coenzyme M reductase [125], which results in the permanent inactivation of the reduced nickel (Ni (I))-tetrapyrrole activation centre [126]. This inactivation prevents methanogens from performing methanogenesis and generating energy. In addition to the damage to MCR, it has been discovered that coenzyme F_{420} undergoes inactivation when exposed to oxygen [127, 128]. H_4MPT and $CODH_2$

have also been detected as being oxygen-labile compounds, causing them to lose their functionality in the presence of oxygen [129] [74].

1.5. Mitigating imbalances within anaerobic digesters

To date, many different techniques have been employed to optimise the operation of anaerobic digesters, especially those used on an industrial scale. These techniques range from monitoring the stability of digesters to a change in reactor design and are briefly detailed below.

1.5.1. Markers for process stability/instability

To aid the prediction of process instability, many different parameters can be monitored. Various sensory devices are often utilised to take measurements from both the liquid and gas phases. Obtaining such readings from sensing devices can be difficult as the devices often become blocked and obscured. However, the benefits of measuring such parameters often outweighs the downsides of the logistics involved.

Chemical oxygen demand and total organic carbon are regularly used in combination with each other to characterise the organic matter content (i.e. all substrates and intermediates). These parameters help infer the organic loading rate into a digester, measuring of the biological conversion capacity of the AD system. Feeding a digester above its OLR is unsustainable due to the accumulation of intermediates, therefore it is important to measure these parameters [130].

VFA concentration is a regularly used process indicator employed by many anaerobic digester operators and, as mentioned previously, is often a cause of instability within a digester [131]. Increase in VFA concentration gives an indication of either unsustainable organic load rate or an inhibition of the methanogens. Early warning of accumulation of VFA allows operators to intervene and potentially reduce the effects before the digester becomes sour [132].

pH measurements are also a very good indicator of process stability. Decreases in pH are often viewed as the most detrimental to the AD process and are researched heavily due to the inhibition of methanogens at pH levels below 6.6 [133]. However increases in pH above neutral can also be very detrimental to the process and can lead to the break-up of microbial granules leading to the failure of the digester [134].

In addition many other parameters can also be used to monitor process stability of an anaerobic digester, these include temperature [135], methane concentration [136] and ammonia levels [137, 138]. Pre-empting instabilities within anaerobic bioreactors by measuring various parameters, allows for intervention before digester failure. Treatments for failing digesters are now widely known to the anaerobic digestion community, for example, low digester pH can be fixed with the addition of lime [139] or sodium carbonate [140]. Often, chemical solutions to aid the re-stabilisation of a digester are available in the form of a commercial product such as those available from Aquafix [141].

1.5.2. Alteration of reactor conditions

Most anaerobic digester systems have a mixing element, which allows for efficient transfer of organic material between the microbial biomass, whilst also allowing the release of gas bubbles. Mixing is often not a continuous process and tends to take place intermittently and depends entirely on the design of the bioreactor and the type of waste being treated [142]. An increase in mixing can be used to relieve digester instability, however over mixing can result in further instability due to the breakdown of sludge microbial granules [143].

The rate of organic loading into a digester can be varied to suit reactor conditions and prevent instability. If concentrations of VFA and other toxic compounds become too high, organic loading may be reduced to allow for recovery and stabilisation of the microbial community before further feeding. There are also occasions where organic loading rate may need to be increased such as when there is a drop in trace element and/or nutrient concentrations [144].

The HRT can vary greatly depending on the type of waste being treated, for example lignocellulose-containing wastes need a longer HRT than less complex material. Studies have shown that increasing the HRT can increase the stability of an anaerobic digester [145, 146] . However this method is not always favourable due to the higher costs associated with this method [147].

Temperature of a bioreactor is also an easily changed variable to suit the requirements of the digester. Higher temperatures (thermophilic reactors 50-60 °C) tend to promote faster reactions and higher gas production, but also destabilise much more rapidly than digesters operating at mesophilic

temperatures (30-40 °C). Digester temperature may be reduced because of substrate build-up or may be increased due to low digester performance [148].

1.5.3. Pre-treating organic material

Many various pre-treatments can be used to help aid the initial stages of anaerobic digester and reduce the HRT required. Mechanical pre-treatment of organic waste involves the disintegration or grinding of solid particles to increase the surface area of the feed, allowing for better contact with the anaerobic microbes [149]. Thermal pre-treatment is another widely used pre-treatment applied to industrial scale waste management. Organic feed is subject to thermophilic temperatures (50-250 °C) prior to the AD process. This treatment enhances the breakdown of pathogen cell membranes and allows for the solubilisation of organic compounds [150]. Chemical pre-treatments are also used to destruct the organic compounds by using either strong acids or alkali. Acidic pre-treatments are often used to enhance the biogas production by improving the hydrolysis stages of AD [151], whereas alkali pre-treatments are generally preferred as a mechanism to aid foreseen souring of the AD digester [152]. In addition, biological pre-treatments may be used to aid the initial breakdown of organic feed material, this usually involves the addition of various enzymes such as peptidase, carbohydrase and lipase [153]. Often combinations of different forms of pre-treatments are used to aid the process of anaerobic digestion [154].

1.5.4. Two and three-stage digesters

The majority of full scale anaerobic digester plants used in Europe rely on continuous one-stage processes [155]. However, there is growing interest in the application of two-phase anaerobic digestion and several research studies have focused their interests on this area [156-158]. This reactor design keeps the acid producing stages physically separate from the methanogenic stages. This allows more control over the process parameters of each of the individual steps such as pH, temperature and aeration. However, this set up requires the optimisation of both the hydrolytic-acidification step as well as the methanogenesis step [159]. Recently, research has also focused on the application of three-stage digesters, which have separate chambers for hydrolysis, acidogenesis and methanogenesis and studies have found that this is one of the most productive reactor set ups [160]. However, the processes require very careful optimisation.

1.5.5. Co-digestion

Another approach for anaerobic digestion technology, is a process known as co-digestion. This approach has experienced increasing interest in recent years and involves the simultaneous digestion of two or more substrates. It was developed to plug some of the shortcomings of using single substrate (SS) wastes. SS wastes are often characterised by low organic loads and very variable nitrogen content, which can be inhibitory to the methanogens. Heavy metal content of some SS wastes can also bring additional complexity. Co-digestion has been found to mitigate some of the drawbacks of SS digestion, increase methane output and improve the economic viability of AD plants [161]. Two main models have been implemented for the co-digestion of agriculture-based AD plants, i)

co-digestion of manures from several different farms together with other organic wastes from industry and residential areas [162, 163], ii) on-farm plants, co-digesting manure with other farm waste such as energy crops [164, 165].

1.6. Synthetic microbial communities (SMCs)

Thanks to the development of next-generation sequencing technologies, recent years have seen a surge in the analysis of microbial communities [166]. These advances have revealed just how complex these natural systems are and the vast potential of microbial ecological power yet to be uncovered. The 'Unified Microbiome Project Initiative' (UMI) prosed by Alivisatos, aims to 'discover and advance tools to understand and harness the capabilities of Earth's microbial ecosystems', by using interdisciplinary approaches to tap into this ecological power [167]. To further enhance these interactions, research is beginning to focus on synthetically engineered microbial community.

1.6.1. What are SMCs?

Synthetic microbial communities can be generally defined as microbial communities that have been created from defined constituents [168]. These defined constituents can either be naturally occurring microbes isolated from the environment, synthetically engineered, or a combination of the two. Synthetic communities have the features of natural communities but with reduced complexity, as only the organisms that are required for a specific function, are incorporated. Two main approaches can be taken when designing a SMC; function first (top-down) or interaction first (bottom-up) [169]. Function first approaches determine the desired function of the selected microbial community,

and then use this definition to characterise its capabilities. Interaction first approaches focus on identifying common interactions between bacterial species, with the expectation that these could be key determinants of the overall community structure and dynamics and function.

Synthetically engineered microbes (SEMs) can be included alongside natural microbes within SMCs. SEMs have gained wide attention due to the developments within synthetic biology, which involves the design and construction of novel artificial biological pathways, organisms or devices. This field of science has grown significantly over recent years, and SEMs now have a wide range of applications in biotechnology, bioenergy and bioremediation [170].

Although still relatively early in their development, SMCs are gaining growing interest due to their potential to capitalise on natural microbial interactions and processes. SMCs have the potential to be controllable, simple and stable, with higher functionality than their natural counterparts [171] and are therefore very attractive to various industries [172].

1.6.2. SMCs and anaerobic digestion

Anaerobic digestion technology is a key process that could benefit from a synthetic engineering approach. The complex nature of the microbial processes involved, along with its instability, makes it an ideal candidate for simplification and engineering. As detailed in the sections above, there have been many approaches towards the optimisation of anaerobic digestion technology; however, to our knowledge, no such work has focused specifically on the microbial communities themselves. The work described in this thesis details work towards a broader interdisciplinary project titled ‘Engineering synthetic

communities for biomethane production', funded by the BBSRC on a strategic longer and larger research grant (sLola) [173]. This project brings together many experts from different universities across the United Kingdom, to engineer the microbial communities involved in anaerobic digestion technology. The main approaches taken for this project are detailed in Figure 1.5.

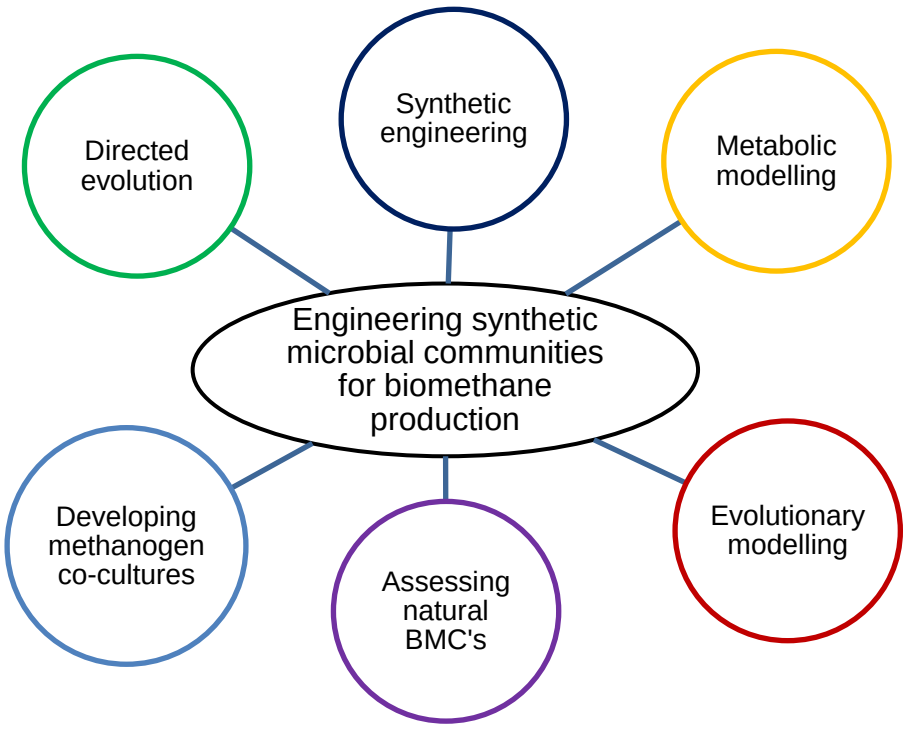

Figure 1.5: Engineering synthetic microbial communities for biomethane production.

Diagram details different focus areas of the BBRSC sLola project funded to Engineer synthetic biomethane producing microbial communities (BMCs).

1.7. Thesis Aims

The work undertaken for this thesis aimed to contribute to the wider goals of the outlined sLola project, whilst also incorporating novel research approaches. Two focus areas were addressed 1) the problem of oxygen intolerance of

methanogens inside anaerobic digesters and 2) the fluctuations in pH caused by variations VFA concentration.

For focus area 1, attention was turned to the natural environment to investigate whether methanogens, with increased tolerance to oxygen, could be identified. Specifically, the tidal mudflats of the River Exe Estuary, by Exmouth, Devon, UK were chosen as the sample site, due to their exposure to oxygen during low tide. Initially, characterisation of the methanogen community was performed using 16S rRNA analyses. This was then followed by enrichment of mudflat samples to assess the activity of methanogens in the surface layers of the sediment, followed by attempted isolation of methanogens.

For focus area 2, the Gram-negative bacterium, *Escherichia coli* was used as a model organism to develop a negative feedback loop against production of the VFA, acetic acid. This first involved the characterisation of a genetic promoter found to be sensitive to both pH and acetate concentration. Once characterised the promoter was used to control an antisense RNA message targeting acetate-producing metabolic pathway.

The aims of this thesis were as follows:

- Investigate the methanogenic depth profiles of estuarine mudflat.
- Identify and isolate methanogens from the natural environment with increased oxygen tolerance.
- Synthetically engineer *E. coli* to regulate its own production of acetate.

2. Chapter two: Materials and Methods

2.1. Sterile conditions

Autoclaving of liquids was performed at 121 °C for 30 minutes using a bench top autoclave (Dixons, Essex, UK). All liquids not appropriate for autoclaving were filter-sterilised through 0.2 µm filters. For large volumes Nalgene Rapid-Flow filters were used (Thermo Fisher Scientific, Massachusetts, USA). When sterile working conditions were necessary, work areas were first cleaned with 70 % ethanol and work was carried out either next to a Bunsen flame or in a biosafety cabinet.

2.2. Strains, vectors and media

All *E. coli* strains, listed in table 2.1, were routinely grown at either 30 °C or 37 °C in a shaking or static incubator in autoclaved Luria-Bertani (LB) broth, M9 minimal medium or on LB agar plates. Where vector selection was necessary, antibiotics, purchased from Sigma-Aldrich (Missouri, USA) were filter-sterilised through a 0.2 µm filter and added to the media in the following concentrations: ampicillin 100 µg/ml, gentamicin 50 µg/ml, chloramphenicol 35 µg/ml. All antibiotics were prepared as 1000 X stock solutions in double distilled water, apart from chloramphenicol, which was prepared in 100 % ethanol.

2.3. Bacterial storage

2.3.1. Short term storage

E. coli strains were stored on LB agar plates or LB broth at 4 °C for periods of weeks.

2.3.2. Long term storage

The Microbank™ Bacterial and Fungal Preservation System (Pro-Lab Diagnostics, Wirral, UK) was used to preserve freezer stocks of all *E. coli* strains. Manufacturer's instructions were followed, and vials were stored at – 80 °C. To revive the cells, a single bead was removed from the vial using a sterile pipette tip and either immersed in LB broth or spread onto an LB agar plate. All *E. coli* strains and vectors used in this study are listed in Table 2.1.

Table 2.1: List of all *E. coli* strains and vectors used in this study.

Bacterial strain/vector	Genotype/comment	Source/Reference
E. coli DH5-α	Cloning host	Lab stock
E. coli YMC10 2841/3236	*thi-1; endA1; hsdR17;*Δ*lacU169; hutC$_k$*	John Innes Centre, Norwich, UK/ [174]
E. coli RB9132	*thi-1; endA1; hsdR17;*Δ*lacU169; hutC$_k$;* Δ*glnL2001*	John Innes Centre, Norwich, UK/ [175]
E. coli RB9132.Δ*pta*	*thi-1; endA1; hsdR17;* Δ*lacU169; hutC$_k$;* Δ*glnL2001;* Δ*pta*	This work
pKD46	Recombineering vector for chromosomal deletions of genes using FRT sites	Lab stock/ [176]
pKD3	Template vectors for FRT-flanked cat cassette	Lab stock/ [176]
pRU1097	GFP reporter vector	Addgene, Cambridge, UK/ [177]
pRU1097.*glnAp2*	GFP reporter vector under the control of *glnAp2* promoter	This work
pRU1097.*t-glnAp2*.as*pta*.*pta*_term	Antisense construct engineered into pRU1097 to inhibit translation of *pta*	This work

2.4. Seed cultures

The term 'seed culture' denotes an LB broth culture or an M9 minimal liquid media culture started by either immersing a microbank bead from a freezer stock or re-suspending a loop-full of cells scrapped from an agar plate into liquid media.

Liquid media was supplemented with an appropriate antibiotic whenever necessary. Seed cultures were typically incubated for 16 hours at 37 °C with shaking.

2.5. Growth curves

To monitor the growth of a bacterial strain, seed cultures were diluted 1/25 into fresh liquid media. Optical density measurements at wavelength 600 nm (OD_{600nm}) were taken every 2-3 hours for a designated length of time (usually 12-16 hrs). The collected optical density values were then plotted against time.

2.6. Molecular biology

2.6.1. Chromosomal DNA extraction

Isolation of chromosomal DNA from pure cultures of bacteria was performed using the Wizard DNA extraction kit (Promega, Wisconsin, USA). Manufacturer's instructions were followed.

2.6.2. Vector DNA extraction

E. coli cells harbouring a desired vector were cultured at 37 °C for roughly 16 hours. Vector DNA was extracted from cultured bacteria using the GeneJET Vector Miniprep Kit (Thermo Fisher Scientific). Manufacturer's instructions were followed. Briefly, cells were lysed, protein and chromosomal DNA precipitate were removed, followed by the purification of the vector DNA using a spin filter.

2.6.3. Extraction of crude DNA for colony PCR

Crude DNA samples were often prepared to screen cells for the presence/absence of certain genes, when total DNA extracts were not required. Generally, a sterile 1 µl loop was used to touch the microbial growth to be screened and immediately submerged in 10 µl of nuclease-free water, contained within a 1.5 ml Eppendorf tube. Water suspensions of cells were then boiled for 5 minutes using a heat block set to 100 °C. This was done to cause the cells to burst and release their DNA. Eppendorf tubes were then centrifuged at full speed for 5 minutes. 1-5 µl of the resulting supernatant was then used as template DNA in the desired PCR reaction.

2.6.4. Extraction of total RNA

Total RNA was extracted from cultured cells using the RiboPure Bacteria kit (Thermo Fischer Scientific). The manufacturer's protocol was followed, this involved disruption of the bacterial cell walls with zirconia beads; phenol extraction of the resulting lysate; followed by a glass-fibre filter purification of the RNA. Resulting RNA underwent DNase treatment to remove any contaminating genomic DNA (gDNA). This treatment involved incubating the RNA sample with DNase 1 and DNase Buffer for 30 minutes at 37 °C. After this time, DNase Inactivation Reagent was added to the mixture, vortexed vigorously and incubated at room temperature for 2 minutes. The mixture was then centrifuged at maximum speed to pellet the inactivation reagent and the RNA transferred to a fresh RNase free 1.5 ml microcentrifuge tube (Thermo Fisher Scientific). Integrity of extracted RNA was analysed via gel electrophoresis (section 2.6.7).

Concentration of RNA was measured using the Thermo Fischer Scientific NanoDrop machine (see section 2.6.9).

Isolated RNA was screened for contamination via PCR with an appropriate primer pair, against a positive control (+ve). Any RNA samples that produced DNA bands at this stage were subject to further rounds of DNase treatment.

2.6.5. Formation of complementary DNA (cDNA) from RNA

Total RNA was converted into cDNA using the reverse transcriptase enzyme SuperScript® III First-Strand Synthesis System (Thermo Fischer Scientific) and random hexamer primers (Thermo Fischer Scientific). The protocol provided with the superscript enzyme was followed. This briefly involved the addition of random primers, total RNA, dNTP mix and sterile distilled water to a volume of 13 µl into a nuclease-free microcentrifuge tube. The mixture was heated at 65 °C for 5 minutes and then incubated on ice for 1 minute. This was then followed by the addition of first-strand buffer, DTT (dithiothreitol) and reverse transcriptase. The mixture was heated at 25 °C for 5 minutes. This was followed by an incubation at 50 °C for 60 minutes and then at 70 °C for 15 minutes to inactivate the reaction. The resulting cDNA was ready for downstream processing.

2.6.6. Polymerase chain reaction (PCR)

PCR cocktail mixes were set up according to guidelines provided on the New England Biolabs, Massachusetts, USA (NEB) website for optimal PCR amplification with Q5 high fidelity DNA polymerase (NEB) [178]. Reactions had a total volume of 50 µl and were carried out in 0.5 ml PCR tubes (Thermo Fisher

Scientific), each containing 10 µl 5X Q5 reaction buffer (NEB), 10 µl 5X High GC enhancer (NEB), 1 µl 10 mM dNTPs (Promega), 2.5 µl 10 µM forward primer (Eurofins, Luxembourg), 2.5 µl 10 µM reverse primer (Eurofins), 0.5 µl Q5 high fidelity DNA polymerase (NEB), 1-5 µl of template DNA and nuclease-free water to make up to total volume. Negative controls (-ve) contained nuclease-free water in place of the template DNA. PCR reactions were performed on a Bio-Rad thermocycler (Bio-Rad Laboratories, California, USA) as follows:

Step 1 – 98 ˚C for 30 seconds

Step 2 – 98 ˚C for 10 seconds
Step 3 – 50-72 ˚C for 30 seconds
Step 4 – 72 ˚C for 30 seconds
} X 35

Step 5 – 72 ˚C for 2 minutes

Final hold 4 ˚C – 10 ˚C

2.6.7. Gel electrophoresis

DNA/RNA separation by gel electrophoresis was used for either:

Size determination of fragments generated by:

1. gDNA extraction
2. RNA extraction
3. Vector DNA extraction
4. PCR

OR the separation of fragments required for cloning purposes.

Gels were formed by dissolving 1% (w/v) agarose in 1X Tris-acetate-EDTA (TAE) buffer and adding a Midori Green (Nippon Genetics Europe, Dueren, Germany) stain to the cooled gel solution, before pouring into a cast and allowing to set. DNA samples were mixed with a 6X gel loading dye (Thermo Fisher Scientific) and pipetted into the gel alongside either a 100 bp plus, 1 Kb or a 1 Kb plus DNA ladder (Thermo Fisher Scientific). Gel electrophoresis was carried out at 100 volts for 30 minutes. If a higher resolution of band separation was required, gels were run at 90 volts for 40 minutes. Band separation was then observed under U.V light using the Gel Doc XR System (Bio-rad, Hercules, California, USA).

2.6.8. DNA purification using gel extraction

Gel purification techniques were often used to carry out DNA purifications in this study. DNA products for purification were electrophoresed on an agarose gel as described above. Following electrophoresis, bands were cut from the gel using a razor blade, under U.V light. Appropriate protective clothing and eyewear was worn always. Excised gel bands were added to 1.5 ml Eppendorf tubes or 15 ml Falcon tubes depending on size of the gel pieces. The gel bands were processed using the GeneJET Gel Extraction kit (Thermo Fisher Scientific) according to the manufacturer's instructions.

2.6.9. Determination of DNA and RNA concentration using Nanodrop

DNA and RNA concentrations were determined using a Nanodrop machine manufactured by Thermo Fisher Scientific. The machine was initialised with

nuclease-free water and blanked with the appropriate solution. 2 µl of DNA or RNA was then loaded onto the machine for quantification.

2.6.10. Determination of DNA concentration using Qubit.

A Qubit Fluorometric Quantitation machine (Thermo Fisher Scientific) was often used for the quantification of DNA intended for next-generation sequencing. Manufacturer's instructions were followed always.

2.6.11. Digest of DNA using restriction enzymes

Enzymes provide by NEB were used to carry out all restriction digest reactions in this study. 1 µg of vector or linear DNA was digested in a total reaction volume of 50 µl. This volume contained 1 µl of each restriction enzyme, appropriate buffer and nuclease-free water to make up to the final reaction volume. The NEBcloner tool, provided on the NEB website, was used to determine the correct buffer, incubation temperatures and incubation times [179]. Immediately after the appropriate incubation steps, the entire sample was mixed with 6X gel loading dye and electrophoresed on an agarose gel. Digested DNA fragments were then purified using agarose gel extraction, as described in section 2.6.8.

2.6.12. Ligation between vector and insert DNA

Ligation reactions were set up in 20 µl volumes using T4 DNA ligase (NEB) according to the protocol supplied with the enzyme. Reaction buffer was added at a 1:10 dilution. Amount of insert added to the reaction was determined by the following formula:

Amount of vector (ng) x [size of insert (Kb)/size of vector (Kb)] x 3

Remaining reaction volume was brought up to 20 µl using nuclease-free water. Reactions were incubated on a thermocycler overnight at 16 °C or at room temperature for 10 minutes.

2.6.13. Gateway vector cloning

The pGEM-T Easy Vector System I (Promega), was used for all Gateway vector cloning described in this report. Cloning was carried out according to manufacturer's instructions. In brief, this involved incubating the desired PCR product (previously A-tailed, described in section 2.6.14) with the vector and DNA ligase. Incubations were performed for 1 hour at room temperature or at 4 °C overnight. Calcium competent *E. coli* DH5-alpha cells were then transformed with the recombinant vector using heat-shock transformation, see section 2.9 for more detail. Cells were plated out onto selective LB agar plates containing X-gal (50 µg/ml), ampicillin (100 µg/ml) and IPTG (0.5 mM). Positive colonies detected by blue/white screening. White colonies were selected and patched onto fresh LB agar/ampicillin plates. Patches were screened for the DNA insert using colony PCR (see sections 2.6.3 and 2.6.6).

2.6.14. A-tailing of insert DNA

The Q5 DNA polymerase enzyme (NEB) used in this study produces blunt-ended PCR products which must undergo A-tailing before being cloned into the pGEM-

T vector. A-tailing is a process of adding 3'A tails to the purified PCR product and was performed according to the following protocol:

The A-tailing reaction contained 5 µl of 10X Taq reaction buffer (NEB), 1 µl of 10 mM dATP (Promega), 0.2 µl of Taq DNA polymerase (5U/µl, NEB), 10-100 ng PCR product for every 100bp of DNA and nuclease-free water up to a total volume of 50 µl. Components were added into a 1.5 ml Eppendorf tube. The reaction was incubated at 72 °C for 20 minutes. After 20 minutes incubation, cloning was proceeded with immediately, as the A-tails generated are gradually lost over time.

2.6.15. Sequencing of PCR products and vector DNA

The value-read Sanger sequencing service provided by Eurofins MWG Operon was used for sequencing of all vectors isolated from *E. coli*. Cells harbouring the desired vector were cultured in LB broth containing the appropriate antibiotic at 37 °C for roughly 16 hours, 200 rpm. Vector DNA was isolated by miniprep and its concentration determined. 50-100 ng/µl of vector DNA in a total volume of 15 µl was sent for sequencing. Sequencing primers (2 µl, 10 µM) were often provided pre-mixed with the sample (total volume 17 µl), alternatively MWG stock primers were used. DNA sequences were sent via email, sequences were downloaded and aligned with a consensus sequence using Clustal X software, downloaded from the Clustal web page [180].

2.7. Competent *E. coli* cells

2.7.1. Electrocompetent *E. coli* cells

Overnight cultures of *E. coli* DH5-alpha cells were diluted 1:100 into 40 ml of fresh LB broth in 200 ml conical flasks. Diluted cultures were incubated at 37 °C at 200 rpm until the OD_{600nm} reached 0.5-0.8. Cells were incubated on ice for 10 minutes before centrifugation at 3,200 *x g* at 4 °C for 10 minutes. Supernatant was discarded, and cells washed in 40 ml ice cold sterile water. Cells were re-centrifuged, and supernatant discarded. Cells were washed with 25 ml of ice cold sterile water and centrifuged and supernatant discarded again. Cells were finally washed with 5 ml of ice cold sterile 10 % glycerol. Cells were centrifuged, and supernatant discarded for the final time. Lastly cells were re-suspended in 500 µl of 10 % glycerol and aliquoted into 100 µl volumes into 1.5 ml Eppendorf tubes (pre-chilled on ice). Electrocompetent cells were either used immediately for electroporation or stored at -80 °C.

2.7.2. Calcium competent *E. coli* cells

Overnight cultures of *E. coli* DH5-alpha cells were diluted 1:100 into 40 ml of fresh LB broth in 200 ml conical flasks. Diluted cultures were incubated at 37 °C at 200 rpm until the OD_{600nm} reached 0.5-0.8. Cells were incubated on ice for 10 minutes before centrifugation at 3,200 *x g* at 4 °C for 10 minutes. Supernatant was discarded, and cells washed in 40 ml ice cold 0.1 M calcium chloride and incubated on ice for 30 minutes. Cells were centrifuged, and the supernatant discarded. Cells were re-suspended in 600 µl of 0.1 M calcium chloride and 300 µl of ice cold 50% glycerol. Cells were then aliquoted into 200 µl volumes in 1.5

Eppendorf tubes (pre-chilled on ice). Cells were then immediately used for heat-shock transformation or stored at -80 °C until needed.

2.8. Electroporation

100 µl aliquots of electrocompetent *E. coli* DH5-alpha cells were thawed on ice for 10 minutes, inside 1.5 ml Eppendorf tubes. For each transformation, 50 ng of vector DNA or control component was added to each aliquot of cells and the tubes incubated on ice for 20 minutes. Each bacteria/vector mix was then added to a pre-chilled 0.2 cm electroporation cuvette (BioRad) and pulsed with 2 kV of electricity (200 Ohms, 25 microFarad). 900 µl of LB broth was added to the cuvette and the mixture transferred into a fresh 1.5 ml Eppendorf tube. The cells were incubated for 1 hour at 37 °C with shaking at 200 rpm. 100 µl of cells from each reaction were plated out neat onto selective LB agar plates. The remaining cells were centrifuged at 17,000 *x g* for 2 minutes. The supernatant was discarded, and the cell pellets were each suspended in 100 µl of LB broth and plated out onto a separate selective LB agar plate. LB agar plates were incubated overnight at 37 °C. Resulting colonies were then patched onto separate LB agar plates and screened for the insert using colony PCR.

2.9. Heat-shock transformation

50 µl aliquots of calcium competent *E. coli* DH5-alpha cells were thawed on ice for 10 minutes, inside 1.5 ml Eppendorf tubes. For each transformation reaction, 50 ng of vector DNA or control component was added to each aliquot of cells and the tubes incubated on ice for 20 minutes. Each bacteria/vector mix was then

heat-shocked at 42 °C for 45 seconds using a water bath. Tubes were immediately returned to ice for 2 minutes. 900 µl of LB broth was added to each of the tubes and the tubes incubated at 37 °C for 1 hour with shaking, 200 rpm. 100 µl of neat mixture from each transformation reaction was then spread onto separate selective LB agar plates. The remaining cells were pelleted by centrifugation at 17,000 *x g* for 2 minutes. The supernatant was discarded, and the cell pellets were each suspended in 100 µl of LB broth and spread onto separate LB agar plates. LB agar plates were incubated overnight at 37 °C. Resulting colonies were then patched onto fresh LB agar plates and screened for the insert using colony PCR.

2.10. Wanner mutagenesis for the deletion of specific *E. coli* genes

The Wanner mutagenesis method as described by Datsenko & Wanner [176] was used to delete specific loci within the *E. coli* genome. To summarise this method, a PCR product containing homology to upstream and downstream regions of the *pta* locus (45 bp either side), FRT (flippase recognition target) sites and a chloramphenicol resistance cassette was generated by using PCR. PCR primers had homology to upstream and downstream regions of the target gene as well as the FRT sites. The pKD3 vector containing the FRT-flanked chloramphenicol cassette was used as template DNA for this PCR reaction. The PCR product was electroporated into the RB9132 strain of *E. coli*, which had been previously transformed with the pKD46 vector expressing the arabinose inducible lamba-red recombinase vector, allowing for homologous recombination of the PCR product (specifically the chloramphenicol marker) with the *pta* locus. Cultures were grown at 30 °C to maintain the pKD46 vector during recombination and shifted to 37 °C

to remove the vector after successful recombination. Deletion of the *pta* locus was confirmed by PCR using *pta* specific primers. Confirmations of pKD46 removal was performed by plating out onto LB/ampicillin plates. As the pKD46 encodes ampicillin resistance, zero growth on these plates was inferred as the successful removal of the pKD46 vector. Confirmation of homologous recombination was performed by plating out on LB chloramphenicol plates.

Flippase (FLP)–FRT recombination was used to remove the central part of the FRT-flanked disruption cassette from the *pta* gene, to leave behind an 81 bp “scar” sequence. The pCP20 vector (conferring ampicillin resistance) was electroporated into cells, which were grown overnight at 30 °C on ampicillin selective plates. Selected colonies were grown overnight at 42 °C to induce recombination and select for the loss of the temperature sensitive pCP20. Colonies were then patched onto a selection of LB plus ampicillin, LB only plates which were grown up at 30 °C. Cells were also patched onto LB plus chloramphenicol plates, grown at 37 °C. Freezer stocks were made of cells were sensitive to both chloramphenicol and ampicillin.

2.11. GFP assays

E. coli RB9132 cells harbouring the GFP reporter vectors used during this investigation, were stored using the Pro-Lab Diagnostics Microbank™ stocks system, as described previously. For each assay, one bead was removed from the appropriate stock and streaked out onto an LB/gentamicin agar plate. Plates were incubated overnight at 37°C. The following day two 5 ml overnight cultures were set up by inoculating 5 ml of unbuffered M9 minimal media (supplemented

with gentamicin, thiamine and 0.4 % (w/v) glucose), using 1 µl loop-full of cells removed from the culture plate. Broth cultures were incubated for roughly 16 hours at 37°C, 200 rpm. After the incubation period, the two cultures were combined and aliquoted into four 2.5 ml volumes into 30 ml Universal tubes. Tubes were centrifuged at 4000 *x g* for 5 minutes at 4 °C. Cells were washed by re-suspending each cell pellet in 1 ml M9 minimal media buffered to either pH 5.5, 6.0, 6.5 or 7.0 and centrifuged again at 4 °C for 5 minutes. Cells were re-suspended again and diluted 1 in 10 into fresh media buffered to the appropriate pH. Cultures were incubated for 2 hours at 30 °C, 200 rpm. After 2 hours, cells were aliquoted in triplicate into a 96 clear flat bottomed plate (200 µl cells per well) and acetate (20 µl), adjusted to the correct pH was added to varying final concentrations (0 mM, 3 mM, 9 mM and 45 mM). Cells were loaded alongside blank media controls. Cells continued to be incubated at 30 °C for 12 hours.

Optical density (OD_{600nm}) and GFP fluorescence (excitation 485 nm; emission 520 nm) were measured every 30 minutes during the 12 hour incubation period, using the Infinite 200 PRO Microplate Reader, with fluorescence capability manufactured by Tecan, Männedorf, Switzerland. Results were normalised against blank controls. GFP fluorescence was normalised against optical density. Averages and standard deviations were calculated for technical replicates. GFP/OD_{600nm} was then plotted against time.

2.12. Cell assays for RT-qPCR sample collection

These methods were used to collect samples required for reverse-transcription quantitative polymerase chain reaction (RT-qPCR) assays described in Chapter 6.

E. coli RB9132/pRU1097.*t-glnAp2.aspta.pta*_term cells were inoculated into two lots of 5 ml unbuffered M9 minimal medium using 1 µl loop-full of cells from an LB agar plate containing gentamicin. Cultures were incubated at 37 °C, 200 rpm overnight (roughly 16 hours). The following morning, the two cultures were combined and mixed gently by inversion and aliquoted into two Universal tubes in 5 ml volumes. This was done to ensure no bias between starting cultures. Tubes were centrifuged at 3500 *x g* for 10 minutes. Following centrifugation, supernatant was discarded, and the pellets washed in 2 ml of M9 minimal medium buffered to the desired pH. Cells in one Universal tube were washed in medium buffered to pH 5.5, cells in the second Universal tube were washed in medium buffered to pH 7.0. Tubes were centrifuged for a second time at 3500 *x g* for 5 minutes and the supernatant discarded. Cell pellets were then re-suspended for a second time in 5 ml of the same medium used for the previous re-suspension. Each re-suspension was used to seed four identical day cultures by diluting 1 in 10 (1 ml of resuspension into 9 ml fresh M9 minimal media buffered to correct pH). Day cultures were incubated at 30°C, 200 rpm for 2 hours. At the 2 hour time point, cells were induced with acetate, this was done by adding 1 ml of sodium acetate stock solution. Stock solutions were made up to different concentrations (0.03 M, 0.1 M and 0.5 M) and adjusted to either pH 5.5 or pH 7.0. 1 ml of 0.03 M was added to 10 ml of medium to give a final concentration of roughly 3 mM, 0.1 M to give 9 mM final concentration and 0.5 M to give a final concentration of 45 mM acetate. Cultures were incubated for 6 hours at 30 °C, 200 rpm.

After 6 hours, culture tubes were centrifuge at 3500 *x g*, 4 °C for 10 minutes. Supernatant was discarded, and the cells re-suspended in 300 µl of RNAlater and stored in three 100 µl aliquots at -80 °C until further processing.

RNA extractions were then performed (see section 2.6.4) on each of the samples followed by cDNA synthesis (see section 2.6.5) and qPCR to detect for the expression of the antisense message (as*pta*) and the *pta* gene.

2.13. qPCR assays

2.13.1. Assay conditions and optimisation

All quantitative PCR (qPCR) assays were run on a Stratagene Mx3000P qPCR machine using the associated MxPro software (Stratagene, California, USA). The Brilliant III ultra-fast SYBR green QPCR master mix provided by Agilent Technologies (Santa Clara, California, USA) was chosen for this investigation. Non-skirted, white, 96-Well PCR plates provided by StarLab (Hamburg, Germany) and ABsolute qPCR Plate Seals, provided by Thermo Fisher Scientific were used throughout the project. The thermocycler conditions used are detailed in Table 2.2 and were followed by a melt curve.

Table 2.2: Thermo-cycling conditions used for quantitative PCR assays

Cycles	Duration of cycle	Temperature
1	3 minutes	95 °C
40	20 seconds	95 °C
	20 seconds	55-60 °C

Oligo primers designed against target genes were supplied by Eurofins MWG Operon (HPSF purified) and optimised prior to the assays. Optimisation of primer pairs entailed varying primer concentrations, annealing temperature and cycle

number using ten-fold dilutions of target cDNA as the template. Fluorescence measurements were taken at the end of each cycle and during the melt curve dissociation. Successful optimisation was inferred from amplification efficiency, melt curves and amplification plots, described below. Melt curves were performed at the end of the qPCR to assess the dissociation-characteristics of the double stranded DNA during heating.

2.13.2. Calculating amplification efficiency for qPCR primers

Each qPCR primer pair was optimised using a series of ten-fold dilutions of template DNA. The cycle threshold (Ct) value is the number of cycles required for a fluorescent signal to cross the threshold value. Optimal efficiency was indicated by even spacing between Ct values generated for each sample of the dilution series (roughly 3.3 cycles). Figure 2.1 shows an example of an amplification plot produced from an optimised qPCR primer pair, and is not related to the work detailed in this thesis.

The Ct values for each of the dilutions were plotted against the log of the dilution factor. The slope of the plotted data was then calculated and slopes values between -3.1 and -3.9 were generally accepted, which indicated an amplification efficiency between 80-110%, (E values 1.8 - 2.1). For each qPCR reaction performed during this study, the default threshold line produced by the MxPro software was used to determine all Ct values.

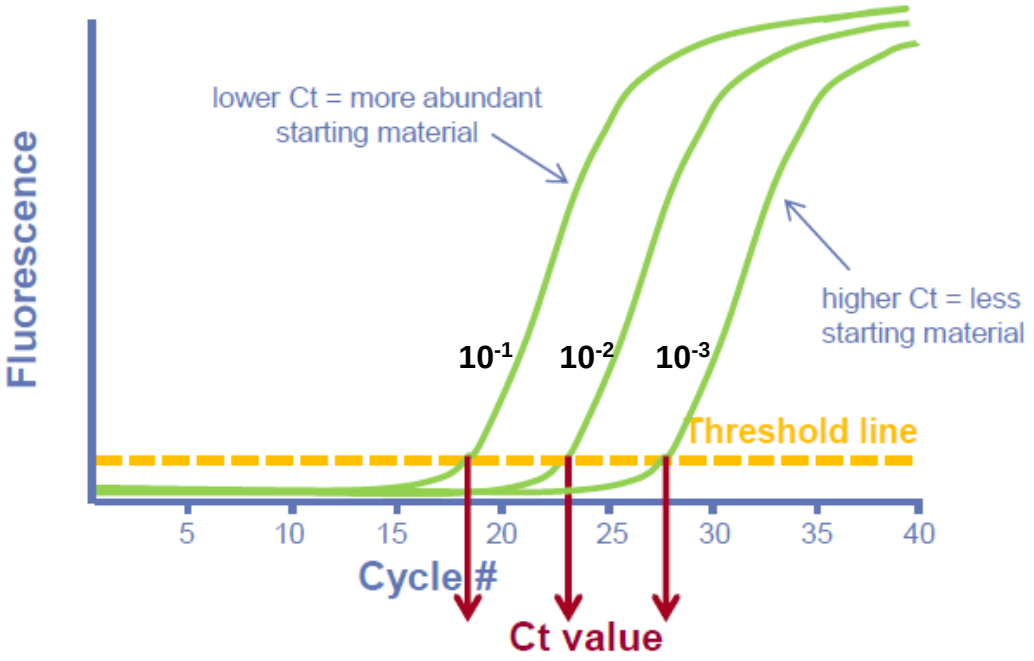

Figure 2.1: Example of qPCR the amplification curves generated from 10-fold serial dilutions of template DNA when using an optimised qPCR primer pair.

Adapted from [181]. This graph is not related to the work detailed in this thesis.

2.13.3. Analysis of amplification plot data

At the end of each reaction, qPCR amplification data was compiled into a Microsoft Excel spreadsheet and fluorescence values plotted against their corresponding cycle number. A sigmoidal amplification curve, denoting the accumulation of fluorescent signal, indicated successful amplification of DNA.

2.13.4. Analysis of melt curve data

SYBR green binds non-specifically to dsDNA and non-specific amplicons, which reduces assay specificity. Melt curves were carried out at the end of each qPCR reaction to detect how many products had been formed. This involved a slow, gradual increase in temperature (from 55 °C to 95 °C), whilst monitoring

fluorescence continually. At a certain temperature, an amplified product would fully dissociate into single strands, this in turn would cause the SYBR green to dissociate from the DNA and fluorescence intensity would decrease. True amplicons usually had melting temperatures of over 80 °C, whereas primer dimers melted at temperatures lower than 80 °C. When optimising qPCR primer pairs, clean, overlapping peaks above 80 °C were desired when amplifying a ten-fold dilution series. If peaks representing primer dimers were detected, the reaction conditions were altered, usually by decreasing primer concentration and increasing temperature slightly and the assay repeated.

2.13.5. Normalising against reference genes

Relative expression levels of target genes were calculated using the following calculation using the $2^{-\Delta\Delta Ct}$ method which can be simplified into the following calculation [182].

$$RE = \frac{(E_{ref})^{Ct\ ref}}{(E_{target})^{Ct\ target}}$$

RE = relative gene expression

E = amplification efficiency (different for each gene)

Ref = reference gene

Target = target gene of interest

2.14. Quantification of acetate production from *E. coli*

The acetate production from both *E. coli* wild type and engineered strains of *E. coli* was quantified by means of an acetate assay. *E. coli* cells were cultured under varying conditions, at given time points, 1 ml samples from cultures were removed and placed into 1.5 ml Eppendorf tubes and centrifuged at full speed to pellet the cells. Resulting supernatant was then deproteinised through a 10 kDa molecular weight cut off spin filter (Amicon Ultra centrifugal filters, Merck Millipore, Massachusetts, USA), and transferred into a fresh 1.5 ml Eppendorf tube. Supernatant was stored at -20 °C until required for acetate quantification.

Acetate quantification was perform using an Acetate Colorimetric Assay Kit provided by Sigma-Aldrich. Manufacturer's instructions were followed. Briefly these methods involved creating standard samples using a 1 mM acetate standard solution, diluted to different final concentrations using the provided acetate assay buffer to create 0, 2, 4, 6, 8, and 10 nmole/well standards. To ensure sample concentrations were within the linear range of the standard curve, they were diluted 1 in 20 in the provided acetate assay buffer, before being loaded into a 96 clear flat-bottomed plate. A reaction mix containing acetate enzyme mix, adenosine triphosphate (ATP), acetate substrate mix and a probe was then added to samples and standards and allowed to incubate for 40 minutes at room temperature, protected from light. Control samples could also be performed which excluded the acetate enzyme from the overall reaction mix. All samples, standards and controls were performed in duplicate. After 40 minutes incubation, the absorbance at 450 nm was measured using a Infinite 200 PRO plate reader (Tecan).

All samples were corrected against blank measurements. The absorbance values obtained from the appropriate acetate standards were used to create a standard curve. The acetate concentrations of samples tested were then inferred from this standard curve and multiplied by the original dilution factor of the sample. Further information on acetate quantification was provided in the manufacturer's protocol.

2.15. Anaerobic methods

2.15.1. Anaerobic chamber

The anaerobic chamber used in this study was the Whitley DG500 anaerobic Workstation with airlock access (Don Whitley Scientific Limited, Shipley, UK). The atmosphere of the chamber was 10 % CO_2, 10 % H_2 and 80 % N_2. Before entering the working area of the chamber, arms were first placed through the attached sleeves, and 2-3 cycles of vacuuming and gassing with 100 % nitrogen were performed before use. Movement of large items into the chamber was done by placing items into the air lock chamber, running a flush cycle and then transferring items into the working area of the chamber via the inner door.

2.15.2. Anaerobic vessels

Anaerobic serum bottles and Balch-type tubes (ChemGlass, New Jersey, USA) were used for the anaerobic cultivation of microbes in liquid media. Serum bottles had a total volume of 100 ml and were typically loaded with up to 30 ml of growth media. Balch tubes had a volume of 25 ml and were typically loaded with 5 – 7 ml of growth media. Bottles and tubes were always sealed with a butyl rubber

stopper followed by an aluminium crimp which exposed the septum of the butyl rubber stopper.

Duran flasks were used during the preparation and storage of larger volumes of anaerobic components. Specially designed Duran flask lids, purchased from Glasgerätebau Ochs, Bovenden, Germany, were used to keep the contents of the Duran flask anaerobic and consisted of a butyl rubber stopper and a screw cap lid.

2.15.3. Degassing of glass wear and plastic wear

All glass wears such as Balch tubes and serum bottles were transferred into the anaerobic chamber for a minimum of 3 hours before use. All plastics used, such as pipettes, petri dishes, sterile loops, Luer-lock syringes and needles required a longer degassing time of 24 hours, due to the ability of plastic to carry dissolved oxygen.

2.15.4. Removal/delivery of liquid anaerobic components

Anaerobic liquid components, such as substrates and seed cultures, were delivered and removed from serum bottles and Balch tubes via the butyl rubber septum using a needle and syringe. Before puncturing, the butyl rubber septum was cleaned with 70 % ethanol and allowed to air dry. This was always done inside the anaerobic chamber using degassed syringes and needles.

2.15.5. Preparation of anaerobic media

Anaerobic liquid medium and anaerobic agar medium were made up of the components listed in in Table A5.4 in the Appendices. The components listed in table above were added into a Duran flask (roughly 2X the total volume of medium required) and made up to the desired volume. Flasks were capped with an anaerobic lid and placed in a water bath set to 80 °C. Four Luer lock needles were pierced through each butyl rubber stopper. Two needles were attached to Tygon laboratory tubing (RS Components, Corby, UK) delivering stream of N_2/CO_2 gas. Two needles were used as an outlet for expelled gas. Flasks were degassed under the stream of N_2/CO_2 for 20 minutes. After 20 minutes, outlet needles were removed from the butyl stoppers, this was immediumtely followed by the needles delivering gas. Once all needles had been removed, the gas cylinder was turned off and the flask removed from the water bath. Flasks were then either autoclaved in batch volumes or transferred into the anaerobic chamber and aliquoted into smaller volumes before autoclaving.

Liquid anaerobic medium (no agar added) was often aliquoted into 5 ml or 30 ml volumes into an appropriately sized vessel, sealed with a butyl rubber stopper and crimped with an aluminium ring before being autoclaved. Balch tubes/serum bottles containing liquid medium were then stored at 4 °C until required. Sterile, degassed vitamin solution, sodium sulphide and appropriate substrates were added prior to inoculation.

Solid anaerobic medium was used in the form of either an anaerobic agar slant (prepared inside a Balch tube) or anaerobic agar plate. For the preparation of anaerobic agar slants, degassed agar medium was aliquoted into Balch tubes in 7 ml volumes. Balch tubes were sealed, crimped and autoclaved. The

autoclave cooled to 60 °C before the tubes were removed and placed inside the anaerobic camber. Sterile degassed vitamin solution, sodium sulphide and appropriate substrates were added to each of the Balch tubes containing liquid agar. Tubes were then swirled and placed at a 20-30 degree angle until the agar medium set. Agar slants were stored short term at 4 °C and used within a week of preparation.

For the preparation of anaerobic agar plates, degassed agar medium was autoclaved in batch volumes inside Duran flasks. Flasks were removed from the autoclave once it had cooled to 60 °C and placed inside the anaerobic cabinet. Lids from the Duran flasks were opened slightly and appropriate volumes of sterile degassed vitamin solution, sodium sulphide and appropriate substrates were added to the liquid agar using syringes. The liquid agar medium was then swirled and poured into plates with the lids placed on top and allowed to set. Once set, plates were placed inside an anaerobic jar and removed from the cabinet for storage at 4 °C and used within a week.

2.15.6. Preparation of anaerobic stock solutions

Anaerobic substrates and medium components, not suitable for autoclaving were prepared aerobically as stock solutions, inside an appropriate vessel such as a Universal tube or Duran flask. Vessel lids were replaced with parafilm and the stock solutions moved into the anaerobic chamber. Stock solutions were degassed for 24 hours. Parafilm was used to allow gaseous exchange without contamination. An anaerobic sealed serum bottle was prepared by placing a sterile and empty serum bottle inside the chamber for 24 hours. Once degassed the serum bottle was sealed with a butyl stopper and aluminium crimp before

autoclaving. Sterile, anaerobic serum bottles were moved back into the anaerobic chamber and filled with degassed stock solutions through a needle and syringe connected via a 0.2 µm filter. If appropriate, stock solutions were moved out of the chamber to be stored at 4 °C.

2.16. Techniques used to study natural methanogenic communities

2.16.1. Environmental sample collection

Acrylic coring devices 10 cm and 25 cm in length and both 4 cm in diameter, were used to obtain the various mudflat sediment core samples used during this investigation. These corers were provided by the Geography department at The University of Exeter. The corers had a sharpened edge and were pushed gradually into the ground with a downwards-rotating motion until the desired depth was reached. Cores were then carefully dug out of the mudflat sediment using a shovel. Ends of the cores were capped and taped and the cores placed inside a polystyrene box containing a small amount of dry ice. Cores containing samples collected for enrichment where first placed inside an anaerobic jar containing a GasPak (Becton, Dickinson and Company, New Jersey, USA). Samples were immediumtely transported back to the lab for processing.

2.16.2. Processing of environmental samples

Once back in the laboratory, sediment cores were pushed out of their acrylic corers and sectioned into the desired sample sizes using a sterilised scalpel. Cores collected for enrichment were sub-sectioned inside an anaerobic cabinet.

Those required only for DNA extraction were sub-sectioned under a biological safety cabinet, under normal aerobic conditions. Separated samples were either directly used for enrichment or stored in zip-lock freezer bags at -20 °C for later DNA extraction.

2.16.3. Total DNA extraction from environmental samples

Depending on starting volume of sediment, total DNA isolation was carried out using either PowerMax Soil DNA Isolation kit (up to 10 g) or PowerSoil DNA Isolation kit (0.25 g) both provided by Mo Bio Laboratories (Carlsbad, USA). For both protocols manufacturer's instructions were followed. Briefly this involved loading the sample into a bead beating tube along with solution containing sodium dodecyl sulfate (SDS). Bead beating the sample for 10 minutes started the homogenization and cell lysis procedure. All bead beating was performed using the Vortex Adapter for 24 (1.5–2.0 ml) tubes and the Vortex-Genie 2 Vortex, both provided by Qiagen (Hilden, Germany). Tubes were then centrifuged at full speed. The supernatant was removed for the precipitation of non-DNA organic and inorganic material, which was then followed by another centrifugation. Resulting supernatant was treated with a high concentration salt solution and passed through a silica membrane. The silica membrane containing bound DNA then underwent washing steps followed by the release of DNA from the membrane into elution solution.

2.16.4. Enrichment of environmental samples

For the enrichment of sediment samples retrieved from the environment, 10 g of sediment per sample was weighed out inside the anaerobic chamber and placed into a sterile 30 ml serum bottle. Serum bottles containing samples were then capped with a butyl rubber stopper and crimped with an aluminium ring. Serum bottles were moved to the bench top where they were purged for 15 minutes with premixed 20 % N_2, 80 % CO_2. Gas was delivered via a needle connected by Tygon laboratory tubing (RS Components) to the gas cylinder and pierced through the septum of the butyl rubber stopper. An unconnected needle was also pierced through the butyl septum and acted as an outlet for expelled gas. After purging, serum bottles were transferred back to the anaerobic chamber and the sediment flooded with 30 ml anaerobic medium, delivered via a needle and syringe. The serum bottles were then shaken gently for 10 seconds. 3 ml of the enrichment suspension was then removed using a needle and syringe and transferred into separate anaerobic serum bottles containing 27 ml of sterile anaerobic medium and an appropriate substrate. Each sample was enriched separately using different substrates. Substrates used were as follows:

- TMA only (20 mM)
- Methanol only (40 mM)
- Acetate only (40 mM)
- A combination of TMA (20 mM) + methanol (40 mM) + acetate (40 mM)

Enrichments were incubated in the dark at approximately 20 °C for up to 6 weeks.

2.16.5. Monitoring gas production from enrichment cultures

Gas production from microbes cultivated inside the enrichment cultures was inferred from the change in pressure inside the serum bottles over time. Pressure measurements were taken using a gas manometer (LEO 2 Ei**,** Keller, Dorset, UK) attached to a needle via a Luer-lock connection. The needle attached to the manometer was placed through the centre of the butyl septum (cleaned with 70 % ethanol) and the pressure read immediumtely. Sub-culturing of active cultures (those producing gas) was usually performed once the gas production halted.

2.16.6. Sub-culturing of enrichments for the isolation of colonies

Successful enrichment cultures underwent rounds of sub-culturing, followed by transferal onto solid agar for the isolation of single colonies.

2.17. Next-generation sequencing

The MiSeq sequencing platform, by Illumina, California, USA, was used throughout this study for both 16S rRNA sequencing and whole genome sequencing. This platform was housed and run by the Exeter Sequencing Service. All data analyses were performed using a Linux computer server.

2.17.1. Preparation of genomic DNA for 16S rRNA sequencing

Genomic DNA was amplified with PCR primers A571F (5'-GCYTAAAGSRNCCGTAGC-3') and UA1204R (5'-TTMGGGGCATRCNKACCT-3') specific for the archaeal 16S rRNA region [59]. PCR product was purified using

gel extraction techniques and the concentration of the purified DNA was determined using a Qubit (Thermo Fisher Scientific).

2.17.2. Preparation of genomic DNA for whole genome sequencing

For whole genome sequencing, genomic DNA was extracted (see section 2.6.1) from target cells (cultured on a plate) and quantified using a Qubit and submitted for sequencing.

2.17.3. Processing of sequencing reads

Upon the completion of Illumina MiSeq sequencing, raw sequencing reads were made available from the Exeter Sequencing Service. Output reads were in FastQ format. Reads were transferred onto a Linux server.

2.17.4. Quality checks

Output from the Illumina MiSeq sequencing platform was provided in the form of FastQ reads [183], which were downloaded onto a Linux server. The ‘FastQC quality control toolkit’ package (Babraham Bioinformatics, [184]), was used to analyse the quality of the raw reads. Attention was paid to the ‘Per Base Sequence Quality’ graphs generated using this tool.

2.17.5. Quality filtering using Trim Galore!

The trimming tool Trim Galore! provided by Babraham Bioinformatics was used for all quality filtering using the following command line options [185].

```
> trim_galore --paired [filenames]
```

2.17.6. Concatenation of paired reads

Quality filtered FastQ reads were concatenated using the Perl script 'concatenate_fastq_pairs' created by Dr David Studholme, University of Exeter. The command line used to run this script is outlined below.

```
> perl concatenate_paired_reads <read_file_1.fastq> <read_file_2.fastq>
```

2.17.7. Performing BLASTn searches

Desired databases for BLASTn searches were downloaded from the internet using the 'wget' command:

```
> wget [link_to_database]
```

Downloaded databases were formatted to make them suitable for blast searches using the 'formatdb' command and the 'pF' option to indicate that the database was a nucleotide database:

```
> Formatdb –pF –i [downloaded database]
```

Blast searches were then performed using the ‘blastn’ command to give reads taxonomic assignment:

```
> blastn -db [path_to_formatted_database] -query [query_file] > [name_of_output.blastn]
```

2.17.8. Analyses of BLASTn output using MEGAN

Blast outputs were imported into MEGAN software (MEtaGenome ANalyzer, version 5.11.3) for analysis. Lowest common ancestor processing was performed to create phylograms using MEGAN5 default settings. Phylograms were created for each dataset [186].

2.17.9. One Codex analysis pipeline

The online sequencing analysis platform, One Codex, was also used for the determination of taxonomy using sequencing files directly loaded onto the server [187]. Further information is provided on the One Codex webpage.

2.18. Methods directly relating to Chapter 3

2.18.1. Sample collection and DNA extraction

The sample site detailed in Figure 3.1 (see Chapter 3) was used for the collection of both the sediment cores analysed during this investigation. For the investigation of the 25 cm depth profile, a sediment core was collected in November 2013. For the investigation of the 4 cm depth profile, a sediment core

was collected in July 2014. Both sediment cores were 4 cm in diameter. Both core collections were carried out at low tide. In the laboratory, cores were sub-sampled into smaller sections and DNA extractions performed. The 25 cm core was sub-sectioned into 0-4 cm, 4-8 cm, 8-12 cm, 12-16 cm, 16-20 cm and 20-25 cm layers. The 4 cm core was sub-sectioned into 0.0-0.5 cm, 0.5-1.0 cm, 1.0-1.5 cm, 1.5-2.0 cm, 2.0-2.5 cm, 2.5-3.0 cm, 3.0-3.5 cm and 3.5-4.0 cm layers (see section 2.6.13).

2.18.2. Amplification of template DNA, Illumina Sequencing and sequence analysis

To confirm the presence of methanogenic organisms, DNA extracted from each layer of the sediment cores underwent PCR amplification, using the methanogen-specific primers ML_F and ML_R [64, 188]. These primers targeted a region of the gene encoding methyl coenzyme A, present only in methanogenic organisms.

DNA extracts were subsequently PCR amplified with the archaeal 16S rRNA primers, A571F and UA1204R [59], gel purified and quantified The amplified archaeal 16S rRNA amplicons were subject to paired-end sequencing using the Illumina MiSeq sequencing platform. Sequencing reads generated, were 300 nucleotides long. Samples were separately barcoded and pooled for sequencing process. Sequences of methanogen-specific and archaeal 16S rRNA PCR primers can be found in Table 2.3 below.

Table 2.3: Primer sequences used for PCR amplification.

Primer	Sequence (5' – 3')	Target	Ref
A571_F	GCYTAAAGSRNCCGTAGC	Archaeal 16S (V4-V7)	[59]
UA1204_R	TTMGGGGCATRCNKACCT	Archaeal 16S (V4-V7)	[59]
ML_F	GGTGGTGTMGGATTCACACARTAYGCWACAGC	*mcrA*	[64, 188]
ML_R	TTCATTGCRTAGTTWGGRTAGTT	*mcrA*	[64, 188]

Quality filtered and joined read files were compared against the RefSeq database [189], using BLASTn. BLAST output files were imported into MEGAN for analysis [186]. MEGAN was used to generate phylograms for each of the sediment core sub-sections. Phylograms representing sub-sections of each sediment core were combined, to allow for the visualisation of the results from the whole sediment cores. Paired reads were also directly fed into the online genomic search engine, One Codex for analysis [187]. See section 2.17 for more information.

2.19. Materials and methods relating directly to Chapter 4

2.19.1. Sample collection and processing

The sample site at the River Exe Estuary mudflats, Exmouth, Devon, UK, was re-visited for the collection of environmental samples on the 30th September 2016. Three 10 cm cores, 4 cm in diameter were collected using acrylic coring devices. Sediment cores were transported back to the laboratory under anaerobic conditions in a cool box.

Sediment samples were processed inside an anaerobic chamber. The top 2 cm of each of the three cores was removed and sub-sectioned into smaller 0.5 cm regions. Corresponding regions of each of the three cores were pooled for

each of the sub-sections (0.0-0.5 cm, 0.5-1.0 cm, 1.0-1.5 cm and 1.5-2.0 cm). The remainder of the soil cores were disposed of.

For total DNA extractions, 0.25 g of sediment was removed from each sample layer and processed using the PowerSoil DNA Isolation Kit (Mo Bio). DNA isolates from each layer were PCR amplified with methanogen-specific primers (ML_F and ML_R) to confirm the presence of methanogens within the sediment samples.

2.19.2. Sample enrichment and monitoring

Sediment samples were enriched on anaerobic growth medium containing either TMA (20 mM); methanol (40 mM); acetate (40 mM); or a combination of TMA/methanol/acetate (medium recipes provided in the Appendices, section A5). Final enrichments each had a total volume of 30 ml and contained approximately 1 g of sediment. Enrichment samples were incubated in sealed anaerobic serum bottles in the dark at ambient temperature (approximately 20 °C) under an atmosphere of 80 % Nitrogen and 20% carbon dioxide for up to 6 weeks. Enrichment cultures containing sterilised (by autoclaving) sediment samples were also set up as controls, to monitor for any microbial growth from contamination. These control enrichments contained a combination of all enrichment substrates (TMA/methanol/acetate).

Due to equipment restrictions, quantification of methane gas produced from the enrichment cultures was not possible. Instead total gas measurements were taken using a LEO 2 Ei gas manometer (Keller). Measurements were performed on a weekly basis.

To further aid the detection of methanogen growth, total DNA was obtained at different stages of enrichment by removing 500 µl of culture and subjecting pelleted cells to DNA extraction using the PowerSoil DNA Isolation kit (Mo Bio). DNA extracts were amplified with the methanogen specific primers ML_F and ML_R. The DNA band intensities of the PCR products were then compared. An increase in band intensity suggested an increase in the number of methanogenic organisms present within the sample.

Accurate optical density readings were hard to obtain for two reasons: 1) the presence of sediment within each enrichment, interfered with overall optical density readings; 2) each OD reading required the removal of 1 ml of culture, which significantly depleted the volume of the culture over the course of the incubation period. For these reasons, I decided not to perform regular optical density readings. Increasing turbidity was used as an additional indicator of microbial growth and was monitored visually over the course of the enrichment period.

2.19.3. Sub-culturing of enrichments

Successful enrichments, were determined as those with high gas production, coupled by an increase in methanogen specific DNA band (detected by PCR). These enrichments were further sub-cultured on fresh liquid anaerobic medium containing the appropriate substrate. Sub-cultures were performed inside anaerobic Balch tubes, had a total volume of 5 ml and were inoculated using 200 µl of liquid culture from the parent enrichment. Sub-cultures were then incubated in the dark at ambient temperature for up to 6 weeks.

2.19.4. Transferring cultures onto solid agar for the isolation of colonies

After subsequent rounds of successful enrichment, cultures were inoculated into solid anaerobic agar slants for the isolation of colonies. For this, 50 µl of the appropriate culture was used to inoculate an anaerobic agar slant, containing the appropriate substrate, within a Balch tube, (Figure 2.2). Agar slants were incubated in the dark at ambient temperature until for up to 3 weeks.

Upon the formation of colonies, agar slants were transferred into an anaerobic chamber and opened. Colonies were removed from the slants using a sterile 1 µl loop and patched anaerobic agar plates. Each patch of microbial growth was tested at regular intervals for methanogenic growth by using crude DNA extractions followed by methanogen-specific PCR. Upon the detection of methanogenic growth, patch samples were streaked out onto fresh agar plates for the isolation of fresh colonies.

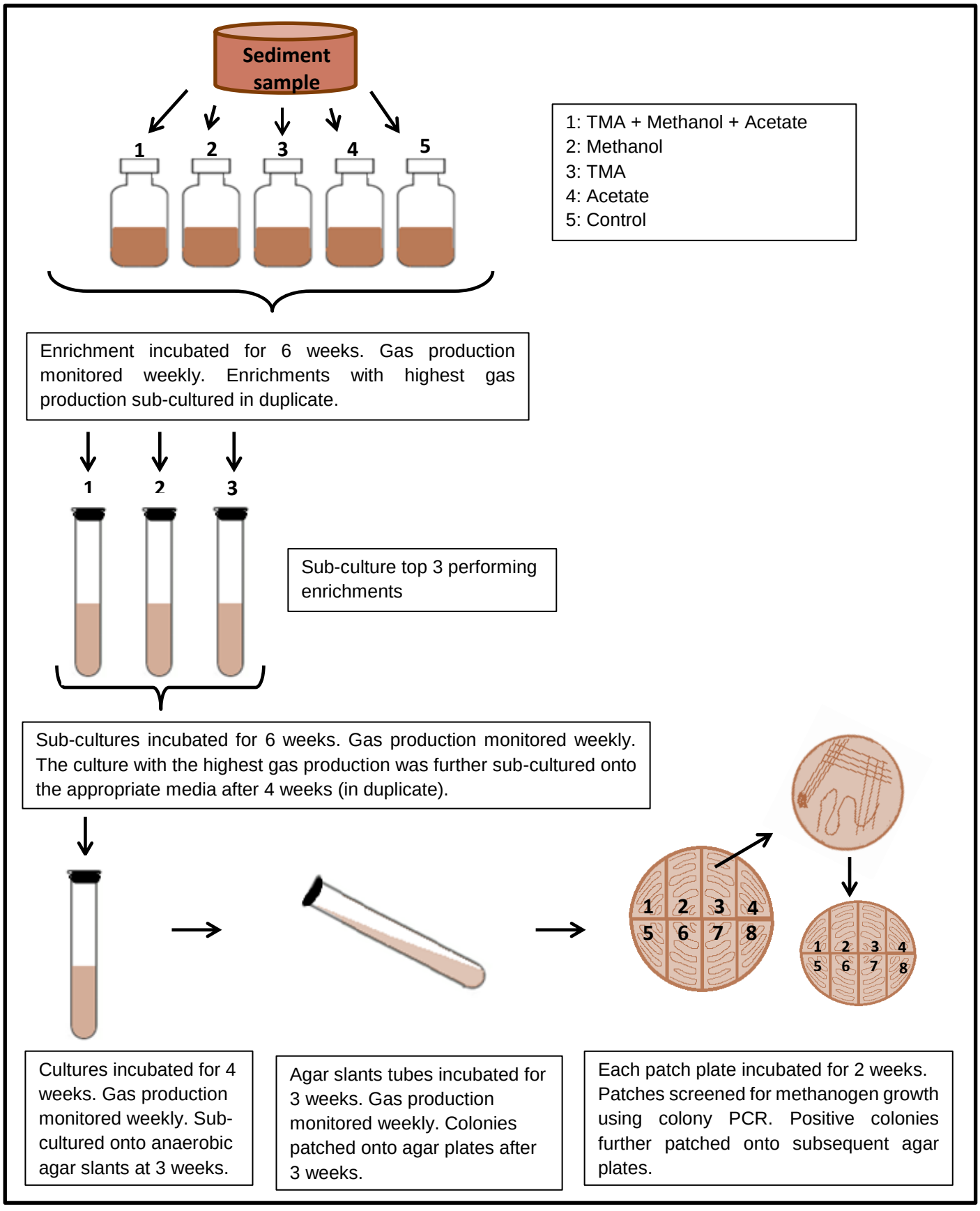

Figure 2.2: Schematic to show the flow of the methods used for the isolation of methanogenic colonies from estuarine mudflat sediment.

2.19.5. Whole genome sequencing and analysis

Total DNA extractions were performed on the desired isolates using the PowerSoil DNA isolation kit (Mo Bio). Extracted DNA was quantified using a Qubit machine (Thermo Fisher Scientific) and sent for whole genome sequencing using the Illumina MiSeq platform (Exeter Sequencing Service). For each sample, paired-end amplicon sequencing with 250 bp reads was performed. Sequencing reads were downloaded onto a Linux server and quality filtered using Trim Galore! [185]. Filtered reads were paired and compared against the archaeal division of the RefSeq genomic DNA database [189] using BLASTn. BLAST output was subsequently fed into MEGAN software for further analysis [186]. See section 2.17 for more information.

2.20. Methods relating directly to Chapter 5

2.20.1. Sourcing of strains and confirmation of genotypes

A culture of *E. coli* strain RB9132 (*glnL* deletion mutant, which codes for NtrB), was donated by Professor Ray Dixon, John Innes Centre, Norwich Research Park [190]. Two *glnL* wild type *E. coli* strains, YMC10 2841 and YMC10 3236, were obtained through donation from Alexander Ninfa, University of Michigan [175]. These were identical wild type strains raised at different sources. To confirm the presence/absence of the *glnL* gene, gDNA extracted from each of the donated strains was subject to PCR amplification with *glnL* specific primers. Confirmation of genotype was then assessed by electrophoresis of the PCR product on a 1 % (w/v) agarose gel and examining for DNA bands under U.V. light.

2.20.2. Generation of *pta* deletion mutant

The *pta* knockout mutant *E. coli* strain required for the characterisation of the *glnAp2* promoter was unavailable from other sources. Instead, a *pta* knockout mutant strain was generated using the Wanner mutagenesis protocol [176]. *E. coli* RB9132 cells were used to create RB9132Δ*pta*, a full description of this can be found in section 2.10. Primers designed for this deletion are described in A3.1 of the appendix.

2.20.3. Cloning of *glnAp2* promoter region

Refer to sections 2.6.11-2.6.14 for more information. The *glnAp2* promoter region containing the promoter and the two NtrC-binding sites was PCR amplified from the *E. coli* RB9132 chromosome. The forward primer glnAp2_F (5'-CGCGTCAAGCTTCAAAGGTCATTGCACCAAC, containing a HindIII site) and the reverse primer glnAp2_R (5'-CTGAGTGGATCCAGTACGTGTTCAGCGGACATAC, containing a BamHI site) were designed, using the *glnAp2* promoter region of *E. coli* strain YMC9 as a guide. These two primers were used in six identical 50 µl PCR reactions to amplify a 251 bp region between positions 93 and 343 in the published DNA sequence (GenBank accession no. M10421). Figure 2.3 provides an annotation of the amplified region.

>gi|146163|gb|M10421.1|ECOGLNALG *E.coli glnALG* operon: *glnA* gene coding for glutamine synthetase, promoter region

TCGCACTACAAAACAGGATCACAAACATCCTCCGCAAACAATATTGCAGAGTCCCTTTGTGATCGC
TTTCACGGAGCATAAAAAGGGTTATCCAAAGGTCATTGCACCAACATGGTGCTTAATGTTTCCATT
GAAGCACTATATTGGTGCAACATTCACATCGTGGTGCAGCCCTTTTGCACGATGGTGCGCATGATA
ACGCCTTTTAGGGGCAATTTAAAAGTTGGCACAGATTTCGCTTTATCTTTTTTACGGCGACACGGC
CAAAATAATTGCAGATTTCGTTACCACGACGACCATGACCAATCCAGGAGAGTTAAAGTATGTCCG
CTGAACACGTACTGACGATG

Key:

glnAp2_F binding site **glnAp2_R binding site** **NtrC~P enhancer site 1** **NtrC~P enhancer site 2**

Predicted Shine-Dalgarno sequence **ATG start site**

Figure 2.3: DNA sequence of the *glnAp2* promoter region from *E. coli* strain YMC9.

Using the genetic sequence of the *glnAp2* promoter region of *E. coli* strain YMC9 as a guide, the *glnAp2* promoter region was PCR amplified from the *E. coli* RB9132 genome using the primer pair glnAp2_F and glnAp2_R. The forward and reverse PCR primer binding sites are highlighted in yellow and blue respectively. The -35 and -10 TATA box binding regions are highlighted in pink and grey respectively. Predicated Shine-Dalgarno sequence is highlighted in dark green and the ATG start site is highlighted in red. This sequence was obtained from the NCBI database (GenBank accession no. M10421) [191].

A-tails were added to the PCR fragment containing the *glnAp2* promoter region (plus restriction sites). The product was then purified and ligated with the pGEM-T vector using the pGEM-T easy vector cloning system I (Promega). The recombinant pGEM-T.*glnAp2* vector was used to transform calcium competent *E. coli* DH5-alpha cells using heat shock transformation. Successful cloning of *glnAp2* was confirmed initially by colony PCR, with the primer pair glnAp2_F/glnAp2_R. Transformants that produced a positive colony PCR were

then subject to miniprep vector extraction. Extracted vector DNA was sent for Sanger sequencing (Eurofins) to confirm the sequence of the *glnAp2* insert.

When required, the *glnAp2* fragment was released from the pGEM-T holding vector using restriction digest techniques. pGEM-T.*glnAp2* was subject to 10 double restriction digest with BamHI and HindIII restriction enzymes, alongside controls. Digest products were mixed with 6X gel loading dye and electrophoresed on a 1 % (w/v) agarose gel.

2.20.4. Preparation of GFP reporter vector

The GFP reporter vector, pRU1097, purchased from Addgene, was used in this investigation. This promoter-less vector contains a gentamicin resistance marker as well as a multiple cloning site ahead of a GFPmut3.1 reporter gene. pRU1097 arrived in *E. coli* DH5-alpha cells and was extracted using miniprep techniques. The extracted vector was subject to 9 identical double restriction digest reactions using BamHI and HindIII restriction enzymes alongside controls. Products from the restriction digests were mixed with 6X gel loading dye and electrophoresed on a 1 % (w/v) agarose gel and imaged under U.V. light.

2.20.5. Ligation and transformations

Restricted and purified pRU1097 vector DNA and restricted and purified *glnAp2* insert DNA were ligated and transformed into calcium competent *E. coli* RB9132Δ*pta* cells to form RB9132Δ*pta*/pRU1097.*glnAp2*. Transformation reactions were plated onto LB gentamicin plates and incubated overnight at 37 °C. Resulting colonies were selected and patched onto fresh LB gentamicin agar

plates and incubated overnight again. Colony PCR's were performed on each patch of *E. coli* cells using PCR primers that overlapped the region of native pRU1097 vector DNA and the inserted *glnAp2* DNA. Transformants that were confirmed as positive by colony PCR were then subject to vector DNA sequencing to confirm the insertion of the *glnAp2* fragment.

2.20.6. Formation of additional cell types

Alongside the formation of RB9132Δ*pta*/pRU1097.*glnAp2*, the cell types RB9132/pRU1097 (promoter-free reporter vector) and RB9132/*pRU1097.glnAp2,* both wild type for the *pta* locus were created. These cell types were used to assay for any leaky expression from the GFP reporter vector itself and to test for fluorescence induction in *pta* knockout cells respectively. Each cell type will be referred to with the following nomenclature:

Cell type 1: RB9132Δ*pta*/pRU1097.*glnAp2*

Cell type 2: RB9132/pRU1097

Cell type 3: RB9132/*pRU1097.glnAp2*

2.20.7. GFP fluorescence assays

Cell types 1, 2 and 3 underwent GFP fluorescence assays under varying pH to assess the natural level of fluorescence produced from each cell type. These assays are described in section 2.11. Unless stated otherwise, all GFP fluorescence data was normalised against the optical density of the *E. coli* culture being tested.

To further investigate the sensitivity of the *glnAp2* promoter to external acetate concentration, *E. coli* Type 1 cells (RB9132Δ*pta*/pRU1097.*glnAp2*) were used and cultured under varying concentrations of external acetate (0 mM, 3 mM, 9 mM, 45 mM) at different pH values (pH 5.5, 6.0, 6.5, 7.0) at 30 °C for 12 hours. Further details can be found in section 2.11.

2.21. Methods relating directly to Chapter 6

2.21.1. Generating a truncated *glnAp2* promoter region (*t-glnAp2*)

The untranslated upstream region of the *glnAp2* promoter was truncated to form a shorter promoter region (denoted as *t-glnAp2*). This truncated promoter regionwas used to direct expression of an antisense RNA. The truncated region was designed not to include the predicted Shine-Dalgarno sequences and ATG start site which would normally initiate ribosome binding to the generated mRNA fragment [192].

The *t-glnAp2* DNA was PCR-amplified from *E. coli* strain RB9132 chromosomal DNA using the forward primer 5'-CGCGTCAAGCTTCAAAGGTCATTGCACCAAC-3' (containing a *Hin*dIII site) and the reverse primer 5'-CTGAGTGGATCCCGTGGTAACGAAATCTGCAA-3' (containing a *Bam*HI site). These primers amplified a 200 bp region between positions 93 and 292 in the published DNA sequence (GenBank accession no. M10421). An annotation of this promoter region and the PCR primers used to clone it can be found in the appendices Figure A4.1.

The *t-glnAp2* region was cloned into the pGEM-T holding vector to form pGEM-T.*t-glnAp2*. The recombinant vector was used to transform calcium

competent DH5-alpha *E. coli* cells. Vector DNA was isolated from positive transformants, sequenced and aligned against the expected sequence of the designed *t-glnAp2* promoter. Freezer stocks of DH5-alpha cells containing pGEM-T.*t-glnAp2,* which had been verified by sequencing were stored -80 °C until needed.

2.21.2. Selection and cloning of antisense fragment targeting *pta*

The *pta* gene was the antisense target. To generate the antisense fragment, a small region of 47 nucleotides upstream of the *pta* translation start site, followed by the first 80 nucleotides of the *pta* gene were PCR amplified from the *E. coli* strain RB9132 genome using the forward primer 5'-TGGGCCCGCTGTTTTGTAACCCGCC-3' (containing an ApaI site) and the reverse primer 5'-CGGATCCATTGCACGGATCACGCC-3' (containing a BamHI site). PCR primers were designed using the *E. coli* K-12 strain C3026 whole genome sequence, region 2516813 to 2517000 [NCBI accession number, CP014272.1]. An annotation of this sequence can be found in the appendices Figure A4.2. PCR amplification generated a fragment 127 base pairs in length. The fragment was named 'as*pta*'.

The antisense fragment was first cloned into the pGEM-T holding vector and used to transform calcium competent *E. coli* DH5-alpha cells. Vector DNA was isolated from transformants, which were identified as positive by PCR, sequenced and aligned against the expected sequence of as*pta*. Freezer stocks of DH5-alpha cells carrying the correct pGEM-T.as*pta* vector were made and stored at -80 °C until needed.

2.21.3. Preparation of terminator fragment

The *pta* operon terminator was chosen as the termination signal for the antisense cassette. This is a Rho-independent terminator (type II terminator), which consisted of inverted repeat sequences followed by a string of uridine bases, which form hairpin structures when transcribed [193]. Due to the hairpin nature of this fragment, PCR amplifications were unsuccessful. The terminator fragment was instead artificially synthesised using GeneArt Gene Synthesis (Thermo Fisher Scientific) and the generated fragment flanked with ApaI and KpnI restriction enzyme sites at the 5' and 3' ends respectively. The fragment arrived in lyophilized form cloned into the pMA-T vector. The vector was rehydrated and used to transform calcium competent DH5 alpha *E. coli* cells, freezer stocks made and stored at -80 °C until later required. This terminator fragment was denoted as '*pta*_term'. An annotation of this sequences is provided in Figure A4.3 in the appendices.

2.21.4. Building the antisense construct

Each component of the antisense cassette was engineered with restriction sites that matched those within the pRU1097 host vector. The truncated promoter region was designed to allow insertion between the HindIII and BamHI sites. The as*pta* message was engineered to allow insertion between the BamHI and ApaI sites. The terminator region designed for insertion between the ApaI and KpnI sites. Each component of the antisense construct was individually cloned into pRU1097 using restriction digests and ligation reactions to form pRU1097.*t-glnAp2.*as*pta*.*pta*_term. The resulting construct was transformed into RB9132 *E. coli* cells (positive for the *pta* locus) to generate the antisense strain

'RB9132_antisense_*pta'* (RB1932/pRU1097.*t-glnAp2.as*pta.*pta*_term). RB9132_antisense_*pta* cells were grown up and subject to vector extraction. Harvested vector DNA was sent for sequencing to confirm the sequence of the antisense construct.

2.21.5. Assessing fluorescence from RB1932/pRU1097.*t-glnAp2*.as*pta*.*pta*_term

Engineered cells were initially screened for fluorescence by adding acetate to concentrations of 0 mM, 3 mM, 9 mM or 45 mM at pH 7.0, to determine if the *t-glnAp2* promoter triggered expression of *gfp* and GFP luminescence upon illumination of cells. These assays were performed using the methods described in section 2.11 (using pH 7.0 only). Fluorescence signal was normalised against OD of the culture and plotted against time.

2.21.6. RT-qPCR assays targeting *pta* and the antisense message

RT-qPCR assays were developed and optimised to target the *pta* gene as well as the as*pta* mRNA and two reference genes, alongside negative controls (-ve). For this investigation *cysG* and the V6 region of the 16S rRNA gene (denoted as *16S_V6*) were chosen as reference genes for the normalisation of qPCR data. RB9132_antisense_*pta* cells were cultured in M9 minimal medium, supplemented with 0.4 % (w/v) glucose, buffered to either pH 5.5 or pH 7.0 and supplemented with varying concentrations of acetate (0 mM, 3 mM, 9 mM and 45 mM) at 30 °C for 6 hours. At the end of the incubation period, cells were harvested by centrifugation and subject to RNA extractions. cDNA pools were created from total RNA extracts and assayed for *pta* expression using qPCR. Further details

are provided in section 2.13. qPCR primer pairs used in this investigation are listed in Table 2.4. Before conversion of RNA into cDNA, RNA was screened for any DNA contamination using end-point PCR and an appropriate primer pair. All qPCR data was normalised using data obtained from reference genes.

Table 2.4. Table of oligo primer pairs used for qPCR amplification of target genes and reference genes.

Target Gene	Target Description	qPCR primers	Primer sequences (5' - 3')	Target Length (bp)	Primer concentrations (nM)	Annealing Temp (°C)	Number of cycles	Efficiency	Reference
cysG	Multifunctional	*cysG*_qpcr_F	TTGTCGGCGGTGGTGATGTC	105	250	60	40	2.03	[194]
		*cysG*_qpcr_R	ATGCGGTGAACTGTGGAATAAACG						[194]
16S_v6	V6 region of 16s rRNA subunit	*V6*_qpcr_967F	CAACGCGAAGAACCTTACC	98	100	60	30	1.88	[195]
		*V6*_qpcr_1046R	CGACAGCCATGCANCACCT						[195]
as*pta*	antisense message against *pta*	as*pta*_qpcr_F	GTGTCCCGTATTATTATGC	80	100	60	40	2.35	This work
		as*pta*_qpcr_R	ATTGCACGGATCACGCCAAG						This work
pta	Targets *pta* gene	*pta*_qpcr_F	GCTAACTACATCAACGC	91	100	55	35	1.99	This work
		*pta*_qpcr_R	GCTGATAACGGAACGC						This work

2.21.7. Acetate assays and growth curves

RB9132_antisense_*pta* cells were tested for acetate production. Cells were grown in either M9 minimal medium, supplemented with 0.4 % (w/v) glucose, buffered to pH 5.5, or to pH 7.0, LB medium (0.4 % (w/v) glucose) or anaerobic growth medium (0.4 % (w/v) glucose). Cells were cultured for 12 hours at 37 °C with shaking, in 30 ml cultures, inside sealed vessels. A colorimetric assay was then used to quantify the amount of acetate in the growth medium. Further details are provided in section 2.14.

For each different growth medium, RB9132_antisense_*pta* and RB9132 wild type cultures were compared. The amount of acetate was normalised against respective OD_{600nm} values to compensate for any differences in growth between the strains. Two biological replicates and two technical replicates were carried out per each condition tested.

3. Chapter three: Investigating methanogenic depth profiles of estuarine mudflat sediment

3.1. Introduction

Up until recent years, methanogens were considered extremely strict anaerobes and the inhibition of methanogenesis by oxygen has previously been addressed in Chapter 1. However, many research articles have described the capabilities of certain methanogens to survive sustained periods of oxygen stress. For example, certain strains of *Methanosarcina barkeri*, have been shown to survive in the presence of oxygen for up to 200 minutes, without a decrease of viability [196]. As the leakage of oxygen can sometimes be an issue for anaerobic digestion technology, the application of aero-tolerant methanogens could potentially be very beneficial.

Most aero-tolerant methanogen discoveries to date, have been made within soils. Amongst this research is a study by Peters and Conrad, 1995; who observed the production of methane from methanogens within aerated soils upon the re-establishment of anoxic conditions [197]. Research has also demonstrated that some methanogen strains possess the genetic features to protect themselves against oxidative stress, [198, 199]. To date, research has primarily focused on rice paddy soils [117, 200, 201] and other environments which often undergo periods of intermittent aeration [202-204]. However, to my knowledge no research has been undertaken to examine the oxygen-tolerant capabilities of methanogens living in estuarine sediments. Like rice paddies, estuarine sediments undergo periods of intermittent aeration due to changes in tidal levels, and therefore carry potential to harbour oxygen-tolerant methanogens. Work described in this chapter aimed to study the methanogenic community within a selected estuarine sediment, to potentially aid the future isolation of oxygen-tolerant methanogens, which may have greater oxygen tolerance capabilities than those previously discovered.

The intertidal mudflats at the River Exe Estuary by Exmouth, Devon, UK were chosen as the sample site for this investigation. Specifically, the 'Duck Pond' area, as it's known to the locals. This site provided easy access during times of low tide. The site undergoes one of the highest aeration periods within the estuary, as it is covered and drained of sea water for approximately equal periods throughout the day, providing an anaerobic environment for methanogenic metabolism and growth [205]. Figure3.1. shows a satellite image map of the Exe Estuary, including the specific location of the sample site. Figure 3.2 describes the salinity gradients within the Exe Estuary.

Sediment cores were sampled and sectioned into various layers and total DNA extractions performed. Samples were initially screened using the methanogen-specific PCR primer pair ML_F and ML_R to indicate weather methanogen DNA was present within the samples. Taxonomic structure of the samples was determined using 16S rRNA sequencing using primers A517F and UA1204R, targeting the variable V4 to V7 regions[59]. These variable regions of the 16S gene detect archaeal diversity, a provided good coverage of methanogenic sequences [59]. Sequencing output from paired-end amplicon sequencing was compared against the RefSeq database, hosted by NCBI, [189] using two-different analysis platforms 1) The MEtaGenome ANalyzer (MEGAN), [186] and 2) The online genome search engine, One Codex [187].

MEGAN, software version 5, was used as the primary analysis tool and is widely used for the analysis of metagenomic datasets, including 16S sequence datasets [206]. Results produced using MEGAN were directly compared with an alternate method of analysis used, the online genomic search engine One Codex, formerly named Helix, which does not use BLAST. This online programme, works

by splitting input reads into a series of overlapping k-mers (DNA sequence k letters long) [207], and searching for matching k-mers within the RefSeq database. One Codex was chosen over other available options for its fast processing time as an alternative approach for read assignment.

Initially a 25 cm core, sectioned into five 4 cm layers and one 5 cm layer was investigated. Methanogenic species were detected within every section of the core, including the very top 0-4 cm layer. This result prompted further investigation into the same sample site using a smaller 4 cm core, separated into 0.5 cm layers, to allow for the very surface layers to be examined.

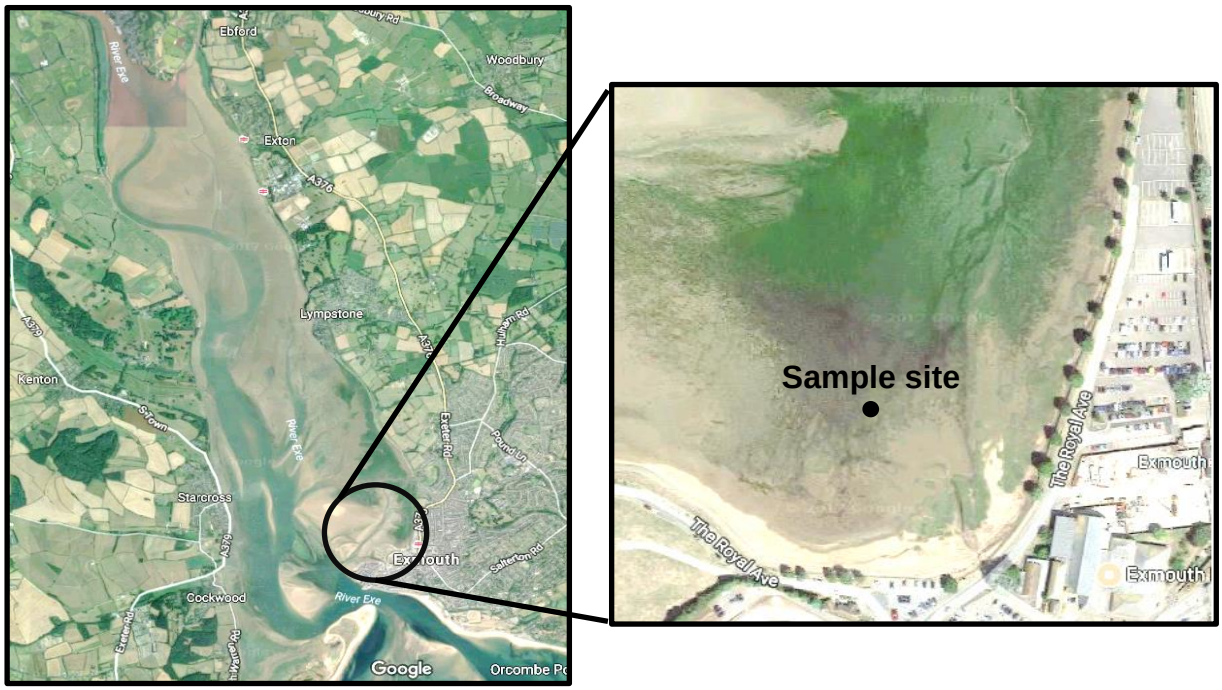

Figure 3.1: Satellite view of the sample site selected for this investigation.

Satellite image of River Exe Estuary, by Exmouth, Devon UK. Source: Google Maps.

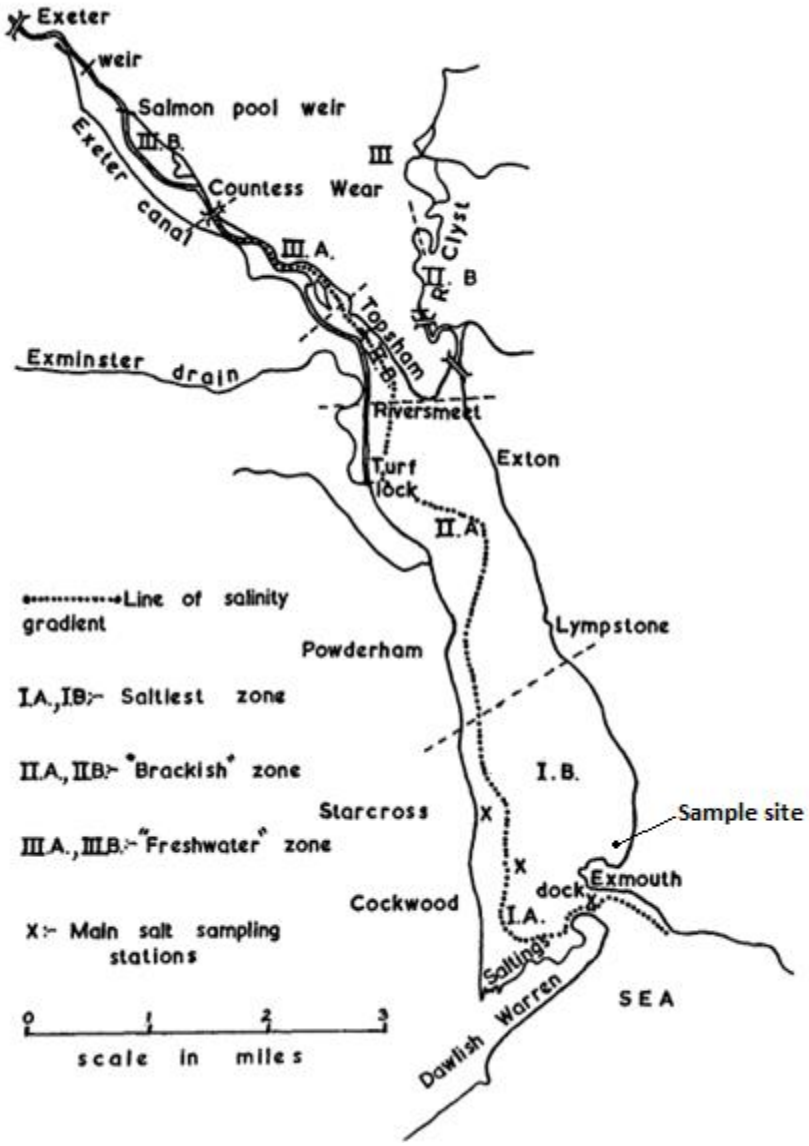

Figure 3.2: Map of the salinity gradients found within the Exe Estuary, Devon UK.

Image sourced from [208].

3.2. Results – Part one: 25 cm sediment core

3.2.1. DNA extraction and quantification

DNA extractions from every layer of the 25 cm sediment core were achieved. A negative correlation between eluted DNA concentration and the depth from which the DNA was extracted were observed; i.e. DNA extracted from 0-4 cm sediment layer had a higher DNA concentration than DNA extracts taken from the 20-25 cm sediment layer. This pattern is clearly seen in the band intensities of the DNA extracts and is also represented graphically (Figure 3.3).

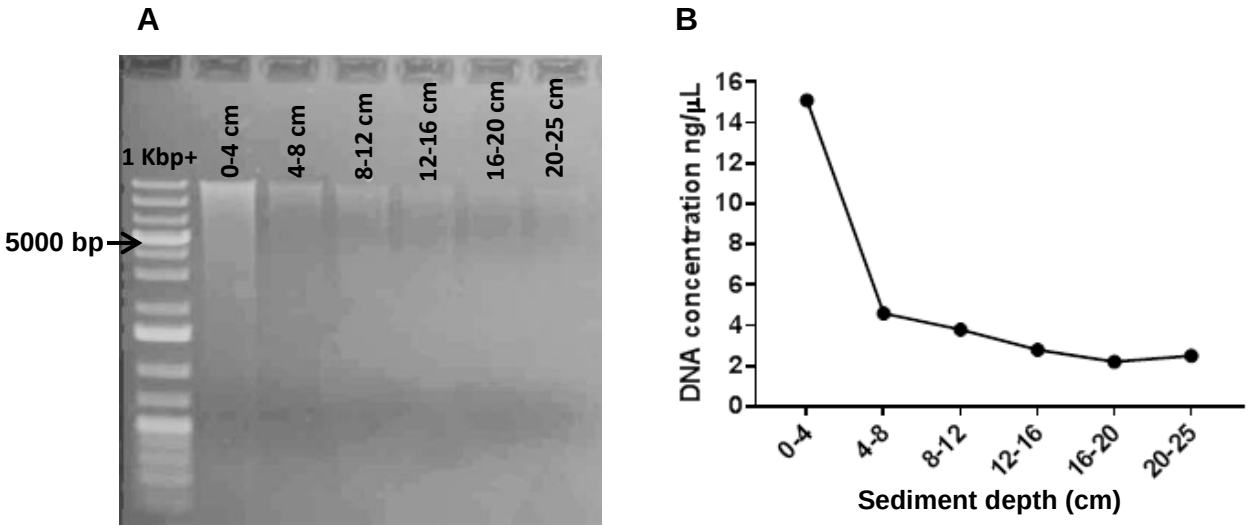

Figure 3.3: DNA extracts isolated from layers of a 25 cm sediment core, sampled from estuarine mudflats at Exmouth, Devon, UK.

DNA was extracted from each layer of a 25 cm sediment core sampled from estuarine mudflats in Exmouth, Devon, UK. A) 10 µl of eluted DNA from each extraction was electrophoresed alongside a 1 Kb plus DNA ladder (Thermo Fisher Scientific). The arrow indicates the 5000 bp DNA marker. B) DNA sample concentrations were quantified using a Nano drop machine (2.6.9) (Thermo Fisher Scientific) and plotted.

3.2.2. PCR amplification using methanogen-specific primers

DNA extracts from each layer of the 25 cm sediment core were PCR amplified with methanogen-specific primers under optimised conditions. A negative control (-ve), containing nuclease-free water in place of template DNA, was also included in the reaction to test for clean reaction conditions. The PCR product was electrophoresed in an agarose gel (Figure 3.4).

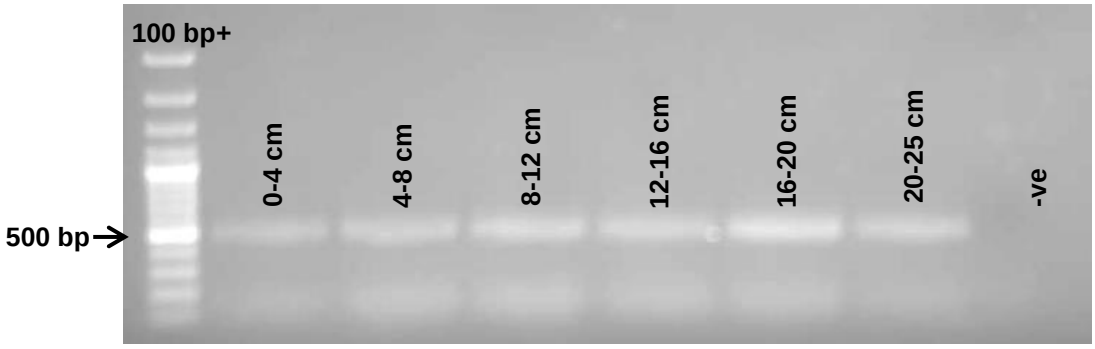

Figure 3.4: PCR product created from DNA extracts of a 25 cm sediment core with methanogen-specific primers.

In separate 0.5 ml PCR tubes, 1 µl of template DNA extracted from each layer of a 25 cm sediment core was amplified with methanogen specific primers (ML_F and ML_R), at optimised conditions. Negative control (-ve)s contained nuclease-free water in place of template DNA. 10 µl of each PCR product was electrophoresed alongside a 100 bp plus DNA ladder (Thermo Fisher Scientific) in a 1 % agarose gel. The arrow indicates the 500 bp DNA marker.

The ML_F and ML_R primers were expected to amplify a 470 bp region of the *mcrA* gene. PCR reactions containing template DNA extracted from each of the layers from the 25 cm sediment core, produced a DNA band. All DNA bands ran very slightly below the 500 bp marker on the 100 bp plus ladder, indicating that

they were the expected size of 470 bp. This result indicated that all layers of the 25 cm core contained methanogenic DNA sequences.

3.2.3. PCR amplification with universal archaeal primers

Target DNA extracted from each layer of the sediment core was amplified with the archaeal specific 16S rRNA primers, A571F and UA1204R. Targeting a region approximately 630 bp in length [59]. Six replicate PCR reactions were carried out per sediment layer. For each set of six replicates, a negative control (-ve), containing nuclease-free water in place of template DNA, was included. PCR product from each of the reactions was electrophoresed in 1 % agarose gels and gel purified. 5 µl of each purified PCR product from was electrophoresed on a second 1 % agarose gel, (Figure 3.5).

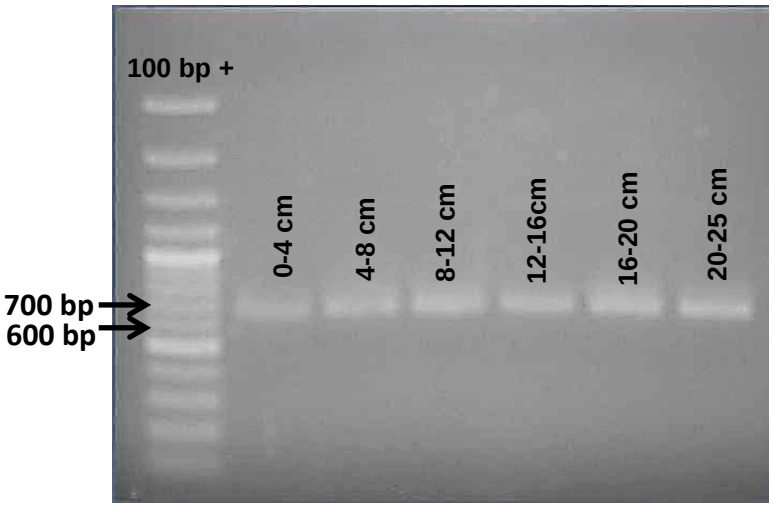

Figure 3.5: Purified archaeal 16S rRNA region from each layer of the 25 cm sediment core. DNA was extracted from the indicated layers of a 25 cm sediment core. DNA extracts were amplified using universal archaeal 16S rRNA PCR primers (A571_F andUA1204_R). Each of the PCR products were purified and run alongside a 100 bp plus DNA ladder (Thermo Fisher Scientific) on a 1% agarose gel, containing Midori Green (Nippon Genetics). The gel was imaged under UV light. The arrows indicate the 600 bp and 700 bp DNA markers.

DNA bands, which migrated between the 600 bp and 700 bp markers on the DNA ladder, were detected in each of the lanes into which purified PCR product was loaded. These bands showed similarities in intensity and indicated successful DNA amplification and purification of the 16S rRNA gene from each of the sediment layers in the 25 cm core.

3.2.4. Quality filtering of sequencing reads

The archaeal 16S regions isolated from each of the sections of the 25 cm core were subject to paired-end amplicon sequencing, using Illumina MiSeq technology. To reduce the error rate of downstream sequencing analysis processes, quality filtering was performed on all sequencing reads. Figures 3.6 and 3.7, illustrate a representative example of the 'Per Base Sequencing Quality' graphs generated by FastQC quality control toolkit (Babraham Bioinformatics, [184]), before and after the quality filtering of sequencing reads. For each base position, in each of the reads within the file in question, a box-whisker type plot is drawn. This includes the following elements: a mediumn value (central red line); the inter-quartile range (yellow box); the upper and lower whiskers representing the 10 % and 90 % points and the mean quality (blue line). The y-axis shows the quality scores; the higher the score the better the base call. The background of the graph divides the y-axis into very good quality calls (green), calls of reasonable quality (orange), and calls of poor quality (red).

The graph seen in Figure 3.6 represents the quality of the sequence reads before quality trimming. The read file used in this example was the forward reads generated during the sequencing of the 0-4 cm sample (0-4_cm_R1). A steep decline in mean quality scores, from good to poor quality, observed around 70 bp

in the reads in question. This indicated the presence of poor quality ends, which is often observed during Illumina MiSeq Sequencing [209] and required removal using Trim Galore! (Babraham Bioinformatics [185]).

Quality checks using FastQC were repeated after trimming with Trim Galore! and showed an improvement in the overall quality of reads, Figure 3.7. Mean quality scores did not fall out of the ‘good quality’ green zone for any positions in the reads after trimming. Similar results were obtained after the trimming of the remaining read files generated for all other samples sequenced.

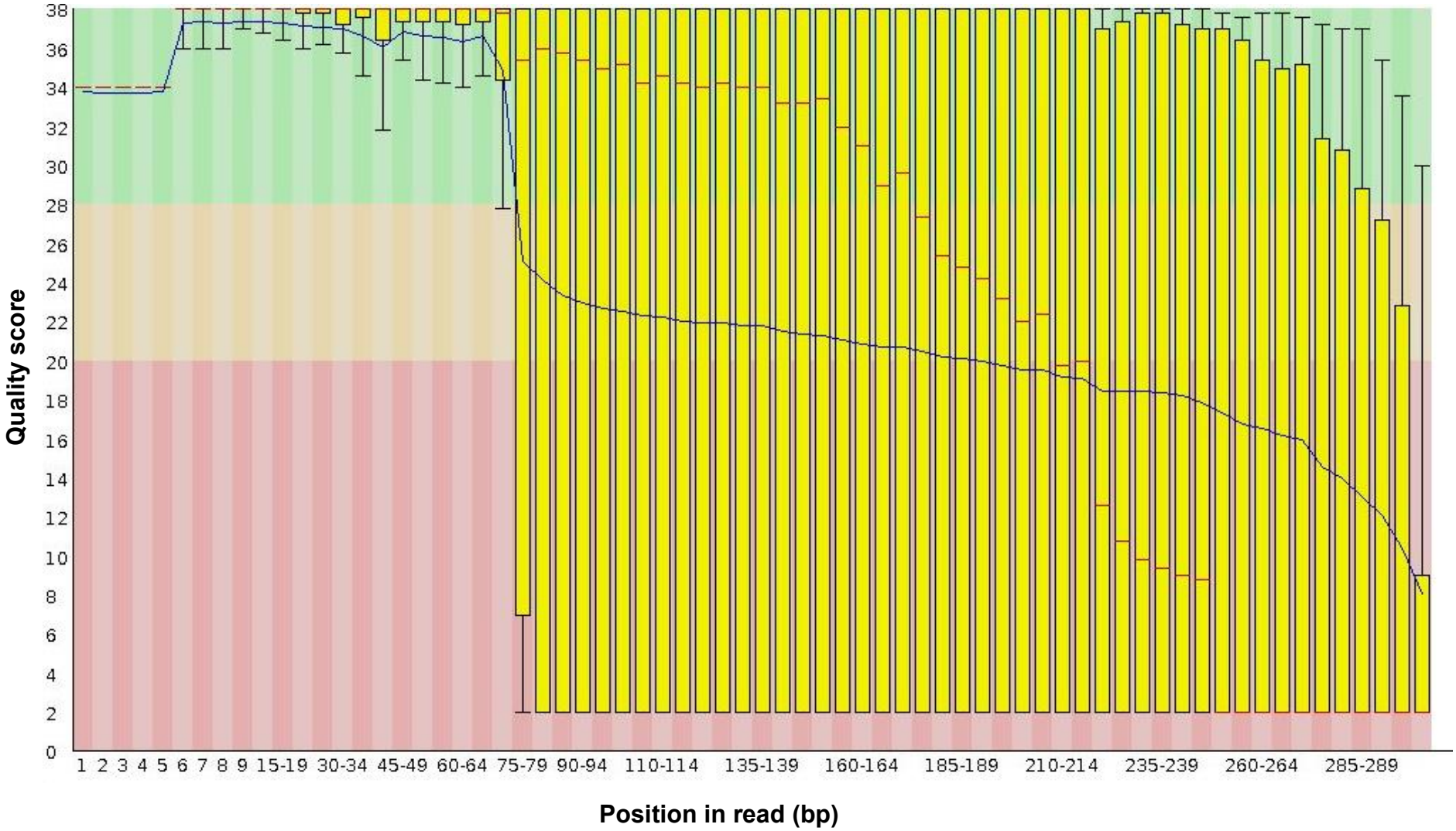

Figure 3.6: Example of 'per base sequence quality graphs' generated using FastQC software (Before trimming).

FastQC quality control toolkit (Babraham Bioinformatics, [184]) was used to assess the quality of sequencing reads within read file 0-4_cm_R1.

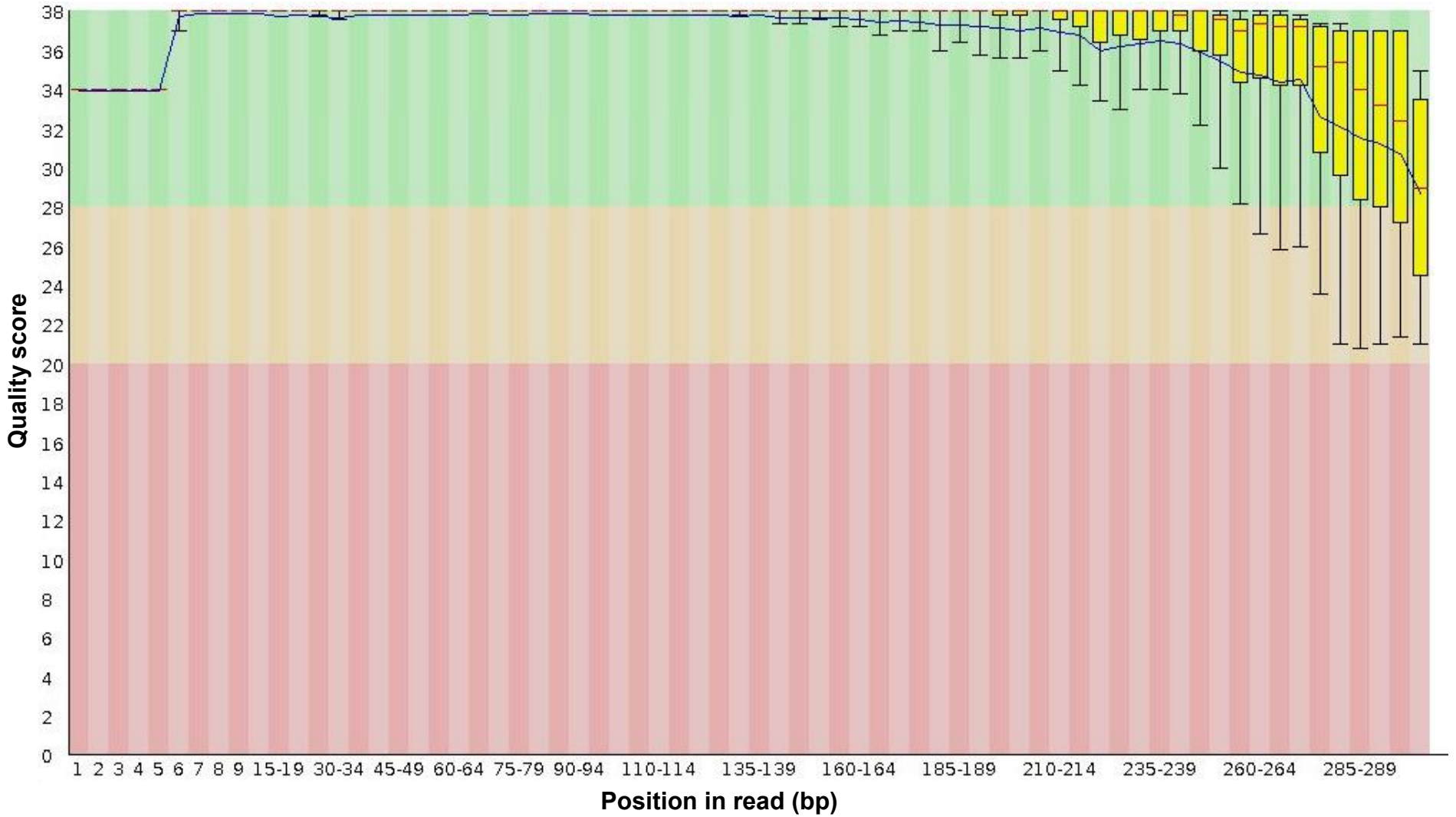

Figure 3.7: Example of 'per base sequence quality graphs' generated using FastQC software (After trimming).

FastQC quality control toolkit (Babraham Bioinformatics, [184]) was used to assess the quality of sequencing reads within read file 0-4_cm_R1.

3.2.5. Analysis using MEGAN (method 1)

The RefSeq database, which contains information on over 54,000 organisms [189] was chosen as the reference database for this investigation. BLAST output files were processed using MEGAN, an analysis tool designed for the processing of metagenomic data. The program processes the results of a BLAST output file to collect all hits of reads against known sequences. It then assigns a taxon ID to each sequence based on the given taxon [210]. This produces a MEGAN file that contains all information needed for analysing and generating graphical and statistical output [186].

MEGAN can estimate and explore the taxonomical content of the BLAST output, using the NCBI taxonomy to summarize and order the results. The program uses a simple algorithm which assigns each of the reads to the lowest common ancestor of the set of taxa that it hit in the comparison. This allows for species-specific sequences to be assigned to taxa near the leaves of the NCBI tree, whereas widely conserved sequences are assigned to high-order taxa closer to the root.

3.2.5.1. Generation of comparison phylogram

To allow for direct comparison between different layers of the sediment core, generated phylograms were combined within the MEGAN interface. A comparison phylogram, seen in Figure 3.8, was generated using normalised read counts. Each node is represented as a bar graph, to demonstrate the relative number of reads assigned to each taxonomic group. Each coloured bar refers to a layer of the sediment core. Where no bar graph is shown, for example at the Methanobacteria node, this indicates that all reads classified as Methanobacteria,

which has a taxonomic rank of ‘class’ were assigned into the more specific taxonomic group, the Methanobacteriales, which has a taxonomic rank of ‘order’. Bar charts generated at each branch point allow for direct comparison of abundance levels of a taxonomic group between different sections of the sediment core.

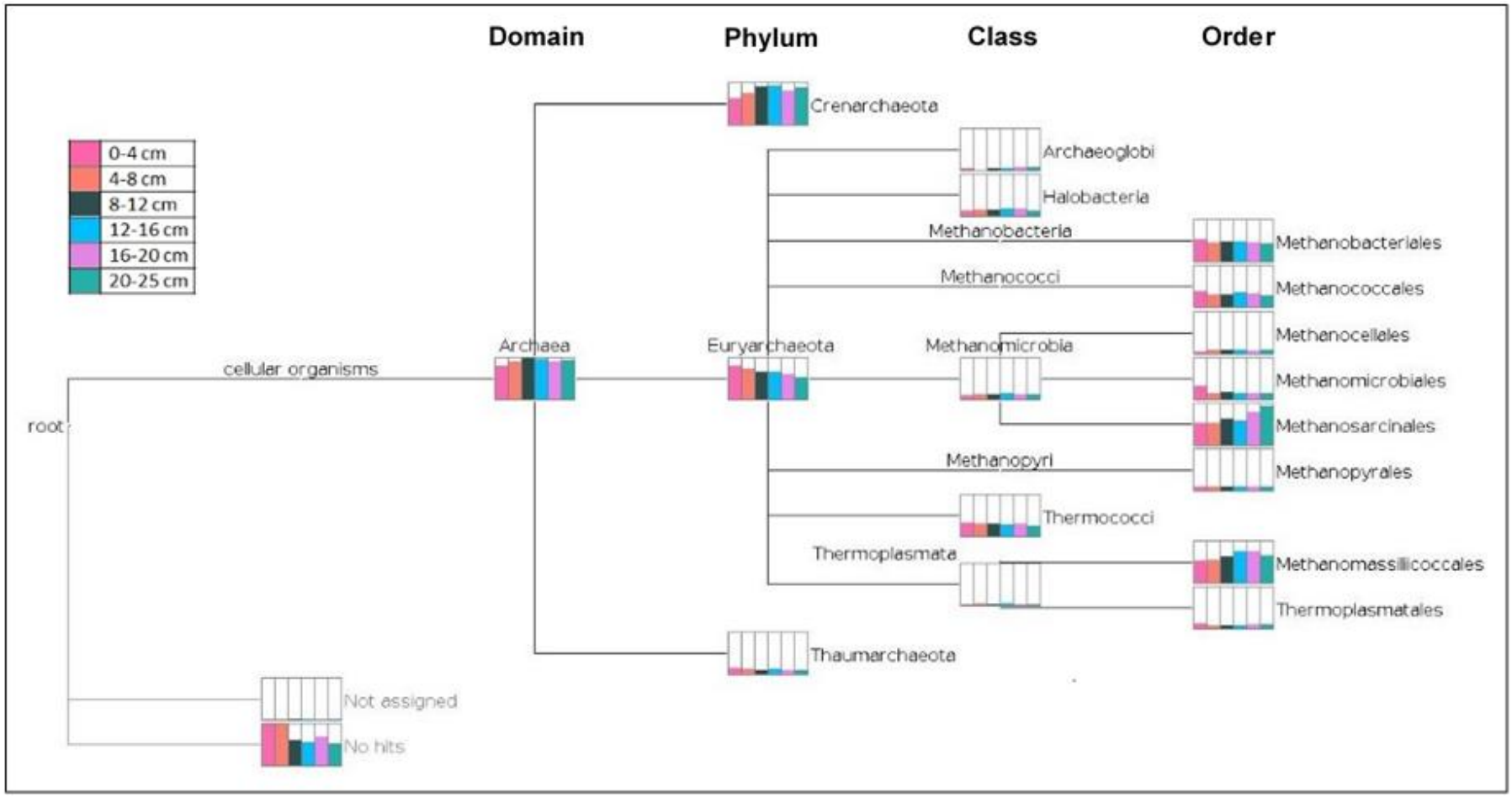

Figure 3.8: Comparison phylogram for the archaeal 16S rRNA sequencing of a 25 cm sediment core.

Reads were quality filtered and BLASTn searched against the RefSeq database. The BLAST outputs generated for each sample were fed in to MEGAN software and a phylogram generated for each sample. The MEGAN interface was used to create a comparisons phylogram, using normalised read counts. Each coloured bar refers to a different layer of the sediment core.

Sequencing of the archaeal 16S rRNA fragment, allowed for the detection of methanogenic sequences as well as other archaeal sequences. For this investigation, only methanogenic sequences were considered.

All methanogenic sequences are first distinguishable at the class level, where they can be separated into the Methanobacteria, Methanococci, Methanomicrobia and the Methanopyri. These groups form part of the Euryarchaeota, which is a phylum of the Archaea domain. All four methanogenic classes were detected within the phylogenetic analysis of the 25 cm sediment core. Methanogenic sequences are classified into a total of seven orders: Methanobacteriales, Methanococcales, Methanocellales, Methanomicrobiales, Methanosarcinales, Methanopyrales and the Methanomassiliicoccales, which were all detected within this 25 cm sediment core. Sequences belonging to the order Methanomassiliicoccales were wrongly classified into the Thermoplasmata class, and belong to the Methanomicrobia. This result is likely due to the relatively recent classification of the Methanomassiliicoccales as a new methanogenic order [68, 211], and it is possible that NCBI is currently out of date.

3.2.5.2. Visualisation of data using bubble charts

In order to better visualise patterns and trends within and between different methanogenic taxa, the combined phylogram in Figure 3.8, was converted into a series of bubble charts using the MEGAN interface [186]. Bubble charts were generated for the top 5 most abundant taxa detected at the class, order, genus or species level. These charts are shown in Figure 3.9.

Figure 3.9: The distribution of reads binned into various taxonomic groups across a 25 cm depth profile, represented by bubble charts using MEGAN software.

MEGAN was used to generate bubble charts to represent the respective abundances of the top 5 methanogenic groups at the class, order, genus or species taxonomic rankings within each of the sections of the 25 cm sediment core. The size of each bubble indicates the relative number of reads binned into that taxonomic group. The larger the bubble, the larger the number of reads classified.

The Methanomicrobia and Thermoplasmata were detected as the most abundant classes. Overall abundance of Methanomicrobia was marginally higher than that of Thermoplasmata, and demonstrated an increasing abundance with increasing depth of the sediment core. The depth profile for the Thermoplasmata class, increased down until a depth of 16-20 cm and was slightly reduced at a depth of 20-25 cm. Methanobacteria, Methanococci and Methanopyri were detected as the third, fourth and fifth most dominant classes respectively.

The top five most dominant methanogenic orders detected were the Methanosarcinales, Methanomassiliicoccales, Methanobacteriales, Methanococcales and the Methanomicrobiales. The trends in abundance of these orders followed the same trend in abundance of their respective parent classes, Methanomicrobia, Thermoplasmata, Methanobacteria and Methanococci. Methanomicrobiales were the least abundant order of the top five, approximately 3.5-fold less abundant that the Methanococci, and belong to the Methanomicrobia.

When classified at the genus level, the dominance of the most abundant methanogenic groups became prominent. *Methanomassiliicoccus* was detected as the most dominant methanogenic genus. This genus was approximately 7-fold more abudant than *Methanobrevibacter*, 9-fold more abundant than *Methanococcoides*, 30-fold more abundant than *Methanococci* and 38-fold more abundant than *Methanosarcina*. This trend was reflected in the dominance of its daughter species, *Methanomassiliicoccus luminyensis*. The depth profile of *Methanomassiliicoccus luminyensis* followed the same trend as its higher taxonomic groups, Methanomassiliicoccus (genus), Methanomassiliicoccales (order) and Thermoplasmata (class).

3.2.6. Analysis using One Codex pipeline (method 2)

Unlike other algorithms that try to reassemble their reads, One Codex compares the values of all its k-mer hits and arrives at the narrowest possible group of organisms that could be in the sample, making the processing time very fast [207].The One Codex interface allowed for comparisons between different layers of the sediment core to be generated and presented in a bar graph format. The minimum percentage abundance required for a taxonomic node to be displayed was set to 3 %. Comparisons were carried at the class, order, genus and species taxonomic levels, Figure 3.10. The One Codex analysis platform does not allow for non-methanogenic taxa to be removed from the graphical display. For this results section, and with the exception of the Thermoplasmata, only methanogenic taxa were considered. In the case of these analyses, sequences identified as 'other' form the nodes that make up less than 3% of the total classified reads. The most dominant class detected was the Methanomicrobia, which demonstrated an increase in abundance with increasing depth. Thermoplasmata was approximately 2.5-fold less abundant that the Methanomicrobia. The Methanococci, Methanobacteria and Methanopyri, were the third, fourth and fifth most dominant classes detected. All had similar overall abundance levels, approximately 9-fold lower than that of Methanomicrobia.

At the order level, the Methanosarcinales were the most abundant and displayed an increase in abundance with increasing depth. The second most abundant order was the Methanomassiliicoccales. The abundance of this order did not vary greatly across the depth of the sediment core. On average, Methanomassiliicoccales were approximately 3-fold less abundant than the Methanosarcinales. The Methanococcales, Methanobacteriales and the Methanocellales were the third, fourth and fifth most abundant methanogenic

classes and were 2-fold, 2.5-fold and 3-fold less abundant than the Methanomassiliicoccales respectively.

The most dominant group detected at the genus level was the *Methanococcoides.* The abundance of this group followed the same pattern of increasing abundance with depth as its parent order, the Methanosarcinales. Second most abundant genus was that of *Methanomassiliicoccus*, which also following the same trend in abundance as its parent order, Methanomassiliicoccales. The abundance of the *Methanococcoides* was approximately equal to the *Methanomassiliicoccales* in the top section of the sediment core. This transitioned to a 4-fold increase in abundance of the *Methanococcoides* as the depth profile of the sediment increased. *Methanosarcina* were the third most abundant genus detected and had comparable abundance to the *Methanomassiliicoccus*. *Methanosaeta* and *Methanocella* were the fourth and fifth most abundance genera detected and were approximately 3-fold less abundant than the *Methanomassiliicoccus*.

The most dominant methanogenic species detected using the One Codex analysis platform was the *Methanococcoides methylutens* followed by *Methanomassiliicoccus luminyensis*. The most notable difference in abundance of these two species is at the top and bottom layers of the sediment core. In the 0-4 cm sample, *Methanomassiliicoccus luminyensis* was 1.5-fold more abundant than *Methanococcoides methylutens.* In the 20-25 cm sample *Methanomassiliicoccus luminyensis* was 3-fold less abundant than *Methanococcoides methylutens*. Other species detected in the top five most abundance species were *Methanopyrus kandleri*, *Methanosaeta harundinacea*

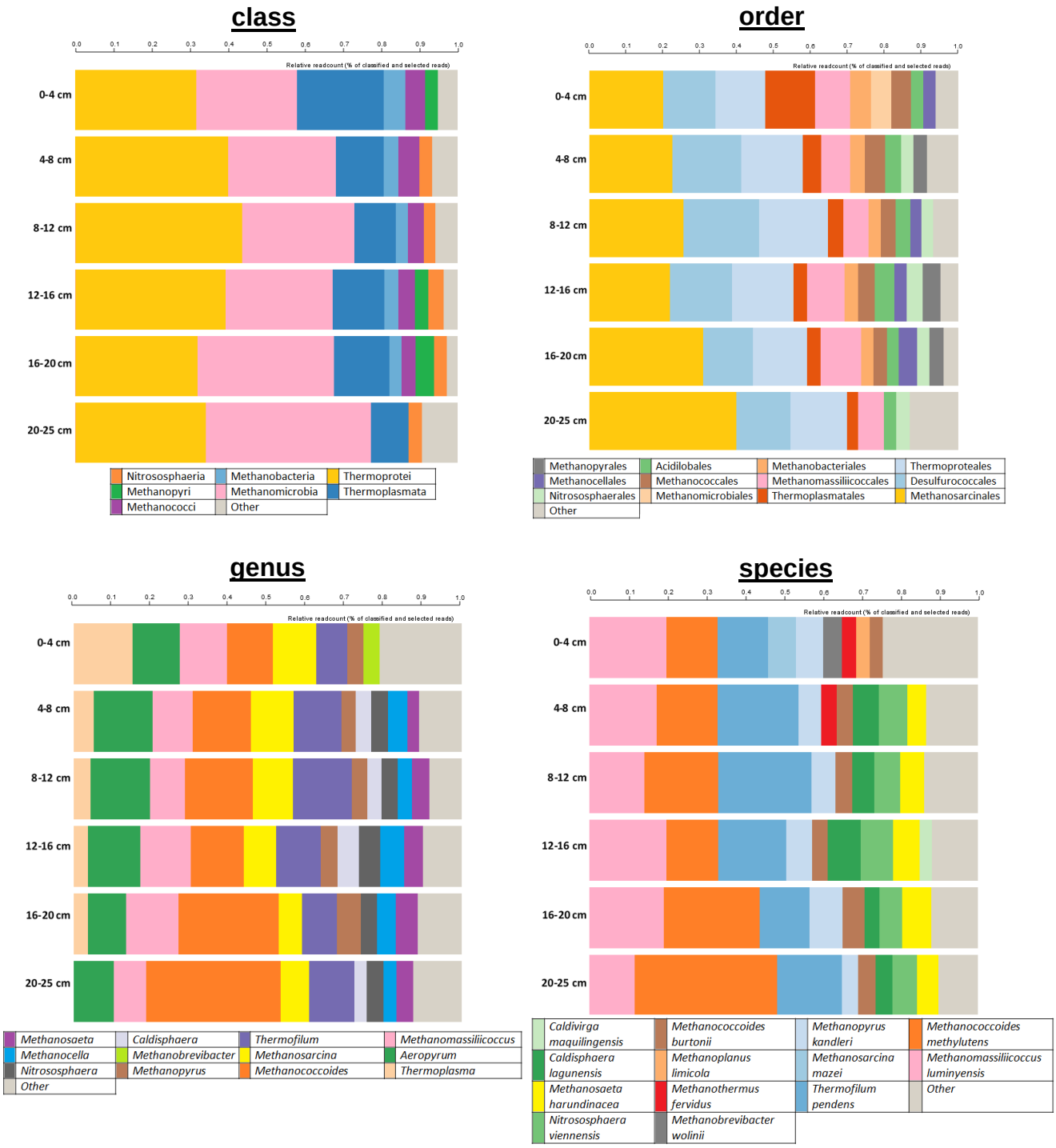

Figure 3.10: The relative distribution of reads binned into various taxonomic groups across a 25 cm depth profile, using One Codex analysis software.

Sequencing reads were generated from the 16S archaeal sequencing of DNA extracted from different depths of a 25 cm sediment core. The One Codex comparison tool was used to compare classifications assigned to each of the samples representing layers of the sediment core. Relative read counts were used. Classifications (min 3 %) were visualised at the class, order, genus and species taxonomic rankings.

and *Methanococcoides burtonii*. *Methanopyrus kandleri*, *Methanosaeta harundinacea* showed approximately similar levels in abundance and *Methanococcoides burtonii* was the least dominant.

3.2.7. Direct comparison of analysis method 1 and analysis method 2

Datasets generated using each of the different analysis methods were compared. For each dataset generated, the percentage proportion of the top five groups at different taxonomic rankings were calculated and plotted (Figure 3.11, Figure 3.12). The most notable trends were noted in the sections below.

The top five methanogenic orders detected were the same using both analysis methods, except for Methanomicrobiales and the Methanopyrales, detected by analysis methods 1 and 2 respectively. Methanosarcinales were the most abundant order of methanogens by both analysis methods. The dominance of the Methanosarcinales was approximately 1.6-fold higher when analysis method 2 was used in comparison to method 1. Both analysis methods established Methanomassiliicoccales as the second most abundant order, however the dominance of this order was approximately 1.8-fold higher when detected using analysis method 1 in comparison to method 2.

Methods 1 and 2 agreed on three of the top five methanogenic family groups detected, the Methanosarcinaceae, the Methanomassiliicoccaceae and the Methanocaldococcaceae. Method 1 detected Methanosarcinaceae and Methanomassiliicoccaceae in approximately equal proportions across the whole depth of the sediment core. Method 2 detected a 1.5-fold increase in abundance in Methanosarcinaceae, and a 1.8-fold decrease in abundance of Methanomassiliicoccaceae when compared to values obtained by analysis

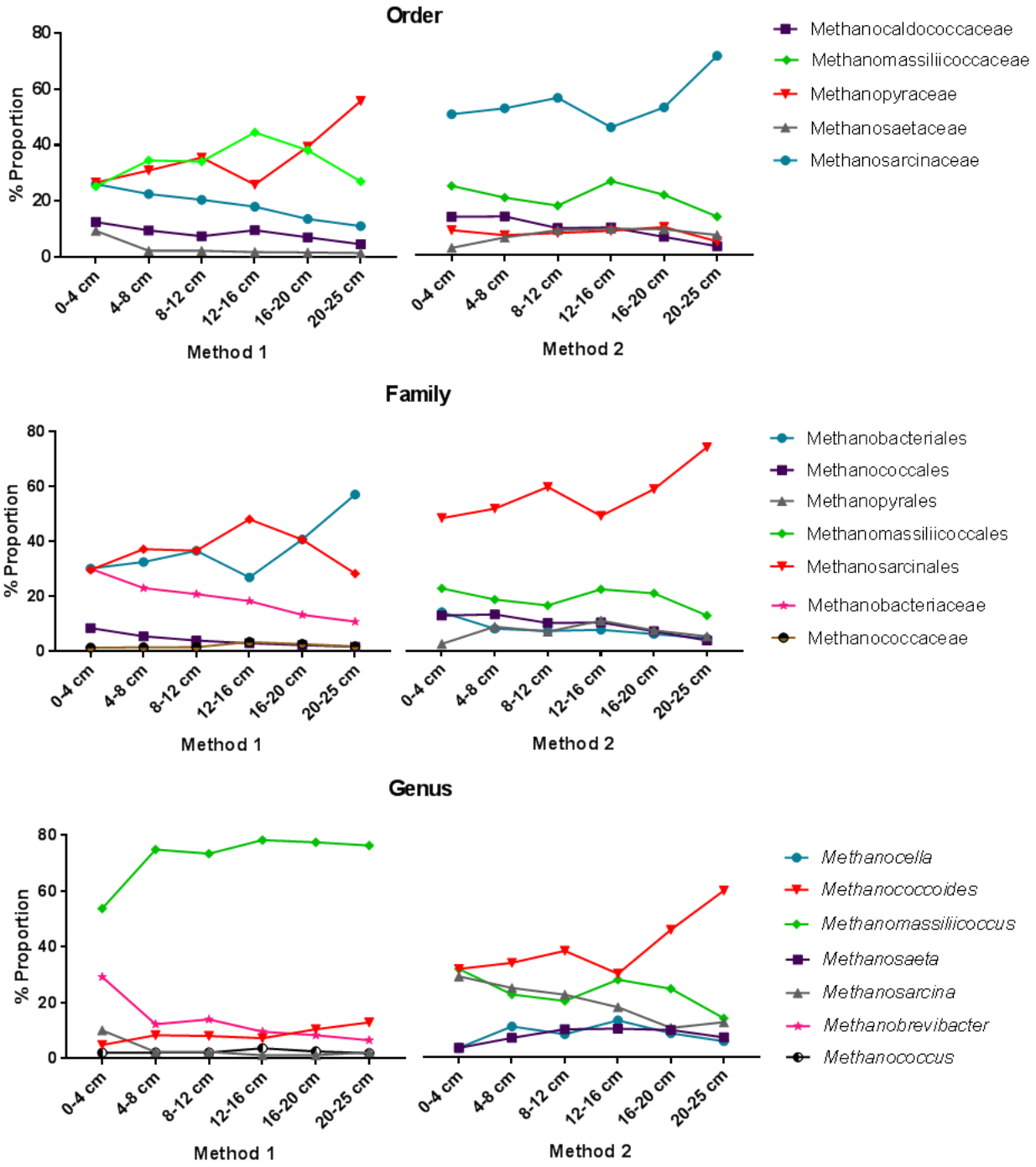

Figure 3.11: Direct comparisons of the phylogenetic analysis assigned to sequencing reads using method 1 versus method 2.

Quality filtered, and paired Illumina sequencing reads were generated from the 16S rRNA archaeal sequencing of DNA extracted from sections of a 25 cm sediment core. Reads were analysed using our two analysis methods. The relative abundances of the top 5 methanogenic groups detected at the order, family and genus level were calculated and plotted.

method 1. Both methods detected opposing patterns in abundance levels of Methanosarcinaceae and Methanomassiliicoccaceae.

When classifying at genus level, the differences in methanogenic groups detected became increasingly prominent. Method 1 detected a clear dominance of the *Methanomassiliicoccus* genus, approximately 3.3-fold higher than the abundance detected using analysis Method 2. Method 2 detected *Methanococcoides* as the most abundant genus, approximately 4.7-fold higher than that detected using analysis method 1. Methanosarcina was detected as being up to 15 times more abundant at sections within the sediment core using method 2 than when using method 1.

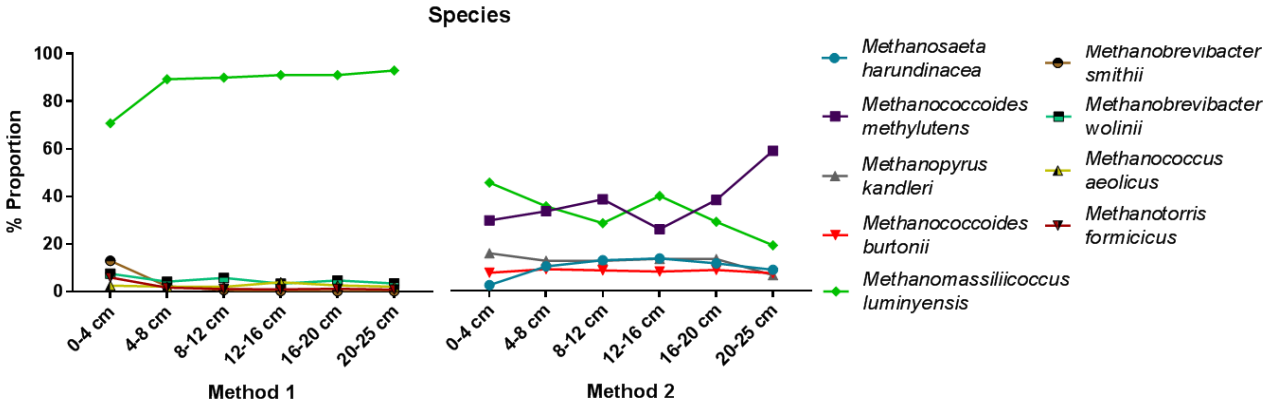

Figure 3.12: Direct comparisons of the phylogenetic analysis assigned to sequencing reads using method 1 versus method 2, at the species level.

Quality filtered, and paired Illumina sequencing reads were generated from the 16S rRNA archaeal sequencing of DNA extracted from sections of a 25 cm sediment core. Reads were analysed using two analysis methods. The relative abundances of the top 5 methanogenic groups detected at the species level.

Methanomassiliicoccus luminyensis was classified as the most abundant species when using analysis method 1. This dominance was very prominent, with all other species detected within the top five being approximately 35-fold to 180-fold less abundant. This abundance was also approximately 3-fold higher over the depth of the sediment core than the levels of *Methanomassiliicoccus luminyensis* using method 2. The most abundant species detected by analysis method 2 was that of *Methanococcoides methylutens,* which was not detected using analysis method 1, however its parent taxa were.

3.3. Part 2 – Methanogenic depth profile over 4 cm

Analysis of the 25 cm sediment core detected methanogenic sequences in every layer of the core, even in the very top 0-4 cm layer. The aim of the second part of this investigation was to discover how close to the very surface of the sediment the methanogens could be detected.

The mudflats at Exmouth were re-visited and new samples taken. A core roughly 10 cm in length was taken and transported back to the lab where it was sectioned into much finer 0.5 cm layers than done previously. Samples 0.0-0.5 cm, 0.5-1.0 cm, 1.0-1.5 cm, 1.5-2.0 cm, 2.0-2.5 cm, 2.5-3.0 cm, 3.0-3.5 cm, 3.5-4.0 cm were then subject to DNA extraction, PCR amplification, sequencing and analyses using the same methods as described for the 25 cm sediment core. For this results section, only the figures detailing the comparisons of the two different analysis methods are detailed. The outcomes of the individual analysis methods are provided in the appendices (section A1).

3.3.1. DNA extraction and quantification

Successful DNA extractions from every layer of the 4 cm sediment core were achieved. A negative correlation between eluted DNA concentration and the depth from which the DNA was extracted was observed. This correlation is clearly represented in Figure 3.13, which gives a graphical representation of the exact DNA concentrations isolated from each sediment samples, quantified using a Nano Drop (Thermo Scientific).

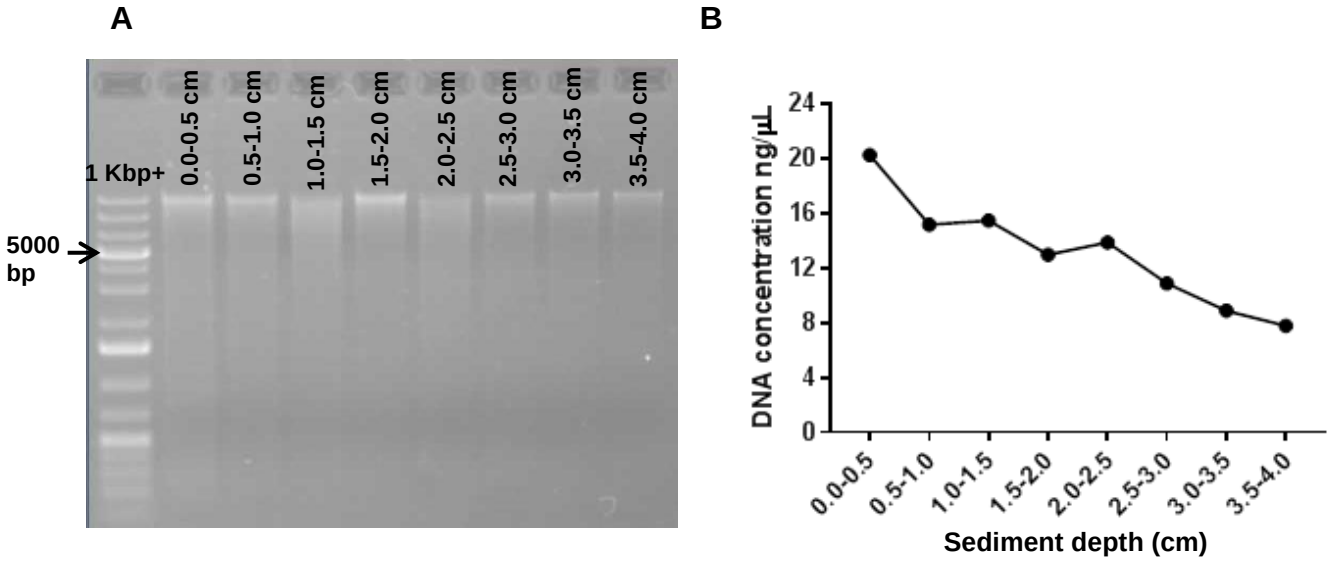

Figure 3.13: DNA extracts isolated from 0.5 cm layers of a 4 cm sediment core, sampled from estuarine mudflats at Exmouth, Devon, UK.

DNA was extracted from each 0.5 cm layer of a 4 cm sediment core. A) 10 µl of eluted DNA from each extraction was loaded into a 1 % agarose gel, containing Midori Green (Nippon Genetics) alongside a 1 kb plus DNA ladder. B) The concentration of each DNA extraction was quantified using a Nano Drop machine (Thermo Scientific). The arrow indicated the 5000 bp DNA marker.

3.3.2. DNA amplification with methanogen-specific primers (ML_F and ML_R)

DNA extracted from each layer of the 4 cm sediment core was subject to PCR with methanogenic specific primers (ML_F and ML_R). Product was electrophoresed on an agarose gel. DNA bands produced indicated the presence of methanogen DNA in every section of the sediment core. See Figure A1.1 in the Appendices.

3.3.3. PCR amplification with universal archaeal 16S PCR primers

Six replicate PCR reactions were carried out with template DNA isolated from each sediment layer. For each set of six replicates, a negative control (-ve), containing nuclease-free water in place of template DNA was included. PCR product from each of the reactions was then electrophoresed in 1 % agarose gels and gel purified. 5 µl of each purified PCR product from was then electrophoresed in a 1 % agarose gel (Figure A1.2, Appendices). These bands showed similarities in intensity and indicated successful DNA amplification and purified of the 16S rRNA gene from each of the sediment layers.

3.3.4. Results using the separate analysis methods

The sequencing and analysis methods used for the 4 cm core were the same as those used previously to sequence and analyse the 25 cm core. . Relative figures produced from analyses with method 1 and with method 2 can be found in the appendences (Figures A1.3, A1.4 and A1.5)

3.3.5. Comparison between methods

Results detected using each of the analysis methods were compared for the 4 cm core. The most notable trends were noted in the sections below (Figure 3.14, Figure 3.15). Except for the Methanomicrobiales, detected using method 1, and the Methanopyrales, detected using method 2, all other orders within the top 5 most abundant were the same when using both analysis methods. Methanosarcinales and the Methanomassiliicoccales were detected as the first and second most abundant orders. The overall abundance of the Methanosarcinales was approximately 1.5-fold higher when using analysis method 2 compared to method 1. The opposite trend was observed for the Methanomassiliicoccales, where a 1.5 fold-decrease in overall abundance was observed when analysis method 2 was used compared to method 1. The Methanobacteriales were the third most abundant order detected, their overall abundance using analysis method 1 was calculated as approximately 2-fold greater than when analysis method 2 was performed.

Except for Methanococcaceace, detected by method 1 and Methanopyraceae detected by method 2, all other families detected within the top 5 were the same using both analysis methods. Methanosarcinaceae and the Methanomassiliicoccaceae to be the first and second most abundant families detected by both methods. As detected with their parent taxa, the Methanosarcinales and the Methanomassiliicoccales, the abundance of Methanosarcinaceae detected using analysis method 2 was 1.5-fold greater than when using method 1. The abundance of the Methanomassiliicoccaceae, was calculated to be 1.5-fold lower when using analysis method 2 compared to method 1.

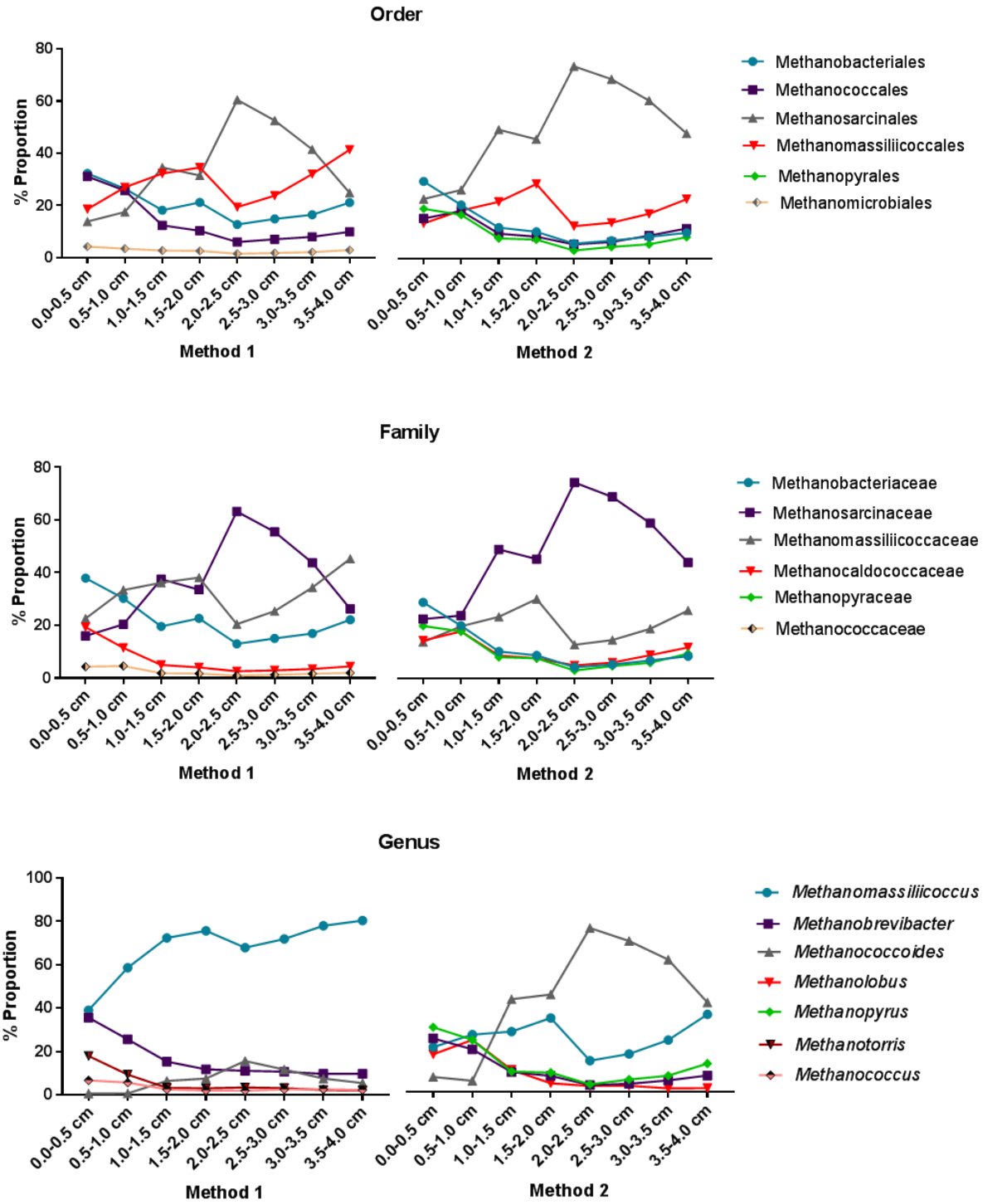

Figure 3.14: Direct comparisons of the phylogenetic analysis assigned to sequencing reads using method 1 versus method 2 for the 4 cm sediment core.

Quality filtered, and paired Illumina sequencing reads were generated from the 16S rRNA archaeal sequencing of DNA extracted from sections of a 4 cm sediment core. Reads were analysed using our two analysis methods. The relative abundances of the top five methanogenic groups detected at the order, family and genus level were calculated and plotted.

At the genus level, trend in taxa identified using our two different analysis methods became distinct from one another. *Methanomassiliicoccus* were determined as the most dominant genus when analysis method 1 was used. This abundance of this genus was calculated as being on average 3-fold greater than it abundance detected using method 2. When analysis method 2 was used, *Methanococcoides* was the most abundant genus and its abundance was calculated as being approximately 7-fold greater over the depth of the sediment core than when analysis method 1 was used. The detection of *Methanobrevibacter* was approximately 2-fold more when using analysis method 1 compared to method 2.

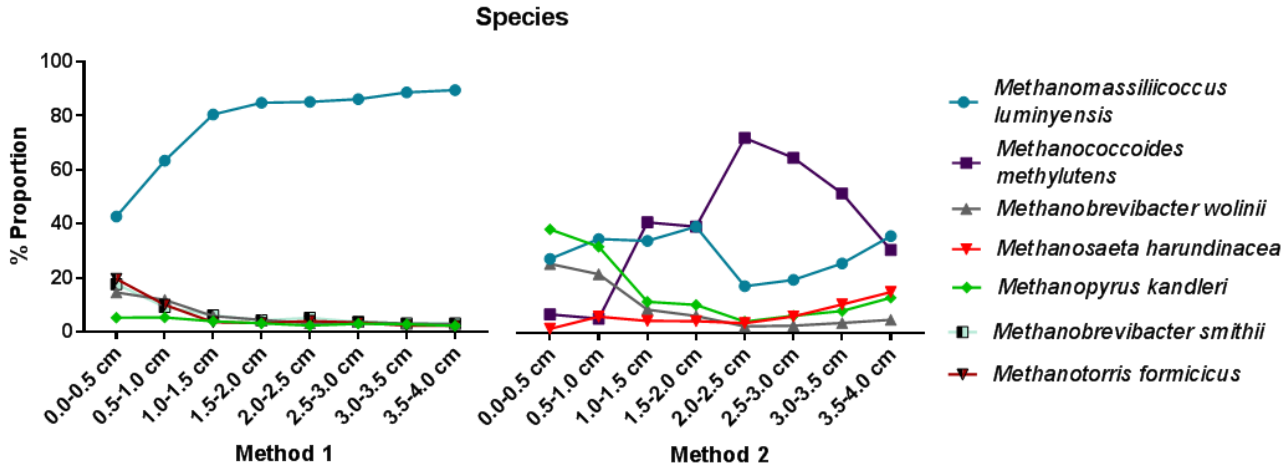

Figure 3.15: Direct comparisons of the phylogenetic analysis assigned to sequencing reads using method 1 versus method 2, for the 4 cm core, at the species level.

Quality filtered, and paired Illumina sequencing reads were generated from the 16S rRNA archaeal sequencing of DNA extracted from sections of a 4 cm sediment core. Reads were analysed using our two analysis methods. The relative abundances of the top five methanogenic groups detected at the species level.

Methanomassiliicoccus luminyensis was classified as the most abundant species when using analysis method 1. As with the results obtained for the 25 cm depth profile, the dominance of *M. luminyensis* was very prominent. The overall trends in abundance of *M. luminyensis* varied greatly depending on the analysis method. The most abundant species detected by analysis method 2 was that of *Methanococcoides methylutens,* which was not detected using analysis method 1. As with its parent taxonomic groups, *Methanococcoides methylutens* demonstrated an increasing abundance up to a depth of 2.5 cm and then sharply decreased throughout the remainder of the sediment core.

3.4. Discussion

As discussed in Chapter 1, methanogens are found in a diverse range of environments, from the sediment of rice paddies and peat bogs, to hydrothermal vents and the digestive tracts of insects and animals. Although initially thought to be strictly anaerobic, methanogens have been found in some environments where they are subject to aeration, indicating that these methanogens may have a degree of oxygen tolerance. The aim of this project was to investigate the depth profile of methanogens within estuarine mudflat sediment of the River Exe Estuary, Devon, UK. This type of environment was chosen due to its intermittent exposure to the atmosphere during low tide. The small number of published studies, focusing on methanogenic communities within estuarine environments, was also a contributing factor to my decision. Of these studies, many have focused on the relation of methanogen community to salinity gradient, which, despite being an important consideration, was not the primary centre of this study. To my knowledge, this is the only study which has focused on estuarine sediment for the discovery of potentially oxygen tolerant methanogens.

Archaeal 16S sequencing was used to investigate the methanogenic community within this chosen environment, using the primer pair A571_F and UA1204_R. These primers had been previously proven to successfully amplify many methanogenic taxa [59]. Recent years have witnessed increasing debate on the consistency and reliability of different metagenomic analysis tools, and it is now common for more than one analysis technique be used [212]. For this investigation, I employed two different analysis techniques to compare the generated datasets against the RefSeq database. For the first (method 1), filtered and paired reads were compared against the RefSeq database using BLASTn and the output analysed using MEGAN software. MEGAN uses lowest common

ancestry to assign taxonomy, a popular technique for the analysis of metagenomic studies, [213, 214]. For the second (method 2), filtered and paired reads were fed directly into the One Codex online analysis tool. This tool that identifies reads using a k-mer mapping approach which also uses the RefSeq database [187].

During the analysis of the of the 25 cm depth profile, the abundance levels of 16S rRNA sequences closely relating to methanogenic taxa detected in the top layer of the sediment core (0-4 cm) were noted. Despite an overall trend of increasing abundance of these sequences with depth, the levels of methanogenic taxa detected in the 0-4 cm layer were often comparable to the levels detected in lower sections of the sediment core, such as the 8-12 cm and 12-16 cm sections. This result was promising as this investigation aimed to identify methanogens in the very top sections of the sediment core. For the second part of this investigation, I endeavoured to discover how close to the very surface of the sediment the methanogens could be detected. For this, the River Exe Estuary mudflats were revisited, and smaller depth of 4 cm was sampled. This 4 cm depth profile was sectioned into smaller 0.5 cm subsamples and studied using the same techniques applied previously for the 25 cm core.

When using method 1 for the analysis of both the 25 cm depth profile and the 4 cm depth profile, very similar trends were produced. Both methods detected sequences closely relating to *Methanomassiliicoccus luminyensis*, an obligate H_2-dependent methylotrophic methanogen as the most dominant at the species level. Analysis of the 25 cm depth profile indicated approximately a 1.3-fold increase in *Methanomassiliicoccus luminyensis* relative abundance between the 0-4 cm and 4-8 cm layer of the sediment core. The abundance of *M. luminyensis*

then remained constant throughout the remaining depth of the sediment core. When analysing the depth profile of *M. luminyensis* over 4 cm, a 2-fold increase was observed in abundance over the first 1.5 cm depth, and then remained constant for the remainder of the depth of the core. This result suggested that the biggest changes in *M. luminyensis* abundance occur over the first 1.5 cm surface layers of the mudflat sediment.

When using method 2, sequences closely relating to *Methanococcoides methylutens*, a methylotrophic methanogen (not H_2-dependent), were detected in high abundance within both sediment cores. However, this dominance was only marginally greater than *M. luminyensis* in the 25 cm sediment core. An interchanging pattern of increasing and decreasing abundance was observed for *M. methylutens* throughout both depth profiles, appeared to directly oppose the trends seen in *M. luminyensis*. This result could suggest that, if present, these two methanogen species were in direct competition with one another for methylated compounds. This competition may also be influenced by the presence of hydrogen-utilising sulphate reducing bacteria (SRB), which will be in direct competition with *M. luminyensis* but not with *M. methylutens*.

Estuaries consist of a freshwater inlet and then become brackish, before progressing to the saltiest zone closest to the sea, the salinity profile of the Rive Exe Estuary can be seen in Figure 3.2. Freshwater sediments zones are often low in sulphate, whereas brackish and salt water zones are high in sulphate. These sulphate gradients affect the abundance of sulphate reducing bacteria (SRB). SRB compete with methanogens for hydrogen and acetate or both, and are therefore capable of outcompeting acetoclastic and hydrogenotrophic methanogens [215]. However, SRB do not utilise methylated compounds and

therefore do not compete with methanogens for substrates such as methylated amines and methanol [215]. Freshwater sediments are often dominated by a range of methanogens, especially acetate-utilising methanogens such as *Methanosaeta* [216]. Whereas brackish and salt zone areas of estuaries are more likely to harbour methylotrophic methanogens, such as *Methanolobus* and *Methanococcoides*. These patterns have been observed during other studies, when comparing a freshwater site (East Bridge Hill) and a saltwater site (Colne Point) of the Rive Colne estuary, Essex, UK [216] and in other similar studies including the work of Webster *et al.,* 2015 [217] and work that have studied either brackish/marine sediments, [218, 219], and freshwater sediments independently [220]. My chosen sample site, was in the saltiest zone of the Exe estuary (see Figure 3.2), which would indicate a high abundance of SRB. This potentially explains why the most abundant methanogens observed are methanogen species capable of utilising methylated substrates.

Trends in abundances of most dominant species were not always reflected in the trends in abundances seen of their relative higher taxonomic groups. When using method 1 to analyse data from both the 25 cm and the 4 cm depth profiles, Methanosarcinaceae were detected as the most dominant family taxa. However, *Methanomassiliicoccus* and *M. luminyensis* were the most dominant at the genus and species level and belong to the Methanomassiliicoccales family, not the Methanosarcinaceae. The profiles produced for the Methanosarcinaceae using both analysis methods 1 and 2 were very similar in both the 25 cm and the 4 cm cores. This suggests that many species belonging to the Methanosarcinaceae were present in the sediment samples, however the reads generated for these species were not be detected at the genus and species taxonomic levels. Given that the most dominant species detected using method 2 was that of the

Methanococcoides methylutens, a member of the Methanosarcinaceae, it is possible that reads classified only as far as Methanosarcinaceae, using method 1, relate closely to *Methanococcoides methylutens.*

These findings indicate a presence of methanogenic organisms in the very surface layers of the mudflat sediment, predominantly those that can utilise methylated compounds for their metabolism. However, the detection of methanogenic DNA does not confirm whether any methanogens present are alive and actively producing methane gas. Further investigation of this sample site using enrichment techniques was required to assess for methanogen activity.

4. Chapter four: Enrichment and identification of methanogens within surface layer estuarine mudflat sediment

4.1. Introduction

Previous 16S analyses of the methanogenic communities in the estuarine mudflat of the River Exe Estuary by Exmouth, detected the presence of methanogenic DNA in the very surface 0.5 cm layer of the sediment. This result was intriguing due to the strict anaerobic nature of the methanogenic archaea, however not a complete surprise, as some studies have identified methanogens from the natural environment with an increased tolerance to oxygen [197-204]. Exposure to oxygen is a problem for all life forms because of the creation of unstable reactive oxygen species (ROS) such as hydrogen peroxide and superoxide. Aerobes typically produce antioxidant enzymes including superoxide dismutase (SOD) and catalase enzymes which can break down ROS into less toxic molecules [221]. Although methanogens do not require oxygen as a terminal electron acceptor, they may be exposed to oxygen and also require a line of defence against reactive oxygen species [203]. There is growing evidence that indicates the presence of antioxidant enzymes within certain species of methanogens. Some methanogens have even been found to produce methane in the presence of low levels of oxygen. *Methanobrevibacter cuticularis*, which was first isolated from the hindgut of termites, is an example of such methanogen. However, the specifics of its ROS defence system are still unclear [222].

The work detailed within this chapter describes the enrichment of methanogenic archaea from the surface sediment layers collected from the mudflats of the River Exe Estuary by Exmouth, Devon, UK. A 2 cm core was sampled and sectioned into 0.5 cm layers. Each layer was then individually enriched on a variety of different substrates. Methanogen growth within enrichments was measured and successful cultures underwent further rounds of sub-culturing for the attempted isolation of methanogenic species. Whole

genome analysis was then performed on the enriched samples for the identification of methanogen species.

4.3. Results

4.3.1. Total DNA extraction and initial screening for methanogens

Before enrichment, a 0.25 g sample of sediment from each layer was subject to total DNA extraction. To confirm the presence of methanogens, DNA (Figure 4.2, panel A) was used as a template and PCR amplified with methanogen specific primers alongside controls (Figure 4.2, panel B).

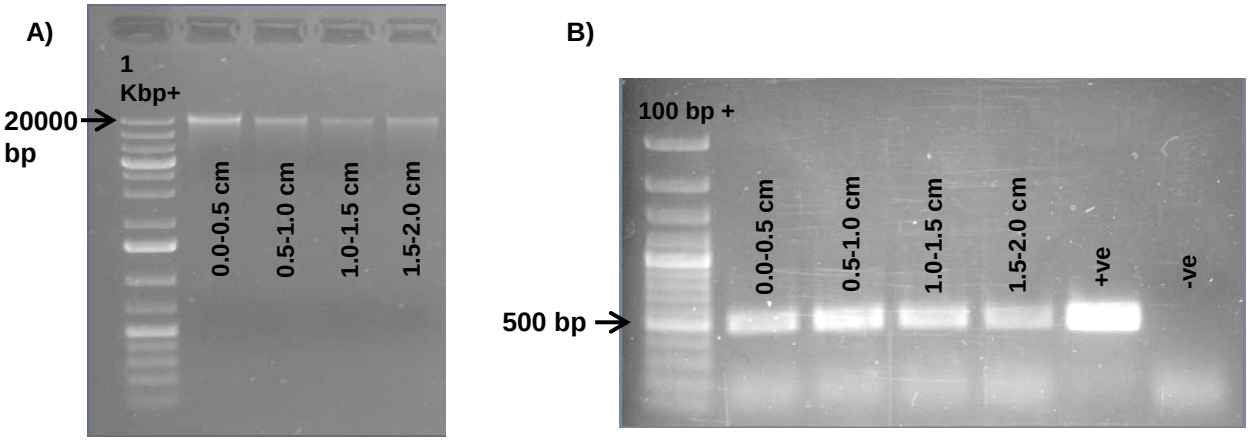

Figure 4.2: DNA extraction and amplification from layers of a 2 cm sediment core, sampled from the River Exe Estuary mudflats, Exmouth, Devon UK.

DNA was extracted from 0.5 cm layers of a 2 cm sediment core using the PowerMax Soil DNA Isolation kit (Mo Bio). A) Gel electrophoresis of raw DNA extract. B) Gel electrophoresis of products generated from DNA amplification with ML_F and ML_R primers; positive control (+ve)s: template = methanogen DNA (donated from Prof. Orkun Soyer's lab, University of Warwick, UK). Negative control (-ve)s: template = nuclease-free water. Sample names are indicated on each of the gel images. DNA ladders, provided by Thermo Fisher Scientific: A) 1 Kb Plus, arrow indicates 20 Kbp marker. B) 100 bp Plus, arrow indicated 500 bp marker.

The ML_F and ML_R primers were expected to amplify a 470 bp region of the methanogen-specific *mcrA* gene. Every PCR reaction containing template DNA extracted from each layer of the 2 cm sediment core produced a DNA band. All

DNA bands ran very slightly below the 500 bp marker of the 100 bp plus ladder, indicating that they were the expected size of 470 bp. This result indicated that all layers of the 2 cm core contained methanogenic DNA sequences. The intensity of the DNA bands produced indicated that the 0.5-1.0 cm layer contained the highest abundance of DNA derived from methanogens.

4.3.2. Progress of enrichment cultures

4.3.2.1. Gas production from enrichment cultures

Total gas pressure was measured weekly from each enrichment, for a period of six weeks after inoculation (Figure 4.3). Increasing gas pressure was interpreted as gas production and for this results section, the progress of enrichments will be discussed in terms of gas production, not pressure.

Sediment layers 0.0-0.5 cm and 0.5-1.0 cm began producing gas after four weeks incubation, whereas sediment layers 1.0-1.5 cm and 1.5-2.0 cm began producing gas after three weeks incubation. For all four sediment layers, a cocktail of TMA, methanol and acetate resulted in the highest gas production over the course of the enrichment period. Enrichments onto ‘TMA only’ and ‘methanol only’ produced comparable results when considering each sediment sample; however, gas production on these substrates was approximately 1.2-fold to 1.4-fold lower than that of the enrichments containing a cocktail of TMA, methanol and acetate. For all four sediment layers, minimal or no gas production was observed for samples enriched in acetate medium. Gas production was also not observed from any control enrichments, which contained sterilised sediment samples.

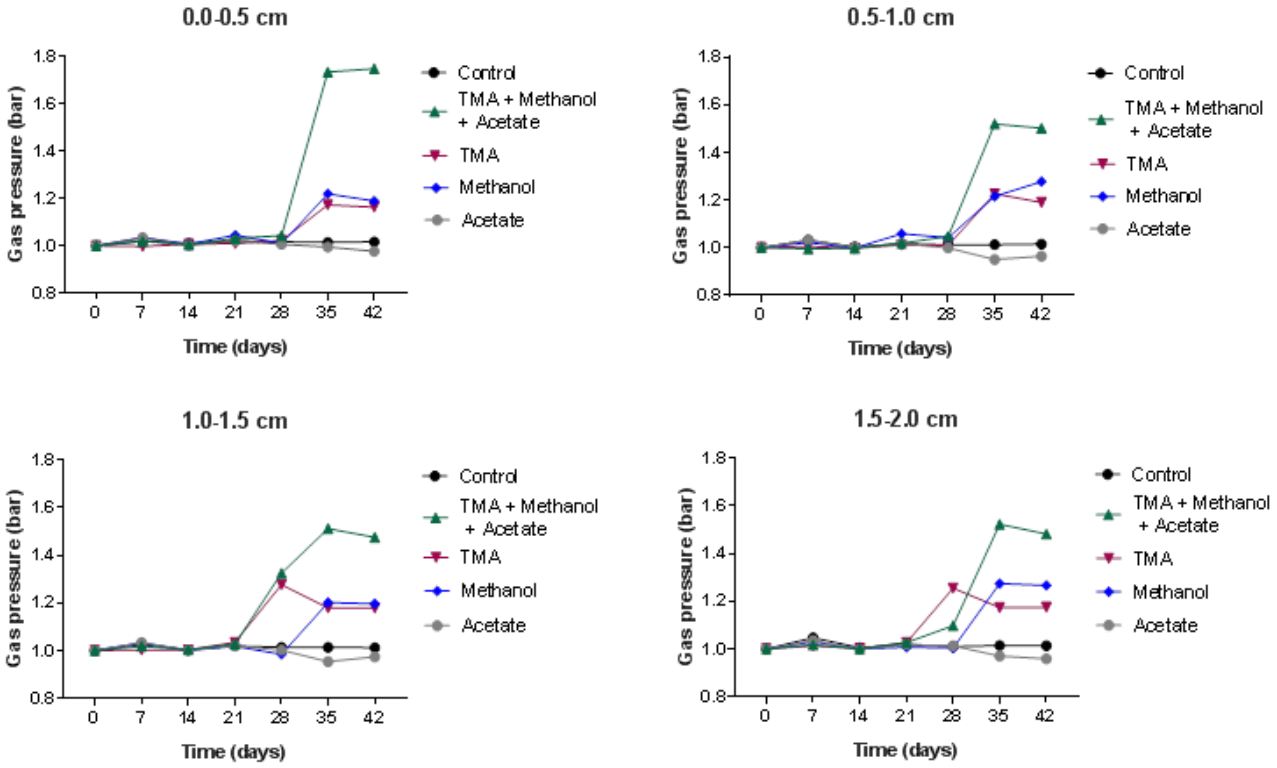

Figure 4.3: Total gas pressure monitored from the methanogen enrichment cultures of estuarine sediment samples.

Gas pressure within each enrichment vessel was monitored weekly for a period of 6 weeks using a gas manometer (Keller). The colour of the plots indicates the substrate onto which the cultures were enriched. The concentrations of substrates used were: TMA, 20 mM; methanol, 40 mM; acetate, 40 mM. Control enrichments contained all three enrichment substrates and were inoculated with sterilised sediment. The title of each graph denotes the sediment layer used to inoculate each enrichment.

Given the success of enrichments grown on a cocktail of TMA, methanol and acetate, these enrichments were directly compared on the same axes seen in Figure 4.4, to observe which sediment layer had the highest production of gas. The very surface 0.0-0.5 cm sediment layer produced the highest volume of gas

when enriched on a cocktail of TMA, methanol and acetate. Gas production from this layer was approximately 1.15-fold higher than all other layers.

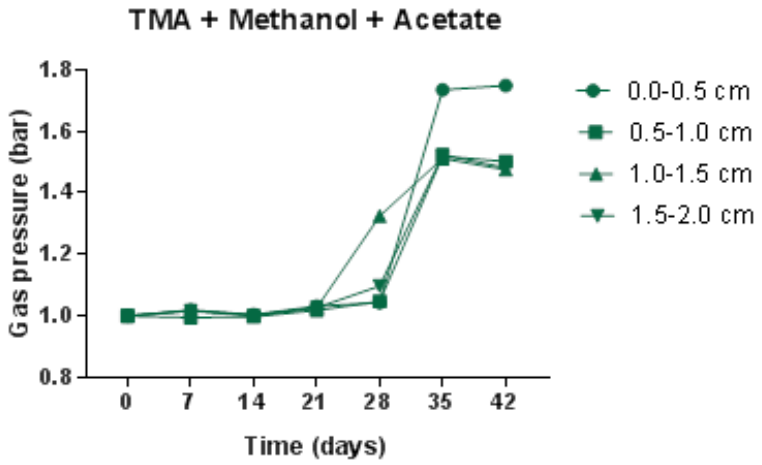

Figure 4.4: Comparisons of gas production of samples enriched on a combination of TMA (20 mM), methanol (40 mM) and acetate (40 mM).

Gas production for all four sediment layers enriched onto a combination of TMA (20 mM), methanol (40 mM) and acetate (40 mM) were compared directly on the same axes.

Throughout the enrichment process, occasional drops in gas pressure were observed. For example, gas pressure observed for 1.0-1.5 cm sample enriched onto TMA dropped between four and five weeks incubation. Although gas production may have halted, gas pressure is not expected to decrease, due to the sealed nature of the culture vessels. Therefore, the observed drop in gas pressure could be due to leakage from the manometer during readings. If the small amounts of gas that are lost during each pressure measurement are not replaced by further gas production, then an overall drop in gas production will be observed.

4.3.2.2. Methanogen-specific PCR screening of enrichment cultures

End-point PCR using methanogen specific primers (ML_F and ML_R) was used to monitor the progress of enrichment cultures. The intensities of the amplicons gave an indication of the enrichment for methanogenic species. Figure 4.5 shows two different examples of how this method was applied. Gel A compares DNA extracts from the 0.0-0.5 cm sediment sample enriched on a cocktail of TMA, methanol and acetate after 1 week incubation and then again after 5 weeks incubation. Gel B compares the 0.0-0.5 cm sediment sample enriched on acetate only vs a cocktail of TMA, methanol and acetate, these DNA extracts were both performed after 5 weeks enrichment.

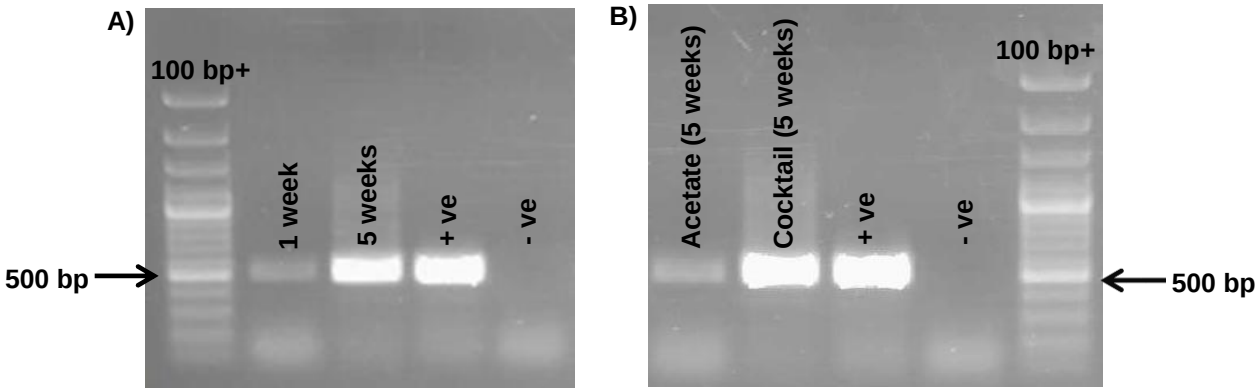

Figure 4.5: Comparison of methanogen DNA band intensities from methanogen enrichment cultures.

DNA extracts from enrichment cultures were subject to PCR with methanogen specific primers (ML_F and ML_R) and band intensities of PCR products compared. Gel A) 0.0-0.5 cm layer enriched onto a cocktail of TMA, methanol and acetate, DNA extractions performed after 1 week incubation and 5 weeks incubation. Gel B) 0.0-0.5 cm layer enriched onto a cocktail of TMA, methanol and acetate compared with the same 0.0-0.5 cm layer enriched onto acetate only. DNA extractions from each enrichment were both performed and subject to PCR after 5 weeks incubation. Positive control (+ve)s: template = methanogen DNA (donated from Prof. Orkun

Soyer's lab, University of Warwick, UK). Negative control (-ve)s: template = nuclease-free water DNA ladder used: 100 bp plus, Thermo Fisher Scientific, arrows indicate 500 bp marker.

Clear differences in band intensities were observed. Bands in Gel A showed an increase in methanogen DNA detected by PCR after five weeks enrichment versus one-week enrichment, suggesting the growth of methanogens. Gel B indicates that methanogens have grown to a higher density in a cocktail of TMA, methanol and acetate versus acetate only. This result suggests the enrichment of methylotrophic methanogens over the five-week incubation period.

4.3.2.3. Turbidity of enrichment cultures

There were noticeable differences in the turbidity of different enrichments. These differences were visually detectable and provided some indication of the progress of the enrichment cultures. Figure 4.6 is an example of sediment layer 0.0-0.5 cm enriched onto a 'cocktail' of TMA, methanol and acetate (picture A) compared with the same sediment layer enrichment onto acetate only (picture B). Pictures were taken after 5 weeks incubation. There was an obvious increase in turbidity of enrichment samples provided with a cocktail of TMA, methanol and acetate, rather than acetate only. This indicated that the presence of either TMA or methanol (or a combination of both) encouraged the growth of organisms, possibly suggesting the enrichment of methylotrophic methanogens and supported the conclusions drawn in section 4.3.2.2.

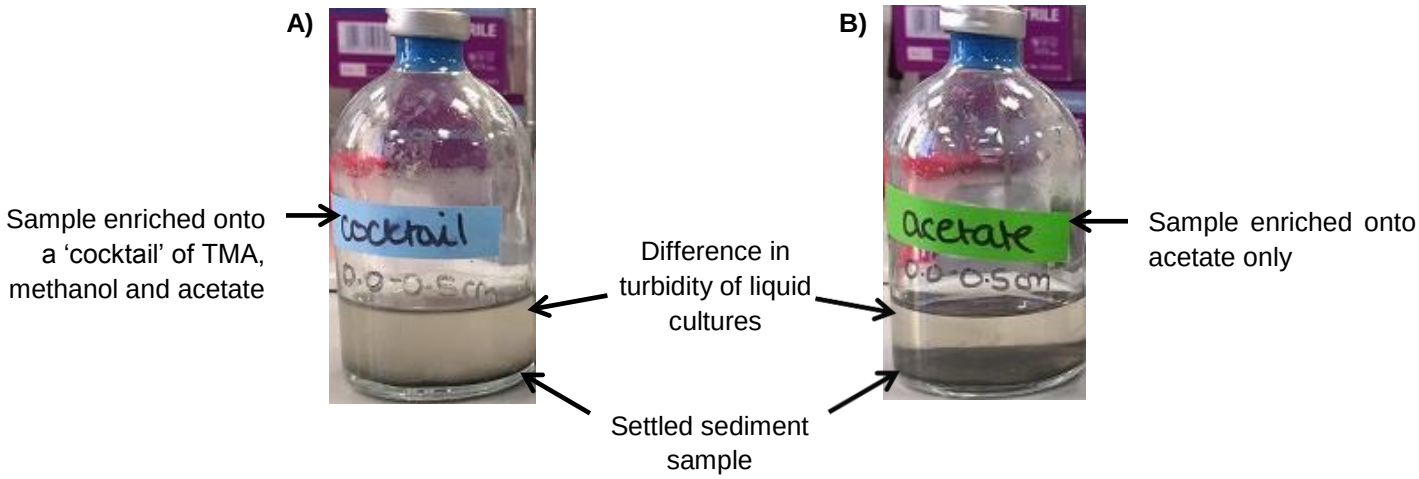

Figure 4.6: Visual example of differing turbidity between enrichment cultures.

Visual comparison of the turbidity of two enrichment cultures each inoculated with the same sediment sample, 0.0-0.5 cm, (samples from the River Exe Estuary mudflats by Exmouth, Devon). Picture A) sediment sample was enriched onto a cocktail of TMA, methanol and acetate. Picture B) sediment sample enriched onto acetate only. Cultures were incubated anaerobically into the dark at ambient temperature (approximately 20 °C) for 5 weeks before pictures were taken.

4.3.3. Gas production from further rounds of sub-culturing

This investigation aimed to isolate methanogenic species from the surface layers of mudflat sediment. The culture containing the 0.0-0.5 cm sample enriched onto a combination of TMA, methanol and acetate was further sub-cultured onto TMA only, methanol only and a combination of TMA/methanol. Each substrate concentration was the same as used previously. Acetate was omitted as a substrate from further investigations due to the lack of gas production from samples enriched onto acetate only. This lack of methanogen enrichment on acetate was also supported by examining DNA band intensities produced in the

Figure 4.5 as detailed earlier. All further enrichments were incubated in the dark at 20°C.

Figure 4.7 displays the gas pressures observed from further rounds of enrichment of the 0.0-0.5 cm sample. The first round of sub-culture was performed in duplicate and gas production was monitored for six weeks. Sub-cultures began producing gas after the first week of incubation, with the highest levels of gas produced from cultures containing a combination of TMA and methanol. This result agreed with previous data obtained from the original enrichments. Lower levels of gas production were observed from cultures containing either TMA only or methanol only. For the second round of sub-culturing (also performed in duplicate), cultures containing only a combination of TMA and methanol were taken forward. This second round of sub-cultures was monitored for four weeks. Gas production was detected within two weeks and peaked after three weeks incubation, at which point the cultures were inoculated onto agar slants.

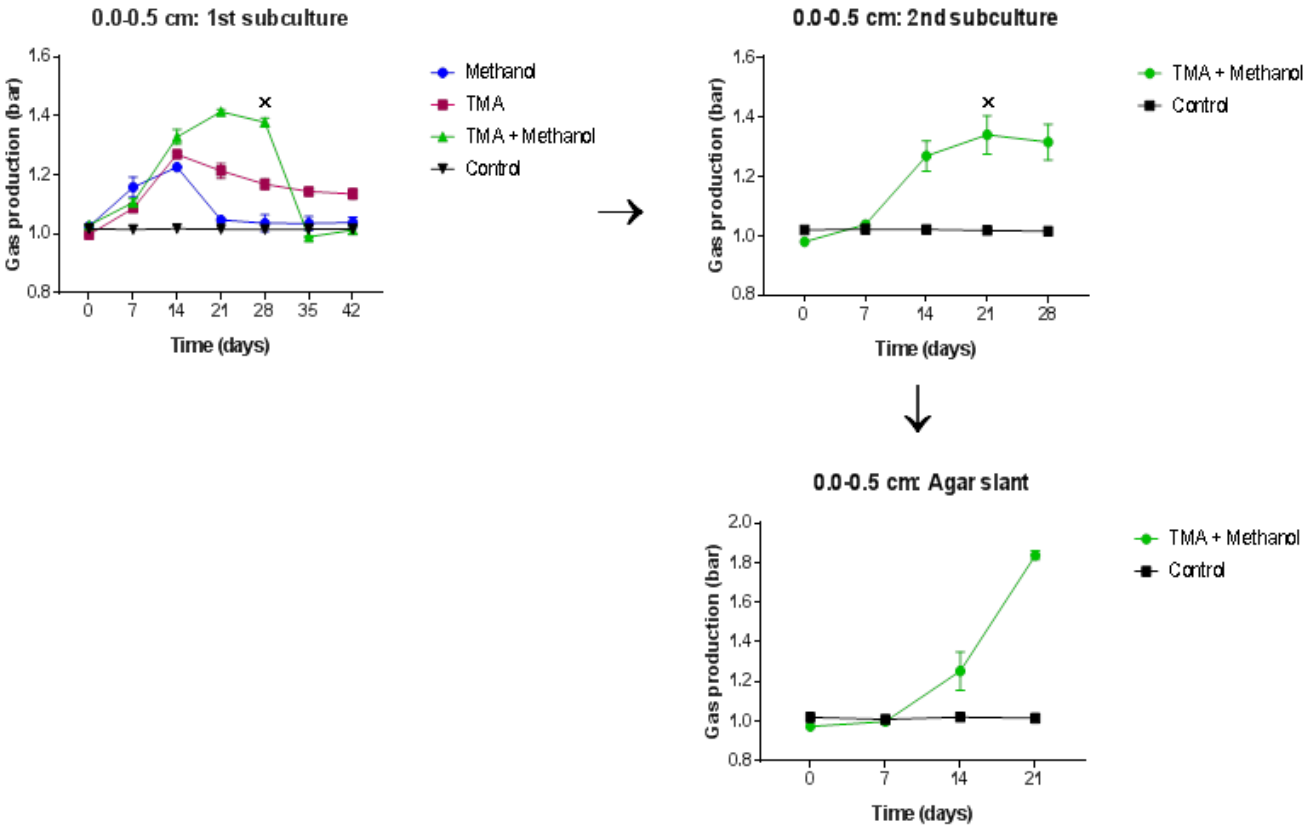

Figure 4.7: Gas production from subsequent rounds of methanogen enrichment of the 0.0-0.5 cm sample.

The colour of the plots indicates the substrate onto which the cultures were enriched. Concentrations of substrates used were: TMA, 20 mM; methanol, 40 mM. All cultures were incubated in the dark at 20 °C. Gas production from each enrichment culture was measured weekly with the use of a manometer (Keller). The 'x' above each graph denotes the week that cultures were further sub-cultured. Duplicate cultures were monitored, the mean pressure values were plotted, and error bars represent standard deviation.

4.3.4. Description of colony formation

After three weeks incubation, the second-round sub-cultures were inoculated onto anaerobic agar slants containing a combination of TMA and methanol. Colony growth was observed on both agar slants within two weeks. An example of this colony formation is displayed in Figure 4.8. Colonies formed on top of a film of microbial growth. Most observable colonies were cream and spherical with irregular edges. Colonies were variable in size and often had a noticeably darker centre, which was orange in appearance.

Figure 4.8: Formation of colonies on an anaerobic agar slant.

Successful enrichment cultures underwent rounds of sub-culturing before inoculation onto solid anaerobic agar slants, for the isolation of colonies. Solid agar contained TMA, 20 mM; methanol, 40 mM. This picture shows an example of colony formation after 3 weeks incubation after inoculation with culture originating from the 0.0-0.5 cm sample. Tubes were incubated in the dark at approximately 20 °C.

4.3.5. Methanogen-specific colony PCR

After three weeks incubation, twelve colonies were removed from the agar slants and patched onto anaerobic agar plates. Plates were covered with aluminium foil to protect from light and incubated within an anaerobic cabinet (approximately 24 °C). The first round of microbial growth was dense and had a dark cream glossy appearance. This growth formed within two weeks incubation. After two weeks, patches were screened for methanogen growth using methanogen-specific PCR. This screening process was then repeated after three weeks. Screening involved removing a 1 µl loop-full of cells from the centre of each patch and performing crude DNA extractions. DNA extracts were then used as template for PCR using ML_F and ML_R primers [61, 192]. The gel images in Figure 4.9 show the PCR products generated from the screening of the twelve patches after being incubated for two weeks (top panel) and after three weeks incubation (bottom panel) against positive and negative controls (-ve).

Bands detected as approximately 500 bp in size were assumed to be that of the methanogen *mcrA* gene. Positive and negative controls (-ve) produced expected results. The amplicons were of different intensities, suggesting different abundances of the *mcrA* gene between the different crude DNA extracts from the cell patches. DNA bands produced from the colony PCR performed after three weeks incubation were much fainter than those produced at the two-week screening (Figure 4.9). This result suggested a decline of the methanogen population within this between week two and three.

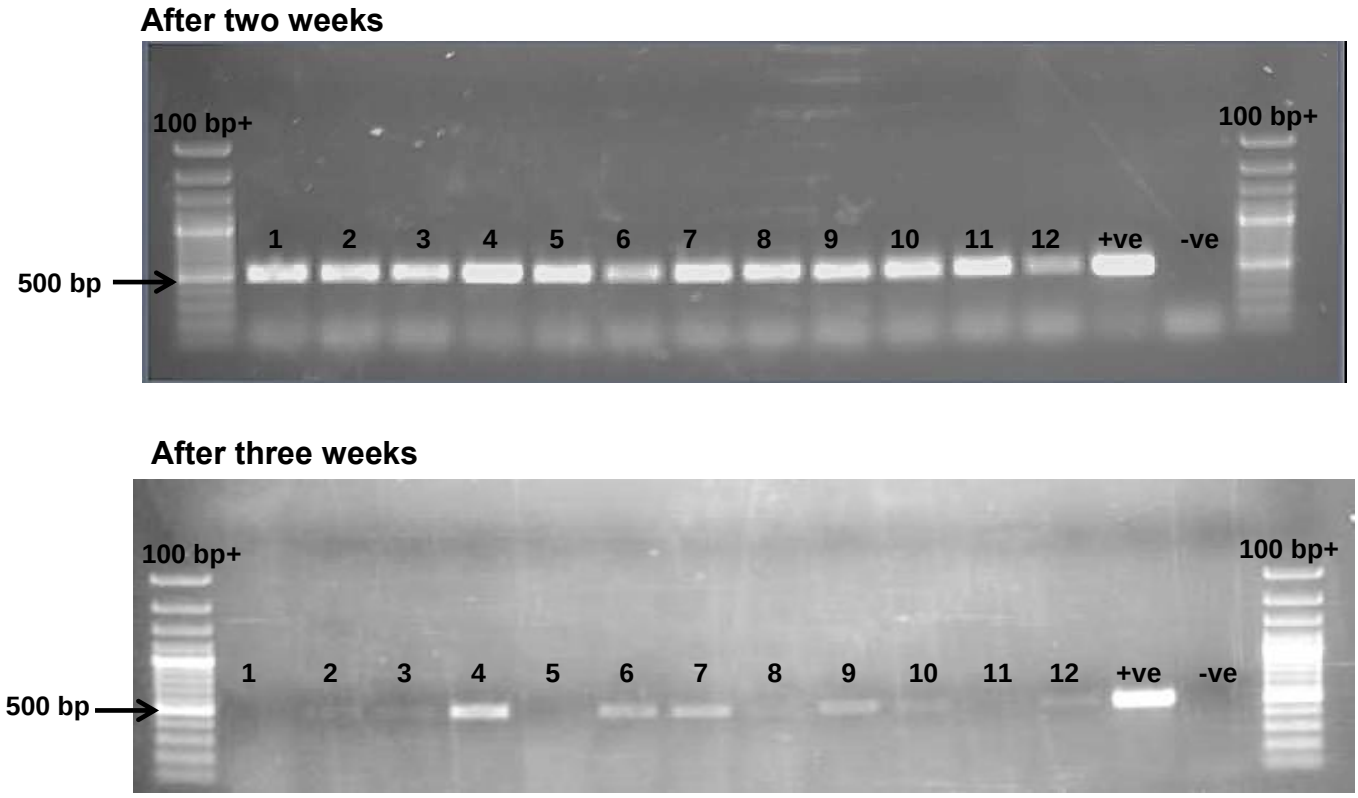

Figure 4.9: *mcrA*-specific PCR products generated from the screening of the first round of isolations for methanogenic organisms.

Potential methanogenic colonies were patched onto solid agar and numbered 1-12. A sample of each patch was subject to crude DNA extraction and screened for methanogens after two weeks incubation (top) and after three weeks (bottom). Screening was performed using methanogen-specific PCR. Band intensities of PCR products were compared. Positive control (+ve): methanogenic DNA (donated from Prof. Orkun Soyer's lab, University of Warwick, UK); negative control (-ve): nuclease-free water. DNA ladder, 100 bp plus (Thermo Fisher Scientific). The arrows indicate the 500 bp DNA markers.

4.3.6. Further re-streaking of methanogen positive colonies

Cells from patches 4, 6, 7, and 9 were re-streaked onto agar plates and incubated for two weeks anaerobically.

Two prominent types of colony morphologies were observed. The first and most dominant morphology (‘morphology 1’), had a translucent appearance that was orange in colour. The microbes forming this morphology often grew to high density, resulting in undefined colony edges. Colony edges that were observed, on occasion, were smooth. The second colony morphology observed (‘morphology 2’), was cream in colour and had a dull appearance with irregular edges. Microbes producing each of these colony morphologies were re-streaked onto fresh anaerobic agar plates and incubated anaerobically before further screening. All morphology 1 colonies, screened throughout the investigation were negative for the presence of methanogens. From herein onwards, only the isolation and screening of morphology 2 will be discussed.

The re-streaking of morphology 2 colonies produced cream colonies very small in size and tightly packed together, which made it difficult to isolate single colonies. This was further complicated by the presence of some morphology 1 colonies, despite the attempted re-streaking of morphology 2 only. Instead of isolating single colonies, six small 2-3 mm regions (labelled A-F) consisting of dense morphology 2 colonies were removed from each streak plate and patched onto fresh anaerobic agar plates. This was done for each of the streak plates originally inoculated with colony 4, 6, 7 or 9. The resulting patches were labelled 4A-F, 6A-F, 7A-F and 9A-F. Patches were incubated for two weeks before methanogen-specific PCR screening was performed. The products of methanogen screening of patches 4A-F produced the best overall results and

were visualised on an agarose gel seen in panel A of Figure 4.10. At this point in the investigation, genomic DNA extractions were performed on patches 4A and 4F and the DNA sent for whole genome shot-gun sequencing (Exeter Sequencing Service). Results from this sequencing will be discussed later in the chapter.

Due to the high intensity of the DNA bands produced during the methanogen-specific screening of patch 4A, cells from this patch were chosen and further streaked out onto fresh anaerobic agar plates. This was done to further isolate morphology 2. Two areas on this streak plate, containing densely morphology 2 colonies (2-3 mm) were identified for patching. These patches were labelled as 4A.1 and 4A.2 and screened for methanogenic organisms after 2 weeks incubation. The results of the PCR screening are displayed in panel B of Figure 4.10.

Screening of patches 4A.1 and 4A.2 using methanogen-specific PCR detected methanogenic organisms in patch 4A.2 but not in 4A.1. All PCR controls gave the anticipated result. Genomic DNA was extracted from patch 4A.2 and sent for whole genome sequencing alongside samples 4A and 4F.

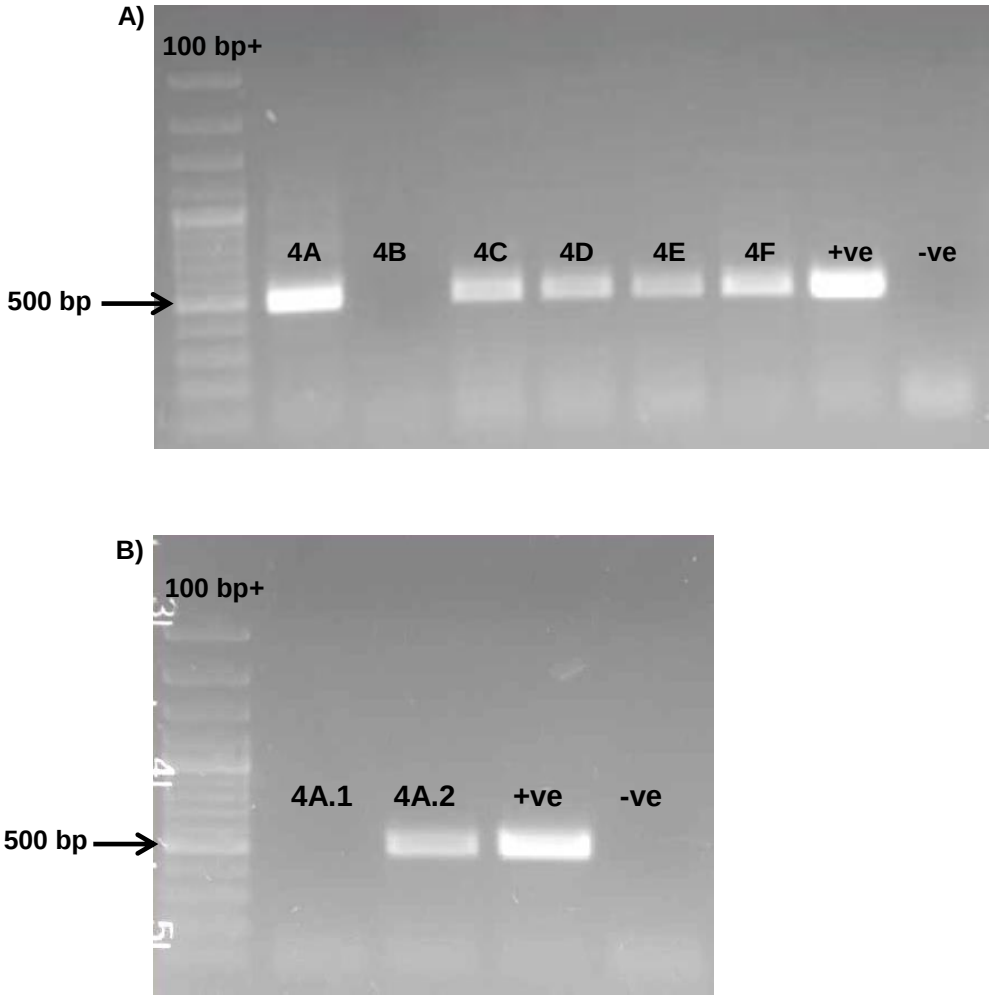

Figure 4.10: Gel electrophoresis of products generated from the 2nd and 3rd rounds of screening for potential methanogenic isolates using colony PCR specific for *mcrA*.

Six areas from the re-streak of microbial patch 4 were patched onto fresh anaerobic agar plates (labelled 4A-4F). Crude DNA extractions were performed on all patches and screened for methanogens using PCR. Patch 4A was further streaked out and another two areas of microbial growth were identified for patching (4A.1 and 4A.2) and methanogen screening. Gel A) Products of screening of patches 4A-4F. Gel B) Products of screening of further isolation from patch 4A. All PCR screenings were run against positive (methanogen DNA) and negative (nuclease-free water) controls. DNA ladder: 100 bp plus (Thermo Fisher Scientific). The arrows indicate the 500 bp DNA markers.

4.3.7. Whole genome sequencing of isolated colonies

Table 4.1 below provides summary of information on the samples sent for whole genome sequencing. All samples originated from 2-3 mm regions of densely packed morphology 2 colonies.

Table 4.1: Summary of enrichment isolates sent for whole genome sequencing

Sample name	Sample information	[DNA] (ng/µl)
4A	Isolate from enrichment of 0.0-0.5 cm sediment sample, grown on a combination of 20 mM TMA and 40 mM methanol.	8.7
4F	Isolate from enrichment of 0.0-0.5 cm sediment sample, grown on a combination of 20 mM TMA and 40 mM methanol.	14.8
4A.2	Sub-isolate of isolate 4A.	9.5

4.3.8. Preparation and analysis of whole genome sequencing data

Reads generated from the whole genome sequencing of each sample were downloaded on a Linux server. Quality checks and filtering were performed on each set of reads before the reads were paired. Read files containing paired reads were compared against the archaeal subset of the RefSeq database [189] using BLASTn. The BLAST output for each sample was fed into MEGAN software [186]. Phylograms were generated to represent each of the whole genome sequencing sample and are shown in Figures 4.11-4.13. The size of the bubble at each node indicates the relative number of reads binned into that taxon.

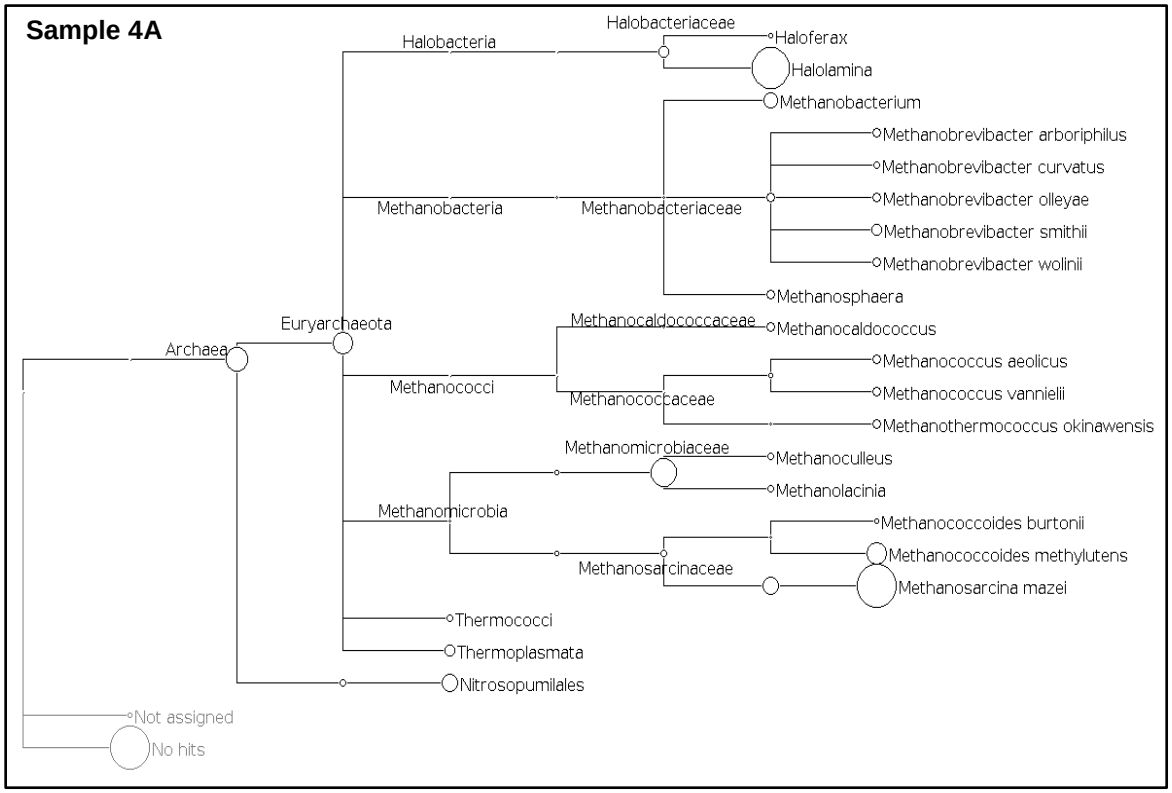

Figure 4.11: Phylogram output of whole genome sequencing of sample 4A compared against the archaeal RefSeq database (Hosted by NCBI, [189]).

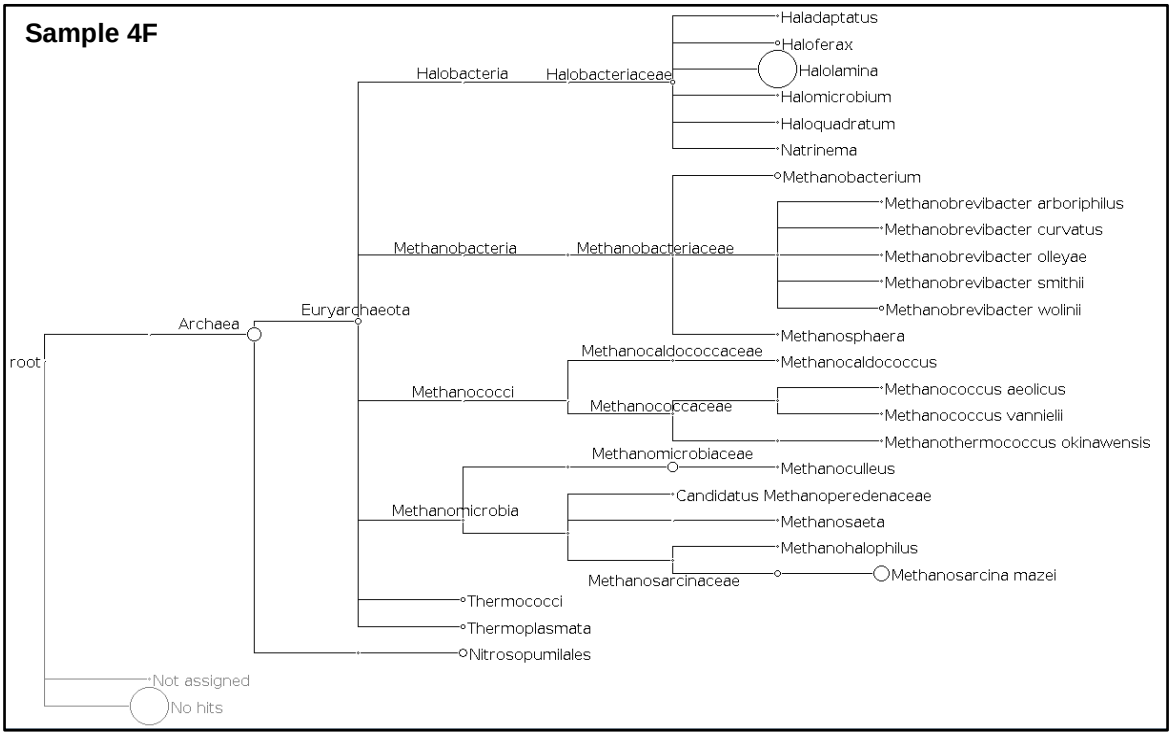

Figure 4.12: Phylogram output of whole genome sequencing of sample 4F compared against the archaeal RefSeq database (Hosted by NCBI, [189]).

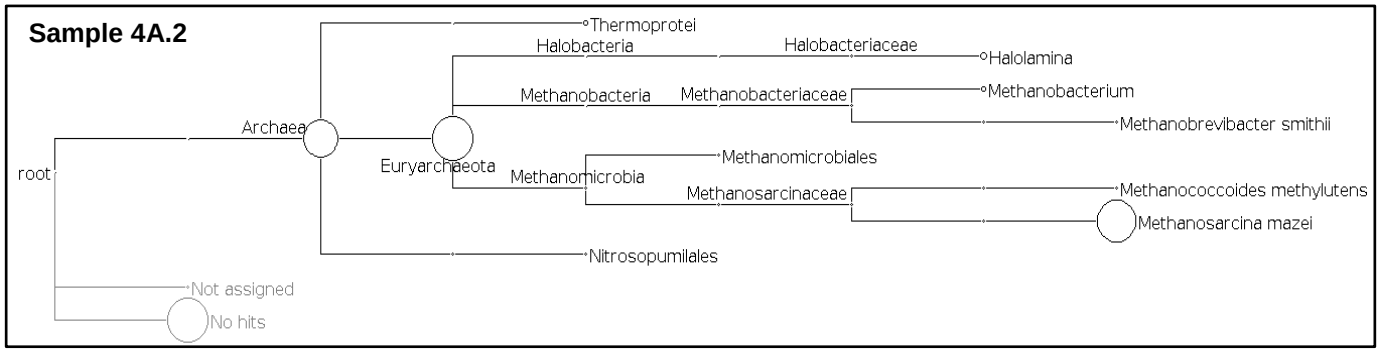

Figure 4.13: Phylogram output of whole genome sequencing of sample 4A.2 compared against the archaeal RefSeq database (Hosted by NCBI, [189])

The phylograms above reveal the likely presence of multiple archaeal species within each of the samples sent for whole genome sequencing. Samples 4A and 4F produced the highest level of taxonomic complexity, for these two samples, classified reads were binned into a total of seven different classes. Three of these classes were the methanogenic classes, Methanobacteria, Methanococci and Methanomicrobia. Sample 4A.2 displayed a much lower complexity in comparison. Reads were classified into only four classes, two of which were methanogenic, Methanobacteria and Methanomicrobia. For all three samples, the highest number of reads classified as methanogens were binned as belonging to the *Methanosarcina mazei* species. A small number reads were classified into as other methanogenic species, such as *Methanobrevibacter smithii* and *Methanoccocoides methylutens*, but not in comparable quantities to that of *M. mazei*. Further information of the different methanogenic genera detected is provided in the table below.

Table 4.2: Methanogenic genera detected within enrichment samples

Genus name	Environment	Substrates	Reference
Methanobrevibacter	Termite gut Human and animal gut Rice paddy soils	Reduction of CO_2 with H_2	[223]
Methanococcus	Salt marsh Deep sea hydrothermal vents	Reduction of CO_2 with H_2	[224]
Methanococcoides	Marine sediments	Methylated compounds	[225]
Methanosarcina	Diverse range of environments	All methanogenic pathways	[226]

Another interesting observation detected from the BLASTn output of the comparison of samples against the archaeal RefSeq database, was the detection of the *Halolamina* genus. A large proportion of reads were binned into this taxa during the analysis of samples 4A and 4F but not during the analysis of sample 4A.2. This taxon was the only non-methanogenic archaeal taxa to be detected in quantities comparable to *Methanosarcina*. This result will be discussed in greater detail, later in the chapter.

4.3.9. Direct comparison between samples 4A, 4F and 4A.2

The number of reads generated during whole genome sequencing varied between each of the different samples. Absolute read counts were used to generate the original phylogenetic trees for each of the BLASTn outputs (Figure 4.11-4.13), and therefore direct comparisons between different samples could not be carried out. To facilitate a direct comparison, a comparison phylogram was generated using MEGAN to include all three samples. This comparison

phylogram was then converted into a series of pie charts, to display the relative proportions of reads from methanogenic taxa at the class, order and species level. The Halobacteria and its lower taxa were also included in this analysis due to the high proportions of *Halolamina* detected within samples 4A and 4F.

The pie charts seen in Figure 4.14 display the different taxa detected during this analysis and their varying proportions within each of the three samples. The species taxa marked as ‘other’ represents the sequences that could not be classified further than the genus level.

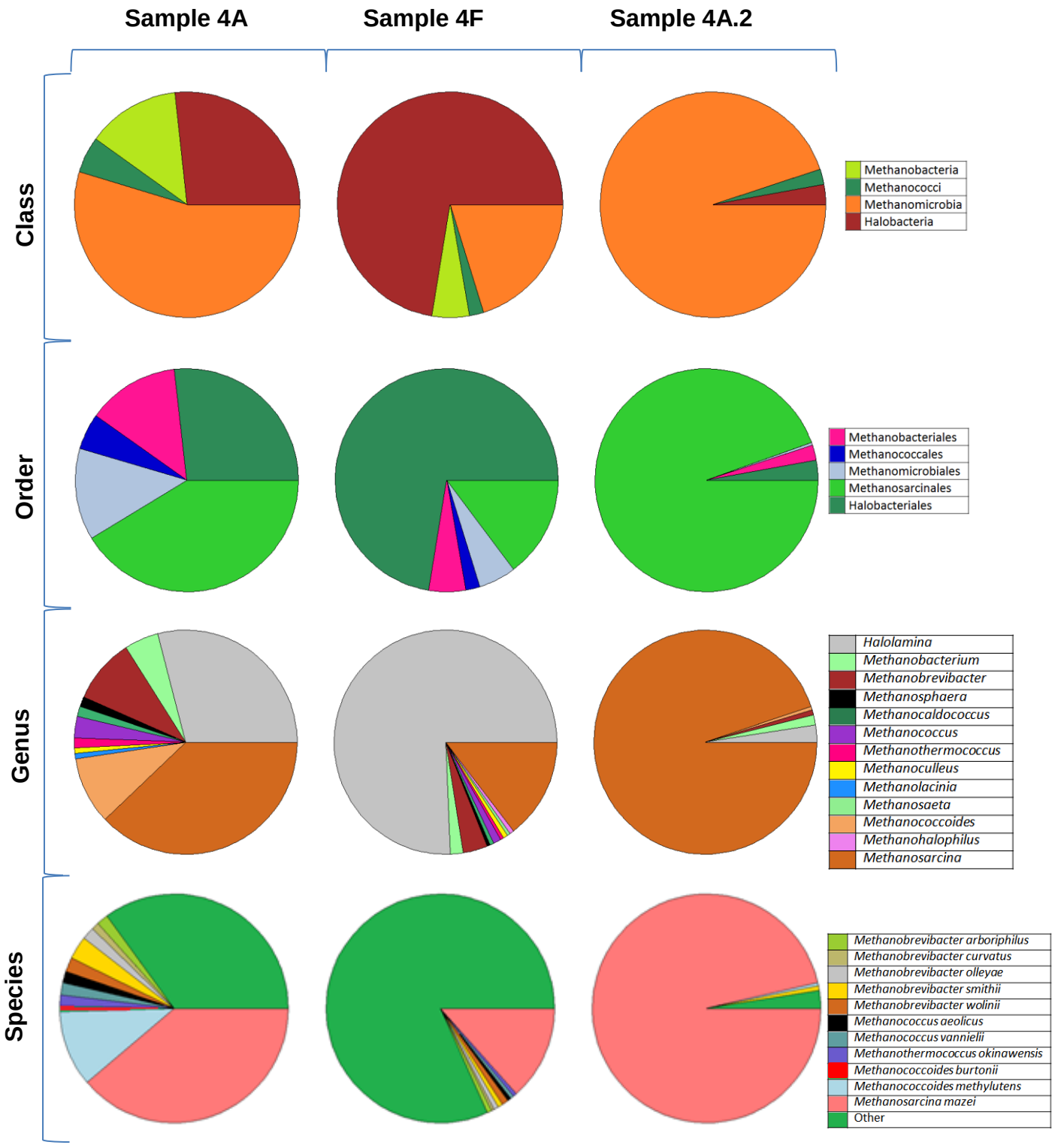

Figure 4.14: Comparison pie charts of all whole genome sequencing samples.

Relative abundances of different phylogenetic groups detected within sample 4A, 4F and 4A.2 were directly compared. Relative read counts were used. The abundance of each phylogenetic group within each sample are shown at the class, order, genus and species level. Pie charts were created using MEGAN5 software [186].

Approximately 70 % of the classified reads generated from sequencing of sample 4A were classified as originating from methanogens at the class level and approximately 30 % of reads were classified as originating from Halobacteria. This dominance of methanogenic taxa was not found in sample 4F, where approximately 70 % of reads were binned as originating from Halobacteria. This differing proportions of Halobacteria to methanogenic sequences between 4A and 4F may reflect the different proportion of the two different cell morphologies in these samples.

When examining the relative proportions of genes from different taxa in sample 4A.2, the differences in samples 4A and 4F became apparent. Approximately 90-95 % of classified reads from 4A.2 were determined as originating from methanogens, specifically *Methanosarcina mazei*. This suggests that additional re-streaking of sample 4A to isolate cell morphology 2, creating sample 4A.2, resulted in further purification of methanogens. The decrease in the proportion of Halobacteria reads supports the possibility that these reads originated from the cell morphology 1.

There is little information provided on *Halolamina* in the literature; therefore, further attempts were made to identify any species of this genus. Reads classified as *Halolamina* were extracted and a proportion of the reads were compared against the whole RefSeq database (rather than the archaeal subset as used previously) using BLASTn [189]. Most extracted reads identified very closely with various strains of *Shewanella*. Upon further investigation into *Shewanella*, I was interested to learn about its colony morphology, which matched that of the description of colony morphology 1, described earlier [227, 228].

4.4. Discussion

Work described in Chapter 3, discovered methanogenic DNA present in the very surface layers of estuarine mudflat sediment. To determine if these surface layers harboured active methanogens, a series of enrichment experiments were performed, followed by rounds of colony isolation. Shot-gun sequencing was used to indicate the identity of the enriched microbes.

Previous metagenomic studies indicated that methylotrophic methanogens often thrive in estuarine environments, such as the one sampled during this investigation [216, 219]. Two methylated compounds, trimethylamine (TMA) and methanol, were chosen as methanogenic growth substrates for the enrichment process, and had previously been successful for enrichment of methanogens [229]. In addition, acetate was also included as a substrate, to enable the growth of any acetoclastic methanogens present within the environmental sample.

Due to equipment restrictions, specific determination of methanogen growth by production of methane gas was not possible. Instead, the enrichment of methanogens was monitored by coupling total gas production with methanogen-specific end-point PCR. It is possible that gases, other than methane were produced at this stage, however a clear correlation was observed between total gas production and methanogen DNA amplicon intensity. These results suggested that an increase in gas production could be used to indicate proliferation of methanogenic species.

Gas production was observed only from enrichments containing methylated substrates and not from enrichments with acetate as the sole substrate. These results suggest successful enrichment of methanogenic

species, specifically methylotrophic methanogens. This observation agreed with other metagenomic studies which witnessed a dominance of methylotrophic methanogens in similar environments, as described in previous discussions (Chapter 3). These results were further backed by methanogen-specific PCR screening.

The highest level of gas production was produced from the enrichment of the very surface layer of sediment (0.0-0.5 cm), onto medium containing TMA and methanol. This suggested that methanogens within this very surface layer of sediment had the highest metabolic activity in comparison to other layers. Further sub-culturing of this sample, followed by enrichment onto agar slants, revealed that liquid cultures were not as pure as initially desired. Large colonies, varying in shape and size formed on top of a film of microbial growth. Initial PCR screening of the cells producing the two dominant colony morphologies, highlighted that the less dominant of the two morphologies, morphology 2, was methanogenic. Isolation and further preservation morphology 2, on anaerobic agar plates proved very challenging and was very difficult to isolate from morphology 1. This initial observation suggested dominance of microbes producing colony morphology 2 on the microbes producing morphology 1.

Three DNA samples, extracted from microbes grown on the anaerobic plates, were selected for sequencing. DNA samples 4A and 4F both originated from combination of cell morphologies 1 and 2. Sample 4A.2 originated from morphology 2 only, with no visible presence of morphology 1. Sequencing analysis indicated that sample 4A and 4F were composed of a combination of methanogenic species and *Halolamina* species plus other non-related species. This was also true for sample 4A.2, however the proportion of methanogenic

sequences observed was much higher and accounted for approximately 95 % of classified reads. Of the methanogenic reads detected in each sample, the majority has the closest identity to *Methanosarcina mazei.* Given the dominance of reads identified as *Methanosarcina mazei* within sample 4A.2, the microbe responsible for the formation of colony morphology 2, was assumed to be *Methanosarcina mazei* or a closely related methanogen. This assumption was also supported by the documented colony morphology of *M. mazei* [230].

M. mazei, originally named *Methanococcus mazei*, was first described by H. A. Barker in 1936 [231]. But it wasn't until 1980 that R. A. Mah successfully isolated *M. mazei* from a laboratory digester and studied a pure culture [230]. Mah described its diverse metabolic range and ability to utilise various substrates including acetate, methanol, methylamine and TMA, enabling it to perform all known routes of methanogenesis. These descriptions explain why my enrichment cultures grew well on a combination of TMA and methanol, but does not explain why enrichments did not thrive on acetate. However due to high abundance of methylated compounds documented in estuarine environments, it is possible that the *M. mazei* strain (or related strains) detected in this study, had already adapted to use methylated compounds and lost its ability to utilise acetate.

It has been previously hypothesised that methanogens lack certain oxygen protection enzymes such as superoxide dismutase (SOD) and catalase, because oxygen is a product of their enzyme activity, which can further propagate production of ROS [232]. However, in 1999, Shima *et al.* discovered that a close relative of *M. mazei*, *Methanosarcina barkeri* exhibited intracellular catalase activity. In 2004, Brioukhanov and Netrusov also detected transcriptional upregulation of a catalase during exposure of *M. barkeri* to sub-lethal

concentrations of hydrogen peroxide [233]. Given the close relationship of *M. barkeri* to *M. mazei*, it is possible that *M. mazei* also possess similar oxygen-protection mechanisms. In 2008, Lui *et al.* noted the ability of a TMA-adapted *M. mazei* strain to tolerate periods of aeration for up to 30 days [234] and in 2011, Kratzer *et al.* noted the presence of superoxide reductase, within *M. mazei* [235]. This protein was named methanoferrodoxin, which was found to contain an iron-sulphur cluster and had the ability to reductively decompose superoxide to peroxid. Other sources of literature also support the presence of antioxidant enzymes in *Methanosarcina* species, such as superoxide reductase (SOR), peroxidase, rubrerythrin, and $F_{420}H_2$ oxidase, which all degrade oxygen radicals and hydrogen peroxide without producing oxygen [199, 236, 237]. The diverse anti-oxidant systems in *Methanosarcina* species in comparison to other lineages of methanogens are credited to their large genomes, facilitating their genetically diverse nature [238].

Methanococcoides methylutens, was the second most dominate methanogen to be detected in samples 4A and 4A.2. *M. methylutens* is normally found in abundance in methylotrophic environments such as marine and estuarine areas and utilises methylated compounds [225]. The colony morphology of *M. methylutens* is described in the literature as yellow, circular, and convex with entire edges [225], and is different to colony morphology 2 that I identified in this study. *M. methylutens* has been identified in many marine and estuarine environments, often in oxygenated areas [239, 240]. However, I could find no evidence to suggest that *M. methylutens* had oxygen-defence mechanisms, such as those documented in *M. mazei*. There is however, speculation that *M. methylutens* could exist in oxygenated environments inside sediment pellets or marine snow, or may have been dispensed into the

environment from faecal material from other living organisms [241]. In addition, the annotation of the whole genome sequence of *M. methylutens* produced by Henriksen *et al.,* 2015, predicted the presence of certain oxygen-defence genes as catalase, peroxidase, SOR, rubredoxin and rubreythrin [242]. This evidence could further support the presence of *M. methylutens* within our enrichment samples.

Our sequencing analyses in combination with previous observations and descriptions within the literature suggest that a methanogen species or strain relating closely to *M. mazei* was enriched and partially isolated during this investigation. This result is interesting due to the lack of detection of sequences closely relating to *M. mazei* during the 16S analysis of the same sample site (Chapter 3). This finding could suggest that *M. mazei* is a minor component of the community sampled at the mudflats of the Rive Exe Estuary. During this investigation, simple anaerobic enrichment cultures were performed under an atmosphere of carbon dioxide and nitrogen, hydrogen was not provided in the culture headspace. *M. luminyensis* was a dominant methanogen detected at the sample site during previous 16S rRNA studies, however was not noted during this enrichment process, most likely because it required hydrogen for growth. Due to *M. mazei's* diverse metabolic range, there was no strict requirement for hydrogen, providing it with a selective advantage over other hydrogen-requiring methanogens. Colony morphology 1 was originally assumed to be that of a *Halolamina* species, however, there was speculation over the classification of reads binned into this genus. Further analyses indicated that reads originally binned as *Halolamina* (an archaeal taxa) matched with greater identity to *Shewanella algae* (a bacterium). This result was also supported by the similarities between the colony morphology of *Shewanella algae* in the literature and the

observations of morphology 1 made during this investigation [227]. This evidence suggests that sequences matching closely with *Shewanella algae* were wrongly classified as *Halolamina* species when compared against the archaeal division of the RefSeq database using BLASTn. After extensive literature searches, there is no explanation for this misclassification.

Despite the uncertainty of the identity of the microbe responsible for morphology 1, it is possible that the *M. mazei* has a form of dependence on this microbe as during the isolation stages of this investigation, morphology 2 was difficult to separate from morphology 1 and would not grow well independently. It is possible that morphology 1 provided some form of protection to *M.mazei* (or a closely related microbe), possibly reducing the redox potential significantly enough for methanogen survival.

5. Chapter five: Characterisation of the glutamine synthetase promoter

5.1. Introduction

Build-up of acetate is well documented problem during anaerobic digestion and is due to an imbalance between acetate producers (acetogenic bacteria) and acetate consumers (the methanogens). Acetate's toxic effects on microorganisms result from its nature as a carboxylic acid. Acetate is excreted in the form of acetic acid, when this acetic acid reaches the outside environment (such as the growth medium), it tends to dissociate, resulting in an influx of protons into the surrounding environment, reducing the overall pH [243]. As discussed in Chapter 1, low pH has a toxic effect on methanogens and can have a direct inhibitory effect on the enzymes involved in methanogenesis, [163, 244]. Due to their important role in the anaerobic digestion process, acetogens have been widely studied and isolated from a number of anaerobic environments such as, intestinal tracts of termites [245], rice paddy soils [246], deep subsurface sediments [247] and waste-water treatment facilities [248]. Their acetate-producing pathways are outlined below.

Acetate production from acetogens occurs through a pathway known as the Wood-Ljungdahl pathway (WLP), and involves the synthesis of acetate from two molecules of CO_2. During heterotrophic acetogenesis, oxidation of glucose first occurs prior to the WLP. This oxidation results in the production of two molecules of acetate and two molecules of carbon dioxide and occurs via a combination of glycolysis, pyruvate:ferredoxin, oxidoreductase and the phosphate acetyl transferase-acetate kinase A (PTA-ACKA) pathway. The reducing equivalents produced during this process are then used by the WLP.

The WLP has two branches, a methyl branch and a carbonyl branch. During the methyl branch (also known as the Eastern branch), one molecule of

CO_2 undergoes reduction by six electrons to a methyl group. During the carbonyl branch (also known as the Western branch) the other CO_2 molecule is reduced to CO (carbon monoxide). Acetyl-CoA is then formed during a condensation reaction between the bound methyl group, CO and coenzyme A. Acetyl-CoA is then converted along the PTA-ACKA pathway to form acetate. These reactions are detailed in Figure 5.1. The production of acetate allows for the regeneration of NAD+ (oxidized form of nicotinamide adenine dinucleotide), which is involved in many metabolic pathways within the cell. Production of acetate also allows for the recycling of coenzyme A, which is required to convert pyruvate to acetyl-CoA [249].

The PTA-ACKA pathway plays a major role in the production of acetate from acetogenic bacteria, converting acetyl-CoA into acetyl-phosphate (AcP) followed by conversion into acetate. The work detailed in this chapter introduces the concept of synthetically engineering acetogenic bacteria for regulation of acetate production through the down-regulation of this pathway.

The PTA-ACKA pathway has been most extensively studied in *E. coli*, due to the problematic nature of acetate accumulation and toxicity during batch culture for industrial scale production of recombinant proteins [250-254]. As a proof of principal project, I chose to use *E. coli* as a model organism for the generation of a negative feedback loop against acetate production. This work was carried out with a view of applying similar techniques in acetogens known to be important to anaerobic digestion. The work described in this chapter characterises the glutamine synthetase promoter, which has been previously described to be sensitive to both pH and external acetate concentration [255].

This promoter was proposed as a genetic controller for the negative feedback loop for the downregulation of acetate production under unfavourable conditions.

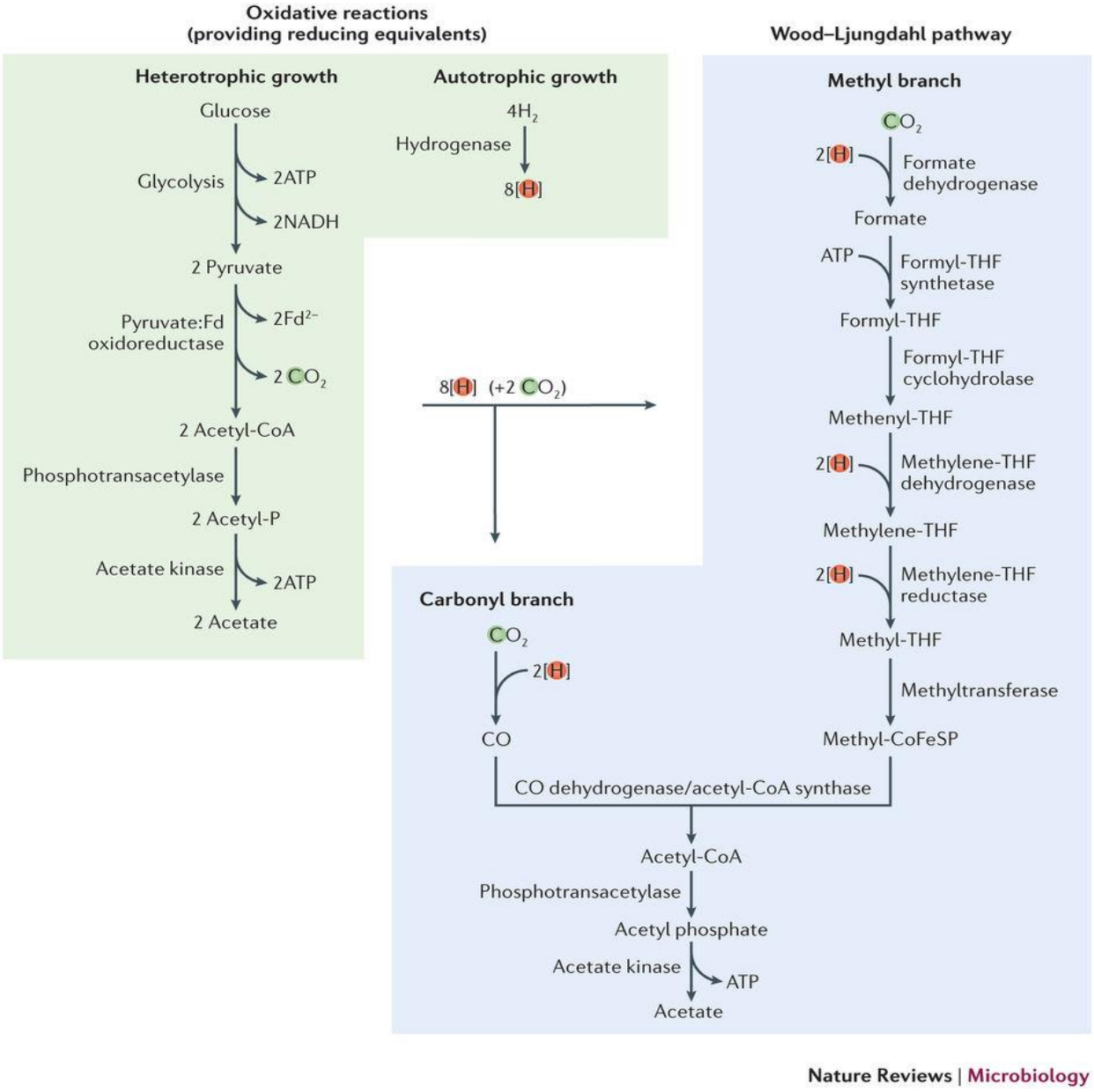

Figure 5.1: The Wood–Ljungdahl pathway of acetogenesis

Figure taken from [256]. Acetogenic bacteria produce acetate from two molecules of carbon dioxide (CO_2) via the Wood–Ljungdahl pathway (WLP). During heterotrophic acetogenesis, glucose is oxidized to two molecules of acetate and two molecules of CO_2 via a combination of glycolysis, pyruvate:ferredoxin oxidoreductase, phosphate acetyltransferase (PTA) and acetate kinase (ACKA). The reducing equivalents are re-oxidized by the reduction of the two molecules of CO_2 to acetate in the WLP. During autotrophic acetogenesis, acetate is formed from $4H_2$ and $2CO_2$.

The initiation of the glutamine synthesis pathway, which plays an essential role in nitrogen metabolism, usually occurs when P_{II} (a nitrogen-sensing protein) controls the phosphorylation of NtrB (nitrogen regulation protein B), NtrB-P then phosphorylates NtrC (nitrogen regulation protein C), which then binds to an enhancer sequence ahead of the *glnAp2* promoter and initiates the transcription of glutamine synthetase, this pathway is outlined in Figure 5.2. By experimenting with *E. coli* cells deficient in NtrB (coded for by the *glnL* gene) and PTA, Bulter *et al* [255] demonstrated that in the absence of NtrB, the glutamine synthetase pathway was no longer sensitive to nitrogen. Instead, induction of *glnAp2* occurred in a dose dependent manner relative to the intracellular concentration of a derivative of acetate, acetyl-phosphate (AcP). By engineering a GFP fluorescence reporter gene under the control of the *glnAp2* promoter, it was shown that the induction of the promoter was dependent on extracellular acetate concentrations and pH potential across the cellular membrane. It was discovered that the lower the pH and the higher the acetate concentration, the greater the induction of the promoter.

The aim of this results chapter was to determine the behaviour of the *glnAp2* promoter under my own laboratory conditions using the *E. coli* RB9132 strain. This was done by subjecting *E. coli* cells containing a GFP reporter plasmid under to the control of the *glnAp2* promoter to varying external pH and acetate concentrations.

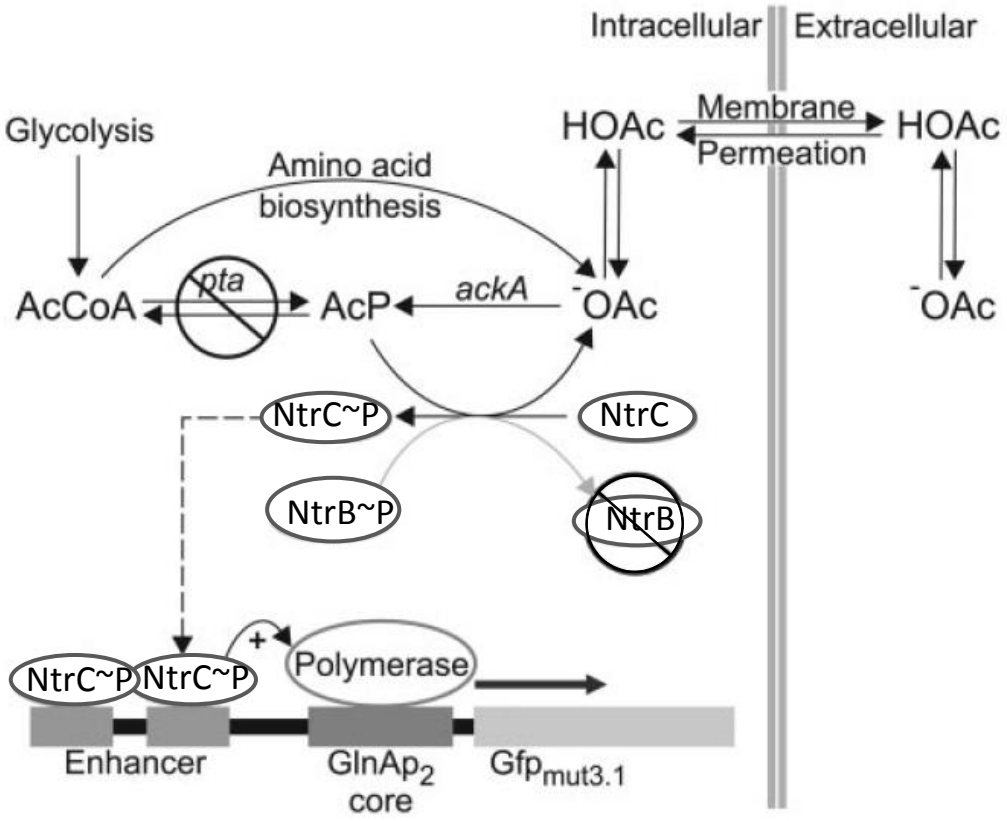

Figure 5.2: The *E. coli* cell–cell communication circuit [255]

Acetate functions as the communication molecule. Acetic acid diffuses freely across the cell membrane, inside the cell; acetate is converted to AcP by ACKA. In the absence of the histidine kinase NtrB, AcP phosphorylates the response regulator NtrC. NtrC-P binds the *glnAp2* enhancer sequence and induces the promoter *glnAp2* [255].

5.3. Results

5.3.1. Confirmation of genotype of *E. coli* strains

The expected result for the amplification with *glnL* specific primers was observed (Figure 5.4). The YMC10 2841 and YMC10 3236 lanes produced bright bands at roughly 500 bp, indicating successful amplification of the 480 bp region of the *glnL* gene. No DNA band was produced in the RB1932 lane indicating that the *glnL* gene is absent in the RB1932 genome. The absence of any DNA bands in the negative control (-ve) lane, indicated that the PCR reaction did not have any contamination.

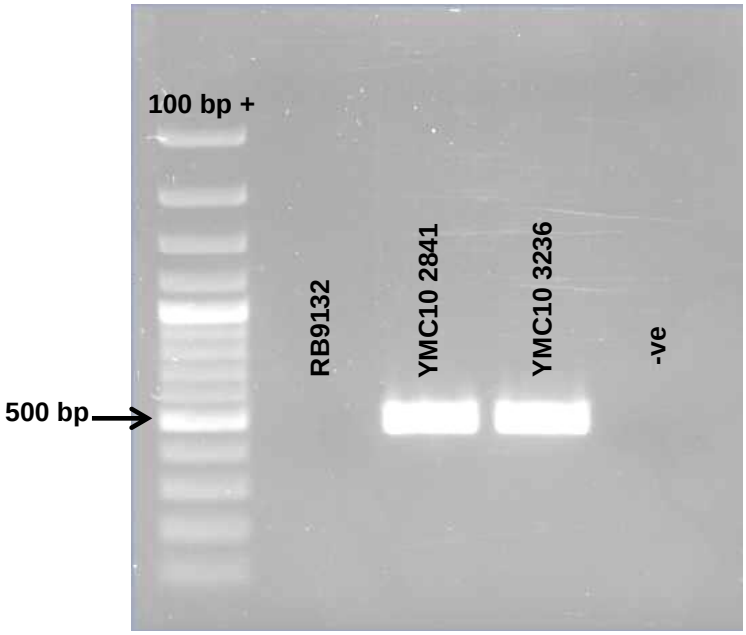

Figure 5.4: Detection of the *glnL* gene *E. coli* strains: RB9132, YMC10 2841, YMC10 3236 via PCR amplification.

Gel electrophoresis of the PCR amplification products of *E. coli* template DNA from different strains with primers specific for the *glnL* (encoding NtrB) locus. The strains from which template DNA was extracted is indicated on the gel image. DNA marker used was a 100 bp plus DNA ladder (Thermo Fisher Scientific), the arrow indicates the 500 bp DNA marker. Negative control (-ve) contained nuclease-free water in place of DNA.

5.3.2. Generation of *pta* knockout mutant in *E. coli* RB9132 cells

The final stages of Wanner mutagenesis involved streaking out cells of potential mutants onto LB chloramphenicol agar plates. The resulting colonies were further patched onto fresh LB chloramphenicol plates and the cells screened for the presence/absence of *pta* using colony PCR designed to amplify a 380 bp region of the *E. coli pta* gene (using primers pta_F and pta_R). The agarose gel image in Figure 5.5 shows the PCR products generated from the colony PCRs of nine potential mutants.

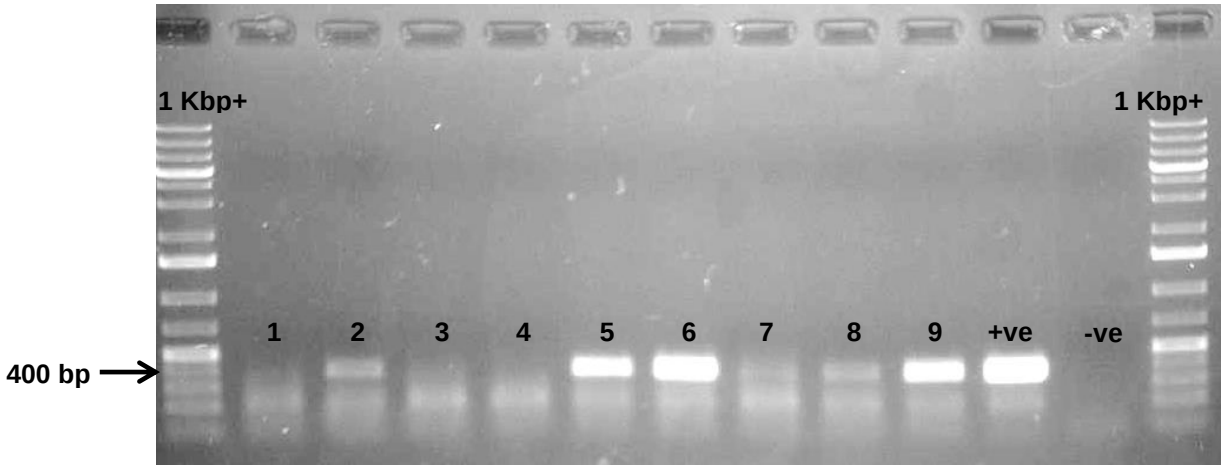

Figure 5.5: Gel electrophoresis of PCR products generated during the screening of potential *E. coli* RB9132∆*pta* mutant cells.

Gel electrophoresis of the PCR amplification products of *E. coli* template DNA from microbial patches of potential *E. coli* RB9132∆*pta* mutants, with pta_F and pta_R primers. The microbial patch number from which template DNA was extracted, is indicated on the gel image. The DNA marker used was a 1 Kbp plus DNA ladder (Thermo Fisher Scientific), the arrow indicates the 400 bp DNA marker. Positive control (+ve) template DNA was extracted *E. coli* strain YMC10 2841. Negative control (-ve) contained nuclease-free water in place of DNA.

Varying degrees of amplicon intensities were observed during the gel electrophoresis of colony PCR products targeting the *pta* gene. The band intensity produced in the patch 6 lane suggests that all *E. coli* cells from this patch had not successfully undergone Wanner mutagenesis. Band intensities seen in other lanes such as for patch 2 and patch 8, suggest that some of the cells within the patches had been successfully mutated but others had not. Cells from patch 4 under went further rounds of growth on LB chloramphenicol agar plates followed by DNA extraction and subsequent PCR's to re-confirm the absence of the *pta* gene. Once confirmed, cell stocks of RB9132Δ*pta* were generated and stored appropriately until needed.

5.3.3. Amplification of *glnAp2* promoter

The *glnAp2* promoter region was PCR amplified from the *E. coli* RB9132 genome. The PCR product was subsequently gel purified. 5 µl of the resulting purified product was electrophoresed on a 1 % (w/v) agarose gel and imaged under U.V light. The gel image is seen in Figure 5.6.

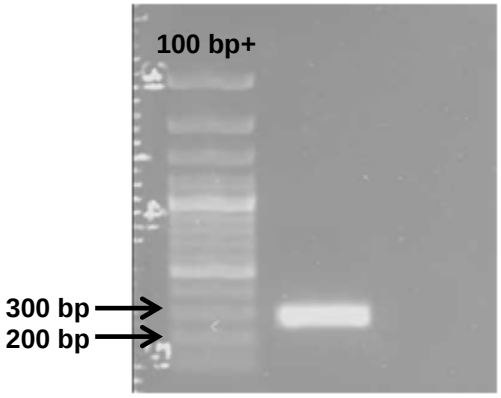

Figure 5.6: Gel electrophoresis of the purified *glnAp2* promoter region amplified from *E. coli* RB9132 chromosomal DNA.

Gel electrophoresis of the purified *glnAp2* promoter from *E. coli* RB9132. The DNA marker used was a 100 bp plus DNA ladder (Thermo Fisher Scientific), the arrows indicate the 200 bp and 300 bp DNA markers.

5.3.4. Confirmation of successful cloning of *glnAp2*

Transformants *E. coli* DH5 alpha cells containing the recombinant pGEM-T.*glnAp2* vector, containing the correct *glnAp2* sequence, were subject to vector DNA extraction. Extracts were sequenced using single read Sanger sequencing (Eurofins). Retrieved sequences were aligned against the correct sequence for the *glnAp2* promoter region to confirm successful cloning of the promoter region. An alignment generated between the sequenced vector and the predicted sequenced for the cloned region can be found in Figure A3.2, in the Appendices.

5.3.5. Release of cloned *glnAp2* promoter region from pGEM-T.*glnAp2*

Figure 5.7, shows the restriction digest products of pGEM-T.*glnAp2*. Double digest reactions produced two sets of DNA bands. Bright bands produced at roughly 3 Kbp represent the linearized the pGEM-T vector DNA, minus the *glnAp2* promoter section. The faint bands highlighted inside the dashed rectangle box produced between the 200 bp and 300 bp DNA markers represent the released *glnAp2* gene. The single digest reaction produced a single bright band just above the 3 kb marker, representing the linearized form of the recombinant pGEM-T.*glnAp2* vector. The 'no enzyme' control DNA band was typical of uncut circular DNA. The negative control (-ve) containing nuclease-free water in place of vector DNA produced no bands indicating a clean restriction digest reaction. The *glnAp2* bands were purified using gel extraction stored at -20 °C until later required.

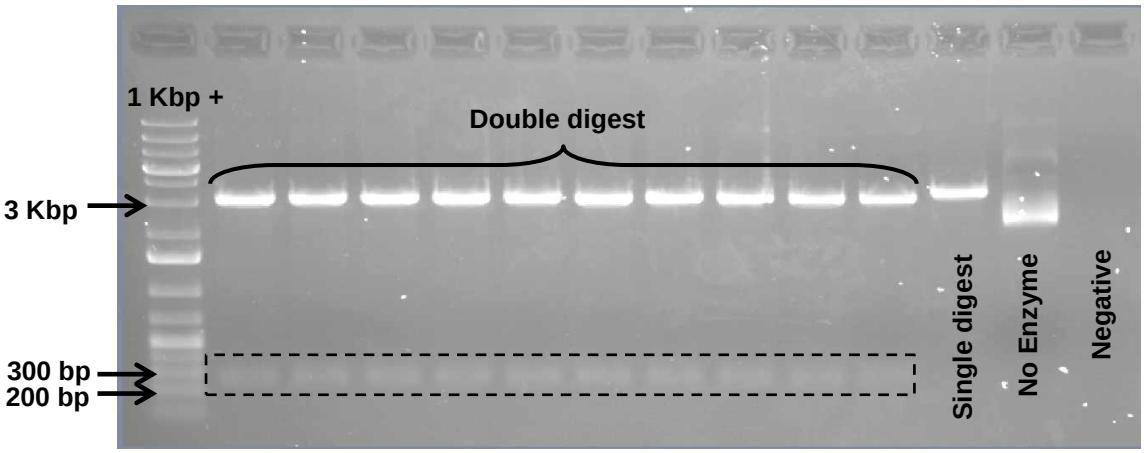

Figure 5.7. Gel electrophoresis of pGEMT.*glnAp2* restriction digest products.

The recombinant vector pGEM-T.*glnAp2 was* isolated from its host cells and subject to double restriction digest reactions with BamHI and HindIII. The single digest reaction used BamHI only, the no enzyme reaction contained nuclease-free water in place of BamHI and HindIII. The negative reaction contained nuclease-free water in place of vector DNA. Faint bands produced inside the dashed rectangular box represent the released *glnAp2*. The DNA ladder used was a 1 Kbp plus DNA ladder (Thermo Fisher Scientific), the arrows indicate the 200 bp, 300 bp and 3 Kbp DNA markers.

5.3.6. Preparation of GFP reporter vector

The products of the restriction digestion of pRU1097 with BamHI and HindIII are shown in Figure 5.8. Double digest reactions produced DNA bands slightly larger than the 5 Kbp marker on the DNA ladder (correct size for the double cut vector, 5,255 bp). The DNA band produced by the single digest reaction was slightly larger than those produced by the double digest, representing the linearized form of pRU1097 which is 5,348 bp in length. The 'no enzyme' control produced bands typical of circular DNA, as the vector DNA in this control remained uncut. The negative control (-ve) reaction containing nuclease-free water in place of vector DNA produced no DNA bands indicating a clean restriction digest reaction. pRU1097 bands restricted with both BamHI and HindIII were isolated and purified using gel extraction techniques and stored at -20 °C until later required.

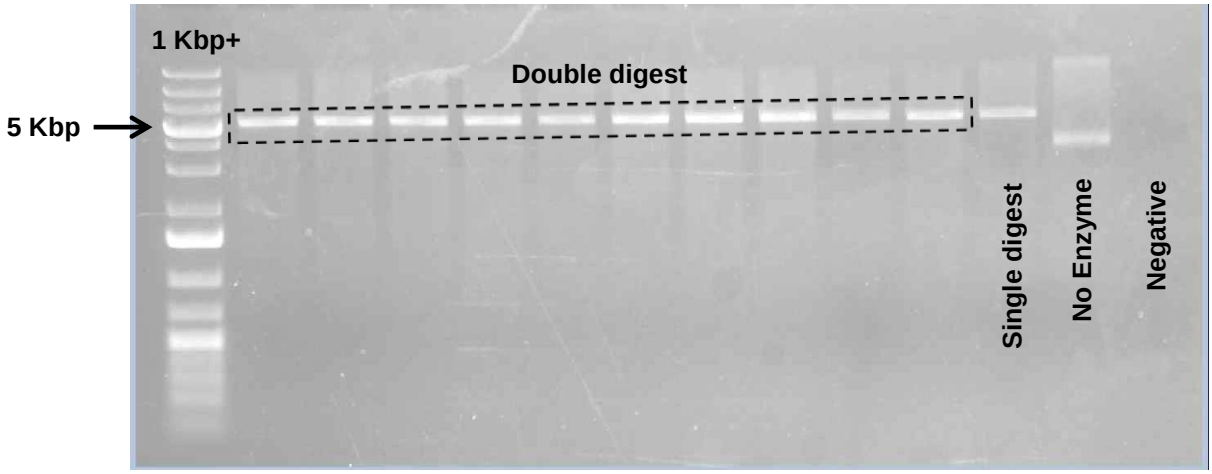

Figure 5.8: Gel electrophoresis of pRU1097 restriction digest products.

pRU1097 was digested using BamHI and HindIII. The single digest reaction used BamHI only, the no enzyme reaction contained nuclease-free water in place of BamHI and HindIII, and the negative reaction contained nuclease-free water in place of vector DNA. Bands produced inside the dashed rectangular box, represent the double cut pRU1097 and were extracted using gel purification. The DNA ladder used was a 1 Kbp plus DNA ladder (Thermo Fisher Scientific), the arrow indicates the 5 Kbp DNA marker.

5.3.7. Ligation of cut pRU1097 with cut *glnAp2* and transformation into *E. coli* RB9132Δ*pta*

The gel image in Figure 5.9 shows the PCR product from the colony PCR targeting the *glnAp2* insertion into the pRU1097 vector.

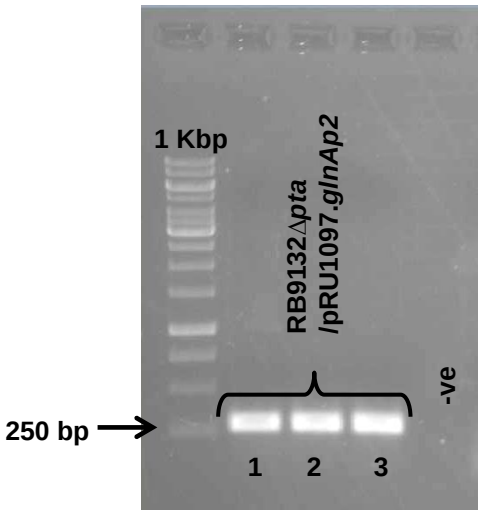

Figure 5.9: Gel electrophoresis of colony PCR products used for the identification of *E. coli* RB9132Δ*pta* cells transformed with pRU1097.*glnAp2*.

pRU1097.*glnAp2* was used to transform into calcium competent RB9132Δ*pta E. coli* cells using heat shock transformation. Resulting colonies were patched onto LB gentamicin agar plates. Patches 1-3 were subject to colony PCR using primers overlapping the vector DNA and insert DNA regions of the recombinant pRU1097.*glnAp2* vector to check for successful transformation. Lanes labelled 1-3 represent the product from these reactions. The negative control (-ve) contained nuclease-free water in place of template DNA. A 1Kb DNA ladder was used (Thermo Fisher Scientific), the arrow indicates the 250 bp marker.

The presence of bright bands in lanes 1-3 in the gel image in Figure 5.9 indicates a successful transformation of RB9132Δ*pta E. coli* cells with the recombinant vector pRU1097.*glnAp2*. The lack of DNA bands in the negative control (-ve) lane also indicates that the colony PCR reaction did not incur and contamination.

Transformants 1-3 were subject to vector extraction using minprep and the vector DNA sent for Sanger sequencing (Eurofins). All three isolates tested positive for the correct sequence of the recombinant pRU1097.*glnAp2* vector and freezer stocks were made for each isolate. From herein onwards, the freezer stock created using isolate 1 was used for all further investigations involving RB9132Δ*pta* /*pRU1097.glnAp2* which will be known as cell type 1.

Cell type 2 (RB9132/pRU1097) and cell type 3 (RB9132/*pRU1097.glnAp2*) were also successfully generated in parallel to cell type 1. All three cells types were subject to characterisation using GFP fluorescence assays

5.3.8. Initial characterisation using GFP fluorescence assays

Cell types were initially characterised by monitoring the GFP fluorescence emitted when incubated in M9 minimal medium, supplemented with 0.4 % (w/v) glucose, buffered to either pH 5.5, pH 6.0, pH 6.5 or pH 7.0 for 12 hours at 30 °C. GFP emission data was normalised against optical density for each dataset. Fluorescence data from all three cell types was plotted onto the same axes, seen in Figure 5.10.

Fluorescence emission from type 2 cells (RB9132/pRU1097), was approximately 12-fold lower than the fluorescence observed when type 3 cells (RB9132/pRU1097.*glnAp2*) were illuminated. This result was expected due to the absence of the *glnAp2* promoter from the GFP reporter vector in type 2 cells. The minimal fluorescence produced by type 2 cells in comparison to type 3 cells indicated that the *glnAp2* promoter can induce detectable levels of fluorescence from the pRU1097 reporter vector. This also indicates that any leaky GFP

expression from pRU1097 can be treated as background and should not cause issues with further investigations. Fluorescence emission from type 3 cells was approximately 5-fold greater than the emission produced when type 1 cells (RB9132Δ*pta*/pRU1097.*glnAp2*) were illuminated. This indicated that the production of the *glnAp2* inducer molecule been mostly inhibited in type 1 cells. As type 1 cells are negative for the *pta* locus, they are unable to convert acetyl-CoA into acetyl-phosphate (AcP) via the action of phosphate acetyltransferase (PTA). This result indicated that AcP, was the inducer molecule for the *glnAp2* promoter.

From GFP fluorescence data produced by type 3 cells, it was also derived that external pH had an influence on the level of GFP fluorescence observed. After 3 hours incubation, type 3 cells cultured at pH 6.0, 6.5, and 7.0 all produced very similar levels of GFP fluorescence, roughly 1.5-fold lower than that produced by type 3 cells cultured at pH 5.5. Between the 3 hour and 6 hour time points, fluorescence produced from cells cultured at pH 6.0, 6.5 and 7.0 began to increase, whilst the fluorescence emitted from cells cultured at pH 5.5 stayed the same. For the remaining 6 hours of the incubation, GFP fluorescence produced by cells cultured at pH 6.0, 6.5 and 7.0 continued to rise whilst GFP fluorescence produced from cells cultured at pH 5.5 stayed approximately linear.

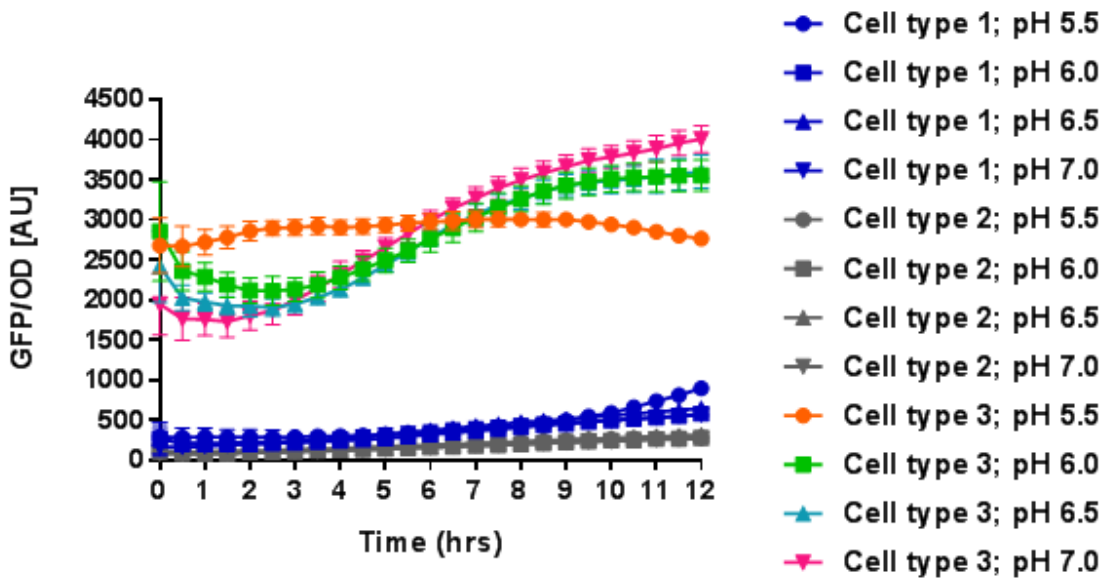

Figure 5.10: GFP fluorescence emitted from cell types 1, 2 and 3 at varying pH.

Cell type 1 (RB9132Δ*pta*/pRU1097.*glnAp2*), cell type 2 (RB9132/pRU1097) and cell type 3 (RB9132/pRU1097.*glnAp2*) were cultured at 30 °C in M9 minimal medium supplemented with 0.4 % (w/v) glucose and adjusted to either pH 5.5, 6.0, 6.5 or 7.0 inside a 96 well plate. GFP fluorescence (excitation 485 nm; emission 520 nm) and $OD_{600\ nm}$ readings were taken every 30 minutes for 12 hours. GFP/OD data for each cell type was calculated and plotted on the same axes. Data sets are labelled according to the characteristics of the *E. coli* cell type in question and the pH of the external medium. Each point represents the mean of the data obtained from three biological replicates, each with three technical replicates. Error bars represent the deviation from the mean.

5.3.9. Influence of external acetate on Type 1 cells

Results described in this section refer to Figure 5.11. Type 1 cells are incapable of the main production pathway for acetate and therefore do not naturally induce GFP expression from the recombinant pRU1097.*glnAp2* vector. By using different external acetate concentrations (0 mM, 3 mM, 9 mM and 45 mM) and pH conditions (pH 5.5, 6.0, 6.5 and 7.0), I was able to monitor the behaviour of *glnAp2* under defined conditions. GFP fluorescence data was normalised against respective OD_{600nm} values and data was grouped based on the concentration of the added acetate.

At all pH levels tested, fluorescence was not detected when cells were cultured in the absence of acetate (0 mM). When cells were cultured with 3 mM acetate, fluorescence was detected from cells cultured at pH 5.5, 6.0, 6.5 or 7.0 after 3 hours incubation. Cells cultured at pH 6.0 showed the highest level of fluorescence, followed by cells at pH 5.5 or pH 6.5. Cells cultured at pH 7.0 produced approximately 2.5-fold lower fluorescence signal after 12 hours when compared to cells cultured at pH 5.5, 6.0 or 6.5. Upon the addition of acetate to a concentration of 9 mM, the pattern of the fluorescence signal was reversed compared to the signal with 3 mM acetate. Cells cultured at pH 7.0 produced the highest fluorescence signal at approximately 12000 [AU], followed by cells cultured at pH 6.5 producing 10000 [AU], pH 6.0 at 9000 [AU] and finally pH 5.5 at 5000 [AU]. The overall fluorescence signal after 12 hours incubation with 9 mM acetate was 2.5 fold greater in cells cultured at pH 7.0 than in cells cultured at pH 5.5.

Upon the addition of 45 mM acetate, fluorescence was detected from illuminated cells cultured at pH 6.0, 6.5 and 7.0 but was not observed from cells

cultured at pH 5.5. Throughout the 12 hour incubation period, cells cultured at pH 7.0 consistently produced the highest levels of fluorescence (14000 [AU] overall), followed by cells cultured at pH 6.5 (9000 [AU] overall) and cell cultured at pH 6.0 (3000 [AU] overall). Figure 5.12 shows a summary of the results from the 12 hour time point after acetate addition. One-way ANOVA analyses did not detect any statistical difference between the florescence emitted from cells cultured in the the presence 3 mM acetate pH 5.5 and those cultured at pH 6.0. This was also true when comparing cells cultured in the presence of 3 mM acetate at pH 5.5 and pH 6.5.

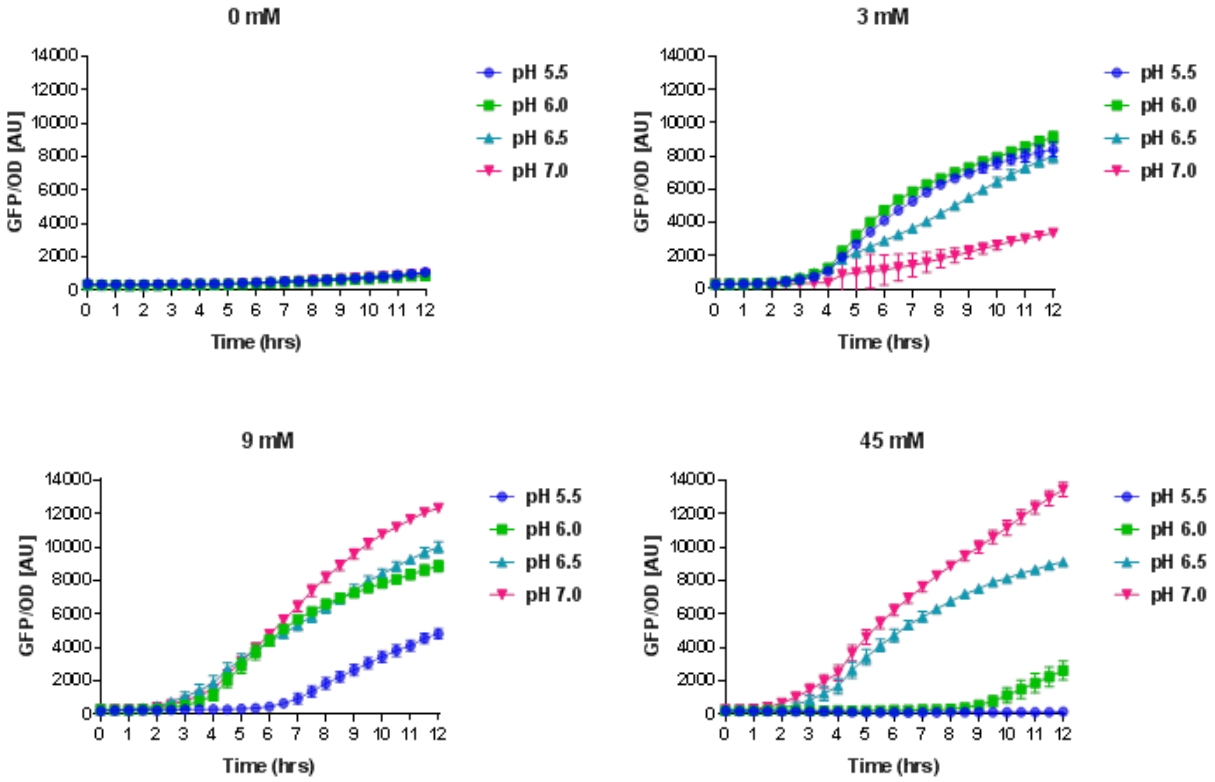

Figure 5.11: glnAp2- GFP reporter expression emitted from cell type 1 at varying pH and external acetate concentration.

Cell type 1 was cultured at 30 °C in M9 minimal medium supplemented with 0.4 % (w/v) glucose and either 0 mM, 3 mM, 9 mM, 45 mM acetate and adjusted to either pH 5.5, 6.0, 6.5 or 7.0 inside a 96 well plate. Fluorescence (excitation 485 nm; emission 520 nm) and $OD_{600\ nm}$ was recorded every 30 minutes for 12 hours.

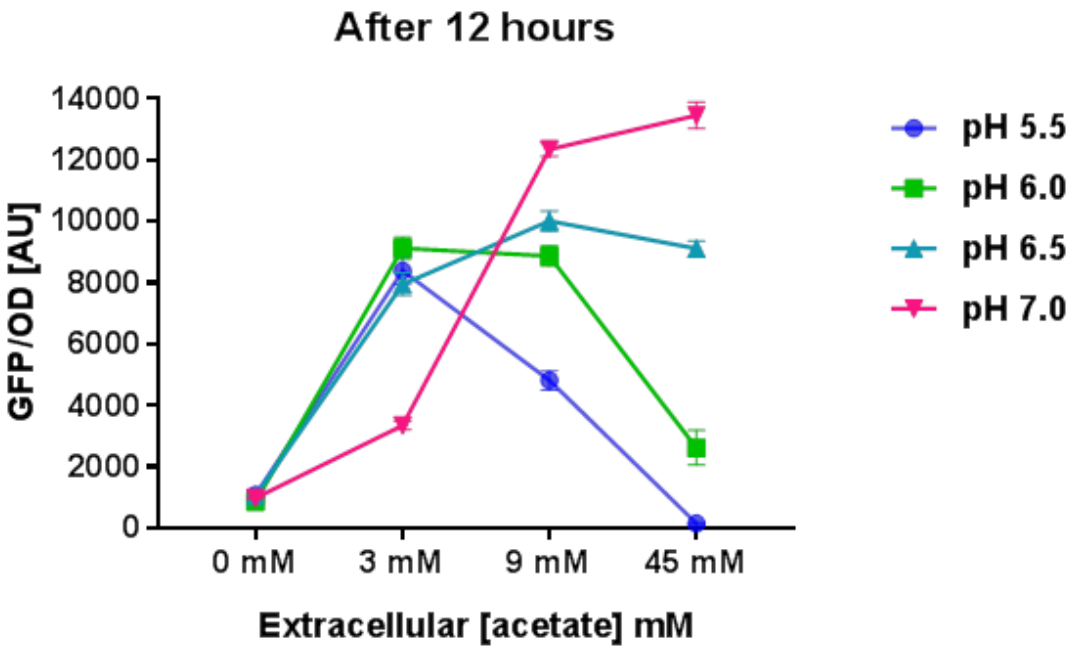

Figure 5.12: GFP fluorescence signal from cell type 1 at varying pH and external acetate concentration after 12 hours of growth at 30 °C in M9 minimal medium.

Cell type 1 was cultured at 30 °C in M9 minimal medium supplemented with 0.4 % (w/v) glucose and either 0 mM, 3 mM, 9 mM or 45 mM acetate and adjusted to either pH 5.5, 6.0, 6.5 or 7.0 in a 96 well plate. Graph represents final GFP fluorescence (excitation 485 nm; emission 520 nm) and $OD_{600\ nm}$ readings after 12 hours incubation.

5.4. Discussion

The work described in this chapter set out to characterise the sensitivity of the *glnAp2* promoter to extracellular pH and acetate concentration, to further support the results obtained by Bulter *et al*., 2004 [255]. For this, I used *E. coli* RB9132 cells, either positive or negative for the *pta* locus. These cells were transformed with a GFP reporter vector, either containing the *glnAp2* promoter (pRU1097.*glnAp2*) or without a promoter (pRU1097). By comparing GFP fluorescence emitted upon the illumination of type 2 cells (RB9132/pRU1097) and type 3 cells (RB9132/pRU1097.*glnAp2*), I was able to determine that the *glnAp2* promoter does induce expression of *gfp*. By comparing type 1 cells (RB9132Δ*pta*/pRU1097.*glnAp2*) with type 3 cells (RB9132/pRU1097.*glnAp2*), I was able to suggest AcP as the inducer molecule for *glnAp2*.

Type 3 cells, cultured at pH 5.5, produced the highest levels of GFP fluorescence, during the first 6 hours of incubation, when compared against the same strain, incubated at pH 6.0, 6.5 and 7.0. This result could be explained by the partitioning of acetate across the cellular membrane at varying pH levels [251]. Low pH i.e. pH 5.5 as opposed to pH 7.0, can facilitate a greater proportion of acetate to become protonated into acetic acid, which has a much greater permeability across the *E. coli* cellular membrane. Due to the presence of the *pta* locus, type 3 cells were capable of producing acetate via the PTA-ACKA pathway, which is likely to have accumulated over the course of the incubation period. During the early stages of incubation (0-6 hrs), when acetate accumulation is predicted to be lower, only the lowest pH, i.e. pH 5.5, provided sufficient pH potential across the cellular membrane to assist the assimilation of acetate. Once assimilated into the *E. coli* cells, acetate is likely to have been converted into AcP by the action of ACKA, allowing for induction of the *glnAp2* promoter.

Between the 3 hour and 6 hour time points, GFP fluorescence produced from cells cultured at pH 6.0, 6.5 and 7.0, increased in an approximately linear fashion with time. It is likely that over this time, the lower protonation rate of acetate occurring under these pH conditions was balanced by increasing external acetate concentration, due to acetate accumulation.

Considering acetate accumulation and pH levels, I expected to see fluorescence increase as the culture time progressed. However, this was not the case when studying data from cells cultured at pH 5.5. At this pH, a plateau was observed in the GFP fluorescence emitted between the 6 and 12 hour time points and was lower than the GFP emitted under other pH conditions. These results may be explained by documented acetic acid toxicity to *E. coli* [243, 251], as it is possible that the accumulated acetate concentration coupled with the increased protonation rates at low pH, led to an influx of acetic acid back through the cellular membranes at pH 5.5. This potentially could cause toxicity to the *E. coli*'s metabolic pathways.

Further investigations were required to determine the effect of external acetate concentration and pH on the induction of the *glnAp2* promoter. For this, cells negative for the *pta* locus were used, preventing the main route of AcP (and therefore acetate) production. By subjecting the cells to varying pH and external acetate concentrations, I was able to have greater control over AcP levels. AcP generation was predicted to be high under low pH (when protonation of acetate was highest) and at high acetate concentration (increasing the concentration of acetate available for protonation). Under these conditions, a greater concentration of acetic acid was predicted to pass across the cellular membrane for conversion into AcP by the action of ACKA.

When cultured with an additional 3 mM acetate, the GFP fluorescence produced indicated that pH levels of 5.5, 6.0 and 6.5 were the most effective pH for inducing expression from the *glnAp2* promoter. When cultured with an additional 9 mM acetate, a pH level of 7.0, indicated the greatest level of expression from the promoter. When acetate concentrations were at their greatest (45 mM), the lowest pH levels became the most ineffective at inducing expression of *glnAp2*. This is likely due to the explained toxicity of acetic acid to cells and further supports that transfer of acetate into *E. coli* cells is controlled by concentration of acetate and pH potential over the cellular membrane.

The results from this study show promising possibilities for the engineering of a negative feedback loop in *E. coli* for the regulation of acetate production. My results indicate that the *glnAp2* promoter can respond to external acetate concentration and pH. Stimulation of the *glnAp2* promoter is triggered under unfavourable culturing conditions, i.e. accumulation of external acetate and a reduction in pH. My results show that the promoter is most sensitive to small amounts of acetate accumulation at lower pH levels.

6. Chapter six: Design, creation and characterisation of an antisense construct targeting *pta*

6.1. Introduction

Antisense RNA's are a form of regulatory RNA and have been known to exist in bacteria for many years. Antisense RNA is capable of base-pairing with messenger RNA to prevent translation of the transcript into protein. Binding of antisense RNA has two effects, the first, is the direct blocking of the ribosomal machinery, the second is the formation of double stranded (ds) RNA, which is rapidly degraded by the double strand specific RNase III. Antisense RNA is commonly used as a form of regulation of bacterial RNA, allowing the upregulation or down-regulation of gene translation [258, 259]. Now with the vast improvement of molecular biology techniques, antisense RNA is a commonly used technology for gene interference and silencing [193].

A paper by Kim *et al* [260], described the use of antisense RNA to target the *pta-ackA* pathway. This study developed set of primers for the generation of antisense oligos against both the *pta* and *ackA* genes. The authors cloned either one or both antisense oligos into a DNA vectors, under the control of the *ackA* promoter and characterised expression of the pathway and the production of acetate. The study found that although mRNA levels of each of the genes were down-regulated in cells containing the antisense, the overall production of acetate was not reduced. They concluded that the *ackA* promoter, may have not been strong enough to result in both down-regulation of mRNA and down-regulation of acetate production. A second paper, by Bakhtiari *et al*. [261], performed a similar study, but this time placed the antisense genes under the control of the much stronger T7 genetic promoter. As a result, they observed a decrease in acetate concentration when antisense targeted the *pta-ackA* pathway. Figure 6.1 details A) the action of the antisense fragment against the translation of the *pta* gene,

and B) how the antisense fragment is cloned from the genome for use in a recombinant vector.

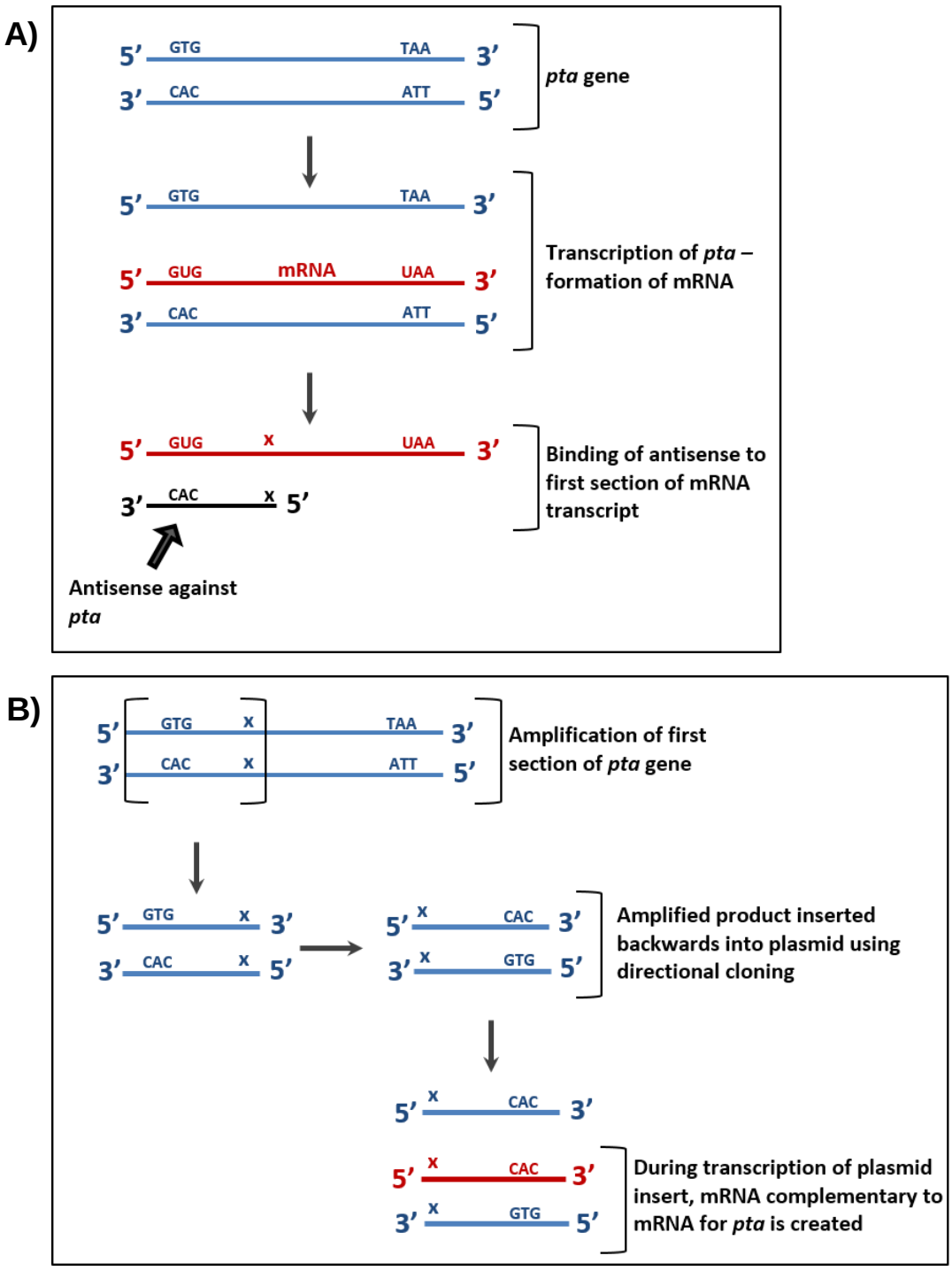

Figure 6.1: Schematic to show the action of the antisense fragment against *pta* translation, and the synthesis of the oligo.

A) The action of the antisense fragment against the translation of the *pta* gene, B) The process of cloning the antisense fragment from the *E. coli* genome. Information sourced from [193].

The work described in this chapter couples the developments of Bulter *et al*. with that of Kim *et al*. by placing the *glnAp2* promoter in control of antisense targeting the *pta* gene. The aim of the investigation was to assess the ability of *glnAp2* induction to control acetate production compared to non-engineered wild type *E. coli* cells.

6.3. Results

6.3.1. Amplification of *t-glnAp2* and as*pta* fragments

PCR was used to amplify the *t-glnAp2* and as*pta* fragments from *E. coli* strain RB9132 DNA. Amplified PCR products were each electrophoresed on a 1 % (w/v) agarose gel and purified using gel extraction. 5 µl from each purified product was electrophoresed on a second agarose gel seen in Figure 6.2 to check the quality of the purified PCR product.

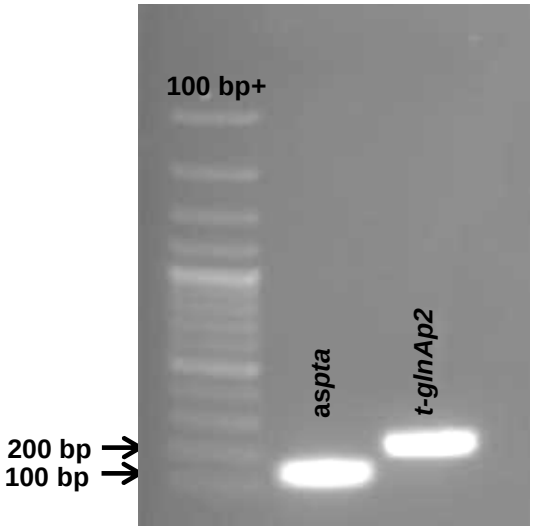

Figure 6.2: Purified antisense_*pta* construct components 'as*pta*' and '*t-glnAp2*'.

Gel electrophoresis of the purified as*pta* region and the *t-glnAp2* promoter region, both isolated from the *E. coli* RB9132 genome. The marker used is a 100 bp plus DNA ladder (Thermo Fisher Scientific). The arrows indicate the 100 bp and 200 bp DNA markers.

6.3.2. Sequencing of *t-glnAp2* and as*pta* fragments

Relevant regions of the pGEM-T.*t-glnAp2* and pGEM-T.as*pta* vectors were sequenced and compared to the expected sequences. Alignments showed that each fragment had been successfully cloned.

6.3.3. Release of cloned DNA fragments from holding vectors

The DNA fragments *t-glnAp2*, as*pta* and *pta*_term was each released from their respective holding vectors using restriction digestion techniques and electrophoresing the product on a 1 % (w/v) agarose gel. Figure 6.3 below, shows an example of the products generated from the digestion of the vector pGEMT.*t-glnAp2,* which was subject to double digest with BamHI, and HindIII. This generated two DNA fragments. The bright DNA bands produced at approximately 3 Kbp represent the linearized the pGEM-T vector DNA, minus the *t-glnAp2* promoter section. The fainter bands highlighted inside the dashed rectangle box, at approximately 200 bp, represent the *t-glnAp2* promoter region. The single digest reaction produced a single bright band marginally larger than the 3 kb marker, representing the linearized form of the recombinant pGEM-T.*glnAp2* vector. The 'no enzyme' control produced DNA bands typical of uncut circular DNA. The negative control (-ve) contained nuclease-free water in place of vector DNA produced no DNA bands, indicating a clean restriction digest reaction.

The released *t-glnAp2,* as*pta* and *pta*_term fragments bands were purified from their respective gels using gel extraction techniques and stored at -20 °C until later required.

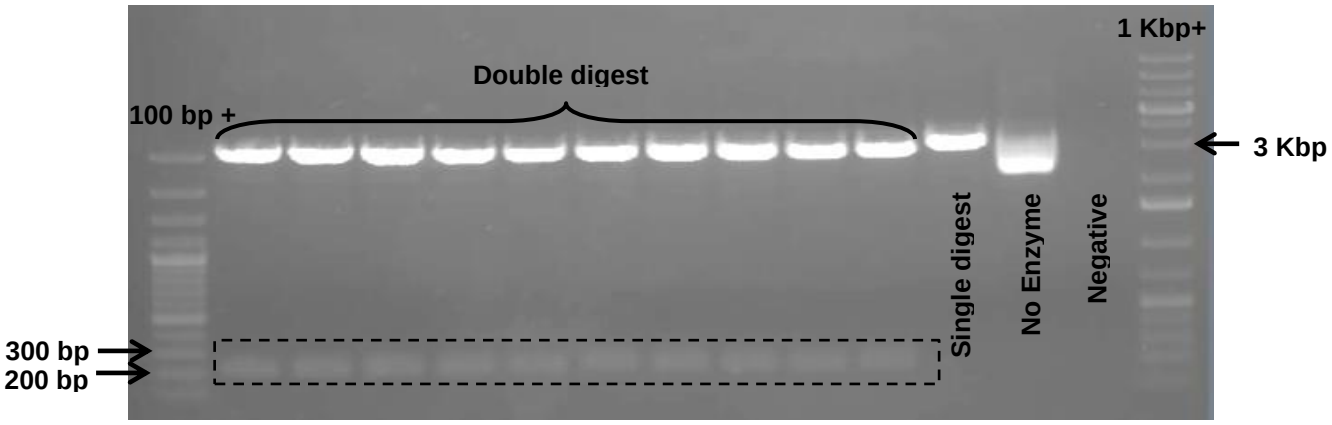

Figure 6.3: Gel electrophoresis of pGEM-T.*t-glnAp2* restriction digest products.

The recombinant vector pGEM-T.*t-glnAp2* was isolated from its host cells and subject to digestion with BamHI and HindIII restriction enzymes. The single digest reaction used BamHI only, the no enzyme reaction contained nuclease-free water in place of BamHI and HindIII. The negative reaction contained nuclease-free water in place of vector DNA. DNA marker, left: 100 bp plus; DNA marker, right, 1 Kbp plus (Thermo Fisher Scientific). Arrows indicate the 200 bp and 300 bp DNA markers (left) and the 3 Kbp DNA marker (right). The dashed rectangular box represents the released *t-glnAp2* fragment.

6.3.4. Building and sequencing of antisense construct against *pta*

The antisense construct was successfully formed within the pRU1097 vector backbone (Figure 6.4) and introduced into *E. coli* RB9132 cells to form RB9132_antisense_*pta* (RB1932/pRU1097.*t-glnAp2.as*pta.*pta*_term). An annotated alignment to confirm the sequence of the antisense construct is provided in Figure A4.4 of the appendices.

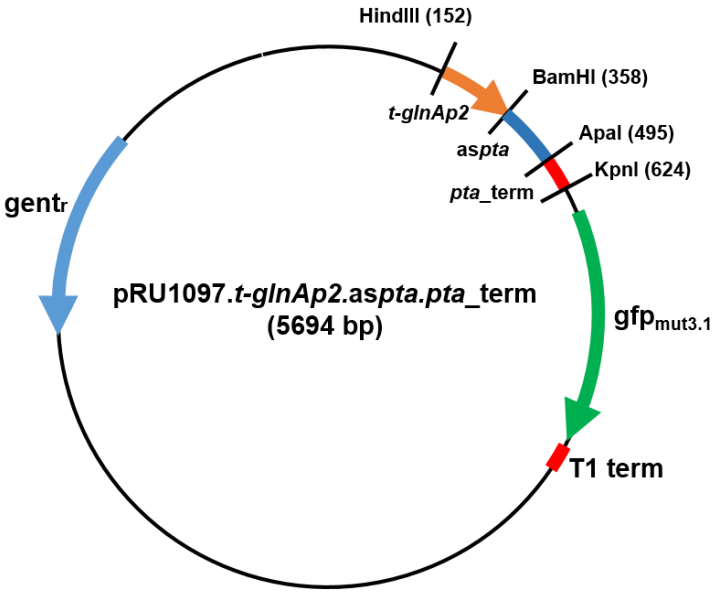

Figure 6.4: Vector map of pRU1097.*t-glnAp2*.as*pta.pta*_term.

The truncated glutamine synthetase promoter *t-glnAp2* and the antisense fragment targeting the *pta* gene (as*pta*) were successfully cloned from the RB9132 genome and placed into the pRU1097 vector backbone. The *pta* terminator fragment was artificially synthesised before placement within the pRU1097 vector backbone, downstream of the as*pta* fragment.

6.4.5. Characterisation of the engineered construct using GFP fluorescence

Both the truncated nature of the *t-glnAp2* promoter region and the presence of the translation termination (*pta*_term) fragment within the antisense construct, should prevent any translation of genes downstream from the *pta*_term region. Therefore, I did not expect to detect any *gfp* expression in RB9132_antisense_*pta.*

RB9132_antisense_*pta* cells were directly compared against Type 1 cells (RB9132Δ*pta*/pRU1097.*glnAp2*) by measuring fluorescence emitted when cultured at pH 7.0 with additional acetate (0 mM, 3 mM, 9 mM or 45 mM) at 30 °C. Under all conditions tested, RB9132_antisense_*pta* cells did not produce

levels of fluorescence higher than the fluorescence emitted by Type 1 cells cultured without the presence of additional acetate (Figure 6.5).

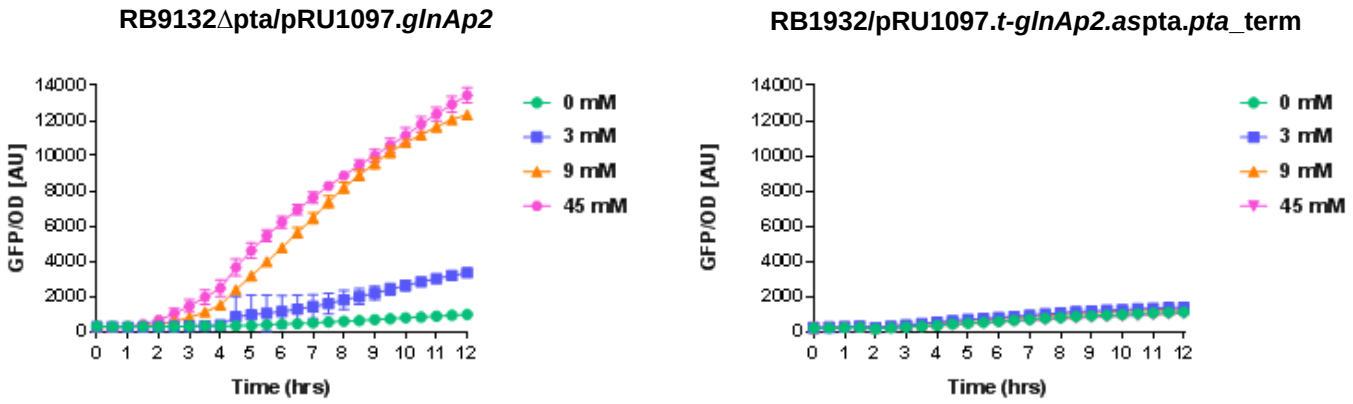

Figure 6.5: GFP fluorescence at pH 7.0 of Type 1 *E. coli* cells vs RB9132_antisense_*pta*.

Left panel: Type 1 cells (RB9132Δpta/pRU1097.*glnAp2*). Right panel: RB9132_antisense_*pta* cells. Cells were cultured at 30 °C in M9 minimal medium supplemented with 0.4 % (w/v) glucose and either 0 mM, 3 mM, 9 mM, 45 mM acetate and adjusted to pH 7.0. GFP fluorescence (excitation 485 nm; emission 520 nm) and $OD_{600\ nm}$ readings were taken every 30 minutes for 12 hours.

6.4.6. RNA extractions

Figure 6.6 shows a representative example of the extracted RNA from RB9132_antisense_*pta* after bacterial growth in the presence of different concentrations of acetate (0 mM, 3 mM, 9 mM, or 45 mM) at pH 5.5. The extracted RNA samples were treated with DNase and electrophoresed in a 1.0 % (w/v) agarose gel. Double bands were observed for all RNA extracts. The bacterial 23S rRNA ran just below the 1.5 Kbp DNA marker and the 16S rRNA ran just under the 1 Kbp DNA marker. Brighter bands, indicating a greater concentration of RNA, were observed from extracts taken from cells that had been exposed to lower concentrations of acetate.

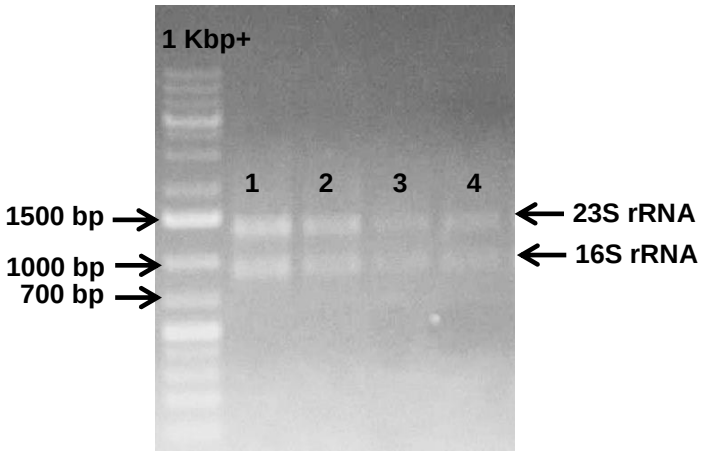

Figure 6.6: RNA extractions from RB9132_antisense_*pta.*

Agarose gel electrophoresis of RNA isolated from *E. coli* cells, strain RB9132_antisense_*pta*. Lanes 1-4 show RNA extracted from cells cultured at pH 5.5 in M9 minimal medium with the addition of 0 mM, 3 mM, 9 mM or 45 mM sodium acetate, respectively. The DNA ladder used was 1 Kbp plus ladder (Thermo Fisher Scientific). The arrows on the left indicate the 700 bp, 1000 bp and 1500 bp DNA markers. Arrows on the right indicate the 16S and 23 S rRNA separated during electrophoresis, respectively.

6.4.7. End-point PCR amplification of RNA and cDNA

Figure 6.7 shows a representative example of the end-point PCR amplification products generated from cDNA template and the corresponding RNA from which it was generated. End-point PCR was performed on RNA extracts to detect any DNA contamination. End-point PCR was performed on synthesised cDNA to ensure that cDNA synthesis had been successful.

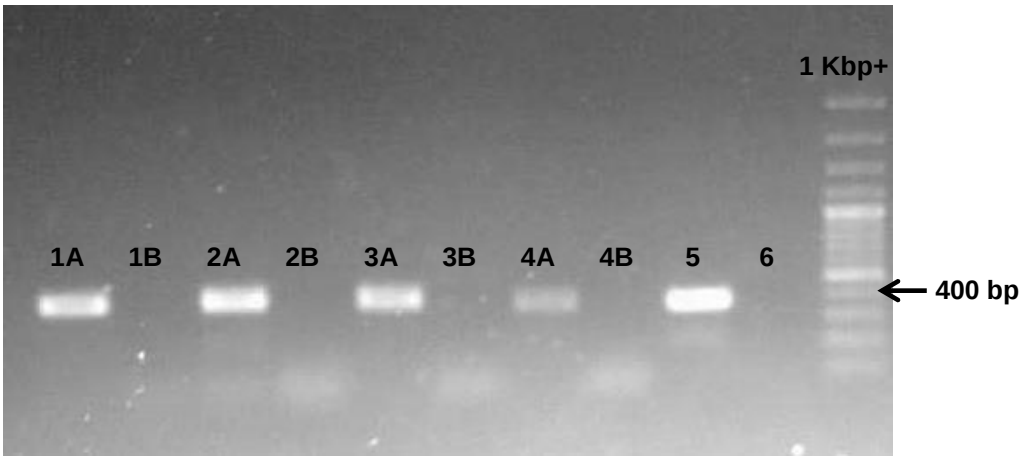

Figure 6.7: Electrophoresis of PCR products produced when using cDNA and RNA as template.

RNA extracted from RB1932/pRU1097.*t-glnAp2*.a*spta*.*pta*_term cells cultured at varying pH in the presence of varying acetate concentrations were converted in to cDNA. cDNA and the parent RNA samples were then subject to end-point PCR targeting the *pta* gene. The numbers 1-4 represent RB9132_antisense_*pta* cells cultured at pH 5.5 and in the presence of 0 mM, 3 mM, 9 mM or 45 mM acetate respectively. The lettering following each of these numbers refer to either the cDNA sample (A) or the RNA extract (B). Lane 5 contains gDNA from the *E. coli* RB9132 strain and lane 6 contains the negative control (-ve) which had nuclease-free water in place of DNA/RNA during the PCR reaction. The DNA ladder used was a 1 Kbp plus ladder (Thermo Fisher Scientific), the arrow indicates the 400 bp DNA marker.

6.4.8. qPCR amplification of target cDNA

All qPCR assays carried out during this investigation were no contaminated with genomic DNA due to repeated rounds of DNase treatment of RNA, to ensure no contamination of samples. Optimised qPCR primers were able to successfully amplify regions of the cDNA and behaved within appropriate parameters advised for qPCR reactions [262]. cDNA amplification targeting *cysG*,*16S_v6*, *pta* and as*pta* was observed from all extracts used for this investigation.

6.4.9. Relative expression of antisense message against *pta*

The following results relate to the data graphs detailed in Figure 6.8. Expression of as*pta* was measured in cells cultured at pH 5.5 and normalised against the reference gene *cysG*. A clear pattern of increasing relative expression was observed as the acetate concentration increased from 0 mM to 45 mM. The error for each data set also increased as acetate concentration increased. This hindered the statistical analysis using one-way ANOVA. The *aspta* expression data was also normalised against a second reference gene, *16S_V6*. The average relative expression of as*pta* increased slightly as additional acetate concentration increased from 0 mM to 3 mM. However, the relative expression of as*pta* was then reduced at higher acetate concentrations of 9 mM and 45 mM. No statistically significant differences within the data set were detected using one-way ANOVA statistical analyses.

Expression data for as*pta* was also collected for cells cultured at pH 7.0. When normalised against the *cysG* reference gene, there was an overall trend of decreasing expression of the as*pta* gene as acetate concentration increased. The level of error calculated for each data set decreased as additional acetate

concentration increased. One-way ANOVA statistical analyses did not detect any statistically significant difference in relative expression of the antisense message normalised against *cysG* at different additional acetate concentrations at pH 7.0. The same dataset was also normalised against the reference gene *16S_V6*. This analysis yielded an overall trend in decreasing expression of the as*pta* message as additional acetate concentration increased. One-way ANOVA statistical analyses did not detect any statistically significant difference in relative expression of the antisense message against *pta* at different additional acetate concentrations at pH 7.0.

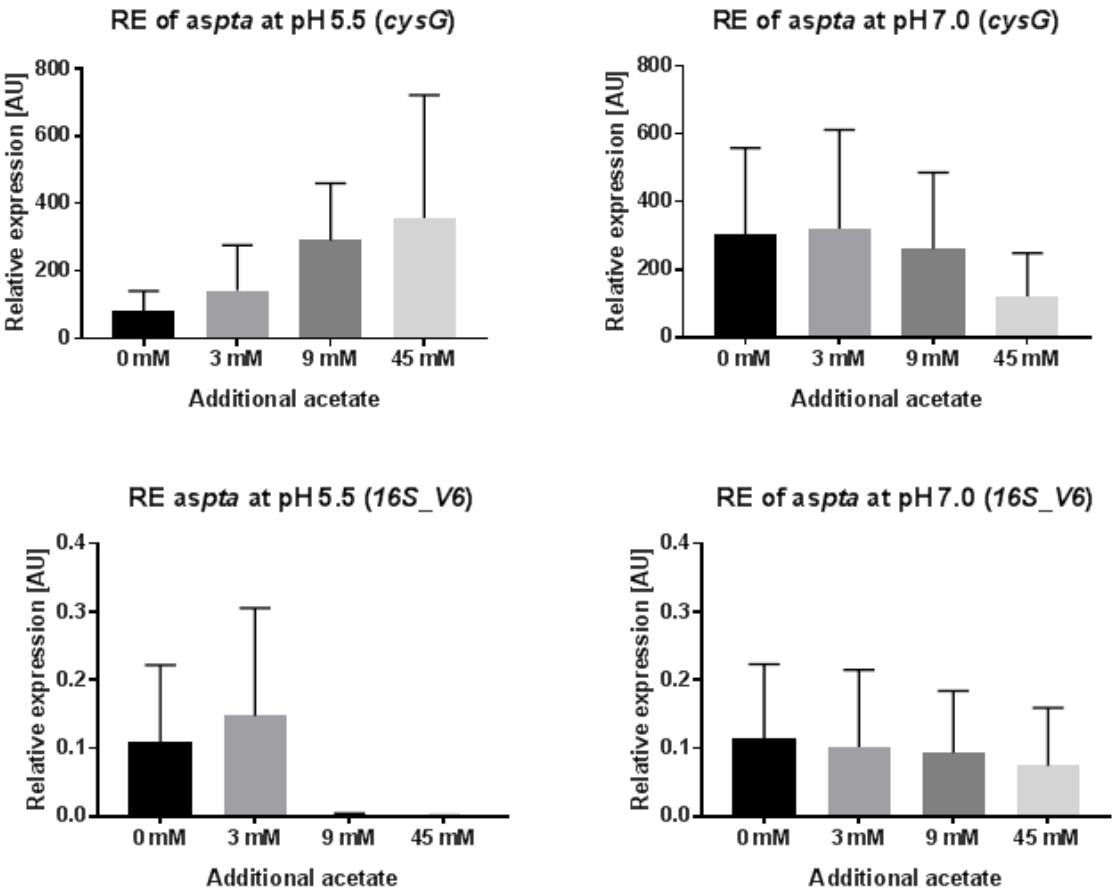

Figure 6.8: Relative expression of *aspta* in RB9132_antisense_*pta* cells at varying additional acetate concentration and pH.

RB9132_antisense_*pta* cells were cultured at either pH 5.5 or pH 7.0 with an additional acetate concentration of 0 mM, 3 mM, 9 mM, or 45 mM at 30 °C for 6 hours. Levels of as*pta* cDNA were measured using qPCR. This data represents two biological replicates, for each biological replicate, three technical replicates were included in the qPCR assay. Expression of the as*pta* target, relative to *cysG* and *16S_V6* reference gene and was calculated using the $2^{-\Delta\Delta Ct}$ method [182]. One-way ANOVA statistical analysis was used to calculate the statistical significance within datasets.

6.4.10. Relative expression of *pta*

The following results relate to the data graphs detailed in Figure 6.9. The *pta* gene expression data collected from cells cultured at pH 5.5 was first normalised against the *cysG* reference gene. This produced a pattern of decreasing relative expression of *pta* as the external acetate concentration changed from 0 mM to 45 mM. One-way ANOVA statistical analyses were performed across the data set and detected a significant drop in expression upon incubation with 9 mM acetate or 45 mM acetate compared with 0 mM additional acetate (*p* values of ≤0.05 and ≤0.0001 respectively). *pta* expression data was also normalised against a second reference gene, *16S_V6*, which also revealed decreasing *pta* expression with increasing additional acetate concentration. Normalisation against *16S_V6,* revealed no *pta* expression after the addition of 9 mM or 45 mM acetate. One-way ANOVA analyses were performed and detected a significant drop in *pta* expression corresponding to a *p* value of ≤0.05 when for treatments of 9 mM or 45 mM acetate when compared to cells that were not treated with acetate (0 mM acetate).

At pH 7.0, opposite trends in *pta* expression with increasing additional acetate, were observed compared to cells cultured at pH 5.5. The addition of 3 mM or 9 mM acetate, did not have a significant effect on the relative expression of *pta*. However, when 45 mM acetate was added, a significant increase in *pta* expression was observed (*p* ≤0.01) compared to every other acetate concentration. The same pattern was observed when the data set was normalised against the *16S_V6* reference gene, (*p* ≤0.05).

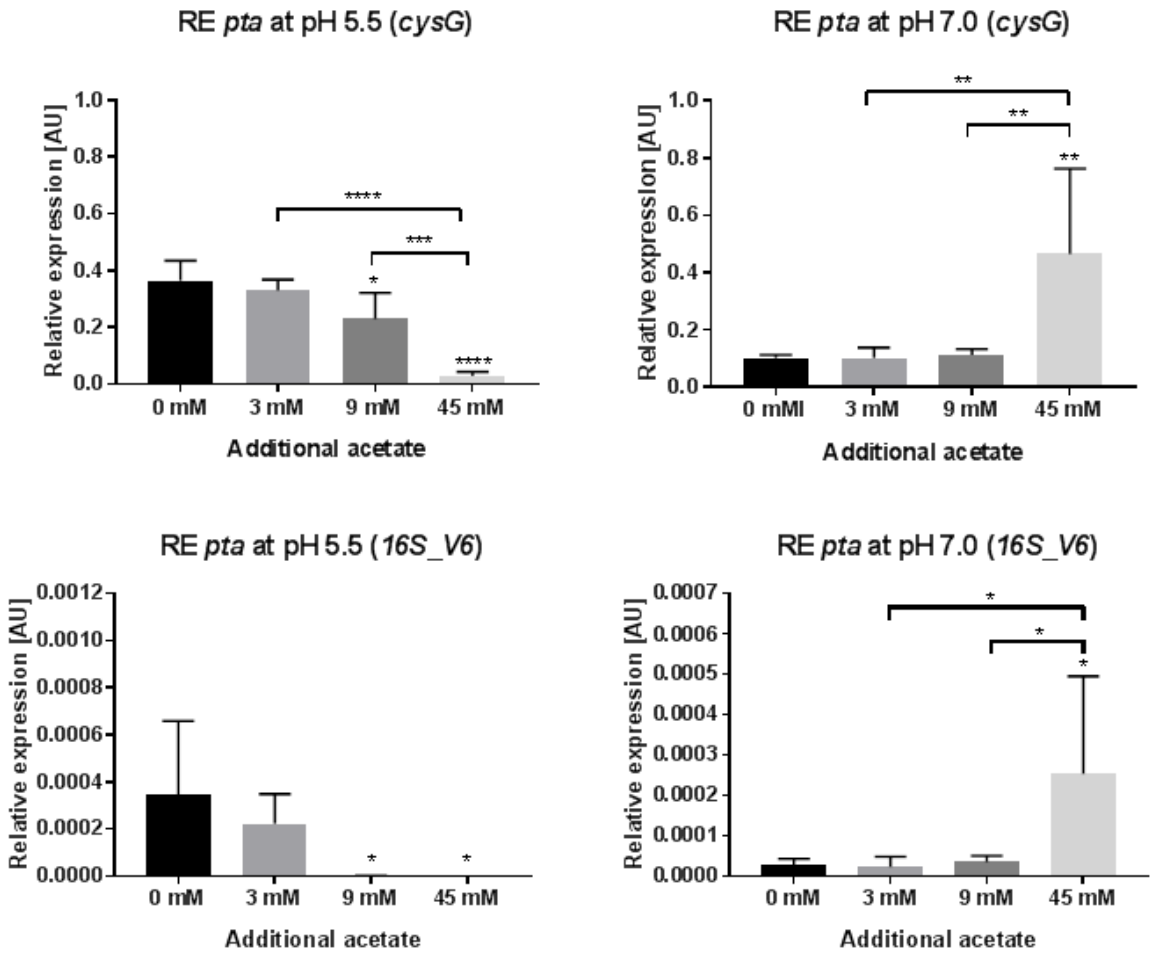

Figure 6.9: Relative expression of *pta* in RB9132_antisense_*pta* cells at varying additional acetate concentration and pH.

RB9132_antisense_*pta* cells were cultured at either pH 5.5 or pH 7.0 with an additional acetate concentration of 0 mM, 3 mM, 9 mM, or 45 mM at 30 °C for 6 hours. Levels of *pta* cDNA were measured using qPCR. This data represents two biological replicates, for each biological replicate, three technical replicates were included in the qPCR assay. Expression of the *pta* target, relative to *cysG* and *16S_V6* was calculated using the $2^{-\Delta\Delta Ct}$ method [182]. One-way ANOVA statistical analyses were used to calculate the statistical significance within datasets.

6.4.11. Comparison of *pta* expression in wild type versus engineered strain

An RT-qPCR assay for the detection of *pta* expression was performed on RB9132 (plasmid free) wild type cells and the RB9132_antisense_*pta* strain. Two biological replicates were performed, each with three technical replicates. The results obtained for the relative expression of the *pta* gene in the RB9132 wild type cells were compared to the averaged data obtained from biological data obtained for RB9132_antisense_*pta* obtained in section 6.4.10 (Figure 6.10).

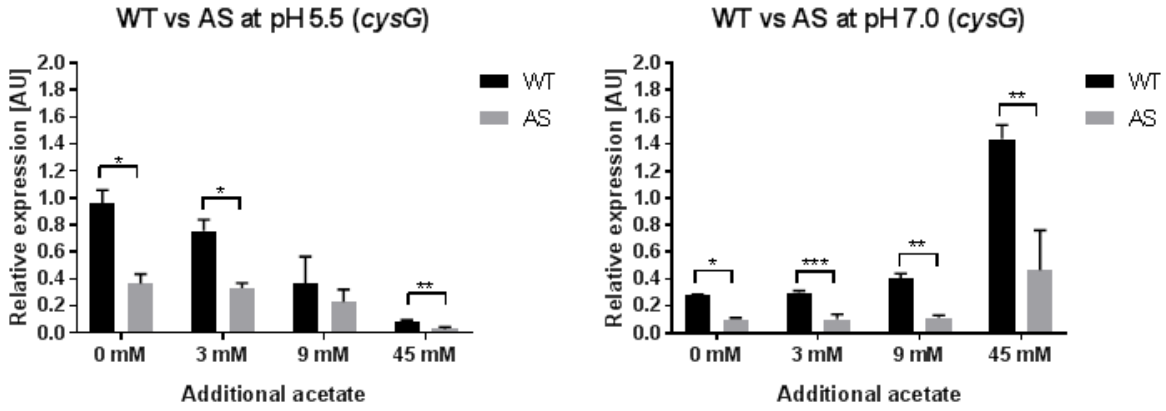

Figure 6.10: Relative expression of *pta* in RB1932 WT cells and RB9132_antisense_*pta* cells at varying additional acetate concentration and pH.

RB9132 wild type cells (WT) and RB9132_antisense_*pta* cells (AS) were cultured at either pH 5.5 or pH 7.0 with an additional acetate concentration of 0 mM, 3 mM, 9 mM, or 45 mM at 30 °C for 6 hours. Levels of *pta* cDNA were measured using qPCR. This data represents two biological replicates, for each biological replicate, three technical replicates were included in the qPCR assay. Expression of the *pta* target, relative to *cysG* was calculated using the $2^{-\Delta\Delta Ct}$ method. One-tailed t-tests were then carried out on each dataset.

RB9132 wild type cells (WT) showed higher levels of relative *pta* expression than the RB9132_antisense_*pta* strain (AS) under all the tested conditions. The *pta* expression patterns of the RB9132_antisense_*pta* and wild type cells were similar, but the relative expression levels were highest in wild type cells. As in the AS strain, *pta* expression decreased gradually with increasing external acetate concentration when the cells were cultured at pH 5.5. When cultured at pH 7.0, relative *pta* expression levels from the wild type cells increased with increasing external acetate concentration, a result that was also observed in the RB9132_antisense_*pta* strain. Under all conditions tested, except pH 5.5, 9 mM, one-tailed t-tests detected a statistical drop in *pta* expression in engineered cells versus the wild type.

6.4.12. Effect of antisense construct on acetate production

Acetate production in RB9132_antisense_*pta*, acetate cultures was quantified and compared to that in wild type RB9132 *E. coli* cultures. Wild type and RB9132_antisense_*pta* strains were cultured in four different types of growth medium (M9 minimal media, supplemented with glucose, pH 5.5 and pH 7.0, LB media and anaerobic growth media) for 12 hours at 37 °C with shaking. Supernatant was removed from the cultures and passed through a 10 kDa Molecular Weight Cut-Off (MWCO) spin filter. The Acetate Colorimetric Assay kit provided by Sigma Aldrich was then used to quantify the concentration of acetate in each sample of supernatant, relative to a previously generated standard curve. One tailed statistical t-tests were carried out on each data set, to assess the significance of the difference in acetate production between RB9132_antisense_*pta* (AS) and RB9132 wild type (WT) strains (Figure 6.11).

Only marginal differences in acetate levels were observed between RB9132_antisense_*pta* and RB9132 wild type strains. Acetate production from antisense strain, was lower relative to the wildtype strain when cultured at pH 5.5 in M9 minimal medium ($p \leq 0.05$). A reduction in acetate production in the antisense strain was also observed when cells were cultured in anaerobic rich medium. However, this reduction in acetate production was not statistically significant.

When cultured in M9 minimal medium buffered to pH 7.0 and in LB medium, acetate production was higher in RB9132_antisense_*pta* strain relative to the RB9132 strain. Although the increase in acetate production from the RB9132_antisense_*pta* strain was only marginal, in each case, these marginal differences were determined as significant using one-tailed t-tests, and each produced a p value of ≤0.01.

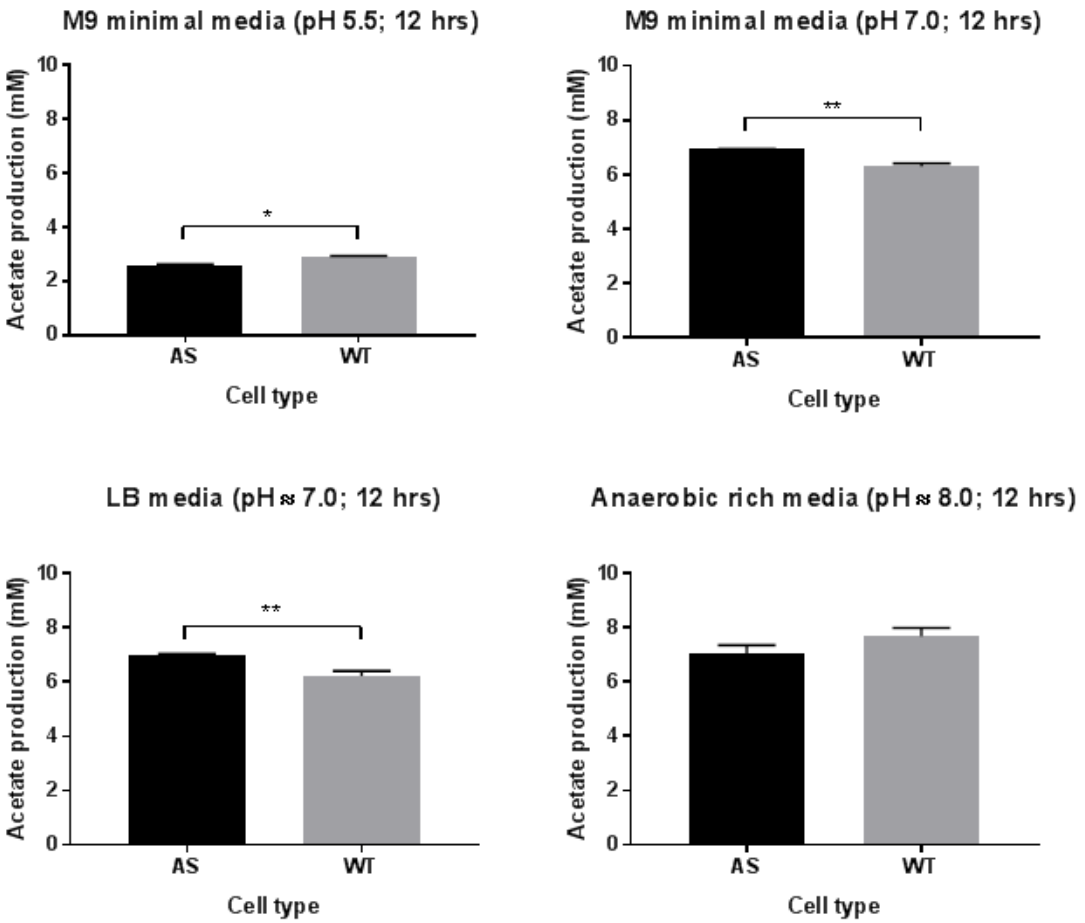

Figure 6.11: Acetate production from RB9132_antisense_*pta* vs RB9132 wild type cells

RB9132 wild type cells (WT) and RB9132_antisense_*pta* cells (AS) were cultured for 12 hours at 37 °C. Cells were cultured in sealed vessels in either M9 minimal medium, buffered to pH 5.5; M9 minimal medium, buffered to pH 7.0; LB medium, roughly pH 7.0 and anaerobic rich medium, all supplemented with 0.4 % (w/v) glucose. Supernatant was subject to acetate quantification, using the Acetate Colorimetric Assay kit (Sigma Aldrich). Acetate concentration was then normalised against the OD_{600nm} of the original culture samples to compensate for any discrepancies in growth between AS and WT strains. One-tailed t-tests were then carried out on each dataset.

6.5. Discussion

To achieve acetate regulation in *E. coli*, I built an antisense construct designed to disrupt translation of *pta*. This gene codes for the enzyme phosphate acetyltransferase (PTA) which is responsible for converting acetyl CoA into acetyl phosphate, which is then converted by acetate kinase into acetate. This construct was controlled by a truncated form of the glutamine synthetase promoter (*t-glnAp2*), which was placed upstream of an antisense coding region (as*pta*). The construct was engineered into the GFP reporter vector, pRU1097, used previously for characterisation of the *glnAp2* promoter (Chapter 5). The recombinant vector was designated as pRU1097.*t-glnAp2*.as*pta.pta*_term, and transformed into calcium competent RB9132 cells (positive for the *pta* locus) to create RB9132/pRU1097.*t-glnAp2*.as*pta.pta*_term. This cell type was denoted as RB9132_antisense_*pta* (and referred to as the antisense (AS) strain).

The *pta* gene was chosen as the antisense target in this study. By regulating antisense production under the control of the characterised glutamine synthesis promoter, I aimed to prevent production of the PTA enzyme under conditions of low pH and high external acetate concentration. These conditions were predicted to increase the expression from the *t-glnAp2* promoter, leading to transcription of the antisense message targeting *pta*. By blocking translation of the *pta* mRNA transcript, it was predicted that this would in turn prevent the generation of the PTA enzyme, and therefore the production of acetate.

Preliminary characterisation using GFP fluorescence assays, indicated that the antisense construct within the pRU1097 vector backbone, prevented expression of GFP gene downstream of the construct. Fluorescence was not expected from RB9132_antisense_*pta* due to the truncation of the upstream

region ahead of the *glnAp2* promoter start site. This truncation prevented the inclusion of the predicted Shine-Dalgarno sequence and therefore the binding of ribosome machinery and translation of mRNA transcripts coding for genes downstream of the promoter. This was an important feature as I did not want ribosomal machinery to bind to the antisense message against *pta*. The *pta* terminator (*pta*_term) is likely to have also prevented expression from the *gfp* gene due to its Rho-independent termination site, which consists of inverted repeat sequences which base pair to form a hairpin loop structure [263]. It is widely accepted that these hairpin structures prevent the RNA polymerase from continuing with elongation of the transcript.

The expression of *pta* cells in the AS strain was quantified using reverse transcription quantitative PCR (RT-qPCR). RT-qPCR is a technique used to detect the expression of a gene of interest, by quantifying the level of the cDNA, which is equivalent to the original level of the mRNA transcript. The antisense construct that I developed, was designed to bind to mRNA transcripts coding for the *pta* gene. Binding of antisense to the *pta* mRNA target, should have, in theory, prevented the translation of the *pta* transcript. By using primers specific to the *pta* gene, the level of *pta* expression (i.e. the level of intact *pta* mRNA transcripts) could be inferred from the degree of PCR amplification. qPCR primers were also designed to target the antisense message itself, to detect expression from the *glnAp2* promoter.

The normalisation of qPCR data against reference genes provided assurance that expression levels detected were a result of defined conditions. The first reference gene used was the *cysG* gene, coding for the multifunctional enzyme, uroporphyrin III C-methyltransferase. This enzyme is involved in

metabolism and the biosynthesis of building blocks and had been previously identified as a stable reference gene [194]. The second reference was the V6 region of the 16S gene, coding for the variable V6 region of the 16S RNA sub unit. However, some caution should be taken when normalising against *16S_V6* reference gene. High amplification was observed for the *16S_V6* gene under all of the conditions tested. These high amplification levels suggested that the *16S_V6* gene may not be an ideal reference gene and therefore not give an accurate representation of the metabolic state of the cells tested. The results obtained for *cysG* produced the expected results and for this discussion, only qPCR results normalised against the *cysG* reference gene will be considered.

Expression of the antisense against *pta* (as*pta*), assessed by qPCR, was detected under all conditions tested. The increase in relative expression of the antisense target with increasing additional acetate concentration at pH 5.5, indicated that the antisense message was upregulated under increasing extracellular acetate concentration. However, the differences in expression were not statistically significant. Results observed at pH 7.0 showed a reverse of those observed at pH 5.5. Overall detection of the antisense message decreased as additional acetate concentration increased, but again, one-way ANOVA analysis did not detect and statistical difference in change in expression levels. It is worth noting that the primers designed to target the antisense message were also capable of detecting the expression of the *pta* gene. This may have led to cross-reactivity causing the expression of the antisense message to be skewed by the expression of the *pta* gene.

Primers designed to target the *pta* gene were designed to target a site close to the end of the mRNA transcript. This was done to first, avoid detection

of the antisense message and secondly, to avoid the 5' end of the mRNA transcripts where rapid degradation occurs [264]. At pH 5.5, relative *pta* expression decreased as additional acetate concentration increased. This result was in line with what we would expect to see in RB9132_antisense_*pta* cells. It is also in line with the pattern in expression levels of the antisense message targeting *pta*, as antisense message expression increased, expression of the *pta* gene decreased. However, the same patterns of expression of both as*pta* and the *pta* gene itself were not observed when RB9132_antisense_*pta* cells are cultured at pH 7.0. A decrease was observed in the expression of as*pta* alongside an increase in *pta* expression as additional acetate concentration increased. This result was particularly notable at an additional acetate concentration of 45 mM.

RB9132_antisense_*pta* cells, exposed to high concentrations of acetate (i.e. 9 mM and 45 mM) at pH 5.5 may become overloaded with acetate, due to the predicted effect of pH and external acetate concentration on the partitioning of acetate across *E. coli* cellular membranes. If these cells are killed during exposure to acetate, I would be unlikely to detect *pta* transcripts. In contrast, at pH 7.0, acetate would have been unable to penetrate the cellular membrane with the same efficiency as at pH 5.5. RB9132_antisense_*pta* cells are therefore likely to tolerate higher levels of acetate at higher pH. This result was also observed in Chapter 5, when the effect of acetate concentration and pH on GFP fluorescence was assessed.

In addition to catalysing the conversion of acetyl CoA into AcP, PTA is also able to act in the reverse direction during the assimilation of acetate from the external environment. Acetate assimilation is usually performed by the AMP-ACS

pathway, however the PTA-ACKA pathway is also known to assimilate acetate when external acetate concentrations are high, leading to an upregulation of *pta* [249]. It is possible that an upregulation of *pta* is observed at high acetate and high pH levels, if the cell is attempting to assimilate the external acetate.

I moved the investigation towards the analysis of the effects of additional acetate concentration on RB9132 cells lacking the antisense construct against *pta* (i.e. RB9132 wild type cells). Results from these qPCR assays reflected the patterns of *pta* expression observed at varying additional acetate concentration and external pH. However, expression of *pta* was higher than that observed in RB9132_antisense_*pta* cells under all the conditions tested. This indicated that although the antisense construct may not behave as predicted, it did influence the levels of mRNA transcripts for *pta*, which may lead to an overall reduced level of PTA in the cell. These results indicated that the antisense construct under the control of the *t-glnAp2* promoter influenced the *pta* transcripts. The next stages of my investigation were to investigate the overall levels of acetate produced from RB9132_antisense_*pta* cells vs the R9132 wild type cells (which did not harbour an antisense mechanism against *pta*).

Previous studies have shown that weak promoters (such as the *ackA* promoter) in control of the as*pta* gene are sufficient to bring down the mRNA transcript levels of *pta*, but are not effective at reducing the overall activity of the PTA enzyme and reducing overall acetate production [260]. Another study had previously found that as*pta* under to the control of the T7 genetic promoter was sufficient to abolish acetate production when cells were induced with IPTG [261]. By engineering an acetate sensing promoter in control of antisense, designed to target genes involved in acetate production, I hoped to create a self-inducing

control circuit for acetate production. This circuit needed to be induced by external acetate concentrations sufficiently enough to block the production of acetate, without the need for an additional inducer molecule such as IPTG. Results obtained from RT-qPCR assays indicated that the *glnAp2* promoter was sufficient to block translation of the *pta* gene. However, results obtained from acetate quantification assays indicated that the overall activity of PTA was not sufficiently reduced to produce a reduction in the overall excretion of acetate from the cell. Growth of the *E. coli* cells also didn't appear to be significantly affected by the presence/absence of the antisense construct under any of the media conditions tested (see Figure A4.5, Appendices). In fact, under the conditions tested, the growth of the antisense strain was slightly improved, an observation previously attributed to the potential regulation of the acetate pathway through antisense mRNA, allowing the cells to keep essential functions operating for survival and maintenance of cellular physiology [260].

7. Chapter seven: Final Discussion and Concluding remarks

7.1. Final discussion

The work described in this thesis focused on the discovery and development of micro-organisms for use in synthetic bio-methane producing microbial communities. Two different problem areas, faced by anaerobic digestion technology, oxygen sensitivity and VFA control, were addressed.

For the first part of this study, I investigated an estuarine tidal mudflat environment, to discover a novel, oxygen-tolerant methanogen, for potential use in bio-methane microbial communities. Initial depth profiling of methanogens using 16S sequencing techniques indicated the presence of methanogens within the very surface layers of the sediment (0.0-0.5 cm). Further investigation into the same sample site, using enrichment cultures, detected the enrichment of a methanogen, which identified closely with the diverse methanogen, *M. mazei.* This methanogen, known to harbour oxygen scavenging mechanisms [235], was enriched from the very surface sediment layer.

Despite promising gas production rates from enrichments, methanogen colonies were difficult to isolate on solid agar and were often outcompeted by the presence of another organism, which I concluded to be related closely with *Shewanella algae.* It is possible that the methanogen colonies had a form of dependence on this neighbouring organism(s) for the provision of additional substrates and the lowering of redox potential. The inability to obtain a pure methanogen culture severely affected my capacity to conclusively identify the methanogen species present. The mixed nature of the culture from which sequences were identified also inhibited the investigation of the methanogen genome for the presence of genes known to be involved in oxygen defence mechanisms (SOD, SOR, catalase, peroxidase, rubrerythrin). However, the

detection of sequences relating closely to *M. mazei* does suggest the methanogen species enriched is also likely to harbour oxygen-tolerance mechanisms.

The remainder of this study addressed the problem of VFA control during anaerobic digestion. For this, acetate production, a common problematic VFA, was targeted. *E coli* was used as a model organism for the design and engineering of a negative feedback loop against acetate production. The work was undertaken with the view to designing similar circuits in common acetogenic bacteria, to form part of a synthetic bio-methane producing community. The chosen controller of this feedback loop, was the glutamine synthetase promoter (*glnAp2*), which had been previously reported to be sensitive to intracellular levels of acetyl phosphate (AcP) [255]. The intracellular levels AcP were thoughtto increase when external pH decreased, and as extracellular levels of acetate increased.

Another way to reduce acetate dissemination could be the complete knock-out either *pta*, *ackA* or both. However, this kind of approach does not take into account the importance of acetate production in *E. coli* metabolism. A complete reduction of acetate production would have not been appropriate for this task, as some acetate release is required. Instead, rather than completely knocking out genes of the *pta-ackA* pathway, I attempted to regulate acetate production using antisense RNA targeting *pta* under the control of *glnAp2.* Using this form of regulation would mean that the formation of the PTA enzyme would only have been disrupted when expression of *glnAp2* was stimulated (i.e. low pH/high external acetate concentration).

Results from the RT-qPCR assays revealed that, in comparison to the wild type, *E. coli* cells harbouring this antisense circuit had reduced levels of *pta* expression. However, there was no clear pattern in the degree of antisense repression on *pta* expression in terms of the external pH and acetate concentration. Also, despite an overall decrease in expression of the *pta* gene in the engineered *E. coli* strains, no significant changes in acetate production from the cells in comparison to wild type were detected. It is possible that the strength of the promoter was not great enough to reduce the overall production of acetate from the engineered strain in comparison to the wild type. This result reflects those of Kim *et al.,* 2003 [260], which used antisense targeting *pta* under the control of the *ackA* promoter. There is, however, evidence to suggest that with a stronger promoter, such as the T7 promoter, overall levels of PTA and therefore acetate production can be reduced using antisense targeting the *pta-ackA* pathway [261].

7.2. Further investigations

7.2.1. Improvement of methanogen enrichment

The lack of pure methanogen culture obtained during this investigation caused great hindrance to my ability to analyse the whole genome sequencing data. Several improvements could be applied to future investigations to advance the enrichment and isolation process. Such improvements could include the addition of antibiotics to kill off any other unwanted species. Additional sub-culturing rounds of liquid cultures in anaerobic Balch tubes could also have been included, to obtain a higher methanogen purity before colony isolation on anaerobic plates. Isolating methanogen species in pure cultures could dramatically improve the

ability to analyse whole genome sequencing datasets with greater accuracy and confidence. This could potentially allow for the assembly of a novel methanogen genome, harbouring oxygen-tolerance mechanisms. In addition to whole genome sequencing analysis, further investigations into a pure methanogen cultures could involve a series of oxygen stress experiments. These experiments could also incorporate transcriptomics to detect if certain oxygen protection genes are upregulated.

7.2.2. Improvement of antisense construct design and characterisation

This study aimed to create a self-sensing negative feedback loop against acetate production, therefore the utilisation of a stronger promoter such as the T7 promoter, would not be appropriate, as an additional inducer molecule (IPTG) would be required. To improve the strength of the *t-glnAp2* promoter, enhancer sequences upstream of the *t-glnAp2* promoter site, could be altered to increase its sensitivity to AcP using splicing overlap extension methods [265]. Such alterations have been successfully performed by Bulter *et al.,* 2004 [255]. Other avenues also could also involve the alteration of the antisense message itself, or the generation of multiple antisense fragments. Different antisense fragments could be generated by the directional cloning of different regions of the *pta* gene, which may have a better ability to bind to the *pta* mRNA transcripts.

7.3. Concluding remarks

Biological organisms have vast potential to perform beyond their current boundaries. The development of synthetic organisms and synthetic microbial communities provides promising opportunities to fulfil this potential. There is still a long way to go for the development of microbial communities for biomethane production. However, the work described in this thesis highlights some key areas, which could be built upon when designing and searching for biomethane-producing community organisms in the future.

Appendices

A1. Figures relating to Chapter 3

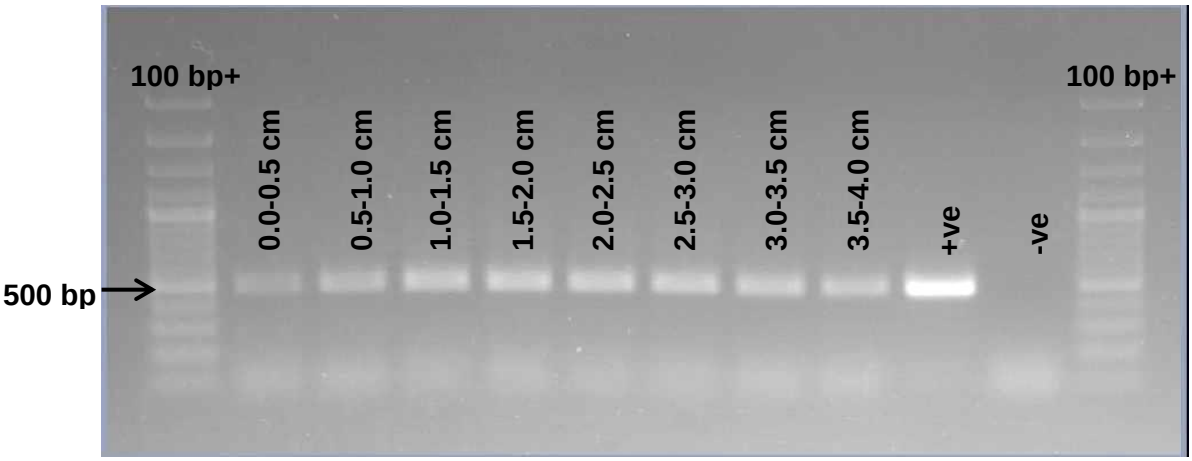

Figure A1.1: PCR product generated from the amplification of DNA extracts from each layer of a 4 cm sediment core with methanogen-specific primers.

1 µl of template DNA extracted from each layer of the sediment core was amplified with methanogen specific primers (ML_F and ML_R). Positive control (+ve)s contained methanogen DNA template. Negative control (-ve)s contained nuclease-free water in place of template DNA. A 100 bp plus DNA ladder was used (Thermo Fisher Scientific). The arrow indicates the 500 bp DNA marker.

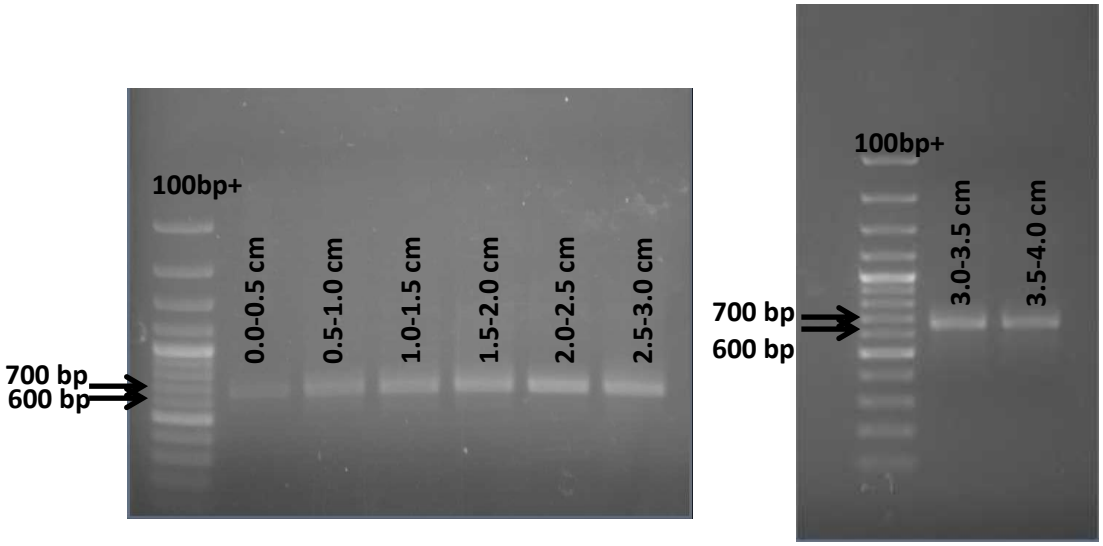

Figure A1.2: Gel electrophoresis of purified PCR products generated from the amplification of extracted DNA from a 4 cm sediment core, using universal archaeal 16S rRNA primers.

DNA was extracted from 0.5 cm layers of a 4 cm mud core. DNA extracts were PCR amplified with A571_F and UA1204_R primers. PCR products were purified and electrophoresed alongside a 1 Kb plus DNA ladder (Thermo Fisher Scientific). The arrows indicate the 600 bp and 700 bp DNA markers.

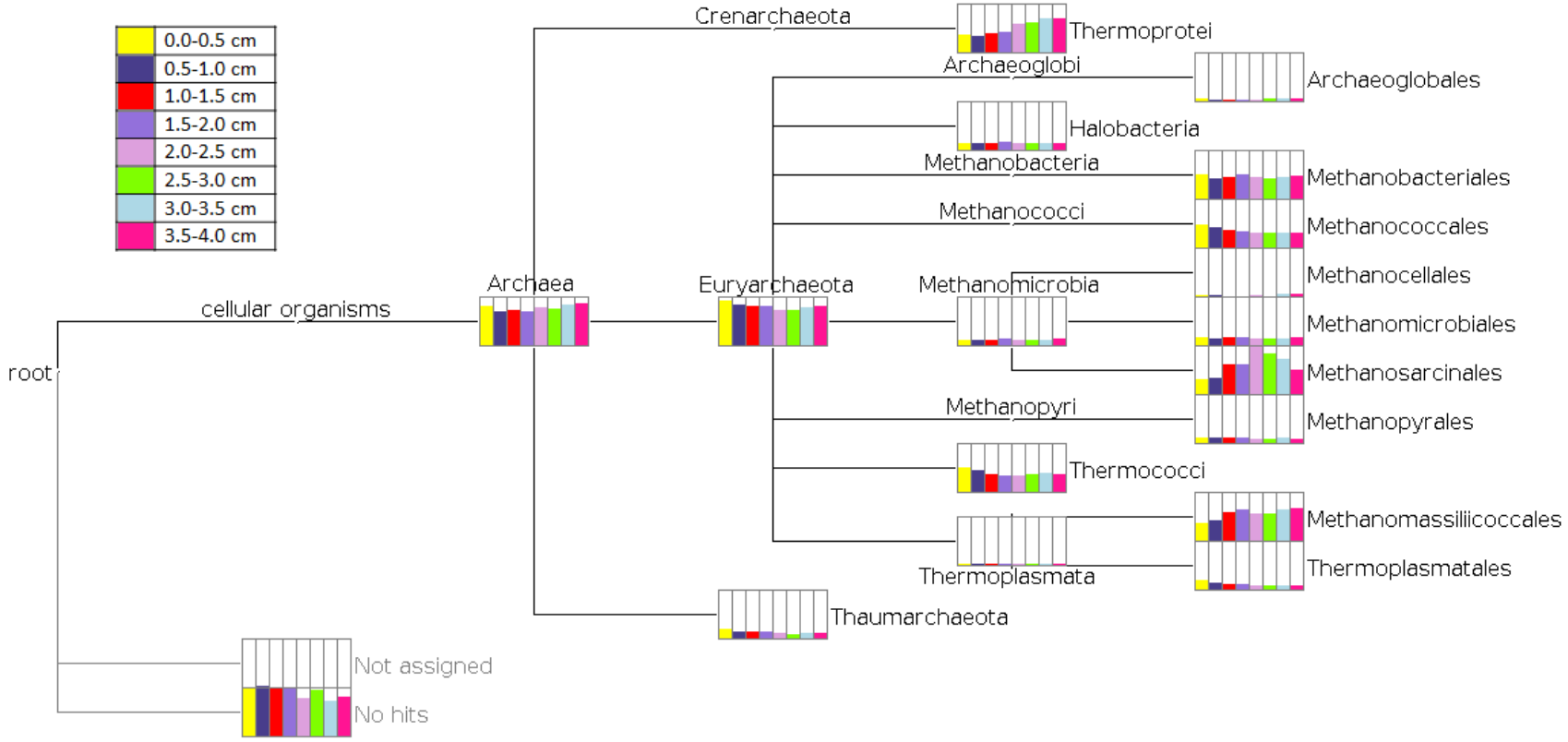

Figure A1.3: Comparison phylogram generated for the archaeal 16S rRNA sequencing of a 4 cm sediment core

Illumina sequencing reads were generated from the 16S rRNA archaeal sequencing of DNA extracted from sections of a 4 cm sediment core. Reads were quality filtered and compared against the RefSeq database using BLAST. The BLAST outputs generated for each sample were fed in to MEGAN to generate a comparisons phylogram, using normalised read counts. Each node is represented as a bar graph, to demonstrate the relative number of reads assigned to each taxonomic group. Each coloured bar refers to a different layer of the sediment core.

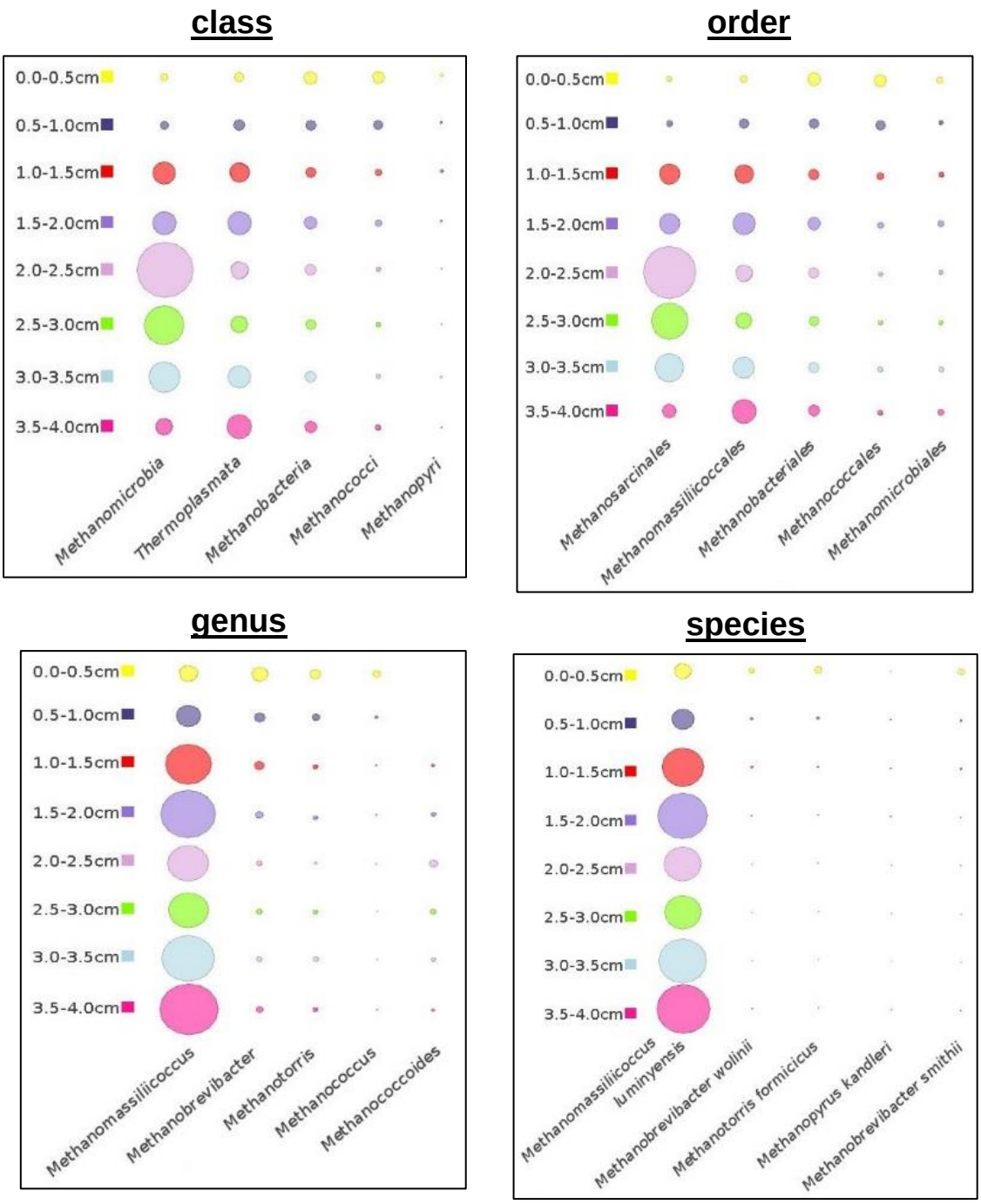

Figure A1.4: The distribution of reads binned into various taxonomic groups across a 4 cm depth profile represented by bubble charts using MEGAN software.

MEGAN was used to generate bubble charts to represent the respective abundances of the top five methanogenic groups at each the class, order, genus or species taxonomic rankings within each of the sections of the 4 cm sediment core. The size of each bubble indicates the number of reads binned into that taxonomic group. The larger the bubble, the larger the number of reads.

Figure A1.5: The relative distribution of reads binned into various taxonomic groups across a 4 cm depth profile, determined using One Codex analysis software.

Quality filtered, and paired Illumina sequencing reads were generated from the 16S rRNA archaeal sequencing of DNA extracted from different depths of a 4 cm sediment core. Read files were loaded into the One Codex online platform. The comparison tool was used to compare the classifications assigned to each of the samples representing descending layers of the mud core. Relative read counts were used (min 3 %). Classifications were visualised at the class, order, genus and species taxonomic rankings.

A2. Figures relating to Chapter 4

There were no additional figures relating to Chapter 4.

A3. Figures and tables relating to Chapter 5

>*pta*

TTTCACACCGCCAGCTCAGCTGGCGGTGCTGTTTTGTAACCCGCCAAATCGGCGGTAACGAAAGAGGATAA
ACCGTGTCCCGTATTATTATGCTGATCCCTACCGGAACCAGCGTCGGTCTGACCAGCGTCAGCCTTGGCGT
GATCCGTGCAATGGAACGCAAAGGCGTTCGTCTGAGCGTTTTCAAACCTATCGCTCAGCCGCGTACCGGTG
GCGATGCGCCCGATCAGACTACGACTATCGTGCGTGCGAACTCTTCCACCACGACGGCCGCTGAACCGCTG
AAAATGAGCTACGTTGAAGGTCTGCTTTCCAGCAATCAGAAAGATGTGCTGATGGAAGAGATCGTCGCAAA
CTACCACGCTAACACCAAAGACGCTGAAGTCGTTCTGGTTGAAGGTCTGGTCCCGACACGTAAGCACCAGT
TTGCCCAGTCTCTGAACTACGAAATCGCTAAAACGCTGAATGCGGAAATCGTCTTCGTTATGTCTCAGGGC
ACTGACACCCCGGAACAGCTGAAAGAGCGTATCGAACTGACCCGCAACAGCTTCGGCGGTGCCAAAAACAC
CAACATCACCGGCGTTATCGTTAACAAACTGAACGCACCGGTTGATGAACAGGGTCGTACTCGCCCGGATC
TGTCCGAGATTTTCGACGACTCTTCCAAAGCTAAAGTAAACAATGTTGATCCGGCGAAGCTGCAAGAATCC
AGCCCGCTGCCGGTTCTCGGCGCTGTGCCGTGGAGCTTTGACCTGATCGCGACTCGTGCGATCGATATGGC
TCGCCACCTGAATGCGACCATCATCAACGAAGGCGACATCAATACTCGCCGCGTTAAATCCGTCACTTTCT
GCGCACGCAGCATTCCGCACATGCTGGAGCACTTCCGTGCCGGTTCTCTGCTGGTGACTTCCGCAGACCGT
CCTGACGTGCTGGTGGCCGCTTGCCTGGCAGCCATGAACGGTGTAGAAATCGGTGCCCTGCTGCTGACTGG
CGGCTACGAAATGGACGCGCGCATTTCTAAACTGTGCGAACGTGCTTTCGCTACCGGCCTGCCGGTATTTA
TGGTGAACACCAACACCTGGCAGACCTCTCTGAGCCTGCAGAGCTTCAACCTGGAAGTTCCGGTTGACGAT
CACGAACGTATCGAGAAAGTTCAGGAATACGTTGCTAACTACATCAACGCTGACTGGATCGAATCTCTGAC
TGCCACTTCTGAGCGCAGCCGTCGTCTGTCTCCGCCTGCGTTCCGTTATCAGCTGACTGAACTTGCGCGCA
AAGCGGGCAAACGTATCGTACTGCCGGAAGGTGACGAACCGCGTACCGTTAAAGCAGCCGCTATCTGTGCT
GAACGTGGTATCGCAACTTGCGTACTGCTGGGTAATCCGGCAGAGATCAACCGTGTTGCAGCGTCTCAGGG
TGTAGAACTGGGTGCAGGGATTGAAATCGTTGATCCAGAAGTGGTTCGCGAAAGCTATGTTGGTCGTCTGG
TCGAACTGCGTAAGAACAAAGGCATGACCGAAACCGTTGCCCGCGAACAGCTGGAAGACAACGTGGTGCTC
GGTACGCTGATGCTGGAACAGGATGAAGTTGATGGTCTGGTTTCCGGTGCTGTTCACACTACCGCAAACAC
CATCCGTCCGCCGCTGCAGCTGATCAAAACTGCACCGGGCAGCTCCCTGGTATCTTCCGTGTTCTTCATGC
TGCTGCCGGAACAGGTTTACGTTTACGGTGACTGTGCGATCAACCCGGATCCGACCGCTGAACAGCTGGCA
GAAATCGCGATTCAGTCCGCTGATTCCGCTGCGGCCTTCGGTATCGAACCGCGCGTTGCTATGCTCTCCTA
CTCCACCGGTACTTCTGGTGCAGGTAGCGACGTAGAAAAAGTTCGCGAAGCAACTCGTCTGGCGCAGGAAA
AACGTCCTGACCTGATGATCGACGGTCCGCTGCAGTACGACGCTGCGGTAATGGCTGACGTTGCGAAATCC
AAAGCGCCGAACTCTCCGGTTGCAGGTCGCGCTACCGTGTTCATCTTCCCGGATCTGAACACCGGTAACAC
CACCTACAAAGCGGTACAGCGTTCTGCCGACCTGATCTCCATCGGGCCGATGCTGCAGGGTATGCGCAAGC
CGGTTAACGACCTGTCCCGTGGCGCACTGGTTGACGATATCGTCTACACCATCGCGCTGACTGCGATTCAG
TCTGCACAGCAGCAGTAATCTCGTCATCATCCGCAGCTTTGCGCTGCGGATATCTGAACCGGAAATAATCA
CTATTTCCGGTTTTTTATTCTCTTAATCTGCATTAATCCTTTCTGATTATCTTGCTTAACTGCGCTACAT

>Forward (5' -3')

**TGTTTTGTAACCCGCCAAATCGGCGGTAACGAAAGAGGATAAACCTAGTGTAGGCTGGAG
CTGCTT**

>Reverse (5'-3')

**TCCGGTTCAGATATCCGCAGCGCAAAGCTGCGGATGATGACGAGATGCATATGAATATCC
TCCTTAGTTCCTA**

Key: 45 bp flanking regions; FRT sites; start of gene; end of gene

Figure A3.1: The *pta* locus within the *E. coli* genome

Predicted sequence of the *pta* gene in *E. coli*, used for the design of PCR primers for the Wanner mutagenesis of the *pta* locus. Primers were designed to flank the *E. coli pta* gene and contained specific FRT sites. Sequence was downloaded from Ensembl bacteria, accession number HUS2011_2802.

Figure A3.2: Sequence of the generated pGEM-T.*glnAp2* vector DNA aligned against the correct sequence for the *glnAp2* promoter region.

A 251 bp region of the glutamine synthetase promoter (*glnAp2*) was PCR amplified from the *E. coli* RB9132 genome using specific primers. The PCR product was subsequently cloned into the pGEM-T easy vector to create pGEM-T.*glnAp2* . pGEM-T.*glnAp2* was used to transform calcium competent DH5-alpha *E. coli* cells using heat-shock transformation. Vector DNA from successful transformants was extracted, sequenced and aligned with the predicted *glnAp2* sequence (GenBank accession no. M10421). Restriction sites are highlighted according to the key.

A4. Figures relating to Chapter 6

>gi|146163|gb|M10421.1|ECOGLNALG E.coli *glnALG* operon: *glnA* gene coding for glutamine synthetase, promoter region

TCGCACTACAAAACAGGATCACAAACATCCTCCGCAAACAATATTGCAGAGTCCCTTTGTGATCGC
TTTCACGGAGCATAAAAAGGGTTATCCAAAGGTCATTGCACCAACATGGTGCTTAATGTTTCCATT
GAAGCACTATATTGGTGCAACATTCACATCGTGGTGCAGCCCTTTTGCACGATGGTGCGCATGATA
ACGCCTTTTAGGGGCAATTTAAAAGTTGGCACAGATTTCGCTTTATCTTTTTTACGGCGACACGGC
CAAAATAATTGCAGATTTCGTTACCACGACGACCATGACCAATCCAGGAGAGTTAAAGTATGTCCG
CTGAACACGTACTGACGATG

Key:

glnAp2_F binding site **glnAp2_R binding site** **NtrC~P enhancer site 1** **NtrC~P enhancer site 2**

Predicted Shine-Dalgarno sequence **ATG start site**

Figure A4.1: DNA sequence of the *t-glnAp2* promoter region from *E. coli* strain YMC9.

Using the genetic sequence of the truncated *glnAp2* promoter region of *E. coli* strain YMC9 as a guide, the region from the *t-glnAp2* promoter region was PCR amplified from the *E. coli* RB9132 genome. The forward and reverse PCR primers, highlighted in yellow and blue respectively were used for the amplification. The -35 and -10 TATA box binding regions are highlighted in pink and grey respectively. Predicated Shine-Dalgarno sequence is highlighted in dark green and the ATG start site is highlighted in red. This sequence was obtained from the NCBI database (GenBank accession no. M10421) [191].

>Escherichia_coli_K-12_CP014272_REGION:2516813-2517000

GCCTGATTTCACACCGCCAGCTCAGCTGGCGGTGCTGTTTTGTAACCCGCCAAATCGGCGGTAACGAA
AGAGGATAAACCGTGTCCCGTATTATTATGCTGATCCCTACCGGAACCAGCGTCGGTCTGACCAGCGT
CAGCCTTGGCGTGATCCGTGCAATGGAACGCAAAGGCGTTCGTCTGAGCGT

Key:

Forward primer; **GTG start site**; **Reverse primer**

Figure A4.2: Upstream and downstream sequences of the *pta* start site within the genome of *E. coli* strain K12.

Using the genetic sequence of the *pta* region of *E. coli* strain K12 as a guide, the as*pta* region was PCR amplified from the *E. coli* RB9132 genome. The forward and reverse PCR primers are highlighted in yellow and blue respectively. The GTG start site of the *pta* gene is highlighted in red. This sequence was obtained from the NCBI database (GenBank accession no. CP014272).

>Escherichia_coli_K-12_CP014272_REGION:2519035-2519226

TAATCTCGTCATCATCCGCAGCTTTGCGCTGCGGATATCTGAACCGGAAATAATCACTATTT
CCGGTTTTTTATTCTCTTAATTTGCATTAATCCTTTCTGATTATCTTGCTTAACTGCGCTGC
ATCAATGAATTGCGCCATCCCACTTTGCATACTTACCACTTTGTTTTGTGCAAGGGAATATT
TGCGCT

Key:

pta stop site; Synthesised terminator region; Hairpin structure

Figure A4.3: The DNA sequence of the Rho-independent terminator for the *pta* gene

Using the genetic sequence of the *pta* region of *E. coli* strain K12 as a guide, the region from the *pta* terminator region was artificially synthesised using GeneArt Gene Synthesis (Thermo Fisher Scientific). The *pta* stop site is highlighted in green. The synthesised region is highlighted in yellow. The underlined bases indicated the inverted repeat sequences that form the hair pin structure of the Rho-independent terminator.

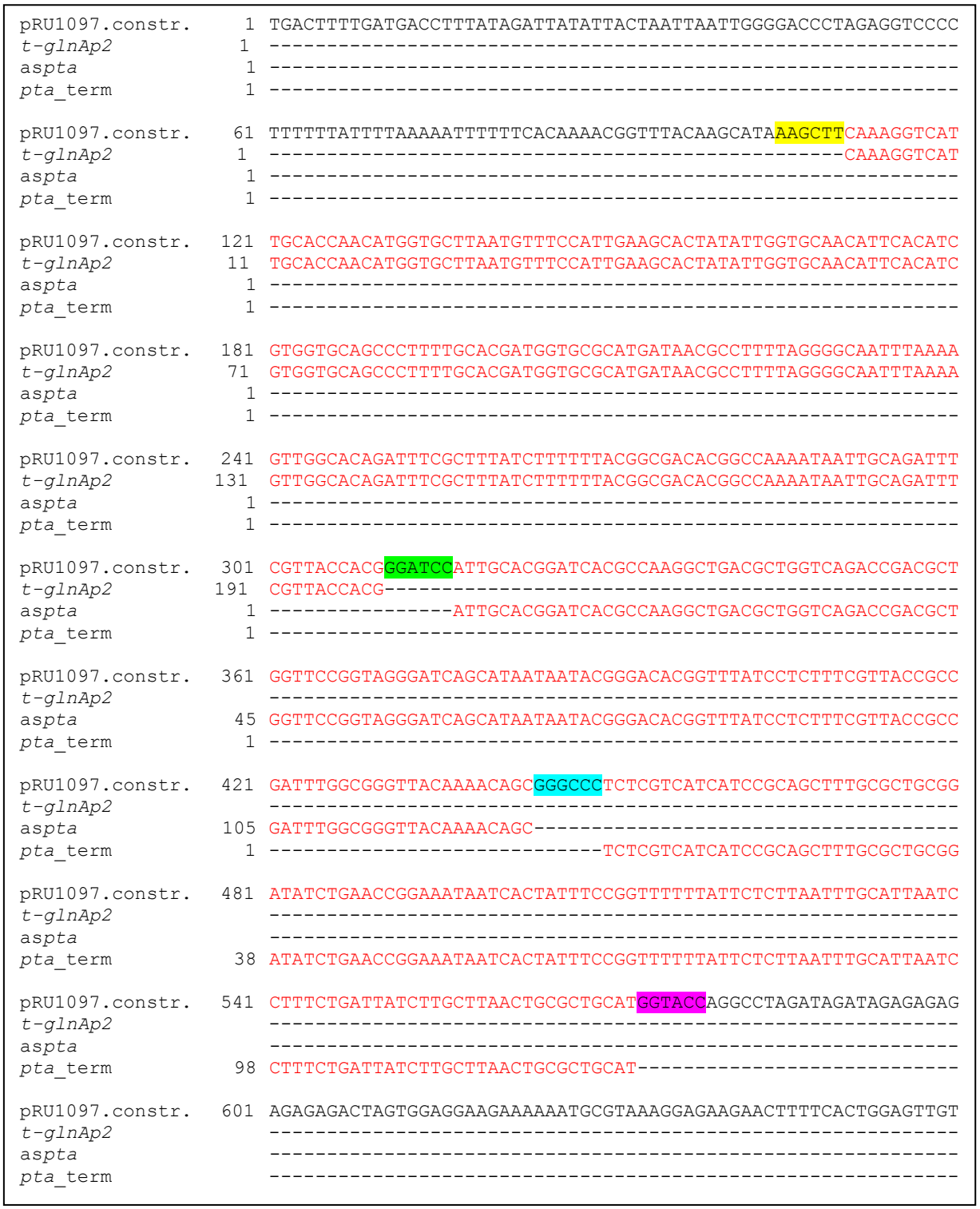

Figure A4.4: Alignment of the antisense construct targeting *pta* against its predicted sequence.

Antisense construct (pRU1907.*t-glnAp2*.as*pta*.*pta*_term) denoted here as 'pRU1097.const.' is aligned against the predicted sequences of the truncated promoter (*t-glnAp2*), the antisense fragment targeting *pta* (as*pta*) and the *pta* terminator region '*pta*_term'. The aligned sequence is shown in red, restriction sites are shown in blue. Restriction sites: HindIII, BamHI, ApaI, KpnI.

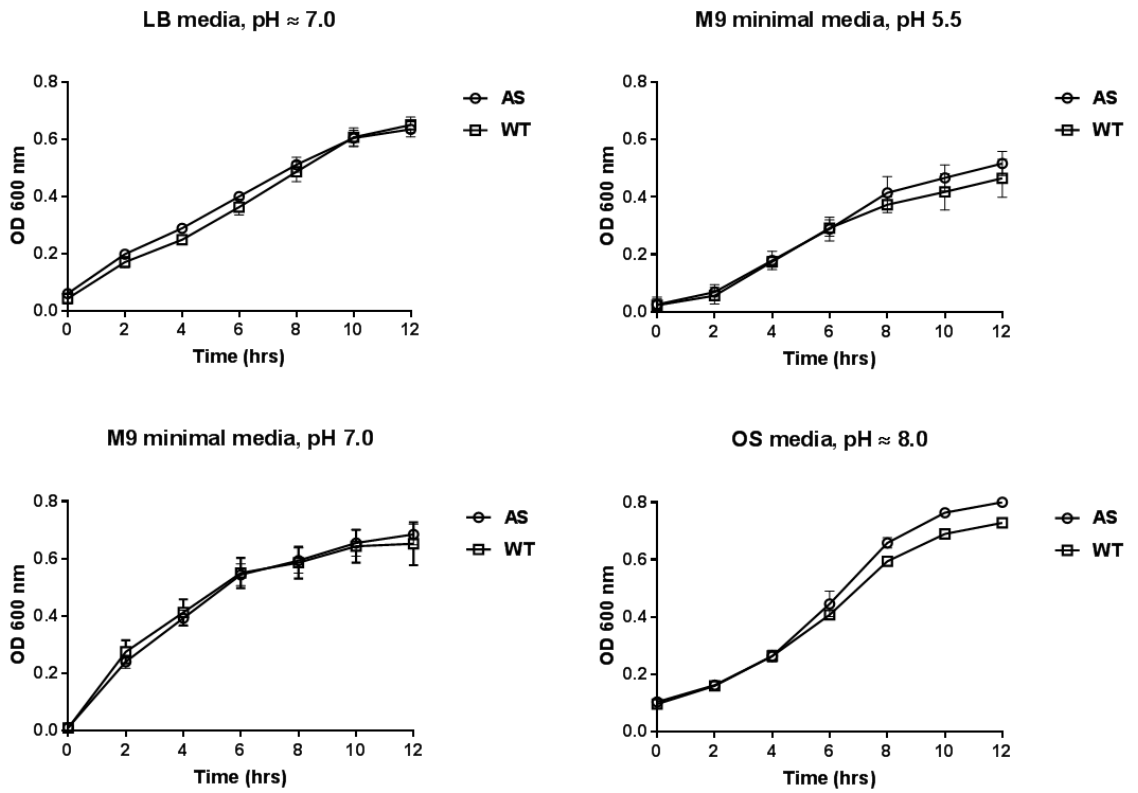

Figure A4.5: Growth curve of *E. coli* strain harbouring antisense construct against *pta* compared with wild type

E. coli RB9132 cells both with and without the antisense construct targeting the *pta* gene were cultured in various growth mediums. Optical density levels (OD_{600nm}) were measured over a 12 hour time period.

A5. Medium recipes

Table A5.1. LB broth medium

Component	Amount required for 1 litre
LB broth powder (high salt)	25 g
Distilled water	Up to a volume of 1 L

- Dissolve broth powder.
- Adjust to desired pH.
- Autoclave.
- Add filter sterilised antibiotics (if required).

Table A5.2. Standard M9 minimal salt solution (1X)

Component	Amount required for 1 litre
5X M9 salts	200 ml
1 M $MgSO_4$	2 ml
0.5 M $CaCl_2$	0.2 ml
20 % (w/v) glucose	20 ml
Thiamine (1 mg/ml)	1 ml
Distilled water	Up to a volume of 1L

- Make components up in bulk, separately.
- Autoclave 5X M9 salts, filter sterilise all other components.
- Make up medium as required, under a biological safety cabinet.
- Filter sterilise once more.
- Store excess at 4 °C until required.

Table A5.3. Buffered M9 minimal salt solution (1X)

Component	Amount required for 1 L
5X M9 salts	200 ml
1 M $MgSO_4$	2 ml
0.5 M $CaCl_2$	0.2 ml
20 % (w/v) glucose	20 ml
Thiamine (1 mg/ml)	1 ml
0.5M MES/MOPS (buffered to the correct pH)	200 ml
0.1 M K_2HPO_4	20 ml
Distilled water	Up to a volume of 1 L

- Make components up in bulk, separately.
- Autoclave 5X M9 salts, filter sterilise all other components.

Make up medium as required, under a biological safety cabinet.

- Store excess at 4 °C until required.

Table A5.4. Anaerobic growth medium

Component	Amount required for 1 L
Salt solution,	978 ml
Sodium bicarbonate	2.5 g
Trace metal solution (100X stock)	10 ml
Yeast extract	2 g
Thiamine (1 mg/ml stock)	1 ml
Cysteine-HCL (100X stock)	10 ml
Vitamin solution (100X stock)	10 ml
Sodium sulphide (50X stock)	20 ml
Glucose stock (20 % (w/v) (optional)	20 ml
Resazurin (1000X stock)	1 mL

- Prepare salt solution and stock solutions separately. Recipes detailed below.
- Add sodium bicarbonate and resazurin to the salt solution.
- Add trace metal solution.

- Add cysteine stock.
- Degas the solution according to the medthod described in section 2.15.5 (Chapter 2).
- Add the vitamin solution.
- If required, add the glucose.
- Add 100 ul of sodium sulphide for every 5 ml of medium.
- Add any desired substrates.

Table A5.5. Salt solution

Component	**Amount required for 1 L**
Sodium chloride	2.17 g
Magnesium chloride, hexahydrate	5.50 g
Calcium chloride, dihydrate	0.14 g
Ammonium chloride	0.50 g
Potassium chloride	0.34 g
Dipotassium phosphate	0.19 g
Distilled water	978 ml

- Add solid components into a 1 L Duran Bottle.
- Add water to dissolve components.
- Use immediumtely, or if storing, separate out into smaller volumes and autoclave.

Table A5.6. Trace metal solution (100X stock solution)

Component	Amount required for 1 L
Nitrilotriacetic acid	1.5000 g
Magnesium chloride, hexahydrate	2.4800 g
Manganese(II) chloride, tetrahydrate	0.5854 g
Sodium chloride	1.0000 g
Ferrous chloride, tetrahydrate	0.0715 g
Cobaltous chloride, hexahydrate	0.1524 g
Calcium chloride, dihydrate	0.1000 g
Zinc chloride, tetrahydrate	0.0853 g
Copper chloride	0.0054 g
Aluminium chloride	0.0103 g
Boric acid	0.0100 g
Molybdic acid sodium salt, dihydrate	0.0100 g
Nickel chloride, hexahydrate	0.0300 g
Sodium selenite, pentahydrate	0.0003 g
Sodium tungstate, dihydrate	0.0080 g
Distilled water	Up to a volume of 1 L

- Dissolve Nitrilotriacetic acid.
- Adjust pH to 6.5 with 1 M KOH.
- Add all other minerals.
- Set final pH to 7.0 with 1 M KOH.
- Autoclave.
- Store at 4 °C until required.

Table A5.7. Vitamin solution stock solution (1000X), anaerobic

Component	Amount required for 1 L
Biotin	0.020 g
Folic Acid	0.020 g
Pyridoxin-HCl	0.100 g
Thiamine-HCl	0.050 g
Riboflavin	0.050 g
Nicotinic acid	0.050 g
D-Ca-Panthotenate	0.050 g
p-Aminobenzoic acid	0.050 g
Vitamin B12	0.001 g
Lipoic acid	0.050 g
Distilled water	Up to a volume of 1 L

- Prepare anaerobic serum bottles by placing uncovered serum bottle inside the anaerobic chamber for 24 hours.
- Seal the serum bottles with a butyl stopper and aluminium crimp.
- Autoclave and place back inside the chamber.
- Add all components into an appropriately sized flask, without a lid.
- In a separate flask add the appropriate amount of distilled water, without a lid.
- Place dry and wet components inside anaerobic cabinet for 24 hrs.
- After 24 hours, mix components and decant into the pre-sterilised anaerobic serum bottle, by using a needle and syringe attached via a 0.2 µm filter.

Table A5.8. Resazurin stock solution (1000X)

Component	Amount required for 1 L
Resazurin powder	1 g
Distilled water	Up to volume of 1 L

- Dissolve powder in water.
- Store in the dark.

Table A5.9. Cysteine stock (100X), anaerobic.

Component	Amount required for 1 L
Cysteine-HCL*H_2O	35.03 g
Distilled water	Up to a volume of 1 L

- Add wet components to dry.
- Autoclave.

Table A5.10. Sodium sulphide stock (50X)

Component	Amount required for 1 L
Na_2S*9H_2O	24 g
Distilled water	Up to a volume of 1 L

- Weigh out the amount of sodium sulphide crystals required carefully.
- Wash the crystals with distilled water and dry on a peeved of microscope paper.
- Fill the crystals into a tube.
- Add the corresponding amount of water required into a second tube.
- Leave both tubes to degas in the anaerobic chamber overnight.
- Mix the components.
- Fill into an anaerobic serum bottle.
- Seal in the anaerobic cabinet.

- Autoclave.

Table A5.11. Thiamine stock (1 mg/ml)

Component	Amount required for 1 L
Thiamine-HCL	1 g
Distilled water	Up to a volume of 1 L

- Add wet components to dry components.
- Filter sterilise.
- Prepare anaerobically if required.

References

1. Demirbas, A., Bioenergy, global warming, and environmental impacts*. Energy Sources*, 2004, **26**(3), p. 225-236.
2. Keller, C.F., Global warming 2007 - An update to global warming: The balance of evidence and its policy implications. *The scientific world journal*, 2007. **7**, p. 381-399.
3. Intergovernmental Panel on Climate Change, Climate change 2014: mitigation of climate change. *Cambridge University Press*, 2015.
4. United Nations, D.o.E.a.S.A., Population Division, *World Population Prospects: The 2015 Revision*, 2015.
5. Hill, J., et al., Environmental, economic, and energetic costs and benefits of biodiesel and ethanol biofuels*. Proceedings of the National Academy of Sciences of the United States of America*, 2006. **103**(30), p. 11206-11210.
6. Mueller, S.A., J.E. Anderson, and T.J. Wallington, Impact of biofuel production and other supply and demand factors on food price increases in 2008*. Biomass & Bioenergy*, 2011. **35**(5), p. 1623-1632.
7. Weiland, P., Biogas production: current state and perspectives*. Applied Microbiology and Biotechnology*, 2010. **85**(4), p. 849-860.
8. Meynell, P.-J., *Methane: planning a digester*. 1976, Dorchester [England]: Prism Press.
9. Penn State University, C.o.A.S. *A short history of anaerobic digestion*. 2014 [Online]; Available from: https://extension.psu.edu/a-short-history-of-anaerobic-digestion [Accessed 06/09/2017].
10. Abbasi T., T.S.M., Abbasi S.A., A Brief History of Anaerobic Digestion and “Biogas”, in Biogas Energy. *SpringerBriefs in Environmental Science*, 2012.
11. Jingura, R.M. and R. Matengaifa. Optimization of biogas production by anaerobic digestion for sustainable energy development in Zimbabwe*. Renewable & Sustainable Energy Reviews*, 2009. **13**(5), p. 1116-1120.

12. Association, A.D.a.B. *History of AD*. 2017 [Online]; Available from: http://adbioresources.org/about-ad/history-of-ad [Accessed 04/05/2017].
13. Darby, D. *Home-made biogas anaerobic digester* 2016 [Online]; Available from: http://www.lowimpact.org/home-made-biogas-anaerobic-digester [Accessed 06/07/2017].
14. Water-technology.net. *Reading Sewage Treatment Works, Reading, United Kingdom*. 2017 [Online]; Available from: http://www.water-technology.net/projects/reading_sewage/reading_sewage2.html [Accessed 06/07/2017].
15. BiogasSA. *Rural Digesters*. 2017 [Online]; Available from: http://www.biogassa.co.za/index.php/91-services-home-articles/81-biogas-rural-digesters [Accessed 06/07/2017].
16. Messenger, B. *Food Waste for Anaerobic Digestion Feedstock Deal for Exeter Agri-Energy in Maine*. 2016 [Online]; Available from: https://waste-management-world.com/a/food-waste-for-anaerobic-digestion-feedstock-deal-for-exeter-agri-energy-in-maine [Accessed 06/07/2017].
17. Braun, R., Anaerobic digestion: a multi-faceted process for energy, environmental management and rural development, *In* P. Ranalli (ed), *Improvement of Crop Plants for Industrial End Uses*. Springer Netherlands: Dordrecht, 2007, p. 335-416.
18. Wolfson, R., *Energy, Environment and Climate*, 2nd edition. U.S.A.N. New York (ed). 2012. p. 96-97.
19. Mohseni, F., et al., Biogas from renewable electricity - Increasing a climate neutral fuel supply. *Applied Energy*, 2012. **90**(1), p. 11-16.
20. Clemens, J., et al., Mitigation of greenhouse gas emissions by anaerobic digestion of cattle slurry. *Agriculture Ecosystems & Environment*, 2006. **112**(2-3), p. 171-177.
21. Szabo, G., et al., The Carbon Footprint Of A Biogas Power Plant. *Environmental Engineering and Management Journal*, 2014. **13**(11), p. 2867-2874.

22. Yvon-Durocher, G., et al., Methane fluxes show consistent temperature dependence across microbial to ecosystem scales. *Nature*, 2014. **507**(7493), p. 488-491.

23. Khalid, A., et al., The anaerobic digestion of solid organic waste. *Waste Management*, 2011. **31**(8), p. 1737-1744.

24. Association, A.D.a.B. *The AD cycle*. 2017 [Online]. Available from: http://adbioresources.org/about-ad/what-is-ad/ [Accessed 23/08/2017].

25. Basiliko, N., et al., Methane biogeochemistry and methanogen communities in two northern peatland ecosystems, New York State. *Geomicrobiology Journal*, 2003. **20**(6), p. 563-577.

26. McDonald, I.R., et al., Molecular ecological analysis of methanogens and methanotrophs in blanket bog peat. *Microbial Ecology*, 1999. **38**(3), p. 225-233.

27. Nercessian, D., et al., Phylogenetic analysis of peat bog methanogen populations. *Fems Microbiology Letters*, 1999. **173**(2), p. 425-429.

28. Horn, M.A., et al., Hydrogenotrophic methanogenesis by moderately acid-tolerant methanogens of a methane-emitting acidic peat. *Applied and Environmental Microbiology*, 2003. **69**(1), p. 74-83.

29. Brauer, S.L., et al., Isolation of a novel acidiphilic methanogen from an acidic peat bog. *Nature*, 2006. **442**(7099), p. 192-194.

30. Lueders, T., et al., Molecular analyses of methyl-coenzyme M reductase alpha-subunit (mcrA) genes in rice field soil and enrichment cultures reveal the methanogenic phenotype of a novel archaeal lineage. *Environmental Microbiology*, 2001. **3**(3), p. 194-204.

31. Kruger, M., P. Frenzel, and R. Conrad, Microbial processes influencing methane emission from rice fields. *Global Change Biology*, 2001. **7**(1), p. 49-63.

32. Peng, J.J., et al., Dynamics of the methanogenic archaeal community during plant residue decomposition in an anoxic rice field soil. *Applied and Environmental Microbiology*, 2008. **74**(9), p. 2894-2901.

33. Delong, E.F., Archaea In Coastal Marine Environments. *Proceedings of the National Academy of Sciences of the United States of America*, 1992. **89**(12), p. 5685-5689.

34. Kendall, M.M., et al., Diversity of Archaea in marine sediments from Skan Bay, Alaska, including cultivated methanogens, and description of Methanogenium boonei sp nov. *Applied and Environmental Microbiology*, 2007. **73**(2), p. 407-414.

35. Colwell, F.S., et al., Estimates of biogenic methane production rates in deep marine sediments at Hydrate Ridge, Cascadia margin. *Applied and Environmental Microbiology*, 2008. **74**(11), p. 3444-3452.

36. Borrel, G., et al., Production and consumption of methane in freshwater lake ecosystems. *Research in Microbiology*, 2011. **162**(9), p. 832-847.

37. Ding, W.X., et al., Key factors affecting spatial variation of methane emissions from freshwater marshes. *Chemosphere*, 2003. **51**(3), p. 167-173.

38. Morvan, B., et al., Quantitative determination of H-2-utilizing acetogenic and sulfate-reducing bacteria and methanogenic archaea from digestive tract of different mammals. *Current Microbiology*, 1996. **32**(3), p. 129-133.

39. Leadbetter, J.R. and J.A. Breznak, Physiological ecology of Methanobrevibacter cuticularis sp nov and Methanobrevibacter curvatus sp nov, isolated from the hindgut of the termite Reticulitermes flavipes. *Applied and Environmental Microbiology*, 1996. **62**(10), p. 3620-3631.

40. Morgavi, D.P., et al., Microbial ecosystem and methanogenesis in ruminants. *Animal*, 2010. **4**(7), p. 1024-1036.

41. Rotmans, J., et al., Stabilizing Atmospheric Concentrations - Towards International Methane Control. *Ambio*, 1992. **21**(6), p. 404-413.

42. Gerardi, M.H (ed)., *The Microbiology of Anaerobic Digesters*. John Wiley & Sons, Inc. 2003 p. 15.

43. Alvarado, A., et al., Microbial trophic interactions and mcrA gene expression in monitoring of anaerobic digesters. *Frontiers in Microbiology*, 2014. **5**, p. 14.

44. Borrel, G., P.S. Adam, and S. Gribaldo, Methanogenesis and the Wood-Ljungdahl Pathway: An Ancient, Versatile, and Fragile Association. *Genome Biology and Evolution*, 2016. **8**(6), p. 1706-1711.

45. Matthieu Girard, J.H.P., Martin Belzile, Stéphane Godbout and Frédéric Pelletier. Biodegradation in Animal Manure Management, *In* Rolando Chamy and Francisca Rosenkranz (ed) *Biodegradation - Engineering and Technology*. Intech, 2013.

46. Ren, Z., et al., Characterization of the cellulolytic and hydrogen-producing activities of six mesophilic Clostridium species. *Journal of Applied Microbiology*, 2007. **103**(6), p. 2258-2266.

47. Nagamani, B. and K. Ramasamy, *Biogas production technology: An Indian perspective.* Current Science, 1999. **77**(1), p. 44-55.

48. Delbes, C., R. Moletta, and J.J. Godon, Monitoring of activity dynamics of an anaerobic digester bacterial community using 16S rRNA polymerase chain reaction - single-strand conformation polymorphism analysis. *Environmental Microbiology*, 2000. **2**(5), p. 506-515.

49. Drake, H.L., A.S. Gossner, and S.L. Daniel, *Old acetogens, new light*, in *Incredible Anaerobes: From Physiology to Genomics to Fuels*, J. Wiegel, R.J. Maier, and M.W.W. Adams (ed). Blackwell Publishing: Oxford. 2008, p. 100-128.

50. Volta, A.c., Lettere del Signor Don Allesandro Volta ... sull'aria infiammabile nativa delle palud*i*. 1777: *Marelli*.

51. Hofmann, A.W., On the Action of Trichloride of Phosphorus on the Salts of the Aromatic Monamines. *Proc. R. Soc. Lond*, 1866. **15**, p. 54-62.

52. Archer, D., Methanogenesis - Ecology, Physiology, Biochemistry And Genetics. *Nature*, 1994. **367**(6464), p. 604-605.

53. Raskin, L., et al., Group-Specific 16s Ribosomal-Rna Hybridization Probes To Describe Natural Communities Of Methanogens. *Applied and Environmental Microbiology*, 1994. **60**(4), p. 1232-1240.

54. Olsen, G.J., et al., Microbial Ecology And Evolution - A Ribosomal-Rna Approach. *Annual Review of Microbiology*, 1986. **40**, p. 337-365.

55. Fox, G.E., et al., Classification Of Methanogenic Bacteria By 16s Ribosomal-Rna Characterization. *Proceedings of the National Academy of Sciences of the United States of America*, 1977. **74**(10), p. 4537-4541.

56. Gray, M.W., D. Sankoff, and R.J. Cedergren, On The Evolutionary Descent Of Organisms And Organelles - A Global Phylogeny Based On A Highly Conserved Structural Core In Small Subunit Ribosomal-Rna. *Nucleic Acids Research*, 1984. **12**(14), p. 5837-5852.

57. Yang, B., Y. Wang, and P.Y. Qian, Sensitivity and correlation of hypervariable regions in 16S rRNA genes in phylogenetic analysis. *Bmc Bioinformatics*, 2016. **17**, p. 8.

58. Grosskopf, R., P.H. Janssen, and W. Liesack, Diversity and structure of the methanogenic community in anoxic rice paddy soil microcosms as examined by cultivation and direct 16S rRNA gene sequence retrieval. *Applied and Environmental Microbiology*, 1998. **64**(3), p. 960-969.

59. Baker, G.C., J.J. Smith, and D.A. Cowan, Review and re-analysis of domain-specific 16S primers. J*ournal of Microbiological Methods*, 2003. **55**(3), p. 541-555.

60. Roesch, L.F., et al., Pyrosequencing enumerates and contrasts soil microbial diversity. *Isme Journal*, 2007. **1**(4), p. 283-290.

61. Bates, S.T., et al., Examining the global distribution of dominant archaeal populations in soil. *Isme Journal*, 2011. **5**(5), p. 908-917.

62. Ispirli, H., F. Demirbas, and E. Dertli, Characterization of functional properties of Enterococcus spp. isolated from Turkish white cheese. L*wt-Food Science and Technology*, 2017. **75**, p. 358-365.

63. Balch, W.E. and R.S. Wolfe, Specificity And Biological Distribution Of Coenzyme M (2-Mercaptoethanesulfonic Acid). *Journal of Bacteriology*, 1979. **137**(1), p. 256-263.

64. Luton, P.E., et al., The mcrA gene as an alternative to 16S rRNA in the phylogenetic analysis of methanogen populations in landfill. *Microbiology-Sgm*, 2002. **148**, p. 3521-3530.

65. Lang, K., et al., New Mode of Energy Metabolism in the Seventh Order of Methanogens as Revealed by Comparative Genome Analysis of "Candidatus Methanoplasma termitum". *Applied and Environmental Microbiology*, 2015. **81**(4), p. 1338-1352.

66. Liu, Y.C. and W.B. Whitman, Metabolic, phylogenetic, and ecological diversity of the methanogenic archaea, *In Incredible Anaerobes: From Physiology to Genomics to Fuels*, J. Wiegel, R.J. Maier, and M.W.W. Adams, (ed). Blackwell Publishing: Oxford. 2008, p. 171-189.

67. Sakai, S., et al., Methanocella paludicola gen. nov., sp nov., a methane-producing archaeon, the first isolate of the lineage 'Rice Cluster I', and proposal of the new archaeal order Methanocellales ord. nov. *International Journal of Systematic and Evolutionary Microbiology*, 2008. **58**, p. 929-936.

68. Borrel, G., et al., Phylogenomic Data Support a Seventh Order of Methylotrophic Methanogens and Provide Insights into the Evolution of Methanogenesis. *Genome Biology and Evolution*, 2013. **5**(10), p. 1769-1780.

69. Rother, M. and J.A. Krzycki, Selenocysteine, Pyrrolysine, and the Unique Energy Metabolism of Methanogenic Archaea. *Archaea-an International Microbiological Journal,* 2010, p. 14.

70. Thauer, R.K., Biochemistry of methanogenesis: a tribute to Marjory Stephenson. *Microbiology-UK*, 1998. **144**, p. 2377-2406.

71. Ritari, J., et al., Molecular analysis of meso- and thermophilic microbiota associated with anaerobic biowaste degradation. *Bmc Microbiology*, 2012. **12**, p. 14.

72. Guyot, J.P. and A. Brauman, Methane Production From Formate By Syntrophic Association Of Methanobacterium-Bryantii And Desulfovibrio-Vulgaris-Jj. *Applied and Environmental Microbiology*, 1986. **52**(6), p. 1436-1437.

73. Widdel, F., Growth Of Methanogenic Bacteria In Pure Culture With 2-Propanol And Other Alcohols As Hydrogen Donors. *Applied and Environmental Microbiology,* 1986. **51**(5), p. 1056-1062.

74. Daniels, L., et al., Carbon-Monoxide Oxidation By Methanogenic Bacteria. *Journal of Bacteriology*, 1977. **132**(1), p. 118-126.

75. Obrien, J.M., et al., Association Of Hydrogen Metabolism With Unitrophic Or Mixotrophic Growth Of Methanosarcina-Barkeri On Carbon-Monoxide. *Journal of Bacteriology*, 1984. **158**(1), p. 373-375.

76. Kiene, R.P., et al., Metabolism Of Reduced Methylated Sulfur-Compounds In Anaerobic Sediments And By A Pure Culture Of An Estuarine Methanogen. *Applied and Environmental Microbiology*, 1986. **52**(5), p. 1037-1045.

77. Dridi, B., et al., Methanomassiliicoccus luminyensis gen. nov., sp nov., a methanogenic archaeon isolated from human faeces. I*nternational Journal of Systematic and Evolutionary Microbiology*, 2012. **62**, p. 1902-1907.

78. Ferry, J.G., Methane From Acetate. *Journal of Bacteriology*, 1992. **174**(17), p. 5489-5495.

79. Scheller, S., et al., Methyl-Coenzyme M Reductase from Methanogenic Archaea: Isotope Effects on the Formation and Anaerobic Oxidation of Methane. *Journal of the American Chemical Society*, 2013. **135**(40), p. 14975-14984.

80. McBride, B.C. and R.S. Wolfe, New Coenzyme Of Methyl Transfer, Coenzyme M. *Biochemistry*, 1971. **10**(12), p. 2317-2324.

81. Taylor, C.D. and R.S. Wolfe, Structure And Methylation Of Coenzyme M (Hsch2ch2so3). *Journal of Biological Chemistry*, 1974. **249**(15), p. 4879-4885.

82. Widdel, F. and R.S. Wolfe, Expression Of Secondary Alcohol-Dehydrogenase In Methanogenic Bacteria And Purification Of The F420-Specific Enzyme From Methanogenium-Thermophilum Strain Tci. *Archives of Microbiology*, 1989. **152**(4), p. 322-328.

83. Ferguson, D.J., et al., Reconstitution of dimethylamine : coenzyme M methyl transfer with a discrete corrinoid protein and two methyltransferases purified from

Methanosarcina barkeri. *Journal of Biological Chemistry*, 2000. **275**(37), p. 29053-29060.

84. Jetten, M.S.M., A.J.M. Stams, and A.J.B. Zehnder, Methanogenesis From Acetate - A Comparison Of The Acetate Metabolism In Methanothrix-Soehngenii And Methanosarcina Spp. *Fems Microbiology Letters,* 1992. **88**(3-4), p. 181-197.
85. Chen, Y., J.J. Cheng, and K.S. Creamer, Inhibition of anaerobic digestion process: A review. *Bioresource Technology,* 2008. **99**(10), p. 4044-4064.
86. Gujer, W. and A.J.B. Zehnder, *Conversion Processes In Anaerobic-Digestion.* Water Science and Technology, 1983. **15**(8-9), p. 127-167.
87. van Lier, J.B., et al., New perspectives in anaerobic digestion. *Water Science and Technology*, 2001. **43**(1), p. 1-18.
88. Bayr, S., et al., Mesophilic and thermophilic anaerobic co-digestion of rendering plant and slaughterhouse wastes. *Bioresource Technology,* 2012. **104**, p. 28-36.
89. Kim, M., Y.H. Ahn, and R.E. Speece, Comparative process stability and efficiency of anaerobic digestion; mesophilic vs. thermophilic. *Water Research*, 2002. **36**(17), p. 4369-4385.
90. Kim, M., et al., Hydrolysis and acidogenesis of particulate organic material in mesophilic and thermophilic anaerobic digestion. *Environmental Technology*, 2003. **24**(9), p. 1183-1190.
91. Yu, H.Q. and H.H.P. Fang, Acidogenesis of dairy wastewater at various pH levels. *Water Science and Technology*, 2002. **45**(10), p. 201-206.
92. Ward, A.J., et al., Optimisation of the anaerobic digestion of agricultural resources. *Bioresource Technology*, 2008. **99**(17), p. 7928-7940.
93. Wang, Y.Y., et al., Effects of volatile fatty acid concentrations on methane yield and methanogenic bacteria. *Biomass & Bioenergy,* 2009. **33**(5), p. 848-853.
94. Bouallagui, H., et al., Bioreactor performance in anaerobic digestion of fruit and vegetable wastes. *Process Biochemistry*, 2005. **40**(3-4), p. 989-995.

95. Nachaiyasit, S. and D.C. Stuckey, The effect of shock loads on the performance of an anaerobic baffled reactor (ABR) .1. Step changes in feed concentration at constant retention time. *Water Research*, 1997. **31**(11), p. 2737-2746.

96. Nachaiyasit, S. and D.C. Stuckey, The effect of shock loads on the performance of an anaerobic baffled reactor (ABR) .2. Step and transient hydraulic shocks at constant feed strength. *Water Research*, 1997. **31**(11), p. 2747-2754.

97. Appels, L., et al., Principles and potential of the anaerobic digestion of waste-activated sludge. *Progress in Energy and Combustion Science*, 2008. **34**(6), p. 755-781.

98. Kato, M.T., J.A. Field, and G. Lettinga, Anaerobe Tolerance to Oxygen and the Potentials of Anaerobic and Aerobic Cocultures for Wastewater Treatment. *Brazilian Journal of Chemical Engineering,* 1997. **14**.

99. Botheju, D., B. Lie, and R. Bakke, Oxygen Effects in Anaerobic Digestion. *Modeling Identification and Control,* 2009. **30**(4), p. 191-201.

100. Botheju, D., B. Lie, and R. Bakke, Oxygen Effects in Anaerobic Digestion - II. *Modeling Identification and Control*, 2010. **31**(2), p. 55-65.

101. Kiener, A. and T. Leisinger, Oxygen Sensitivity Of Methanogenic Bacteria. *Systematic and Applied Microbiology*, 1983. **4**(3), p. 305-312.

102. Jarrell, K.F., Extreme Oxygen Sensitivity In Methanogenic Archaebacteria. Bioscience, 1985. **35**(5), p. 298-302.

103. Borja, R., C.J. Banks, and Z.J. Wang, Effect Of Organic Loading Rate On Anaerobic Treatment Of Slaughterhouse Waste-Water In A Fluidized-Bed Reactor. *Bioresource Technology*, 1995. **52**(2), p. 157-162.

104. Borja, R. and C.J. Banks, Response Of An Anaerobic Fluidized-Bed Reactor Treating Ice-Cream Waste-Water To Organic, Hydraulic, Temperature And Ph Shocks. *Journal of Biotechnology*, 1995. **39**(3), p. 251-259.

105. Visser, A., Y. Gao, and G. Lettinga, Effects Of Short-Term Temperature Increases On The Mesophilic Anaerobic Breakdown Of Sulfate Containing Synthetic Waste-Water. *Water Research*, 1993. **27**(4), p. 541-550.

106. Akuzawa, M., et al., Distinctive Responses of Metabolically Active Microbiota to Acidification in a Thermophilic Anaerobic Digester. *Microbial Ecology*, 2011. **61**(3), p. 595-605.

107. Ahring, B.K., Methanogenesis In Thermophilic Biogas Reactors. *Antonie Van Leeuwenhoek International Journal of General and Molecular Microbiology, 1*995. **67**(1), p. 91-102.

108. Mendez-Acosta, H.O., et al., Monitoring anaerobic sequential batch reactors via fractal analysis of pH time series. *Biotechnology and Bioengineering*, 2013. **110**(8), p. 2131-2139.

109. Rallis, I., et al., Novel sensing techniques for industrial scale bio-digesters, *In* 17th International Conference on Optical Fibre Sensors, Pts 1 and 2. M. Voet, et al., (ed). Spie-Int Soc Optical Engineering: Bellingham. 2005, p. 110-113.

110. Williams, R.T. and R.L. Crawford, Methane Production In Minnesota Peatlands. *Applied and Environmental Microbiology*, 1984. **47**(6), p. 1266-1271.

111. Wust, P.K., M.A. Horn, and H.L. Drake, Trophic links between fermenters and methanogens in a moderately acidic fen soil. *Environmental Microbiology*, 2009. **11**(6), p. 1395-1409.

112. Brauer, S.L., et al., Characterization of acid-tolerant H-2/CO2-utilizing methanogenic enrichment cultures from an acidic peat bog in New York State. *Fems Microbiology Ecology*, 2006. **57**(2), p. 206-216.

113. Trcek, J., N.P. Mira, and L.R. Jarboe, Adaptation and tolerance of bacteria against acetic acid. *Applied Microbiology and Biotechnology,* 2015. **99**(15), p. 6215-6229.

114. Russell, J.B., Another Explanation For The Toxicity Of Fermentation Acids At Low Ph - Anion Accumulation Versus Uncoupling. *Journal of Applied Bacteriology*, 1992. **73**(5), p. 363-370.

115. Hickey, R.F. and M.S. Switzenbaum, Thermodynamics Of Volatile Fatty-Acid Accumulation In Anaerobic Digesters Subject To Increases In Hydraulic And

Organic Loading. *Research Journal of the Water Pollution Control Federation,* 1991. **63**(2), p. 141-144.

116. Wang, Q.H., et al., Degradation of volatile fatty acids in highly efficient anaerobic digestion*. Biomass & Bioenergy*, 1999. **16**(6), p. 407-416.

117. Yuan, Y.L., R. Conrad, and Y.H. Lu, Responses of methanogenic archaeal community to oxygen exposure in rice field soil. *Environmental Microbiology Reports*, 2009. **1**(5), p. 347-354.

118. Barley, M.E., A. Bekker, and B. Krapez, Late Archean to Early Paleoproterozoic global tectonics, environmental change and the rise of atmospheric oxygen*. Earth and Planetary Science Letters*, 2005. **238**(1-2), p. 156-171.

119. Fetzer, S. and R. Conrad, Effect Of Redox Potential On Methanogenesis By Methanosarcina-Barkeri. *Archives of Microbiology*, 1993. **160**(2), p. 108-113.

120. Thauer, R.K., et al., Methanogenic archaea: ecologically relevant differences in energy conservation. *Nature Reviews Microbiology*, 2008. **6**(8), p. 579-591.

121. Touati, D., Superoxide Dismutases in Bacteria and Pathogen Protists. *Cold Spring Harbor Monograph Archive*. 1997. **34**, p. 447-4931997.

122. Storz, G. and J.A. Imlay, Oxidative stress*. Current Opinion in Microbiology*, 1999. **2**(2), p. 188-194.

123. Imlay, J.A., Iron-sulphur clusters and the problem with oxygen*. Molecular Microbiology*, 2006. **59**(4), p. 1073-1082.

124. Imlay, J.A., How oxygen damages microbes: Oxygen tolerance and obligate anaerobiosis*. Advances in Microbial Physiology.* 2002. **46**: p. 111-153.

125. Nagle, D.P. and R.S. Wolfe, Component-A Of The Methyl Coenzyme-M Methylreductase System Of Methanobacterium - Resolution Into 4 Components*. Proceedings of the National Academy of Sciences of the United States of America-Biological Sciences*, 1983. **80**(8), p. 2151-2155.

126. Cedervall, P.E., et al., Structural Insight into Methyl-Coenzyme M Reductase Chemistry Using Coenzyme B Analogues*. Biochemistry*, 2010. **49**(35), p. 7683-7693.

127. Schonheit, P., H. Keweloh, and R.K. Thauer, Factor F420 Degradation In Methanobacterium-Thermoautotrophicum During Exposure To Oxygen. Fems Microbiology Letters, 1981. **12**(4), p. 347-349.

128. Kiener, A., W.H. Ormejohnson, and C.T. Walsh, Reversible Conversion Of Coenzyme F-420 To The 8-Oh-Amp And 8-Oh-Gmp Esters, F-390-A And F-390-G, On Oxygen Exposure And Reestablishment Of Anaerobiosis In Methanobacterium-Thermoautotrophicum. *Archives of Microbiology,* 1988. **150**(3), p. 249-253.

129. Escalantesemerena, J.C., K.L. Rinehart, and R.S. Wolfe, Tetrahydromethanopterin, A Carbon Carrier In Methanogenesis. *Journal of Biological Chemistry*, 1984. **259**(15), p. 9447-9455.

130. Monnet, F. An Introduction to Anaerobic Digestion of Organic Wastes, 2003 [Online]. Available from: http://www.remade.org.uk/media/9102. [Accessed 12/02/2017].

131. Pullammanappallil, P.C., et al., Expert system for control of anaerobic digesters. *Biotechnology and Bioengineering,* 1998. **58**(1), p. 13-22.

132. Ahring, B.K., M. Sandberg, and I. Angelidaki, Volatile Fatty-Acids As Indicators Of Process Imbalance Is Anaerobic Digesters. *Applied Microbiology and Biotechnology*, 1995. **43**(3), p. 559-565.

133. Mosey, F.E. and X.A. Fernandes, Patterns Of Hydrogen In Biogas From The Anaerobic-Digestion Of Milk-Sugars. *Water Science and Technology,* 1989. **21**(4-5), p. 187-196.

134. Sandberg, M. and B.K. Ahring, Anaerobic Treatment Of Fish-Meal Process Waste-Water In A Uasb Reactor At High Ph. *Applied Microbiology and Biotechnology*, 1992. **36**(6), p. 800-804.

135. Peces, M., S. Astals, and J. Mata-Alvarez, Response of a sewage sludge mesophilic anaerobic digester to short and long-term thermophilic temperature fluctuations. *Chemical Engineering Journal,* 2013. **233**, p. 109-116.

136. Michaud, S., et al., Methane yield as a monitoring parameter for the start-up of anaerobic fixed film reactors. *Water Research*, 2002. **36**(5), p. 1385-1391.

137. Raju, C.S., et al., NIR Monitoring of Ammonia in Anaerobic Digesters Using a Diffuse Reflectance Probe. *Sensors*, 2012. **12**(2), p. 2340-2350.

138. PoggiVaraldo, H.M., et al., Inhibition of mesophilic solid-substrate anaerobic digestion by ammonia nitrogen. *Applied Microbiology and Biotechnology,* 1997. **47**(3), p. 284-291.

139. Zhang, J.S., et al., Anaerobic digestion of food waste stabilized by lime mud from papermaking process. *Bioresource Technology*, 2014. **170**, p. 270-277.

140. Georgacakis, D. and D. Dalis, Controlled Anaerobic-Digestion Of Settled Olive-Oil Waste-Water. *Bioresource Technology*, 1993. **46**(3), p. 221-226.

141. Aquafix. Anaerobic Digester Upset & Troubleshooting, 2017 [Online], Available from: https://teamaquafix.com/anaerobic-digester-upset-troubleshooting/ [Accessed 11/09/2017].

142. Burton, C.H. and C. Turner, *Manure Management: Treatment Strategies for Sustainable Agriculture*. Silsoe Research Institute, 2003.

143. McMahon, K.D., et al., Anaerobic codigestion of municipal solid waste and biosolids under various mixing conditions - II: Microbial population dynamics. *Water Research*, 2001. **35**(7), p. 1817-1827.

144. Verstraete, W., et al., Anaerobic bioprocessing of organic wastes. *World Journal of Microbiology & Biotechnology*, 1996. **12**(3), p. 221-238.

145. Dareioti, M.A. and M. Kornaros, Effect of hydraulic retention time (HRT) on the anaerobic co-digestion of agro-industrial wastes in a two-stage CSTR system. *Bioresource Technology*, 2014. **167**, p. 407-415.

146. Shi, X.S., et al., Effect of Hydraulic Retention Time on Anaerobic Digestion of Wheat Straw in the Semicontinuous Continuous Stirred-Tank Reactors. *Biomed Research International*, 2017: p. 6.

147. Smil, V., *Biomass Energies*. Springer US, 1983.

148. Hao, J.X. and H. Wang, Volatile fatty acids productions by mesophilic and thermophilic sludge fermentation: Biological responses to fermentation temperature. *Bioresource Technology*, 2015. **175**, p. 367-373.

149. Elliott, A. and T. Mahmood, Comparison of Mechanical Pretreatment Methods for the Enhancement of Anaerobic Digestion of Pulp and Paper Waste Activated Sludge*. Water Environment Research*, 2012. **84**(6), p. 497-505.

150. del Rio, A.V., et al., Thermal pre-treatment of aerobic granular sludge: Impact on anaerobic biodegradability*. Water Research*, 2011. **45**(18), p. 6011-6020.

151. Mussoline, W., et al., The Anaerobic Digestion of Rice Straw: A Review. C*ritical Reviews in Environmental Science and Technology,* 2013. **43**(9), p. 895-915.

152. Torres, M.L. and M.D.E. Llorens, Effect of alkaline pretreatment on anaerobic digestion of solid wastes. *Waste Management,* 2008. **28**(11), p. 2229-2234.

153. Lin, Y.Q., D.H. Wang, and L.S. Wang, Biological pretreatment enhances biogas production in the anaerobic digestion of pulp and paper sludge. *Waste Management & Research*, 2010. **28**(9), p. 800-810.

154. Ariunbaatar, J., et al., Pretreatment methods to enhance anaerobic digestion of organic solid waste*. Applied Energy*, 2014. **123**, p. 143-156.

155. Lissens, G., et al., Solid waste digestors: process performance and practice for municipal solid waste digestion*. Water Science and Technology*, 2001. **44**(8), p. 91-102.

156. Ince, O., Performance of a two-phase anaerobic digestion system when treating dairy wastewater*. Water Research*, 1998. **32**(9), p. 2707-2713.

157. Zhu, H., et al., Co-production of hydrogen and methane from potato waste using a two-stage anaerobic digestion process*. Bioresource Technology*, 2008. **99**(11), p. 5078-5084.

158. Chen, X., et al., Improving biomethane yield by controlling fermentation type of acidogenic phase in two-phase anaerobic co-digestion of food waste and rice straw. *Chemical Engineering Journal*, 2015. **273**, p. 254-260.

159. Llabresluengo, P. and J. Mataalvarez, The Hydrolytic Step In A Dry Digestion System. *Biological Wastes*, 1988. **23**(1), p. 25-37.

160. Lu, Y., et al., Characteristics of hydrogen and methane production from cornstalks by an augmented two- or three-stage anaerobic fermentation process. *Bioresource Technology*, 2009. **100**(12), p. 2889-2895.

161. Mata-Alvarez, J., S. Mace, and P. Llabres, Anaerobic digestion of organic solid wastes. An overview of research achievements and perspectives. *Bioresource Technology*, 2000. **74**(1), p. 3-16.

162. El-Mashad, H.M. and R.H. Zhang, Biogas production from co-digestion of dairy manure and food waste. *Bioresource Technology*, 2010. **101**(11), p. 4021-4028.

163. Murto, M., L. Bjornsson, and B. Mattiasson, Impact of food industrial waste on anaerobic co-digestion of sewage sludge and pig manure. *Journal of Environmental Management*, 2004. **70**(2), p. 101-107.

164. Lehtomaki, A., S. Huttunen, and J.A. Rintala, Laboratory investigations on co-digestion of energy crops and crop residues with cow manure for methane production: Effect of crop to manure ratio. *Resources Conservation and Recycling*, 2007. **51**(3), p. 591-609.

165. Cavinato, C., et al., Thermophilic anaerobic co-digestion of cattle manure with agro-wastes and energy crops: Comparison of pilot and full scale experiences. *Bioresource Technology*, 2010. **101**(2), p. 545-550.

166. Wooley, J.C. and Y.Z. Ye, Metagenomics: Facts and Artifacts, and Computational Challenges. *Journal of Computer Science and Technology,* 2010. **25**(1), p. 71-81.

167. Alivisatos, A.P., et al., A unified initiative to harness Earth's microbiomes. *Science*, 2015.

168. Sivasubramaniam, D. and A.E. Franks, Bioengineering microbial communities: Their potential to help, hinder and disgust. *Bioengineered*, 2016. **7**(3), p. 137-144.

169. Grosskopf, T. and O.S. Soyer, Synthetic microbial communities. *Current Opinion in Microbiology*, 2014. **18**, p. 72-77.

170. Purnick, P.E.M. and R. Weiss, The second wave of synthetic biology: from modules to systems*. Nature Reviews Molecular Cell Biology*, 2009. **10**(6), p. 410-422.

171. Brenner, K., L.C. You, and F.H. Arnold, Engineering microbial consortia: a new frontier in synthetic biology. *Trends in Biotechnology*, 2008. **26**(9), p. 483-489.

172. Jagmann, N. and B. Philipp, Reprint of Design of synthetic microbial communities for biotechnological production processes*. Journal of Biotechnology*, 2014. **192**, p. 293-301.

173. lab, O. Engineering Synthetic Microbial Communities for Biomethane Production, 2017 [Online] Available from: http://osslab.lifesci.warwick.ac.uk/adLola.html [Accessed cited 05/092017].

174. Backman, K., Y.M. Chen, and B. Magasanik, Physical And Genetic-Characterization Of The Glna-Glng Region Of The Escherichia-Coli Chromosome*. Proceedings of the National Academy of Sciences of the United States of America-Biological Sciences,* 1981. **78**(6), p. 3743-3747.

175. Atkinson, M.R. and A.J. Ninfa, Characterization Of Escherichia-Coli Glnl Mutations Affecting Nitrogen Regulation. *Journal of Bacteriology*, 1992. **174**(14), p. 4538-4548.

176. Datsenko, K.A. and B.L. Wanner, One-step inactivation of chromosomal genes in Escherichia coli K-12 using PCR products. *Proceedings of the National Academy of Sciences of the United States of America,* 2000. **97**(12), p. 6640-6645.

177. Karunakaran, R., et al., A family of promoter probe vectors incorporating autofluorescent and chromogenic reporter proteins for studying gene expression in Gram-negative bacteria. *Microbiology-Sgm*, 2005. **151**; p. 3249-3256.

178. Biolabs, N.E. PCR Using Q5® High-Fidelity DNA Polymerase (M0491) 2017 [Online]. Available from: https://www.neb.com/protocols/2013/12/13/pcr-using-q5-high-fidelity-dna-polymerase-m0491 [Accessed 05.01.17].

179. Biolabs, N.E. *NEBCloner*. 2017 [Online]. Available from: https://nebcloner.neb.com/#!/, [Accessed 18.06.17].

180. Clustal. *Clustal W / Clustal X*. 2017 10/09/2017]; Clustal X download page]. Available from: http://www.clustal.org/clustal2/.

181. Lange, A., *Primer Design and Assay Optimisation for Quantitative PCR.* 2016.

182. Livak, K.J. and T.D. Schmittgen, Analysis of relative gene expression data using real-time quantitative PCR and the 2(T)(-Delta Delta C) method. *Methods*, 2001. **25**(4), p. 402-408.

183. Cock, P.J.A., et al., The Sanger FASTQ file format for sequences with quality scores, and the Solexa/Illumina FASTQ variants*. Nucleic Acids Research,* 2010. **38**(6), p. 1767-1771.

184. Bioinformatics, B. *FastQC*. 2017 [Online]. Available from: https://www.bioinformatics.babraham.ac.uk/projects/fastqc/, [Accessed 10/09/2017].

185. Bioinformatics, B. *Trim Galore!* 2017 [Online]. Available from: https://www.bioinformatics.babraham.ac.uk/projects/trim_galore/, [Accessed 10/09/2017].

186. Huson, D.H., et al., *Metagenome analysis using megan*. Proceedings of the 5th Asia- Pacific Bioinfomatics Conference 2007, ed. D. Sankoff, L. Wang, and F. Chin. Vol. 5. 2007, Covent Garden: Imperial College Press. 7-16.

187. Krol, A. One Codex and Microbiology's Search Problem. 2015 [Online]. Available from: http://www.bio-itworld.com/2015/2/9/one-codex-microbiologys-search-problem.html, [Accesed 06/08/2017].

188. Juottonen, H., P.E. Galand, and K. Yrjala, Detection of methanogenic Archaea in peat: comparison of PCR primers targeting the mcrA gene. *Research in Microbiology, 2006*. **157**(10), p. 914-921.

189. O'Leary, N.A., et al., Reference sequence (RefSeq) database at NCBI: current status, taxonomic expansion, and functional annotation. *Nucleic Acids Research*, 2016. **44**(D1), p. D733-D745.

190. Studholme, D.J. and R. Dixon, Domain architectures of sigma(54)-dependent transcriptional activators. *Journal of Bacteriology*, 2003. **185**(6), p. 1757-1767.

191. Reitzer, L.J. and B. Magasanik, Expression Of Glna In Escherichia-Coli Is Regulated At Tandem Promoters. Proceedings of the National Academy of Sciences of the United States of America, 1985. **82**(7), p. 1979-1983.

192. Kozak, M., Initiation of translation in prokaryotes and eukaryotes. *Gene*, 1999. **234**(2), p. 187-208.

193. Hebert, C.G., J.J. Valdes, and W.E. Bentley, Beyond silencing - engineering applications of RNA interference and antisense technology for altering cellular phenotype. *Current Opinion in Biotechnology*, 2008. **19**(5), p. 500-505.

194. Zhou, K., et al., Novel reference genes for quantifying transcriptional responses of Escherichia coli to protein overexpression by quantitative PCR. *Bmc Molecular* Biology, 2011. **12**, p. 9.

195. Wang, Y. and P.Y. Qian, Conservative Fragments in Bacterial 16S rRNA Genes and Primer Design for 16S Ribosomal DNA Amplicons in Metagenomic Studies. *Plos One*, 2009. **4**(10), p. 9.

196. Fetzer, S., F. Bak, and R. Conrad, Sensitivity Of Methanogenic Bacteria From Paddy Soil To Oxygen And Desiccation. *Fems Microbiology Ecology*, 1993. **12**(2), p. 107-115.

197. Peters, V. and R. Conrad, Methanogenic And Other Strictly Anaerobic-Bacteria In Desert Soil And Other Oxic Soils. *Applied and Environmental Microbiology,* 1995. **61**(4), p. 1673-1676.

198. Brioukhanov, A., et al., Protection of Methanosarcina barkeri against oxidative stress: identification and characterization of an iron superoxide dismutase. *Archives of Microbiology,* 2000. **174**(3), p. 213-216.

199. Erkel, C., et al., Genome of Rice Cluster I archaea - the key methane producers in the rice rhizosphere. *Science*, 2006. **313**(5785), p. 370-372.

200. Ma, K. and Y.H. Lu, Regulation of microbial methane production and oxidation by intermittent drainage in rice field soil. *Fems Microbiology Ecology*, 2011. **75**(3), p. 446-456.

201. Ueki, A., et al., Survival of methanogens in air-dried paddy field soil and their heat tolerance. *Water Science and Technology*, 1997. **36**(6-7), p. 517-522.

202. Kim, S.Y., et al., Comparative analysis of soil microbial communities and their responses to the short-term drought in bog, fen, and riparian wetlands. *Soil Biology & Biochemistry*, 2008. **40**(11), p. 2874-2880.

203. Angel, R., D. Matthies, and R. Conrad, Activation of Methanogenesis in Arid Biological Soil Crusts Despite the Presence of Oxygen. *Plos One*, 2011. **6**(5), p. 8.

204. Freeman, C., et al., Contrasted effects of simulated drought on the production and oxidation of methane in a mid-Wales wetland. *Soil Biology and Biochemistry*, 2002. **34**(1), p. 61-67.

205. Times, T. *Exmouth Dock Tide Times*. 2017 [Online]; Available from: https://www.tidetimes.org.uk/exmouth-dock-tide-times#axzz2vg9fpyqf, [Accessed 07/07/2017].

206. Mitra, S., M. Stark, and D.H. Huson, Analysis of 16S rRNA environmental sequences using MEGAN. *Bmc Genomics*, 2011. **12**, p. 7.

207. World, B.-I. One Codex and microbiology's search problem. 2015 [Online]; Available from: http://www.bio-itworld.com/2015/2/9/one-codex-microbiologys-search-problem.html. [Accessed 04/06/2016].

208. Gillham, M.E., Vegetation Of The Exe Estuary In Relation To Water Salinity. *Journal of Ecology*, 1957. **45**(3), p. 735-756.

209. Fuller, C.W., et al., The challenges of sequencing by synthesis. *Nat Biotech*, 2009. **27**(11), p. 1013-1023.

210. Sayers, E.W., et al., Database resources of the National Center for Biotechnology Information. *Nucleic Acids Research*, 2009. **37**, p. D5-D15.

211. Iino, T., et al., Candidatus Methanogranum caenicola: a Novel Methanogen from the Anaerobic Digested Sludge, and Proposal of Methanomassiliicoccaceae fam. nov and Methanomassiliicoccales ord. nov., for a Methanogenic Lineage of the Class Thermoplasmata. *Microbes and Environments,* 2013. **28**(2), p. 244-250.

212. Garcia-Etxebarria, K., M. Garcia-Garcera, and F. Calafell, Consistency of metagenomic assignment programs in simulated and real data. *Bmc Bioinformatics*, 2014. **15**, p. 10.

213. Huson, D.H., et al., Integrative analysis of environmental sequences using MEGAN4. *Genome Research,* 2011. **21**(9), p. 1552-1560.

214. Dumont, M.G., et al., Classification of pmoA amplicon pyrosequences using BLAST and the lowest common ancestor method in MEGAN. *Frontiers in Microbiology*, 2014. **5**, p. 11.

215. Oremland, R.S. and S. Polcin, Methanogenesis And Sulfate Reduction - Competitive And Noncompetitive Substrates In Estuarine Sediments. *Applied and Environmental Microbiology,* 1982. **44**(6), p. 1270-1276.

216. Purdy, K.J., et al., Comparison of the molecular diversity of the methanogenic community at the brackish and marine ends of a UK estuary. *Fems Microbiology Ecology*, 2002. **39**(1), p. 17-21.

217. Webster, G., et al., Archaeal community diversity and abundance changes along a natural salinity gradient in estuarine sediments. *Fems Microbiology Ecology*, 2015. **91**(2), p. 18.

218. Banning, N., et al., Investigation of the methanogen population structure and activity in a brackish lake sediment. *Environmental Microbiology*, 2005. **7**(7), p. 947-960.

219. Munson, M.A., D.B. Nedwell, and T.M. Embley, Phylogenetic diversity of Archaea in sediment samples from a coastal salt marsh. *Applied and Environmental Microbiology,* 1997. **63**(12), p. 4729-4733.

220. Earl, J., et al., Development of temporal temperature gradient electrophoresis for characterising methanogen diversity. *Microbial Ecology,* 2005. **50**(3), p. 327-336.

221. Scandalios, J.G., Oxidative stress: molecular perception and transduction of signals triggering antioxidant gene defenses. *Brazilian Journal of Medical and Biological Research*, 2005. **38**(7), p. 995-1014.

222. Tholen, A., M. Pester, and A. Brune, Simultaneous methanogenesis and oxygen reduction by Methanobrevibacter cuticularis at low oxygen fluxes. *Fems Microbiology Ecology*, 2007. **62**(3), p. 303-312.

223. Miller, T.L., et al., Isolation Of Methanobrevibacter-Smithii From Human Feces. *Applied and Environmental Microbiology,* 1982. **43**(1), p. 227-232.

224. Jeanthon, C., et al., Methanococcus vulcanius sp. nov., a novel hyperthermophilic methanogen isolated from East Pacific Rise, and identification of Methanococcus sp. DSM 4213(T) as Methanococcus fervens sp. nov. *International Journal of Systematic Bacteriology,* 1999. **49**, p. 583-589.

225. Sowers, K.R. and J.G. Ferry, Isolation And Characterization Of A Methylotrophic Marine Methanogen, Methanococcoides-Methylutens Gen-Nov, Sp-Nov. *Applied and Environmental Microbiology,* 1983. **45**(2), p. 684-690.

226. Galagan, J.E., et al., The genome of M-acetivorans reveals extensive metabolic and physiological diversity. *Genome Research*, 2002. **12**(4), p. 532-542.

227. Nath, R., et al., Isolation of Shewanella algae from rectal swabs of patients with bloody diarrhoea. *Indian Journal of Medical Microbiology*, 2011. **29**(4), p. 422-U150.

228. Dey, S., et al., Shewanella algae in acute gastroenteritis. *Indian Journal of Medical Microbiology*, 2015. **33**(1), p. 172-175.

229. Lai, M.C., et al., Methanosarcina mazei strain O1M9704, methanogen with novel tubule isolated from estuarine environment. *Current Microbiology*, 2000. **41**(1), p. 15-20.

230. Mah, R.A., Isolation And Characterization Of Methanococcus-Mazei. *Current Microbiology*, 1980. **3**(6), p. 321-326.

231. Barker, H.A., Studies upon the methane-producing bacteria. *Archiv für Mikrobiologie,* 1936. **7**(1), p. 420-438.

232. Jennings, M.E., et al., *Expression of a bacterial catalase in a strictly anaerobic methanogen significantly increases tolerance to hydrogen peroxide but not oxygen.* Microbiology-Sgm, 2014. **160**, p. 270-278.

233. Brioukhanov, A.L. and A.I. *Netrusov, Catalase and superoxide dismutase: Distribution, properties, and physiological role in cells of strict anaerobes. Biochemistry-Moscow*, 2004. **69**(9), p. 949-962.

234. Liu, C.T., et al., Evaluation of methanogenic strains and their ability to endure aeration and water stress*. Current Microbiology*, 2008. **56**(3), p. 214-218.

235. Kratzer, C., et al., Methanoferrodoxin represents a new class of superoxide reductase containing an iron-sulfur cluster. *Febs Journal*, 2011. **278**(3), p. 442-451.

236. Jenney, F.E., et al., Anaerobic microbes: Oxygen detoxification without superoxide dismutase*. Science*, 1999. **286**(5438), p. 306-309.

237. Lumppio, H.L., et al., Rubrerythrin and rubredoxin oxidoreductase in Desulfovibrio vulgaris: a novel oxidative stress protection system*.* J*ournal of Bacteriology*, 2001. **183**(9), p. 2970-2970.

238. Maeder, D.L., et al., The Methanosarcina barkeri genome: Comparative analysis with Methanosarcina acetivorans and Methanosarcina mazei reveals extensive rearrangement within methanosarcinal genomes*. Journal of Bacteriology*, 2006. **188**(22), p. 7922-7931.

239. Sieburth, J.M., C1 Bacteria In The Water Column Of Chesapeake Bay, Usa .1. Distribution Of Subpopulations Of O2-Tolerant, Obligately Anaerobic, Methylotrophic Methanogens That Occur In Microniches Reduced By Their Bacterial Consorts. *Marine Ecology Progress Series*, 1993. **95**(1-2), p. 67-80.

240. Cynar, F.J. and A.A. Yayanos, Enrichment and characterization of a methanogenic bacterium from the oxic upper layer of the ocean. *Current Microbiology*, 1991. **23**(2), p. 89-96.

241. van der Maarel, M., et al., Detection of methanogenic archaea in seawater particles and the digestive tract of a marine fish species. *Fems Microbiology Letters*, 1999. **173**(1), p. 189-194.

242. Henriksen, J.R., Luke,J., Reinhart,S., Benedict,M.N., Youngblut,N.D., Metcalf,M.E., Whitaker,R.J. and Metcalf,W.W. *Methanococcoides methylutens MM1, complete genome.* 2015 [Online]; Available from: https://www.ncbi.nlm.nih.gov/nuccore/CP009518.1. [Accessed 06/07/2017].

243. Roe, A.J., et al., Inhibition of Escherichia coli growth by acetic acid: a problem with methionine biosynthesis and homocysteine toxicity. *Microbiology-Sgm*, 2002. **148**, p. 2215-2222.

244. Franke-Whittle, I.H., et al., Investigation into the effect of high concentrations of volatile fatty acids in anaerobic digestion on methanogenic communities. *Waste Management,* 2014. **34**(11), p. 2080-2089.

245. Breznak, J.A., *Acetogenesis from Carbon Dioxide in Termite Guts*, in *Acetogenesis*, H.L. Drake (ed). 1994, Springer US: Boston, MA. p. 303-330.

246. Rosencrantz, D., F.A. Rainey, and P.H. Janssen, Culturable populations of Sporomusa spp. and Desulfovibrio spp. in the anoxic bulk soil of flooded rice microcosms. *Applied and Environmental Microbiology,* 1999. **65**(8), p. 3526-3533.

247. Liu, S. and J.M. Suflita, H2-Co2-Dependent Anaerobic O-Demethylation Activity In Subsurface Sediments And By An Isolated Bacterium. *Applied and Environmental Microbiology*, 1993. **59**(5), p. 1325-1331.

248. Adrian, N.R. and C.M. Arnett, Anaerobic biodegradation of hexahydro-1,3,5-trinitro-1,3,5-triazine (RDX) by Acetobacterium malicum strain HAAP-1 isolated from a methanogenic mixed culture. *Current Microbiology*, 2004. **48**(5), p. 332-340.

249. Wolfe, A.J., The acetate switch. *Microbiology and Molecular Biology Reviews*, 2005. **69**(1), p. 12-50.

250. Farmer, W.R. and J.C. Liao, Reduction of aerobic acetate production by Escherichia coli. *Applied and Environmental Microbiology*, 1997. **63**(8), p. 3205-3210.

251. Eiteman, M.A. and E. Altman, Overcoming acetate in Escherichia coli recombinant protein fermentations. *Trends in Biotechnology*, 2006. **24**(11), p. 530-536.

252. De Mey, M., et al., Minimizing acetate formation in E-coli fermentations. *Journal of Industrial Microbiology & Biotechnology*, 2007. **34**(11), p. 689-700.

253. Kakuda, H., et al., Identification And Characterization Of The Acka (Acetate Kinase A)-Pta (Phosphotransacetylase) Operon And Complementation Analysis Of Acetate Utilization By An Acka-Pta Deletion Mutant Of Escherichia-Coli. *Journal of Biochemistry*, 1994. **116**(4), p. 916-922.

254. Castano-Cerezo, S., et al., An insight into the role of phosphotransacetylase (pta) and the acetate/acetyl-CoA node in Escherichia coli. *Microbial Cell Factories*, 2009. **8**, p. 19.

255. Bulter, T., et al., Design of artificial cell-cell communication using gene and metabolic networks. *Proceedings of the National Academy of Sciences of the United States of America*, 2004. **101**(8), p. 2299-2304.

256. Schuchmann, K. and V. Muller, Autotrophy at the thermodynamic limit of life: a model for energy conservation in acetogenic bacteria. *Nature Reviews Microbiology*, 2014. **12**(12), p. 809-821.

257. Waters, L.S. and G. Storz, Regulatory RNAs in Bacteria. *Cell*, 2009. **136**(4), p. 615-628.

258. Dolnick, B.J., Naturally occurring antisense RNA. *Pharmacology & Therapeutics*, 1997. **75**(3), p. 179-184.

259. Brantl, S., Regulatory mechanisms employed by cis-encoded antisense RNAs. *Current Opinion in Microbiology*, 2007. **10**(2), p. 102-109.

260. Kim, J.Y.H. and H.J. Cha, Down-regulation of acetate pathway through antisense strategy in Escherichia coli: Improved foreign protein production. *Biotechnology and Bioengineering*, 2003. **83**(7), p. 841-853.

261. Bakhtiari, N., et al., Down Regulation of ackA-pta Pathway in Escherichia coli BL21 (DE3): A Step Toward Optimized Recombinant Protein Expression System. *Jundishapur Journal of Microbiology*, 2014. **7**(2), p. 9.

262. BIO-RAD. *qPCR Assay Design and Optimization*. 2017; Available from: http://www.bio-rad.com/en-uk/applications-technologies/qpcr-assay-design-optimization?ID=LUSO7RIVK. [Accessed 03/02/2017].

263. Carafa, Y.D., E. Brody, and C. Thermes, Prediction Of Rho-Independent Escherichia-Coli Transcription Terminators - A Statistical-Analysis Of Their Rna Stem-Loop Structures. *Journal of Molecular Biology,* 1990. **216**(4), p. 835-858.

264. Luciano, D.J., et al., Differential Control of the Rate of 5 '-End-Dependent mRNA Degradation in Escherichia coli. *Journal of Bacteriology*, 2012. **194**(22), p. 6233-6239.

265. Horton, R.M., PCR-Mediated Recombination And Mutagenesis. *Molecular Biotechnology*, 1995. **3**(2), p. 93-99.